SEDIMENTOLOGY OF THE BHUBAN FORMATION IN AND AROUND AIZAWL, MIZORAM

A THESIS SUBMITTED IN PARTIAL FULFILLMENT OF THE REQUIREMENTS FOR THE DEGREE OF DOCTOR OF PHILOSOPHY

GAUTAM RAJ BAWRI
MZU REGD. NO.: 1506813
PH.D. REGD. NO.: MZU/Ph.D./1090 of 27.04.2018

DEPARTMENT OF GEOLOGY
SCHOOL OF EARTH SCIENCES AND NATURAL RESOURCES MANAGEMENT
FEBRUARY 2024

SEDIMENTOLOGY OF THE BHUBAN FORMATION IN AND AROUND AIZAWL, MIZORAM

BY

Gautam Raj Bawri
Department of Geology

Supervisor: Prof. K. Srinivasa Rao
Joint Supervisor: Dr. Bubul Bharali

Submitted
In partial fulfillment of the requirement of the Degree of Doctor of Philosophy in Geology of Mizoram University,
Aizawl

DEPARTMENT OF GEOLOGY
MIZORAM UNIVERSITY
A Central university established by an Act of Parliament
Accredited 'A' Grade by NAAC in 2019
AIZAWL: MIZORAM-796004

Prof. K. Srinivasa Rao

Phone: 7005609873
Email: ksrao@mzu.edu.in

CERTIFICATE

This is to certify that the thesis entitled "**Sedimentology of the Bhuban Formation in and around Aizawl, Mizoram"** submitted by **Gautam Raj Bawri** in fulfillment of Doctor of Philosophy in Geology is an original work and has not been submitted elsewhere for other degree. It is recommended that this thesis be placed before examiners for the award of the degree of Doctor of Philosophy.

Dated:
Place: Aizawl

(DR. BUBUL BHARALI)
Joint Supervisor

(PROF. K. SRINIVASA RAO)
Supervisor

DECLARATION

MIZORAM UNIVERSITY

FEBRUARY, 2024

I **GAUTAM RAJ BAWRI**, hereby declare that the subject matter of this thesis is the record of work done by me, that the contents of this thesis did not form basis of the award of any previous degree to me or to do the best of my knowledge to anybody else, and that the thesis has not been submitted by me for any research degree in any other University / Institute.

This is being submitted to Mizoram University for the Degree of **Doctor of Philosophy** in Geology.

Date:

Place: Aizawl

(**GAUTAM RAJ BAWRI)**
Department of Geology,
Mizoram University, Aizawl-796004

(Dr. Jimmy Lalnunmawia)	**(Prof. K. Srinivasa Rao)**	**(Dr. Bubul Bharali)**
Head	Supervisor	Joint Supervisor

ACKNOWLEDGMENTS

I extend my heartfelt gratitude to my supervisors, **Prof. K. Srinivasa Rao** and **Dr. Bubul Bharali**, Department of Geology, at Mizoram University and the Department of Geology at Pachhunga University College, Aizawl, respectively for their unwavering support, invaluable guidance, meticulous review of the thesis and constant encouragement throughout the duration of this thesis work.

I am sincerely grateful to **Dr. Jimmy Lalnunmawia**, Head of the Department for his continuous guidance, unwavering support, and provided the laboratory facility during my research work.

I am also immensely grateful to, Dr. V. Vanthangliana, Dr. Kavita Devi, Dr. J. Malsawma, Dr. Paul Lalnuntluanga, Dr. Susheel Kumar, and Dr. Santonu Ghosh and all the dedicated office staff of the Department of Geology at Mizoram University and Department of geology Pachhunga University College for their invaluable support and cooperation.

I would also like to extend my gratitude to the Director and the Head of the Geochemical Division, CSIR-National Geophysical Research Institute (NGRI), Uppal Road, Hyderabad for granting me the opportunity to conduct geochemical analysis in their laboratory.

I also extend my sincere gratitude to Dr. Develeena Mani Tiwari, Centre for Earth, Ocean and Atmospheric Sciences (CEOAS), University of Hyderabad, Hyderabad for her invaluable assistance and guidance during my research work. Her support has been instrumental in the success of my endeavors. Additionally, I would like to thank Dr. M. Ram Mohan for assisting me during my geochemical analysis. Furthermore, I extend my special thanks to Mr. Mintu Saikia, ONGC, Sivasagar for his help in laboratory work, particularly in the preparations of thin sections for my samples.

I am grateful for the financial support from the University Grants Commission and Mizoram University (UGC-MZU), Government of India, which made it possible to conduct this research work.

I would like to express my gratitude to my parents, elder brother **Gakul Bawri** and **Dr. Amal Bawri** for their unwavering patience, understanding, financial support,

and moral encouragement throughout my research work. Their prayers and support were invaluable to me and I deeply appreciate their constant encouragement.

I wish to express my special thanks to Dr. Ajanta Sharma, Dr. Meghali Gogoi, Dr. Raghu Protim Rakshit, and Dr. Parakh Protim Phukon for their valuable guidance and encouragement.

I extend my heartfelt thanks to **Sristi Sarkar,** Jonmenjoy Barman, Arman Boruah, Dr. Arup Bhowmik, Debojit Rabha, Rupendra Chakma, Ananya Buragohain, Arnabneel Gogoi, Pralay Kumar Boro, Abdul Rajak Ahmed, Diganta Baishya, Liza Gogoi, Saurabh Chetia, Dikshit Bokotial, Debashish Sarma, Debashish Das, Habibullah Ahmed, and also Research Scholars in the department of geology, Mizoram University, Aizawl for their unwavering support and moral encouragement.

Date:

Place: Aizawl

(GAUTAM RAJ BAWRI)
Department of Geology
Mizoram university
Aizawl-796004

TABLE OF CONTENTS

List of Figures

List of Tables

CHAPTER – 1
INTRODUCTION

1.1 Introduction

Tectonically, Mizoram is a part of the Surma Basin, and associated with the eastward subduction of the Indian plate along the Arakan Yoma suture during the Miocene period, followed by the subsequent formation of the Indo-Burmese Orogenic belt (Nandy, 1982) (Fig. 1.1). The Cenozoic rocks of Mizoram are represented by the Surma Basin, often referred to as the Greater Bengal Basin's northern extension in the geological past. The Surma Basin has evolved similarly to the Bengal Basin which was initiated by the collision between the Indian plate and the Burmese plate (Nandy et al., 1983; Dasgupta, 1984; Bharali et al., 2017).

As the collisions continued, the sea level regression in an S-W direction resulted in the transition of sedimentary sequences into an N-S trending hill range (Tiwari and Kachhara, 2003). Geologically, the Mizoram part is encompassed within the Neogene Surma Basin, which is characterized by a Succession of elongated and folded hill ranges exhibiting an arcuate shape with westward convexity. Based on the lithological variations, the Tertiary sequence of the Mizoram Fold Belt (MFB) has been classified into the Barail Group (Late Oligocene), Surma Group (Upper Oligocene-Miocene), and Tipam Group (Late Miocene-Early Pliocene), as shown in Table 1.1.

It extends across an area of approximately 21,081 km^2 and is located between the latitudes of 22º00'N and 24º30'N, along with longitudes 92°15′E and 93°25′E, respectively. The Miocene succession of Mizoram is one of the thickest sedimentary columns of the region and is a repeated succession of Paleogene to Neogene argillaceous and arenaceous rocks. According to the previous investigations, the entire basin is composed of sandstone, silty-sandstone, shale, mudstone, and their combination along with a few pockets of calcareous sandstone, fossiliferous siltstone, and intraformational conglomerate (Tiwari and Kachhara, 2003).

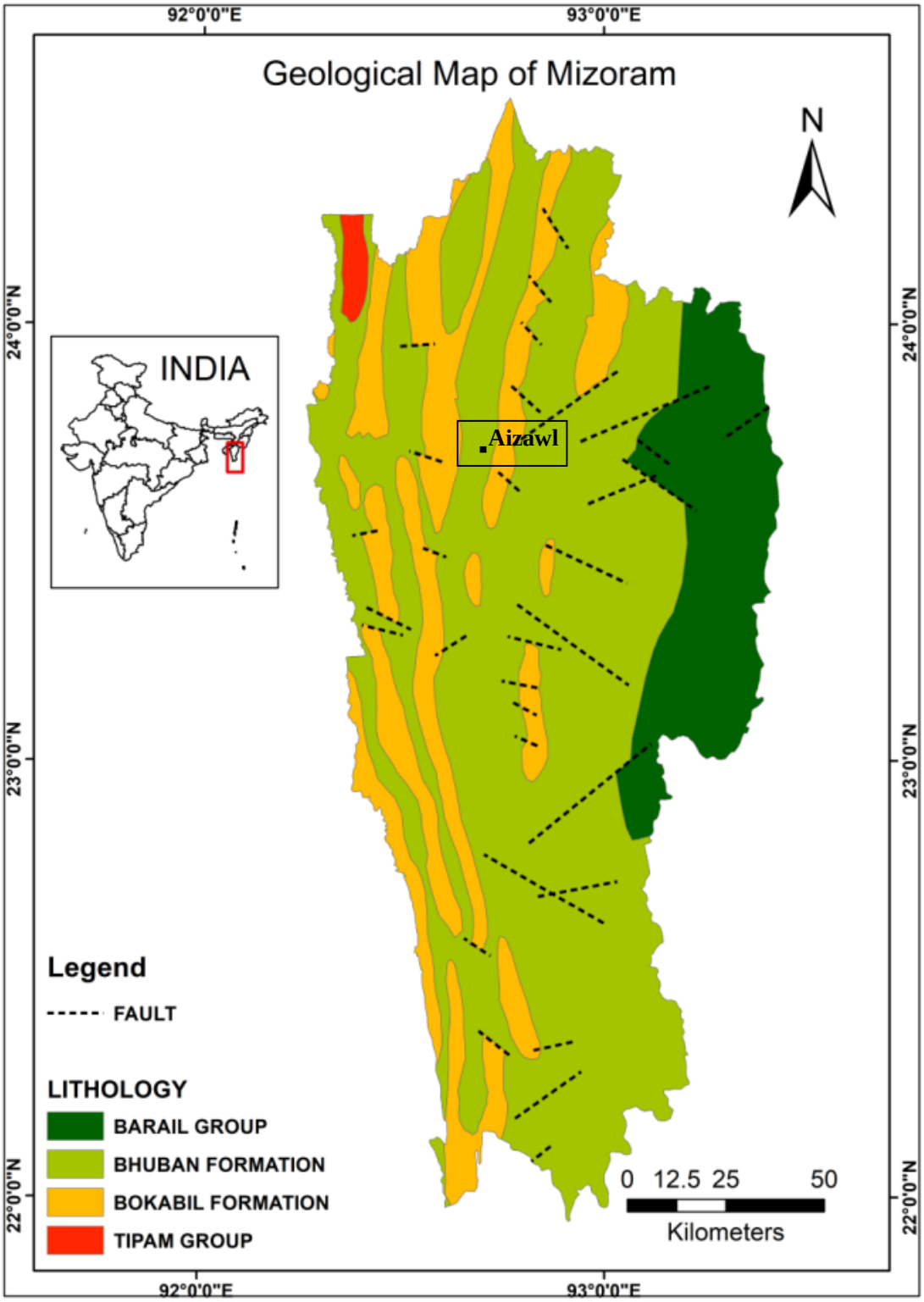

Figure 1.1. Geology and structural map of Mizoram (after GSI, 2013 & Barman and Rao, 2021).

Table 1.1. Stratigraphic succession of Mizoram (Modified after Karunakaran, 1974; Ganju, 1975; Tiwari and Kachhara, 2003; Mandokar, 2000; Barman and Rao, 2021).

Age	Group / Formation		Thickness	Gross lithology	Depositional environment
Recent	-		-	Gravel, silts, and clays	Fluvial and alluvial
----------Unconformity----------					
Early Pliocene to Late Miocene	Tipam		+ 900 m.	Friable sandstone with occasional clay bands	Fluvial
----------Conformable and transitional contact ----------					
Miocene	S	Bokabil	+ 950 m.	Shale, siltstone, and sandstone	Shallow marine
	U	----------Conformable and transitional contact ----------			
To	R	B H U B A N	Upper (+1100 m.)	Arenaceous predominating with sandstone, shale, and siltstone	Shallow marine, near shore to lagoonal
Upper Oligocene	M A		----------Conformable and transitional contact --------		
			Middle (+1000 m.)	Argillaceous predominating with shale alterations and sandstone	Deltaic
			--------Conformable and transitional contact --------		
			Lower (+900 m.)	Arenaceous predominating with sandstone, silty shale	Shallow marine
----------Unconformity obtained by faults----------					
Oligocene	Barail		(+ 3000 m.)	Shale, siltstone, and sandstone	Shallow marine
---------- Lower contact not exposed ----------					

This research investigates a section of the well-exposed Miocene Bhuban Formation in the Aizawl District of Mizoram, where these marine sedimentary sequences, characterized by significant deposition, are recognized as the depocenter of the Surma Basin (Tiwari and Kachhara, 2003).

The previous researchers La Touche (1891), Hayman (1937), and Franklin (1948) laid the foundation. Nevertheless, Ganju (1975), Nandy et al. (1983), Dasgupta (1984), and Tiwari et al. (2003, 2007, 2011) extensively worked on the Surma Basin, providing valuable information on the regional geological framework, tectonic settings, paleontology, magneto stratigraphy, etc.

This present research work has been selected for consolidating the discrepancies in the litho-unit division as suggested by the earlier researchers and a deficiency in adequate geological information. Consequently, the present study involves a comprehensive outcrop mapping and preparation of a vertical litho-column for the Bhuban Formation in the selected sections. A comprehensive petrographic analysis, encompassing diagenesis of the Bhuban sandstones has been carried out. This study also includes an attempt to the granulometric analysis, heavy mineral analysis, and whole-rock geochemistry of sandstones in parts of the Aizawl district. Additionally, a Sequence stratigraphic model has been prepared for the Bhuban Formation of the study area. Furthermore, the study area is also an important aspect of its distinctive geodynamic setting and the rocks are geologically suitable for hydrocarbon prospects.

1.2 Physiography

The Mizoram situated as the southernmost state of India is sharing the international borders with Myanmar and Bangladesh. Geographically, it comprises curved N-S anticlinal hill ranges, spanning an area of 21,081 km^2, with an average elevation of 1,000 meters above mean sea level. The Phawngpui hill ranges situated in Lawngtlai District and also recognized as the Blue Mountains is acknowledged as the highest peak in the state, reaching an elevation of 2157 meters above Mean Sea Level (MSL). The landscape primarily consists of steep gorges and narrow valleys, with major rivers generally flowing along these valleys in a northerly or southerly direction. The important rivers in the state of Mizoram are the Tlawng (Dhaleswari), Tuirial (Sonai), Tuivawl, and Tut (Gutur) courses flowing towards the Barak Valley in the state of Assam. The significant southernly flowing rivers, including the Chhimtuipui

(Koladyne) and Karnafulid originated from Myanmar and the southern corner of Mizoram state.

1.3 Climate

The climate is generally considered to be mild and pleasant. Winter temperatures in Mizoram are between 11°C and 21°C, and summer temperatures are between 20°C and 30°C. The monsoon brings an average of 250 mm of rain a year, which changes the normal weather in the area. It doesn't rain much or at all in the winter.

1.4 Geological Significance

The Assam-Arakan Basin encompasses an extensive continental mass in the Indian Terrain, spanning northeastern India, Bangladesh, and a portion of Myanmar. This basin covers an area of about 100,000 km^2 in India, including Assam, Mizoram, Manipur, Tripura, Meghalaya, and parts of Arunachal Pradesh. Due to the complex geological setup of the area that is being examined, as well as the area being geologically suitable for hydrocarbon occurrences and accumulation of hydrocarbons in the area is attracting scientists from both the academic community and the industrial sector. The widely distributed Cenozoic rocks of the Bhuban Formation are well exposed in the study area. The earlier scientific works in the proposed area of study a very little work, particularly on the petrography and geochemistry of the Bhuban sandstone of the Surma Basin. The proposed area exhibits good exposure to Cenozoic rocks. However, there is a lack of a scientific database in the studied area especially in terms of petrographical and geochemical aspects. It requires a comprehensive analysis of both the petrographical and geochemical aspects integrated with other proxies which is useful for better understanding the Surma Basin setup.

1.5 Previous Literature

The Surma Basin is located in an important geotectonic zone, however, it is rarely visited by researchers because of its rough terrain and isolated position. There has been very little research conducted in the Surma Basin. However, important work by early researchers has made it possible to understand the basin's regional perspective (Ganju, 1975; Nandy et al., 1983; Dasgupta, 1984). Tiwari et al. (2011). *Skolithos* and *Cruzianaichno* facies were found in the Bhuban Formation of Aizawl, Tiwari et al. (2011). They said that the sandy substrate changed to a poorly sorted soft substrate,

and high energy conditions were found in the foreshore zone and low energy conditions were found in the shoreface offshore zone. In addition, Rajkonwar et al. (2013) suggested that based on ichnofossils, the Middle Bhuban Formation exposed in and around Aizawl was influenced by fluctuating energy conditions in the foreshore to shoreface/offshore zone of the shallow marine environment. The magnetostratigraphic studies revealed that the Upper Bhuban Formation has a faster rate of sedimentation than the Middle Bhuban Formation (Tiwari et al. 2007 and Malsawma et al. 2010).

Chenkual, et al. 2010 analyzed heavy mineral assemblages found in the Tertiary rocks of the Teidukhan anticline, Kolasib district, Mizoram. Their analysis revealed that the source rock of the sediment is complex, encompassing igneous rock, pegmatite, high-rank metamorphic rocks, and reworked sediment supply.

Sarma and Chutia (2013) analyzed the petrography and heavy minerals of Tipam sandstones exposed on the Tipam hill of the Sita Kunda area in Upper Assam. Their analysis suggests that the provenance of Tipam sandstones was predominantly mixed and dissected arc type. Additionally, some sandstones indicate their derivation from quartz recycled origin. Furthermore, the study found that Tipam sandstones originate from both igneous and metamorphic sources.

Devi (2014) examined the textural characteristics and depositional environment of olistostromal sandstones in Ukhrul, Manipur. The study revealed that the sandstones exhibit high variability in size and shape, with a predominantly texturally and mineralogically immature composition. Additionally, most of these sandstones display an unimodal distribution. The dominant environment observed in the study was marine turbidity.

Sonowal and Laskar (2017) analyzed the textural characteristics of Jiadhal River sediments in Dhemaji district, Assam. The findings indicate that the sediments range from medium to very fine sand and are generally well to moderately sorted. They exhibit a range of skewness from negative to very positive and a kurtosis from very platykurtic to very leptokurtic. The varying mean size of the medium to very fine sand suggests fluctuations in the energy of the depositional environments.

Haider (2016) conducted grain size analysis along the Eastern Makran coastline area, in Pakistan. The study found that most samples exhibit a very fine to

fine-grained sand distribution, with only two samples showing a medium-grained standard deviation. This indicates that the grain size sorting of the sediment samples ranges from very well sorted to moderately sorted, with a few poorly sorted. Additionally, the particle population displays a range from very fine skewed to very coarse skewed, as demonstrated by the skewness.

The Surma Group of rocks extended into the Bengal Basin predominantly consists of quartzolithic sandstones with a few feldspathic and quartz arenitic types of sediments deposited from a quartzose recycled orogen provenance that indicates a moderate to high silica concentration (Rahman et al. 2007). The boundary between the active continental margin and the passive margin setting was established by using the tectonic setting. These sandstones are thought to have originated from felsic parent rocks as shown by the REE patterns.

Based on petrographic and diagenetic studies on Surma sandstone from several studies from the Bangladesh gas fields by Farhaduzzaman et al. (2015) stated that the Surma Group of sandstones are predominantly sublithic arenite to sub-feldspathic arenite with diagenetic characteristics such as quartz cement (overgrowth), authigenic clays, carbonate cement, dissolution-replacement, and compaction.

Lalnunmawia et al. (2014) have examined the sandstones and classified them as litharenite and sublitharenite types in the Bhuban sandstones of the Durtlang road section in Aizawl district, likely to have originated from the Himalaya Orogen and the Indo-Burmese collision tectonic zone.

Numerous studies using geochemical and petrological methods have been undertaken in the nearby Bengal Basin and northeastern regions of India. Najman et al. (2008) employed biostratigraphy, petrography, geochemistry, isotopic analysis, and seismic techniques to examine the Paleogene record of Himalayan erosion in the Bengal Basin of Bangladesh. Their findings concluded that the Barail Formation, consisting of deltaic sandstones ranging in age from the Late Eocene to early Miocene (38 to 21 Ma), represents the primary source of Himalayan-derived detritus entering the Bengal Basin.

Similarly, Devi and Mondal (2008) explored the provenance and tectonic settings of the Barail (Oligocene) and Surma (Miocene) Groups in the Surma-Barak basin, Manipur. They categorized the Barail and Surma sandstones as sublitharenite

and litharenite, respectively, formed from the collision-suture fold belt. The Surma sandstone was attributed to quartzose recycled orogen and transitional recycled orogen, with the provenance believed to be craton interior and quartzose recycled orogen. They proposed a "humid and semi-humid climate" for the source areas of these formations. According to the provenance ternary diagram, Barail and Surma sandstones are suggested to have originated from the Collision suture and Fold Thrust belt.

Bracciali et al. (2015) utilized various methods, including U-Pb detrital zircon and rutile analysis, isotopic (Sr-Nd and Hf) analysis, and petrography, to elucidate the change in the source of the Neogene paleo-Brahmaputra deposit in the Surma basin. The study suggests that the uplift of the Tibetan Plateau has increased river gradients and stream strength, resulting in the capture of the Yarlung Tsangpo River by the Brahmaputra. These methods indicate that detrital minerals were sourced from Cenozoic metamorphism, with contributions from the Yarlung Tsangpo River.

Chaudhuri et al. (2020) used petrographical and geochemical methods to study the compositional changes in the Mesozoic sedimentary record during the evolution of the pericratonic rift basin of Kutch. The investigation revealed felsic source rocks, indicated by various parameters such as the dominance of arkosic sandstone, zircon concentration, trace element abundance and ratios, and enrichment of LREE with negative Eu anomaly. The study proposed "intermediate to intense weathering in the source area with immature to mature sediments." Tectonic settings analysis suggested that the Kutch Basin originated in passive margin settings during the Mesozoic Era.

Zoramthara (2015) conducted research work on the grain size analysis of the Tipam Group of sandstones in the Kolasib district, Mizoram. It shows that the Tipam sandstones are not deposited in a single environment but, rather in mixed or transitional environments.

The whole rock geochemistry of Tertiary sediments from the Mizoram foreland basin was studied by Hussain and Bharali (2019) categorized the rocks as quartz arenite and sublith-arenite based on the mineral compositions. The Chemical Index of Alteration (CIA) and Chemical Index of Weathering (CIW) values suggested that the source rock for the Barail and Surma sandstone had undergone moderate weathering.

Chondrite-normalized Rare Earth Element (REE) analyses of the Surma and Barail sandstones indicated a felsic magmatic source.

1.6 Objectives of the study

1) Preparation of facies map based on the facies analysis.
2) To interpret the modes of transport of sediments and depositional environments of the study area.
3) To study the sequence stratigraphy of the study area.
4) To decipher the tectono provenance of the study area

1.7 Geological setting and Study area

The Surma Basin, located in the North-eastern part of India, spans latitudes 21°56' to 24°31' and longitudes 92°16' to 93°26', with an average elevation of 1000 meters above sea level. It originated due to the collision between the Indian and Burmese plates, resulting in intermittent subsidence and significant sediment deposition during the Tertiary period (Ganju,1975; Nandy et al.,1983; Dasgupta, 1984). Tertiary clastic sequences of the Surma Basin have undergone folding and faulting, forming North-South trending hill ranges across Mizoram. The Tertiary sequences include the Oligocene Barail Group, the Miocene Surma Group, and the Mio-Pliocene Tipam Group. The Surma Group of rocks is dominantly exposed in most parts of the basin, the central part became thickest and is considered to be the depocenter of the basin (Tiwari et al. 2013). Although the Barails are not subdivided, the Surma Group is divided into Bhuban and Bokabil Formations based on litho association (Evans, 1964; Nandy, 2001). The Bhuban Formation is further divided into Upper, Middle, and Lower Formations based on lithological variations, primarily comprising sandstone, shale, and siltstone. The Middle Bhuban Formation constitutes a significant portion of the Surma Group and is enriched with argillaceous sediments. The Bhuban formation exhibits alternate transgressive–regressive sequences of transitional shallow marine deposits influenced by fluvial processes (Tiwari & Mehrotra, 2002; Tiwari et al., 2011; Bharali et al., 2021). The Tipam Group, mainly composed of coarse-grained sandstones with shale bands, was deposited in estuarine and fluvial settings (Sinha and Sastri 1973; Ranga Rao 1979). These Tertiary

sedimentary sequences are primarily sourced from Himalayan granitoids, with minor contributions from nearby Indo-Burmese orogens (Hussain and Bharali, 2019).

The study area encompasses the Surma Group of the Miocene Bhuban Formation, which falls within the Upper Bhuban Formation and Middle Bhuban Formation of the Aizawl District of Mizoram ranging from early to middle Miocene age. Geographically, the study area extends from latitude 23°38' to 23°46' N and longitude 92°43' to 92°49' E, with a maximum elevation of 1159 meters (MSL) covering toposheets no. 84-A/10, 84-A/14, 84-A/15 (Fig. 1.2). The examined Bhuban sandstones are characterized by fine to medium grains, buff in color, and exhibit massive bedding with limited outcrops. Conversely, the shales are described as dark grey, firm, and compact. In the present research work, geological mapping is conducted in four road sections of the Aizawl district of Mizoram where rocks are mainly from the Upper and Middle Bhuban Formations of the Surma Group. Thickness measurements of various sedimentary beds are recorded to prepare a litho-column for each section.

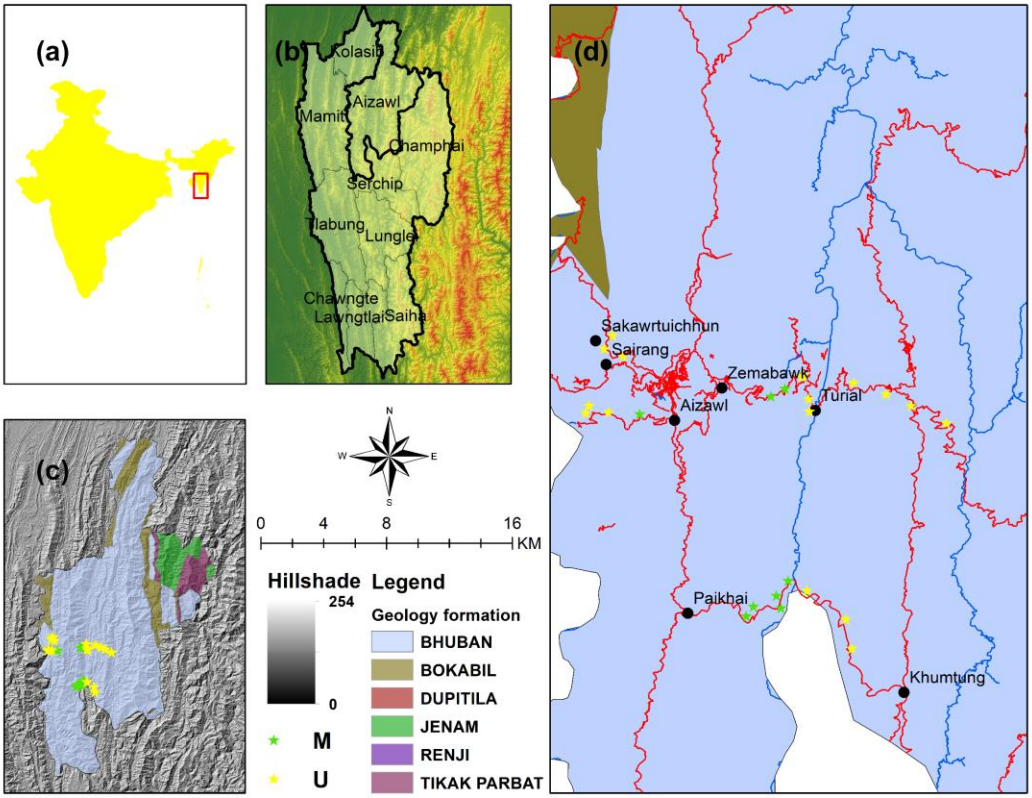

Figure 1.2. Location map representing the inset maps of districts (b), (c), and (d) related to the geology of the study area and location of the samples. Note: - The NE corner of the Aizawl district in the inset map (c) borders with the Manipur state and the geology of the area included in the inset map (M - representing the Middle Bhuban Formation and U - representing Upper Bhuban Formation)

CHAPTER - 2

METHODOLOGY

2.1 Research Methodology

To attain the research objectives, the present study employs the following methods and techniques which are mainly categorized into three parts.

2.2 Literature Review

The previous literature in a specific area provides valuable insights into the various aspects of geology and research activities within the study area. It aids in identifying gaps and limitations in previous works. For this present study, a review of previous work done on the Bhuban Formation of the Surma Group is undertaken focusing on sedimentological studies. The collection of research papers, scientific reports, and theses took place at the Central Library of Mizoram University, Aizawl, and Dibrugarh University, Dibrugarh. Additionally, some of the literature-related materials were gathered from INFLIBNET (www.inflibnet.ac.in) and Research Gate (www.researchgate.net).

2.3 Field investigations

The fieldwork for this present study entails a comprehensive investigation of lithological facies variations, along with the measurement of bedding planes and thickness, and the analysis of sedimentary structures within the Surma Group of Bhuban sandstones. To accurately document sampling locations and other significant points of interest, GPS coordinates were also recorded. Detailed data on textural properties and sedimentary structures, including features like current bedding and ripple marks, ball and pillow, cross-stratification, etc were meticulously recorded during the fieldwork, and supplemented with field photographs for visual reference (Fig.2.1). The study spanned across four geological sections within the Surma Group, of both Upper Bhuban and Middle Bhuban Formations namely:

1) Zemabawk-Tuirial, (2) Aizawl-Reiek, (3) Sairang- Sakawrtuichhun and (4) Paikhai Section.

2.3.1 Instruments Used: A handheld Garmin GPS (Global Positioning System), base map (toposheets), digital camera, measuring tape, Brunton compass, portable hand

drill machine, sample bags, hammer, chisel, field notebooks, haversack, and other tools are mostly used during the fieldwork (Fig2.2).

2.3.2 Sample Collection: Sandstone samples from the Surma Group were collected from each geological proposed section for various laboratory analyses. These analyses include rock thin section study, heavy mineral study, grain size analysis, and whole-rock geochemistry.

2.4 Laboratory analysis: It involves the following steps

a) Geological mapping, Litho-column preparation, and Sequence Stratigraphy analysis,

b) Rock Thin-Section study and heavy mineral identification,

c) Granulometric analysis, and

d) Geochemical analysis.

Finally, an attempt has been made to understand the characteristics of collecting Bhuban sandstones, tectonic setting, provenance, paleoclimatic conditions, different weathering parameters, and depositional setting of the Surma Group of Bhuban sandstones in the study area by combining laboratory experiments along with field observations.

2.4.1 Geological mapping, Litho-column preparation, and Sequence Stratigraphy analysis

A litho-column typically includes a systematic description of lithological features such as rock type, texture, colour, bedding characteristics, grain size, sedimentary structures, and fossil content observed within each stratigraphic unit of a particular area. This detailed documentation enables researchers to identify and interpret various sedimentary facies and depositional environments, ranging from fluvial and deltaic systems to marine and aeolian environments.

In the present study, the litho-column and geological maps for each proposed section were meticulously constructed using data collected during the fieldwork. To investigate the lithofacies analysis, comprehensive vertical litho-columns were generated for each section within the Surma Group of Bhuban Sandstone, employing geological traverses across the study area. These columns were constructed based on meticulous measurements of various litho-units, measurements of bed thickness, observations of sedimentary structures, grain size, and fossil content exposed in the

study region. Again, this prepared litho-column serves as a valuable tool for sequence stratigraphic analysis, providing detailed information on lithological units, boundaries, stacking patterns, and depositional environments of the studied area. Its integration with other stratigraphic data allows for a comprehensive understanding of basin evolution and the development of sequence stratigraphic models for sedimentary basins. The present study conducted lithofacies analysis and sequence stratigraphy to assess the depositional environment and the development of sequence stratigraphic models for sedimentary basins of the Surma Group of Bhuban Sandstones. The geological map and lithocolumn of the study area were prepared using software such as SedLog v3.1, CorelDraw X7, and ArcGIS10.3.

2.4.2 Rock Thin-Section Study and Heavy Mineral Identification

To determine the mineralogical compositions, textural characteristics, and diagenetic signatures of Bhuban sandstone, 20 representative samples were collected from proposed field sections and analyzed using petrographic modal counting techniques. The petrological study and compositional analyses of the selected samples were carried out at the Optical Petrographical Laboratory, Department of Applied Geology, Dibrugarh University. Modal composition analyses involved counting at least 500 points per thin section using the standard procedure and Gazzi-Dickinson's point-counting technique (Dickinson and Suczek, 1979; Dickinson et al., 1983). Additionally, the Bhuban Sandstone samples were classified based on their detrital framework components, primarily comprising quartz, feldspar, lithic fragments, mica, cement, and matrix. With the help of petrographical modal counting techniques, detailed mineralogical analyses including diagenetic evolution were conducted as well, and using the modal analysis data, interpretations related to petrographic classification, tectonic setting, provenance and climatic conditions of sandstone samples have been derived.

Heavy mineral analysis was conducted on the selected 26 samples at the sedimentology laboratory, Department of Geology, Mizoram University. Although there are many alternative ways to separate minerals, Bromoform (sp. gr. 2.89) and Thoulet's solution are frequently employed with different specific gravities (sp. gr. 3.40). In this study, the Bromoform liquid was used for heavy mineral separation. Due to the hard and compact nature of the rock samples, their breakdown for heavy mineral

separation was not feasible, thus, the method proposed by Folk (1982) was adopted. To remove authigenic clay, carbonate, and ferruginous coatings on the grains, approximately 50 gm of samples for heavy mineral separation were gently crushed, thoroughly washed, and then treated alternately with Hydrogen Peroxide, distilled water, dilute Hydrochloric acid, and Stannous Chloride for 5 to 10 minutes. The minerals were subsequently separated in a funnel using Bromoform to extract heavy minerals. The extracted minerals were mounted on slides with Canada Balsam for microscopic examination to determine the relative abundance of heavy minerals in each sample, using Galehouse's Ribbon Counting Method (1971).

2.4.3 Granulometric study

To ascertain the textural characteristics, transportation agencies, and depositional environment from the grain size analysis, 26 representative sandstone samples were selected from the different field sections and analyzed in the sedimentology laboratory, Department of Geology, Dibrugarh University. Sandstone samples underwent a 24-hour water soak to loosen the grain bonds and were subsequently dried under the Sun. Each sample was disintegrated with an agate mortar, and 100 gm of each disintegrated sample was taken for sieve analysis using an automatic sieve shaker machine. The standard sieves of the American Society for Testing Materials (ASTM) specifications were used. These sieves have openings that increase uniformly in multiples of $4\sqrt{2}$, starting from an opening of 0.045 mm (325 mesh). The sieves were arranged with the coarsest mesh size at the top and the finest at the bottom (in the order of 35, 45, 60, 80, 120, 170, 230, and 325), with ½ Phi (Ø) intervals. A pan was placed at the bottom to collect the silt and clayey fractions. The entire setup was then placed on a Ro-Tap mechanical Sieve shaker for 15 minutes, and the weight of each stack's samples was carefully recorded. In the present study, the size of various grades is expressed by using the phi (Ø) scale, as defined by Krumbein (1934). The size data were then grouped into phi (Ø) scale intervals. The cumulative frequency curves for each sample were plotted on an arithmetic probability scale, with cumulative frequency percentages on the ordinate (y-axis) and phi (Ø)-sizes on the abscissa (x-axis). The statistical textural parameters such as graphic mean size (M_Z), inclusive graphic standard deviation (σ_1), inclusive graphic skewness (S_K), graphic

kurtosis (K_G), and linear discriminant functions, etc. were calculated by using this graph.

2.4.4 Geochemical Analysis

For whole-rock geochemical analysis, 20 representative sandstone samples were powdered by grinding at the sedimentology laboratory, Department of Geology, Mizoram University, India. After grinding, 20 gm of each sample was meticulously packed to prevent contamination. The samples were prepared for analyzing X-ray Fluorescence Spectroscopy (XRF) and High Resolution-Inductively Coupled Plasma Mass Spectroscopy (HR-ICP-MS) to identify the major oxides, trace elements, and rare earth elements present in the sandstone samples. The investigations were carried out at the National Geophysical Research Institute (NGRI) in Hyderabad, India. To measure major oxides, pressed pellets were prepared from the powdered sample with a mesh size of 200µm, employing the Axiasm AX 4 kW Sequential Wavelength Dispersive X-ray Fluorescence Spectrometer (WD-XRF). The powdered samples were subsequently dissolved in an HF: HNO_3 solution through an open digestion procedure for the analysis of trace and rare earth elements. Following the dissolution, the sample solutions were subjected to analysis using a High Resolution-Inductively Coupled Plasma Mass Spectrometer (HR-ICP-MS).

Figure 2.1. Field photographs from the study area: (A) alternate layers of sandstone and shale overlaid by massive sandstone (Tuirial road section) (B) vertical burrows (skolithos), (C) massive sandstones in Paikhai road section), (D) current bedding in sandstone (E) alternate layers of siltstone and shale with sandstone (near Paikhai) and (F) shale beds alternate with sandstone beds (Sairang).

Figure 2.2. The instruments used during fieldwork and laboratory work mainly involve (A) GPS, (B) Ro-Tap mechanical sieve shaker (C) Brunton Compass (D) Agate mortar and pestle (E) Separating funnel equipment assembled for heavy mineral separation. (F) Leica-DM750P Trinocular Polarizing Microscope fitted with CCD camera.

CHAPTER -3
SEDIMENTOLOGICAL INVESTIGATIONS AND SEQUENCE STRATIGRAPHIC FRAMEWORK

3.1 Lithofacies description of the field sections

Facies encompass the combined lithologic characteristics, including bed thickness, grain size, bed geometry, sedimentary structures, and fossil content. These elements help deduce the origin and depositional environment of the sediment (Teichert, 1958). Sedimentary facies, based on their origin, fall into three main groups: (i) terrigenous, formed from particles eroded from older rocks and transported to the deposition site, (ii) biogenic, composed of whole or fragmented shells and other hard parts of organisms, and (iii) chemical, resulting from inorganic precipitation from a solution. Facies association pertains to the collection of sedimentary facies used to characterize a specific sedimentary environment. Walther's Law (1937) states that the vertical successions of facies not only represent changes in the environment over time but can also be used to reconstruct past landscapes (Reading, 1978; Feibel, 2013). In the present study, the following geological sections from the Bhuban formation have been covered. (Table. 3.1) and (Figure 3.1).

Table 3.1. Studied sections (location) details along with GPS coordinates (longitudes and latitudes).

Sections	Locations (GPS)		Elevations (m)
	Top of section	Bottom of section	
Zemabawk-Tuirial	23°43′ 445″ N 92°46′ 276″ E	23°43′ 392″ N 92°47′ 454″E	204 m-696 m
Aizawl-Reiek	23°42′ 808″ N 92°39′ 835″ E	23°42′ 738″ N 92°38′ 781″ E	489 m-1111 m
Sakawrtuichhuan-Sairang	23°45′ 890″ N 92°40′ 568″ E	23°45′ 985″ N 92°40′ 527″ E	199 m-801 m
Paikhai	23°36′ 200″ N 92°43′ 982″ E	23°36′ 142″ N 92°45′ 645″ E	515 m-828 m

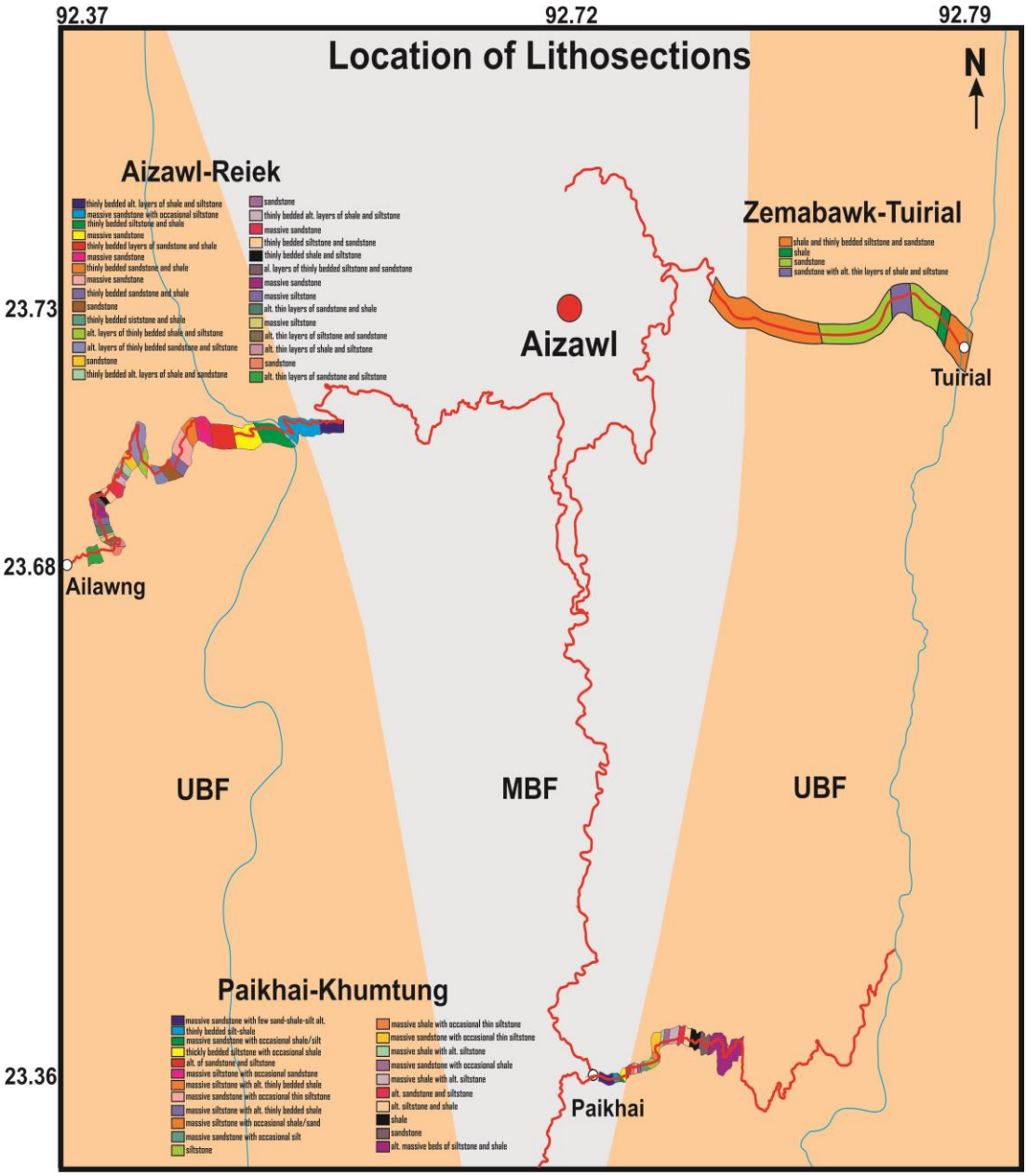

Figure. 3.1. Facies map of the studied lithosections, Aizawl, Mizoram.

3.2 Zemabawk-Tuirial Road Section (ZT)

Zemabawk-Tuirial Road section belongs to the Surma Group of the Bhuban Formation which is situated in the northern part of the Aizawl District, Mizoram. Lithologically, this section comprises a coarsening upward sequence at the bottom which is overlain by fining upward. The section is dominantly composed of massive sandstone and subordinate shale-siltstone and shale. The dominant sedimentary structures of this section are vertical burrows (*skolithos*), amalgamated sandstone beds, planner laminations, and hummocky cross stratifications (Fig 3.2). The details measured Litho column of the Zemabawk-Tuirial Road section is shown in (Fig 3.3 and Fig.3.4). In this section, there are mainly two types of system tracts that have been observed falling stage system tract (FSST) and low stand system tract (LST) (Fig. 3.2). Based on the field observation (litho-column) and the preservation of sedimentary structures such as vertical burrows (*skolithos*), planner laminations, and hummocky cross stratifications indicative of deposition in the transitional environment i.e., tidal flat environment.

Figure 3.2. The field photographs show the sedimentary structures (a) hummocky cross stratifications (b) vertical barrows and (c) planner laminations.

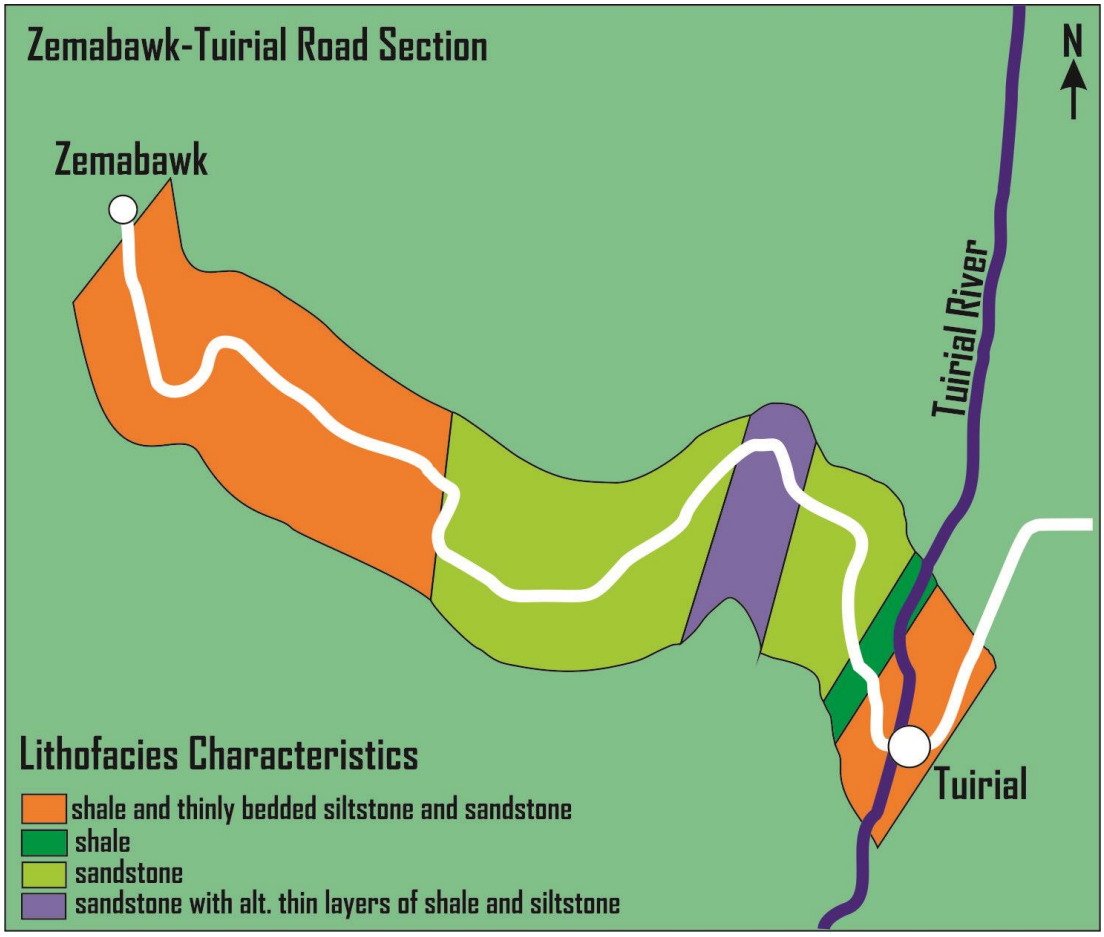

Figure 3.3. Lithofacies map of the Zemabawk-Tuirial road section, Aizawl, Mizoram.

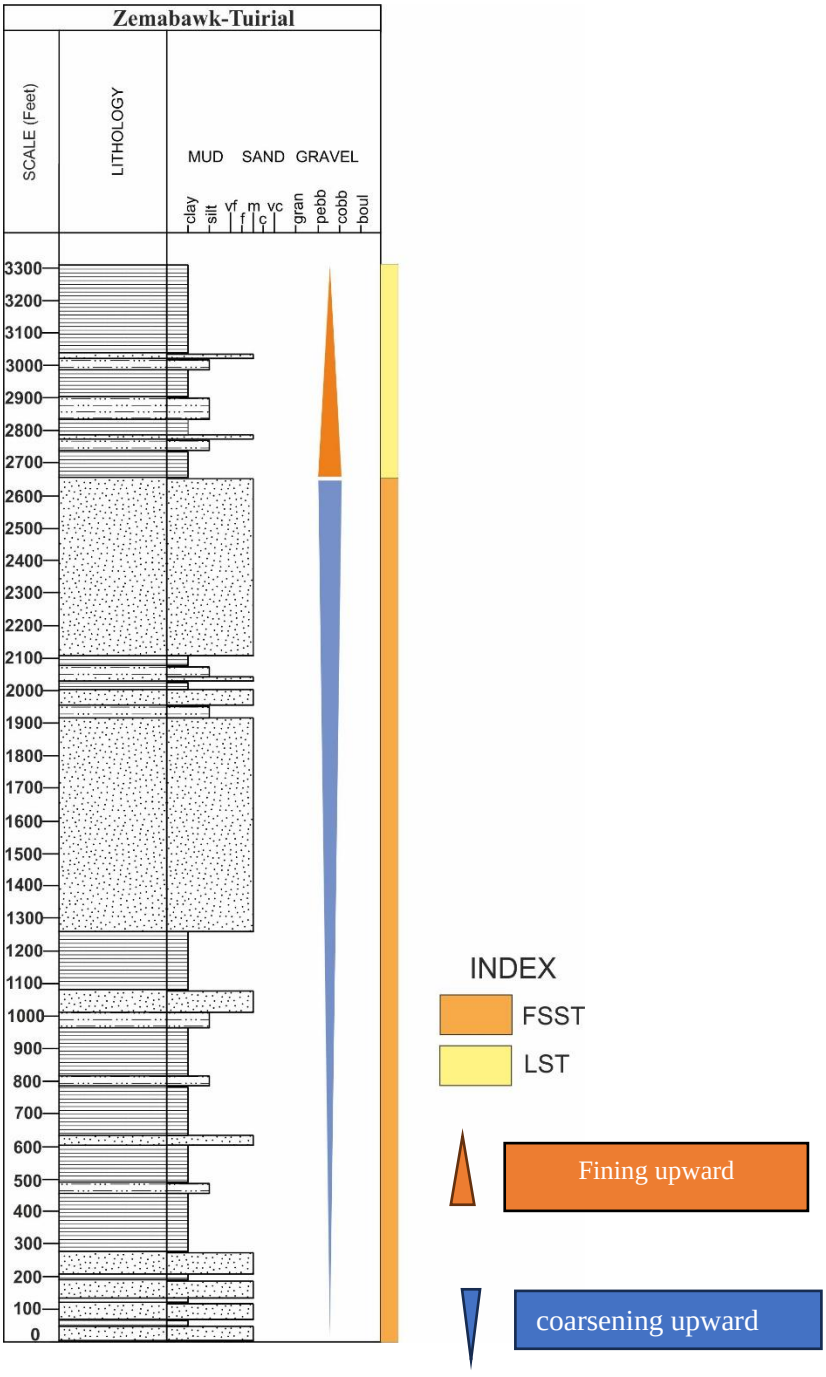

Figure 3.4. The detailed lithocolumn of the Zemabawk-Tuirial road Section (ZT) shows the distribution of lithologies, and sequence stratigraphic framework.

3.3 Aizawl-Reiek Road Section (AR)

The Aizawl-Reiek Road section belongs to the Surma group of the Bhuban Formation comprising fine to medium, grained sandstone bed along with shale and siltstone bed. A well representation of a coarsening upward section is observed in this section, where massive sandstone beds are at the top of the section, while the middle portion of the section is composed of the massive siltstone beds, and the bottom layer of the section is comprised of the alternate layers of siltstone and shale with sand bed. Ball and Pillow, planner lamination, and cross-bedding are the dominant sedimentary structures present in this section (Fig. 3.5). The detailed Litho-column of the measured section is shown in (Fig.3.6 and Fig. 3.7a, 3.7b, 3.7c, 3.7d ,3.7e). In the Aizawl-Reiek section is mainly falling stage system tract (FSST) and low stand system tract (LST) are present.

Based on the field observation (litho-column) the presence of amalgamated sandstone beds, siltstone–shale beds, planner lamination, and cross-bedding point toward deposition in a fluvial environment.

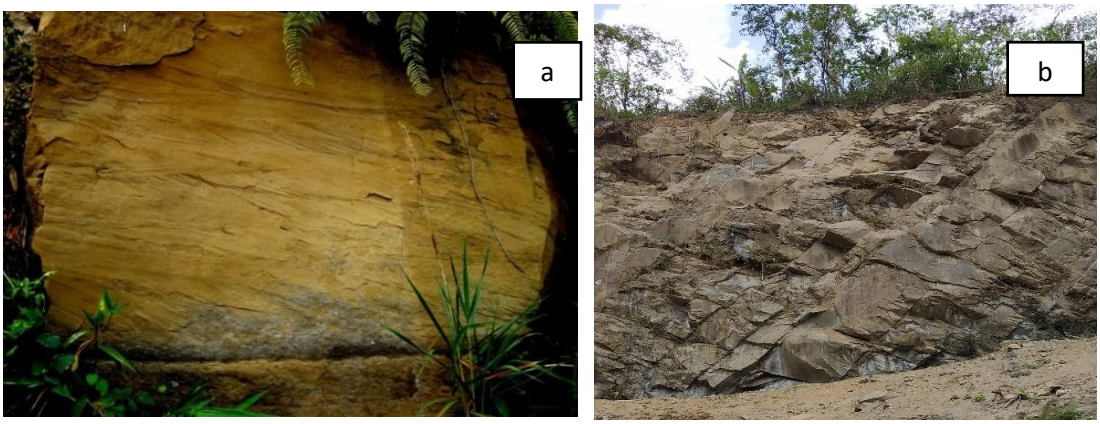

Figure 3.5. The field photograph shows the sedimentary structures (a) cross-bedding and (b) amalgamated sandstone beds.

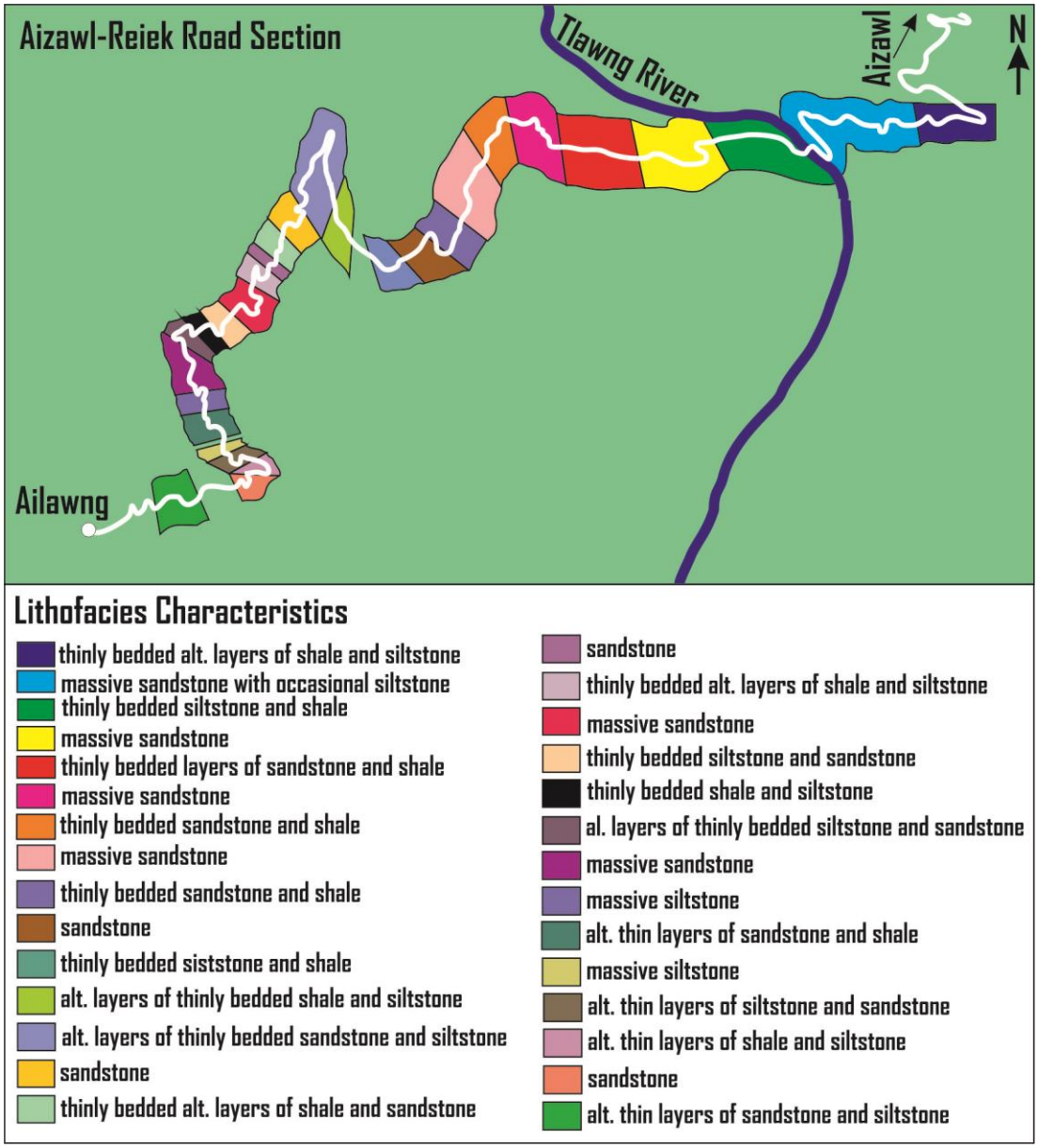

Figure 3.6. Lithofacies map of the Aizawl-Reiek road section, Aizawl, Mizoram.

a

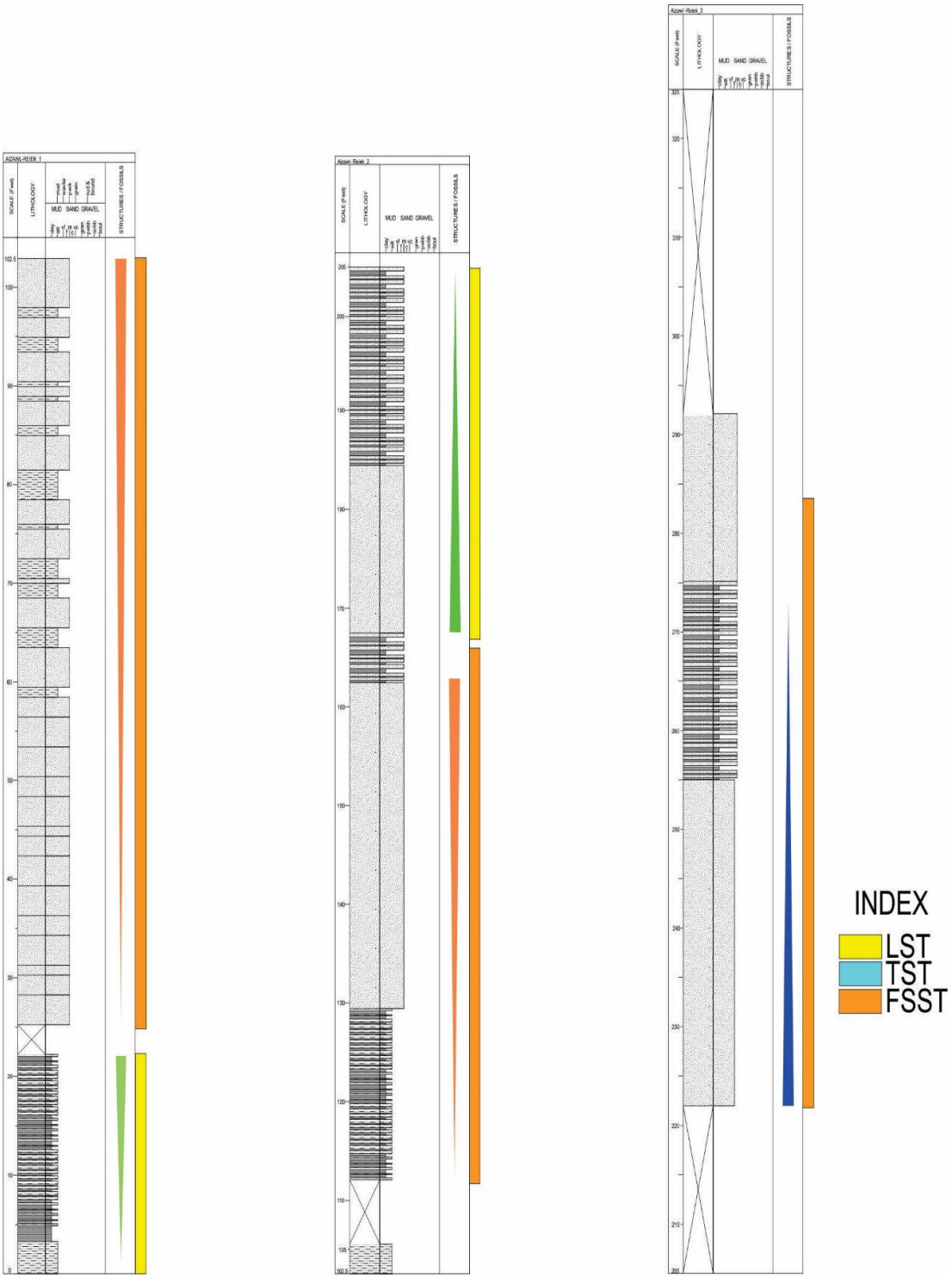
AZAM-REEK 1
Azawi Reek 2
Azawi Reek 3
SCALE (Feet)
LITHOLOGY
MUD SAND GRAVEL
STRUCTURES / FOSSILS
INDEX
LST
TST
FSST

b

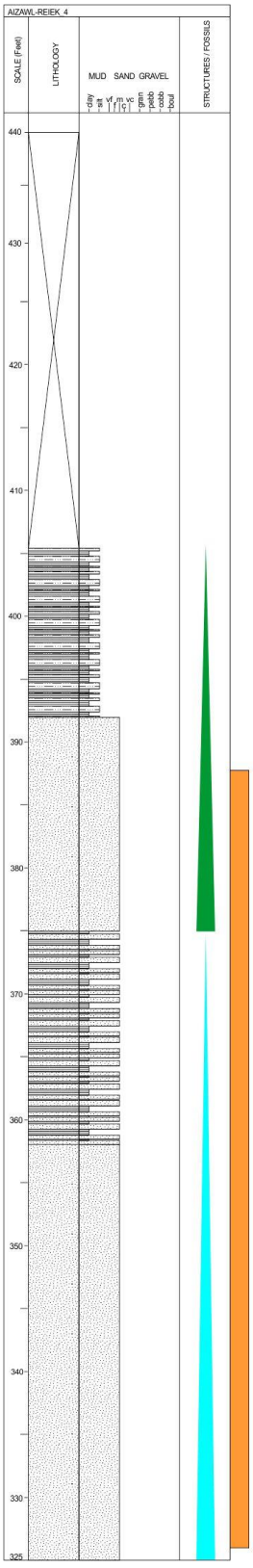

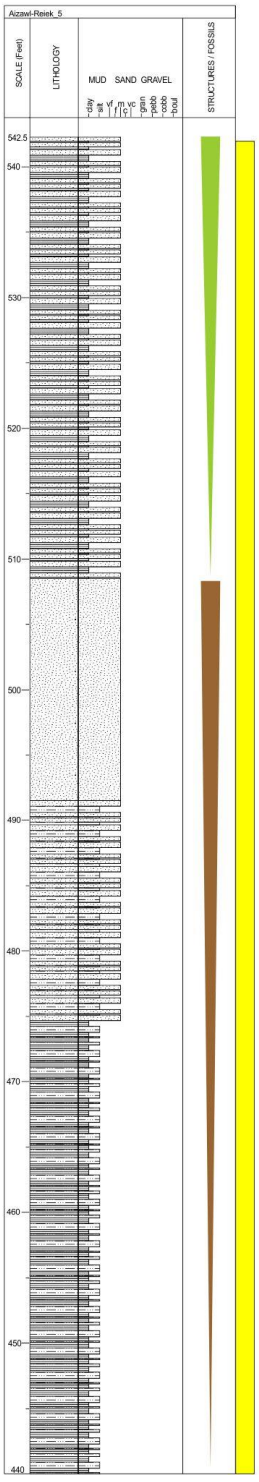

INDEX

LST

TST

FSST

C

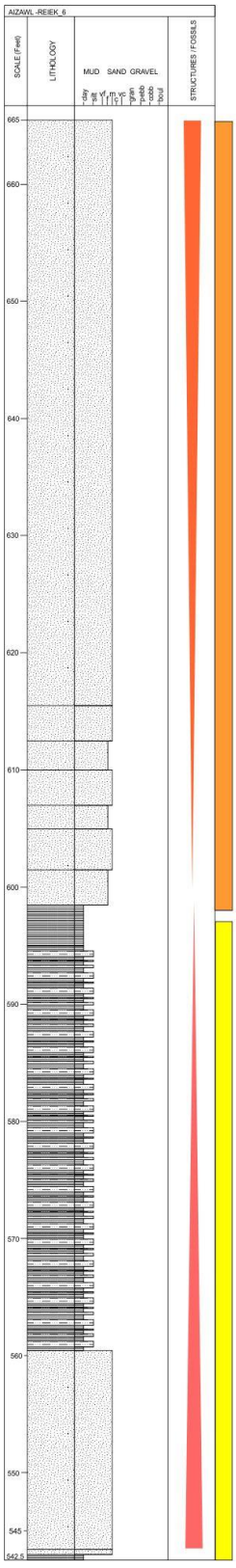

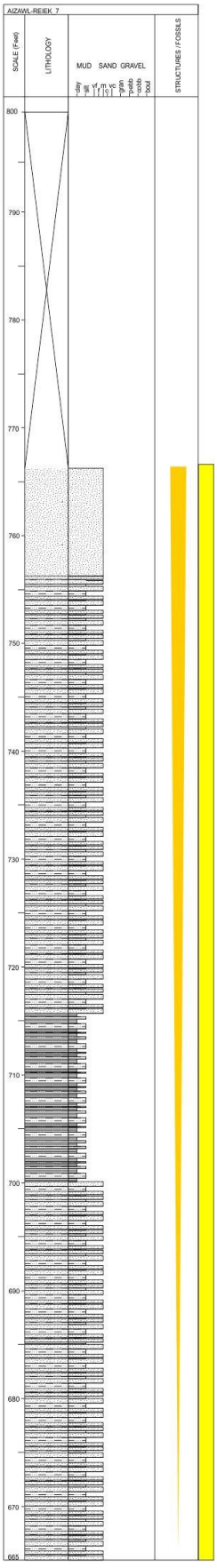

INDEX

LST

TST

FSST

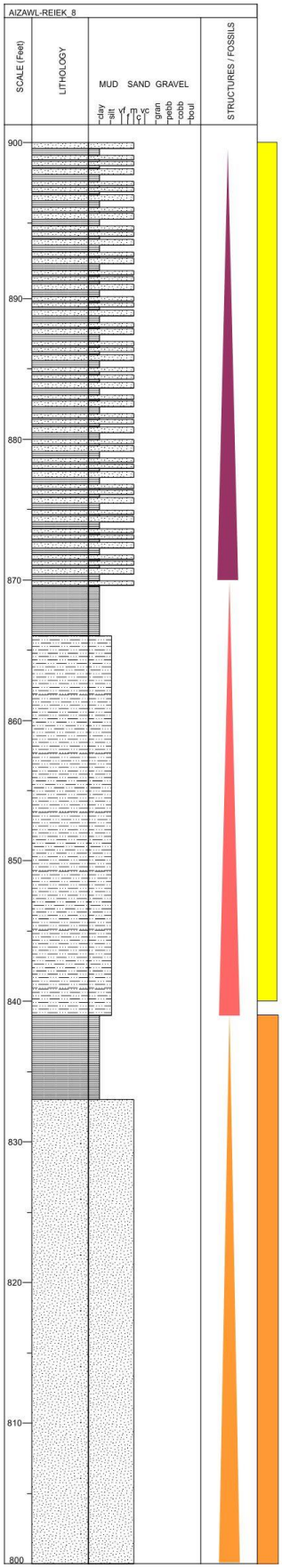

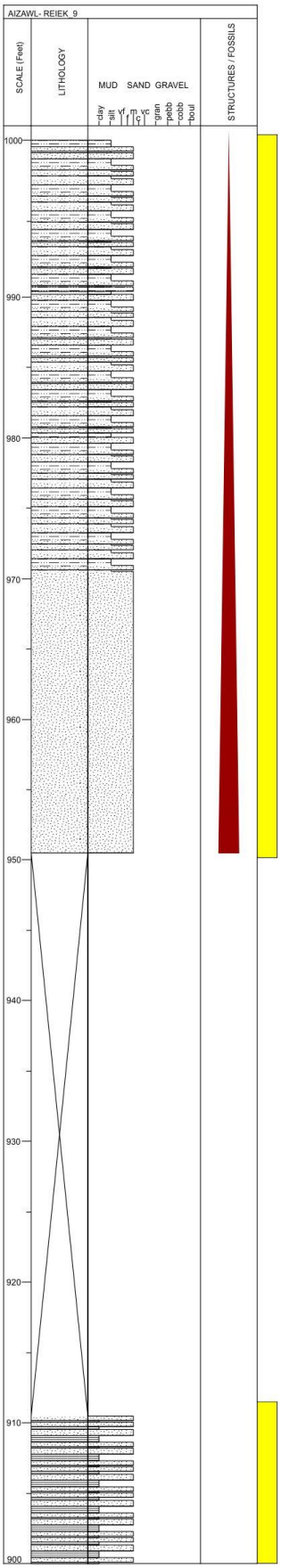

d

INDEX

LST

TST

FSST

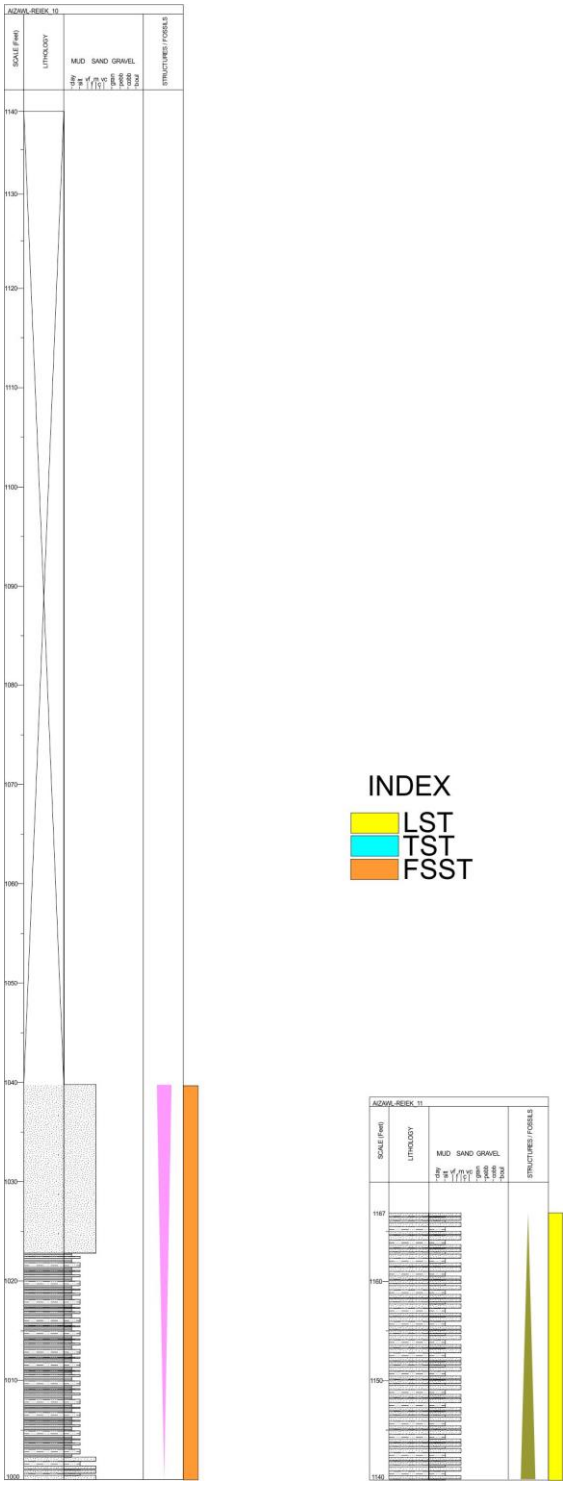

e

Figure 3.7 (a), (b), (c), (d), and (e) the detailed lithocolumn of Aizawl-Reiek road section (AR) shows the distribution of lithologies, and sequence stratigraphic framework.

3.4 Sakawrtuichhuan- Sairang Road Section (SS)

The studied section is part of the Surma group of Bhuban formation situated in the western part of the Aizawl district. Lithologically, in this section, a well representation of coarsening upward is observed at the base which is overlain by fining upward indicating the both transgressive and regressive phases of sediment deposition. The section is dominantly comprised of siltstone and alteration bed with siltstone and sandstone in its lower part and thickly bedded to massive sandstone with shale in the upper part. The sedimentary structures observed along this section is mainly parallel laminations and, hummocky cross-stratification (Fig. 3.8). The detailed lithocolumn of the measured section is given in (Fig. 3.9.). In the Sakawrtuichhuan- Sairang Road Section (SS) section is mainly falling stage system tract (FSST), low stand system tract (LST), and transgressive system tract (TST) are present. Based on the field observation (litho-column) and the presence of alterations of siltstone and sandstone beds, parallel laminations and, hummocky cross-stratification point towards deposition in shallow marine environment.

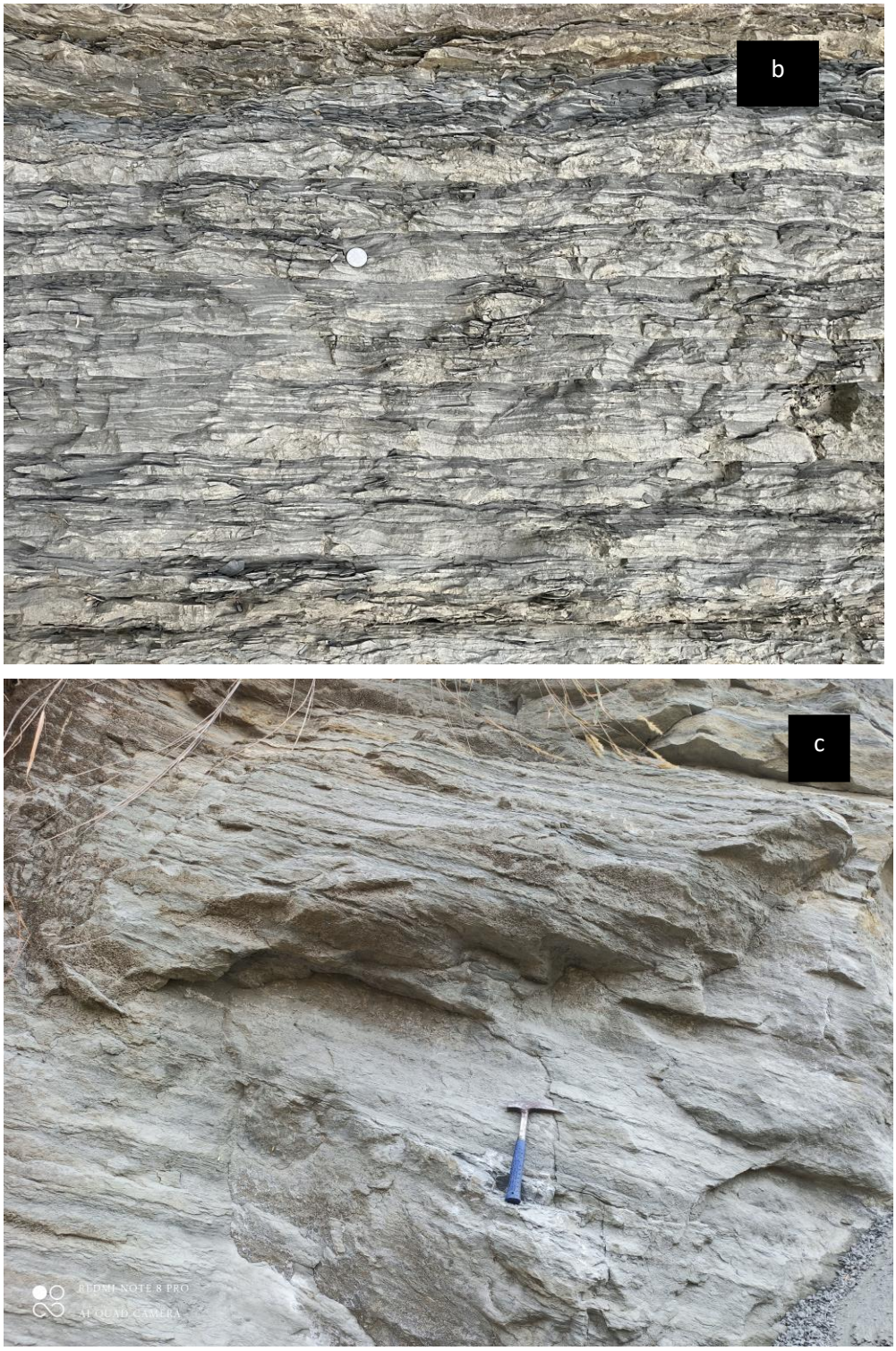

Figure 3.8.- Field photograph showing the sedimentary structures (a) siltstone and sandstone beds (b) Parallel Lamination and (c) hummocky cross-stratification,

Figure 3.9. The detailed lithocolumn of Sakawrtuichhuan- Sairang road section (SS) showing the distribution of lithologies, and sequence stratigraphic framework.

3.5 Paikhai Road Section (PK)

The Paikhai road Section belongs to the Surma Group of the Bhuban Formation composed of fine to medium grained massive sandstone along with siltstone and shale. Overall, this section shows coarsening upward at the base and fining upward at the top which represents a transgressive and regressive phase of sediment deposition. The majority of the sediments are fine grained consisting mostly of siltstone with shale and alternatively deposited with the thick beds of sandstone. The measured section shows cyclic sedimentation of sandstone, interbedded shale-siltstone, sand-silt intercalations, and thin to thickly-bedded sandstone. The dominant sedimentary structures present in this section are ripple marks, cross-stratification, and planner lamination is shown in (Fig.3.10). The details of the measured lithocolumn of the Paikhai road Section are shown in (Fig.3.11 and Fig.3.12a, 3.12b, 3.12c, 3.12d 3.12e, 3.12f, 3.12g, 3.12h, 3.12i, 3.12j, 3.12k, and 3.12l). This section is occupied with all the system tracts such as the falling stage system tract (FSST), low stand system tract (LST), transgressive system tract (TST), and high stand system tract (HST). Based on Field observation (Litho-Column) of the presence of massive sandstone beds, ripples mark, cross-stratification, and planner lamination point towards deposition in a fluvial environment.

Figure 3.10.- field photograph showing the sedimentary structures (a) Ripple Marks and (b) Massive Sandstone bed (c) alteration bed sandstone and shale.

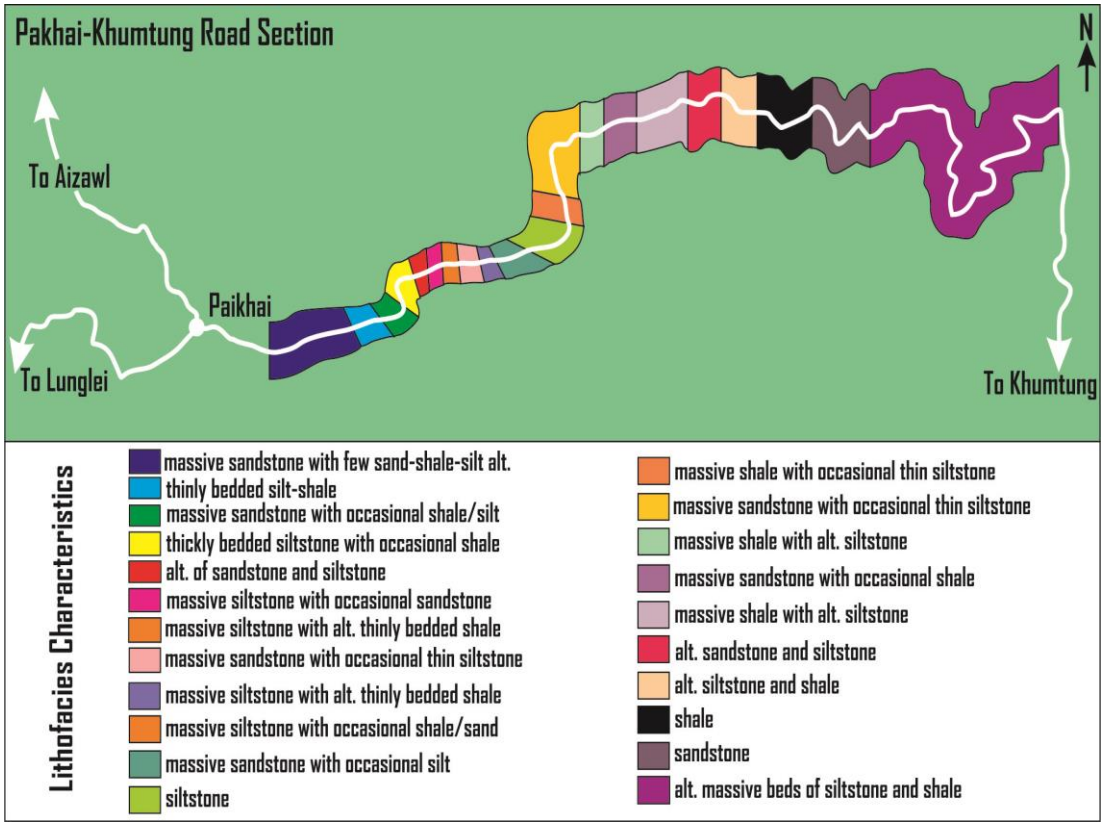

Figure.3.11. Lithofacies map of Paikhai road section, Aizawl, Mizoram.

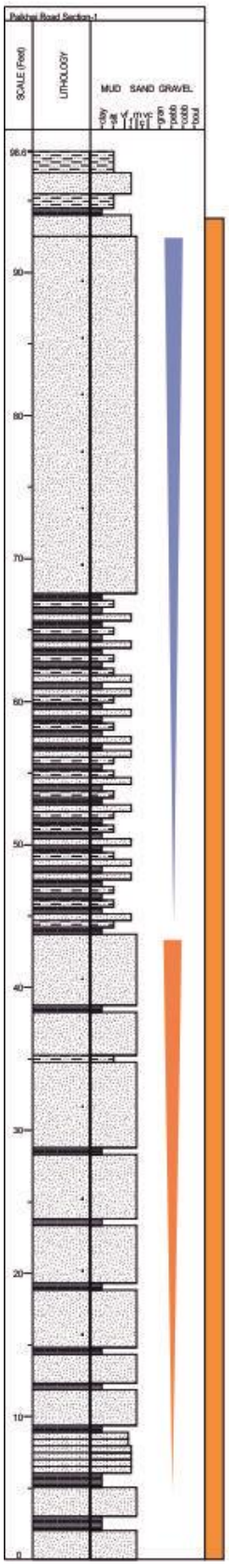

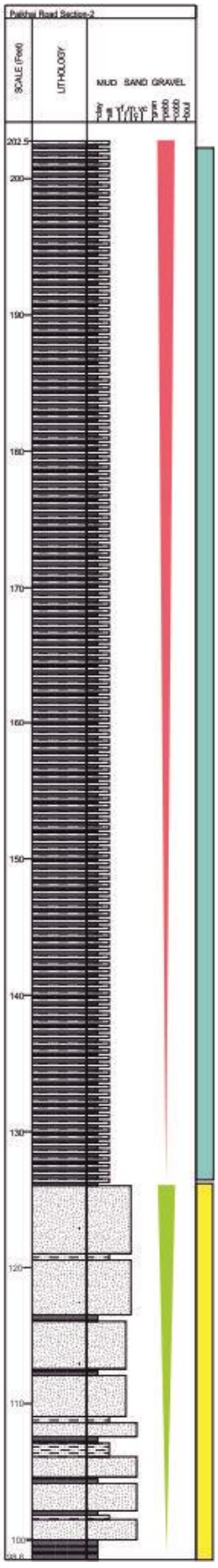

a

INDEX

LST

TST

FSST

HST

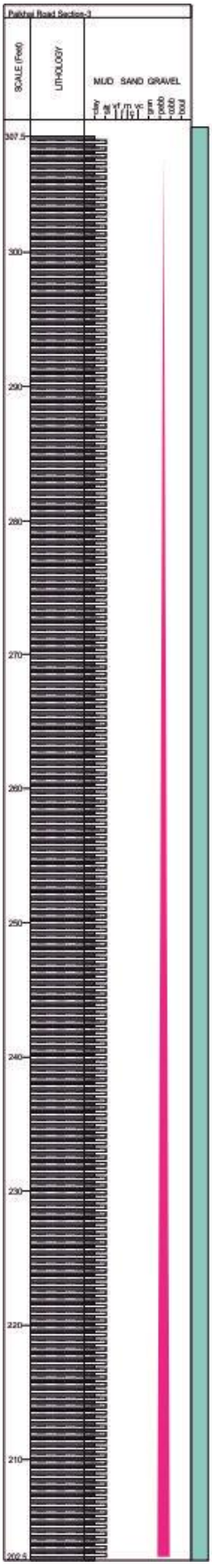

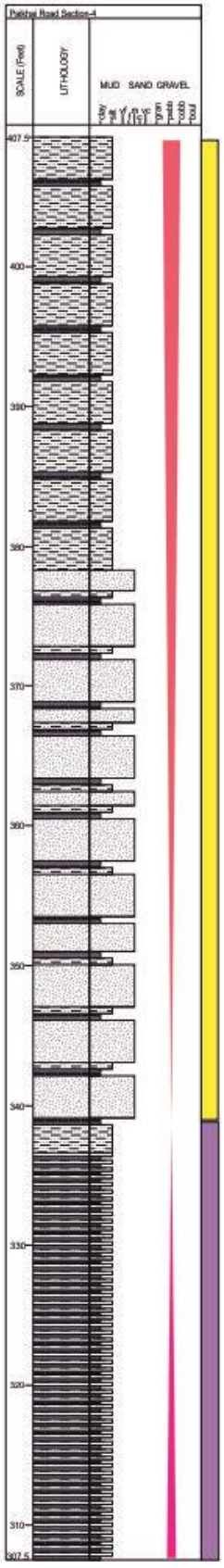

b

INDEX

LST

TST

FSST

HST

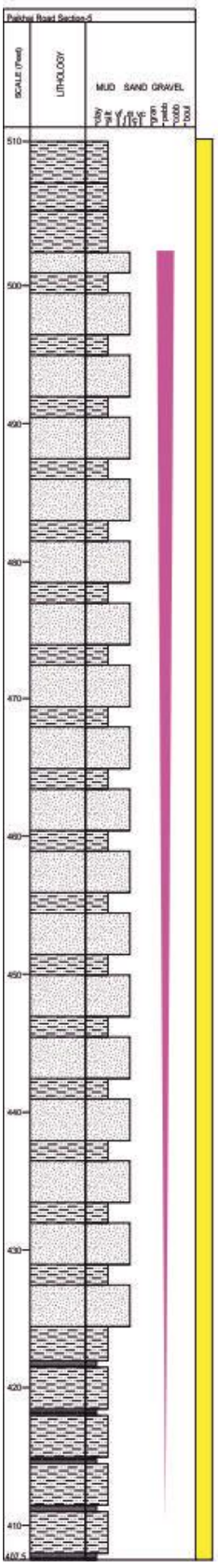

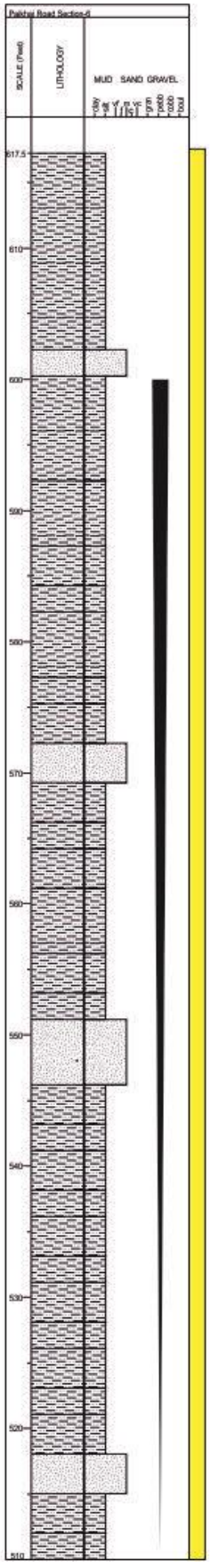

C

INDEX

LST

TST

FSST

HST

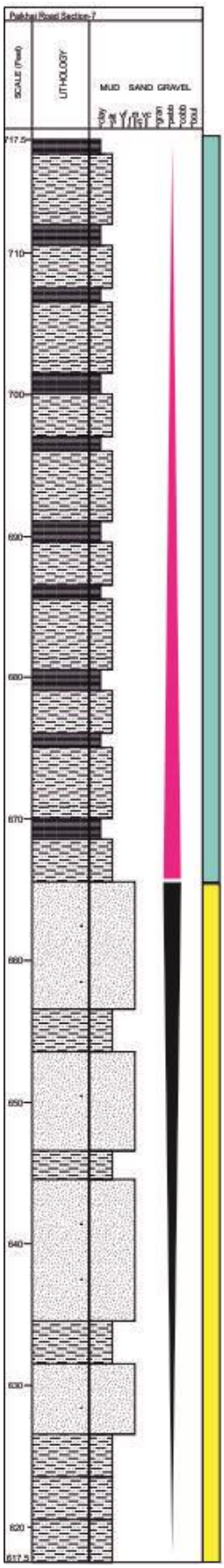

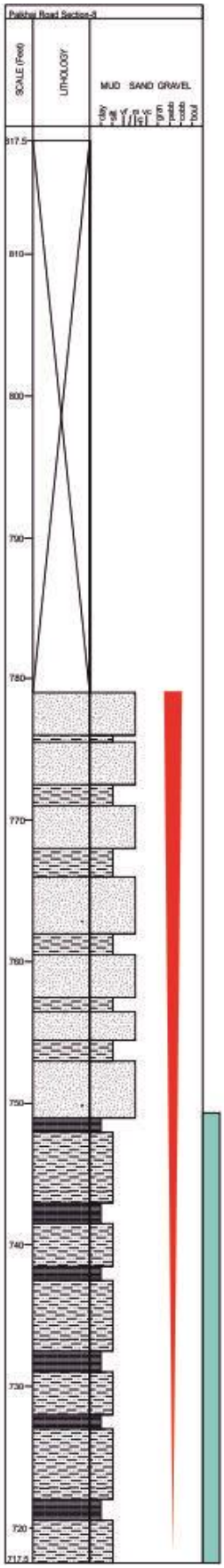

d

INDEX

LST

TST

FSST

HST

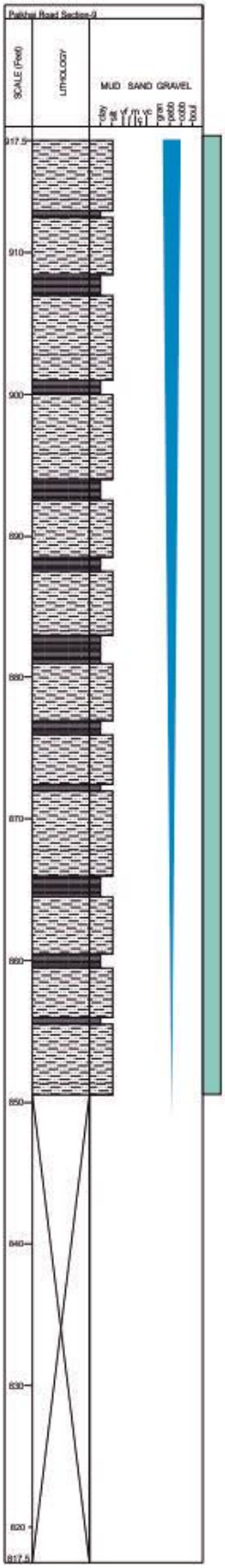

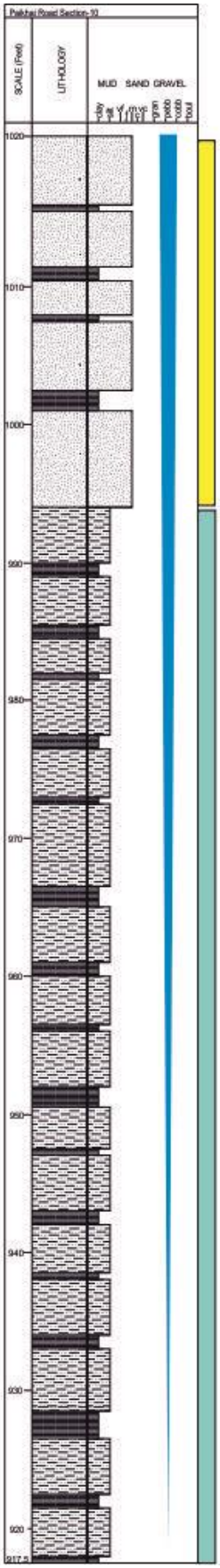

e

INDEX

LST

TST

FSST

HST

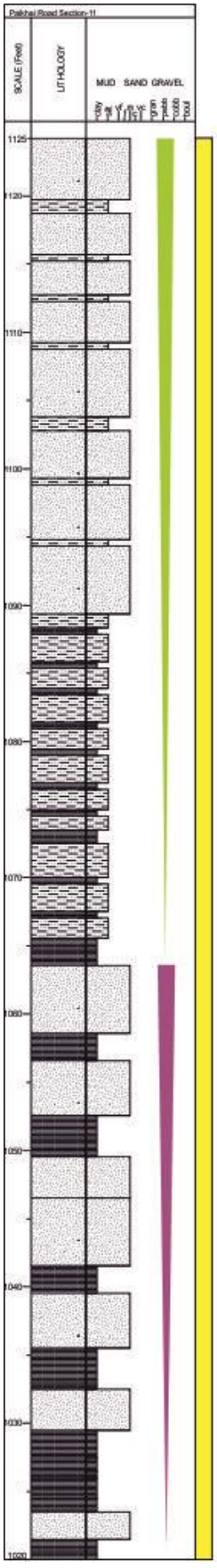

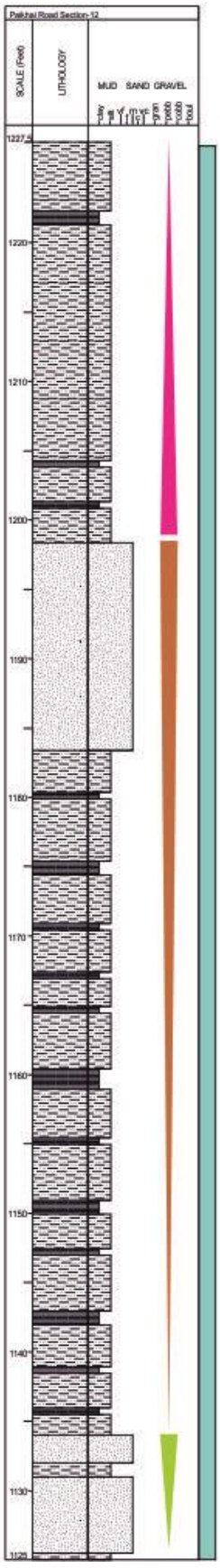

f

INDEX

LST

TST

FSST

HST

g

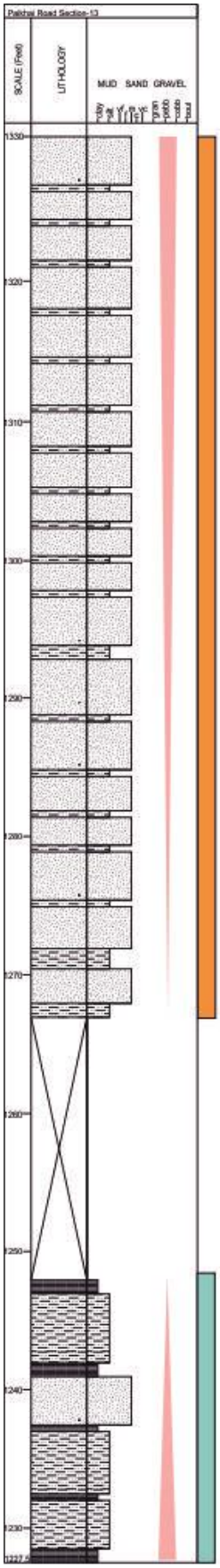

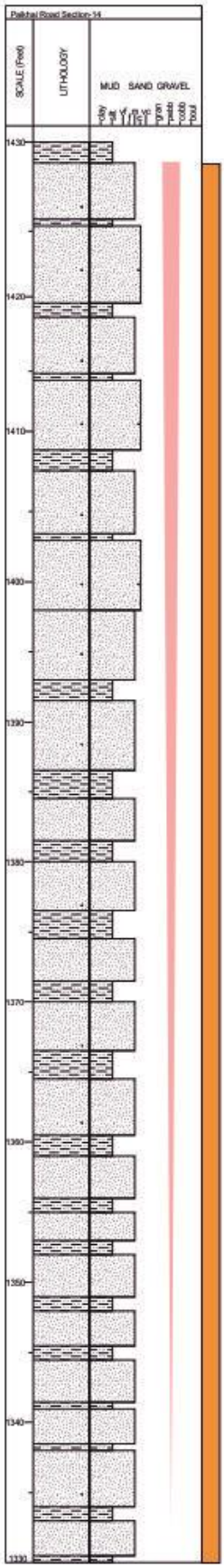

INDEX

LST

TST

FSST

HST

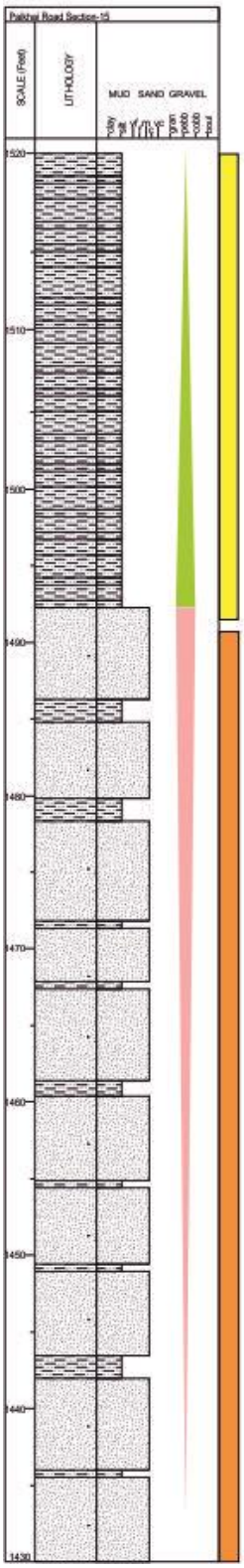

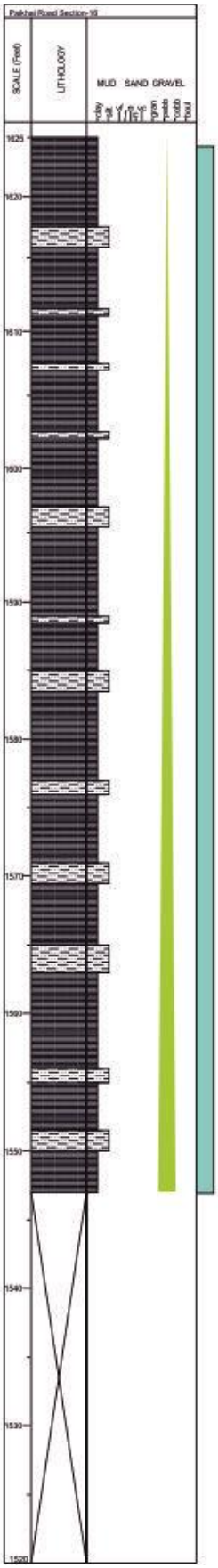

h

INDEX

LST

TST

FSST

HST


Pakhal Road Section-17
SCALE (Feet)
LITHOLOGY
MUD SAND GRAVEL
clay
1735
1730
1720
1710
1700
1690
1680
1670
1660
1650
1640
1630
1625
Pakhal Road Section-18
SCALE (Feet)
LITHOLOGY
MUD SAND GRAVEL
clay
1840
1830
1820
1810
1800
1790
1780
1770
1760
1750
1740
1735
INDEX
LST
TST
FSST
HST

j

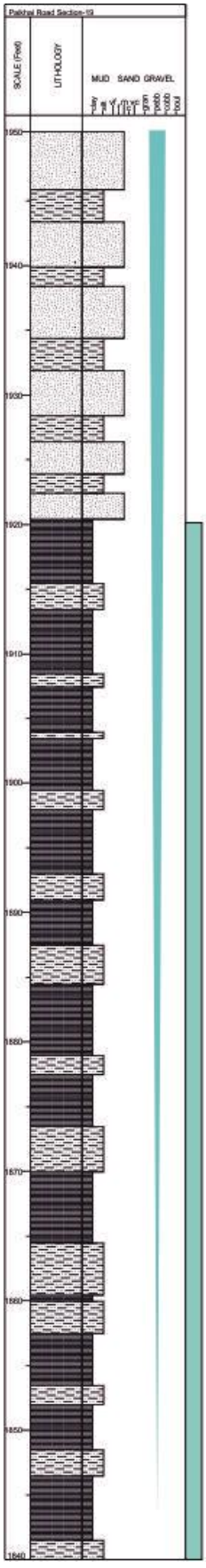

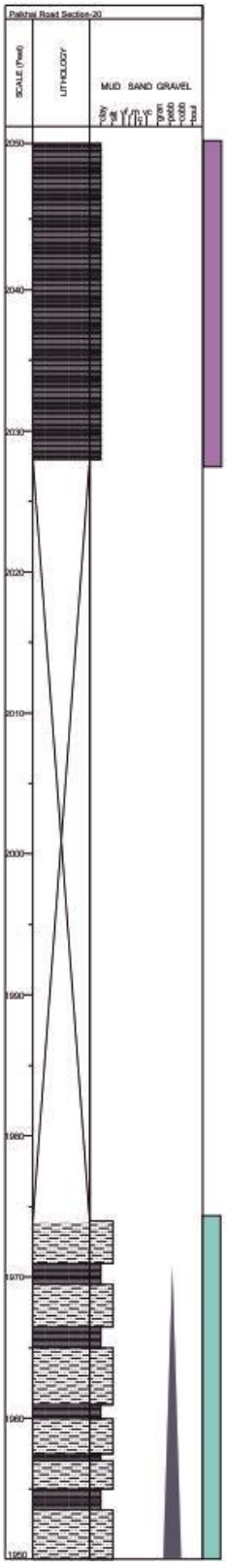

INDEX

LST
TST
FSST
HST

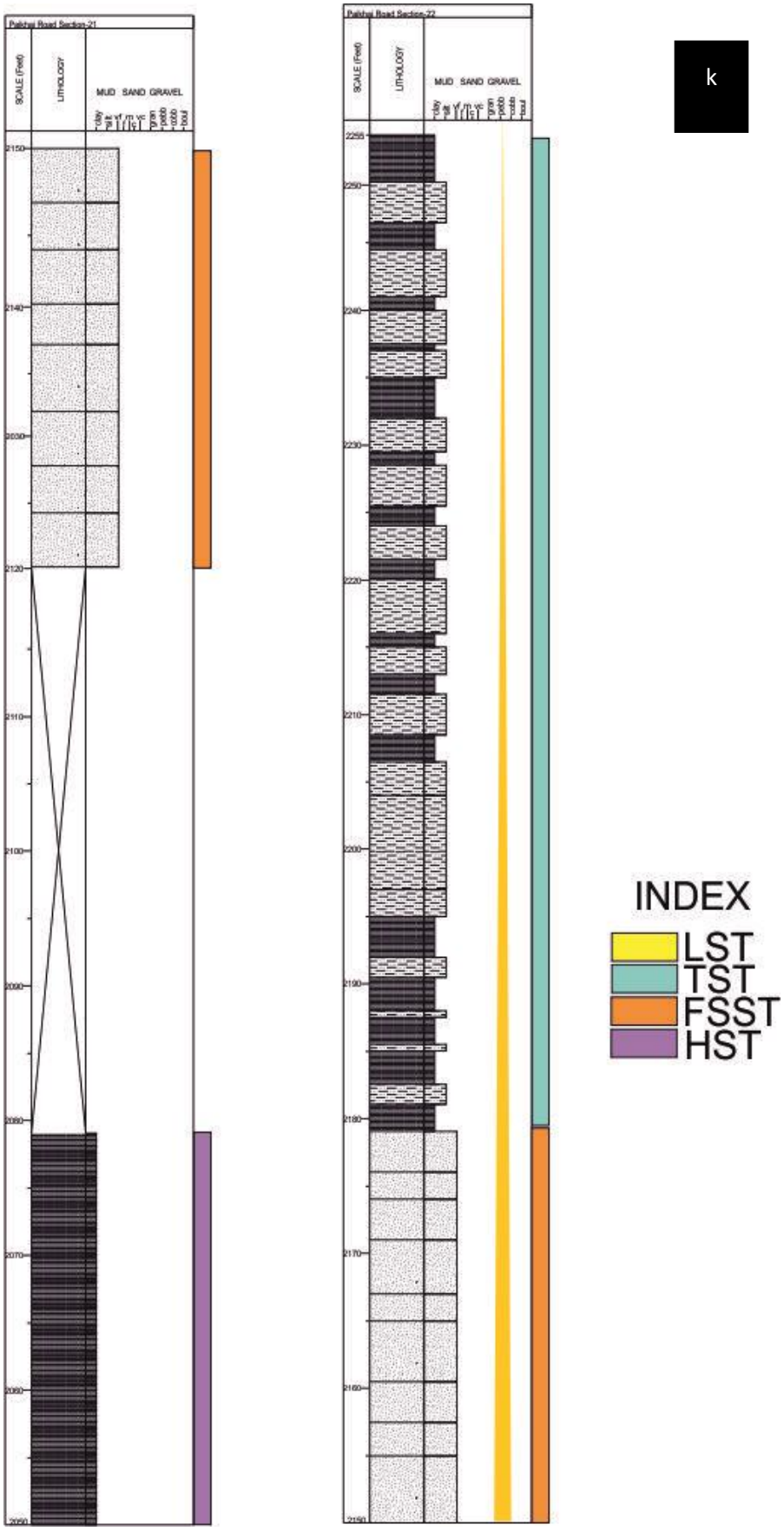
Pakhaj Road Section-21
SCALE (Feet)
LITHOLOGY
MUD SAND GRAVEL
clay
silt
vf
f
m
c
vc
gran
pebb
cobb
boul
2150
2140
2130
2120
2110
2100
2090
2080
2070
2060
2050
Pakhaj Road Section-22
SCALE (Feet)
LITHOLOGY
MUD SAND GRAVEL
2255
2250
2240
2230
2220
2210
2200
2190
2180
2170
2160
2150
k
INDEX
LST
TST
FSST
HST

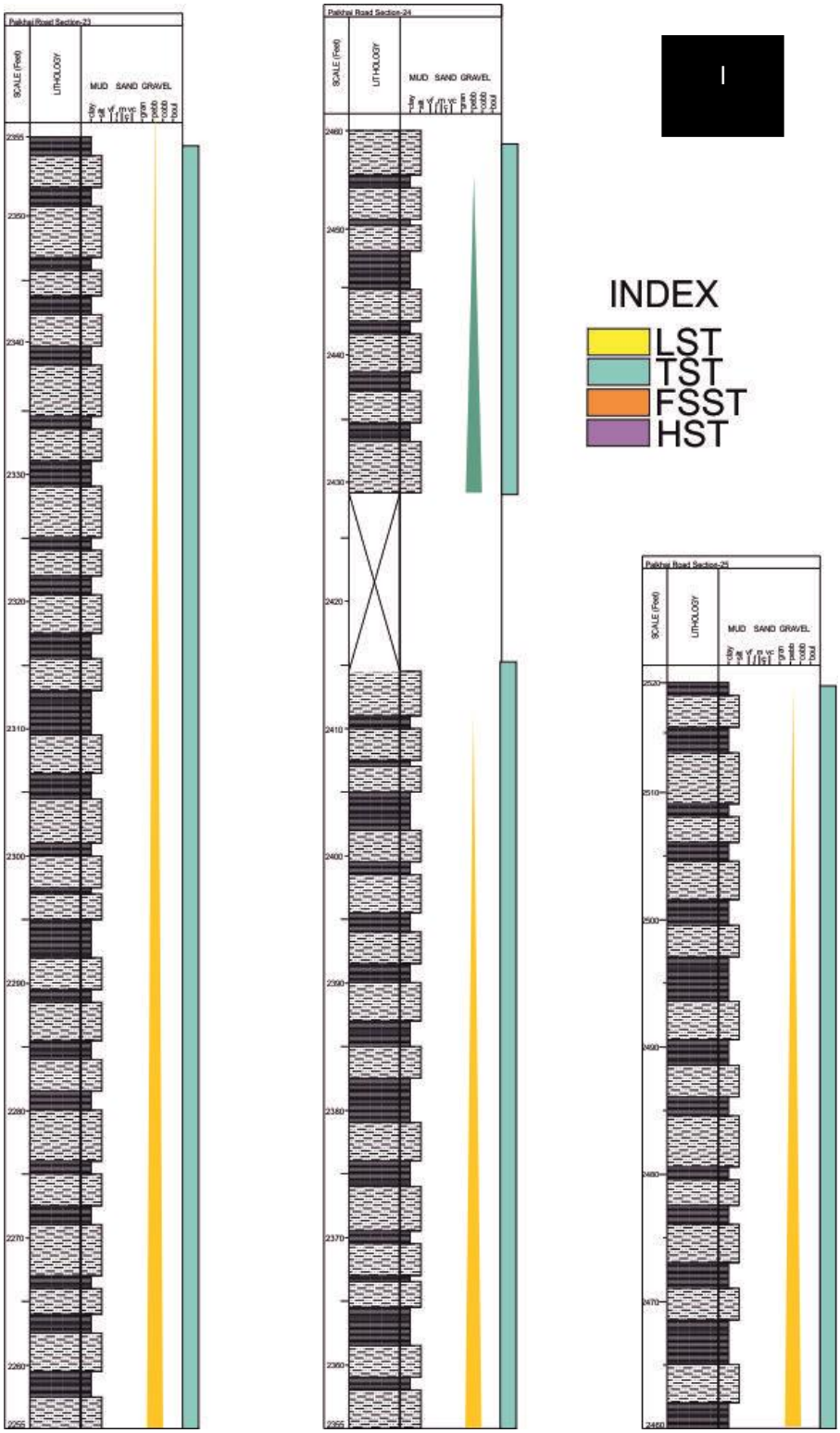

Figure 3.12. (a), (b) (c), (d), (e) (f) (g) (h), (i) (j), (k), and (l)the detailed lithocolumn of Paikhai road section (PK) showing the distribution of lithologies, and sequence stratigraphic framework.

3.6 Sequence Stratigraphic Analysis

Sequence stratigraphy is based on the analysis of stratigraphic surfaces, referred to as unit boundaries, which indicate alterations in depositional trends. These surfaces are employed for correlation purposes (Embry et al. 2007). In sequence stratigraphic analysis, the key surfaces often used include (i) Sub-aerial unconformity or correlative conformity (ii) Ravinement surfaces (RS) (iii)Transgressive ravinement surface (iv)Transgressive surface (v) Transgressive surface of erosion (vi) Maximum regressive surface (MRS) (vii) Regressive surface of marine erosion (RSME) (viii) Maximum flooding surface (MFS) (Sloss et al, 1949; Shanmugan, 1988; Catuneanu, 2006; Suter et al., 1987; Galloway and Sylvia, 2002; Blum and Aslan, 2006; Hunt and Tucker, 1992; Mitchum et al., 1977; Stamp, 1921; Bruun, 1962; Swift et al., 1972; Swift, 1975; Dalrymple et al. 1994; Catuneanu, 2006; Galloway, 2001; Forgotson, 1957; Frazier, 1974; Vail et al. 1977; Plint, 1988; Embry, 2002; Galloway and Sylvia, 2002; Bradshaw and Nelson, 2004; Cantalamessa and Celma, 2004; Catuneanu, 2006; Embry, 2001; Cross and Lessenger, 1997; Schlager, 2005; Catuneanu et al, 1998; Catuneanu, 2006; Posamentier and Allen, 1999; Van Wagoner et al, 1988).

According to the Exxon model, (Fig. 3.13), a sequence can be divided into four parts such as system tracts: falling stage system tract (FSST), low stand system tract (LST), transgressive system tract (TST), and high stand system tract (HST). These system tracts are separated by sequence stratigraphic surfaces such as flooding surfaces (FSs), maximum flooding surfaces (MFSs), and regressive surfaces (RSs). Terms like progradation (during FSST), retrogradation (during TST), and aggradations (during LSST) are commonly used to describe the shifting nature of facies along a continental margin. The transgressive surface (TS) or flooding surface (FS) marks the transition from a regressive falling stage system tract (FSST) trend below to a transgressive systems tract (TST), and it is bordered by the maximum flooding surface (MFS) above. The maximum flooding surface (MFS) marks the shift from a transgressive TST trend below to a slightly regressive high stand system tract (HST), which is capped by the sequence boundary (SB) of FSST. This model was developed by Van Wagoner et al. (1988) and further refined by Posamentier and Vail (1988).

To conduct a sequence stratigraphic analysis of a sedimentary formation, it's essential to examine various sections both across and along the strike length. This involves carefully measurements of each section, noting down lithological properties, sedimentary structures, textures, and flow regimes of individual facies. Subsequently, facies analysis within each section and correlating their strike length among different sections are carried out to establish the wider depositional system and provide a comprehensive sequence stratigraphic framework for the individual formation. Therefore, the primary tools for sequence stratigraphic analysis involve studying the stacking patterns of strata, identifying key bounding surfaces, and reconstructing facies. Unlike other branches of stratigraphy that rely heavily on empirical data, sequence stratigraphy is more interpretation-based. Various sequence stratigraphic models exist, but the most widely used is the EXXON model (Jervey, 1988), which has been modified by several researchers over time (Van Wagoner et al., 1988; Embry, 1993; Hunt 84 and Tucker, 1992; Helland-Hansen and Gjelberg, 1994; Posamentier and Allen, 1999).

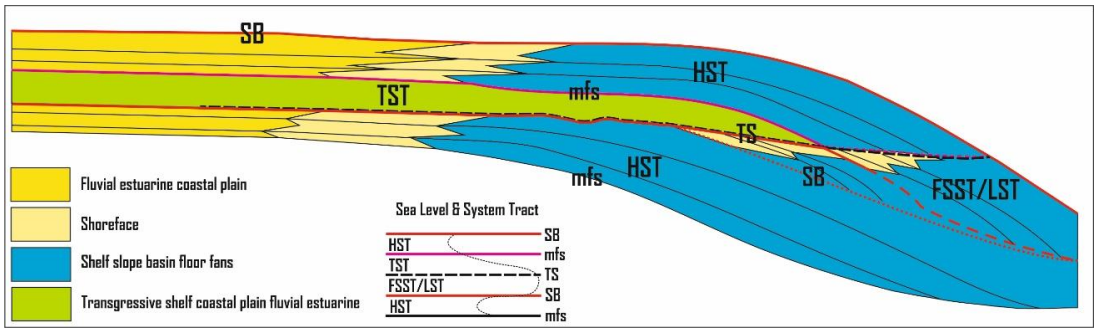

Figure 3.13. Sequence stratigraphic EXXON model (modified after Posamentier and Allen, 1999).

A traditional genetic sequence consists of three main parts: the Lowstand Systems Tract (LST), Transgressive Systems Tract (TST), and Highstand Systems Tract (HST). Within this sequence, there are two significant surfaces the Maximum Flooding Surface (MFS) and the Sequence Boundary (SB). The LST is comprised of deposits that accumulate after the beginning of a rise in relative sea level, during a normal regression phase. It forms a wedge shape and is defined at the bottom by the subaerial unconformity and/or the correlative conformity (Catuneanu, 2011, 2017).

Transgressive Systems Tract (TST) consists of deposits that gather from the start of transgression until the point of maximum transgression along the coast, just before the renewed regression of the Highstand Systems Tract (HST). The top of the TST is marked by the Maximum Flooding Surface (MFS) and displays features like backstepping, onlapping, and retro-gradational clinoforms, with a tendency to thicken towards the landward side in siliciclastic systems (Catuneanu, 2011). The HighStand Systems Tract (HST) comprises progradational deposits formed when sediment accumulates at a rate faster than the increase in accommodation during the later phases of rising relative sea levels (Catuneanu, 2011). This system's tract is topped by the subaerial unconformity and its correlative conformity, following the definition by Posamentier and Allen (1999), and exhibits prograding and aggrading clinoforms.

In this present study, an attempt has been made to establish the sequence stratigraphic framework by analyzing the lithostratigraphic column from field observations and the presence of sedimentary structures.

An attempt has also been made to conceptualize a depositional regime for Bhuban sediments (Surma Group) of the study area, (Fig. 3.14) based on lithology, bed geometry, and sedimentary structures. The dominant fluvio–tidal environment has also been envisaged with also minor contribution to the Shallow marine Environment.

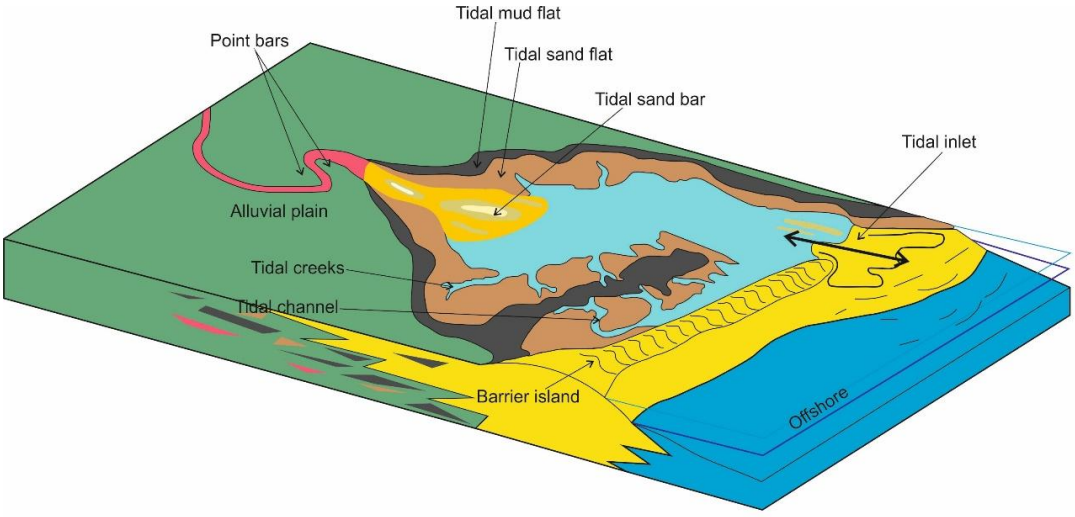

Figure 3.14. The conceptual depositional model of the Bhuban sediments in the study area.

CHAPTER- 4
SANDSTONE PETROGRAPHY

4.1 Introduction

The sedimentary rocks are essential sources of information about past orogenic conditions, and their compositions can provide insights into the evolution of provenance and tectonic settings (Johnsson, 1993). The petrographic study can reveal the nature of the source regions, the tectonic setting of the sedimentary basin, and the paleoclimate conditions of particular regions. A petrographical study is necessary to know the characteristics of sedimentary rock such as the degree of compaction, cementation, and effect of pressure solution (Blatt, 1967; Pettijohn, 1975; Quasim et al. 2021). It also helps in understanding the degree and type of tectonism, which controls or indicates an association of rocks in the source area. The analysis petrography, using various ternary plots (QFL, Q_mFL_t, etc.,), has been employed in describing the tectonic settings and helps to understand and interpret plate interactions in the geologic past (Ingersoll, 1978; Dickinson and Suczek, 1979; Dickinson et al. 1983).

The petrographic observations under the microscopic study reveal that the framework grains such as quartz, K-feldspar, plagioclase, and rock fragments constitute the essential mineral compositions of the rocks. Additionally, framework grains of a few other minerals, including biotite, muscovite, zircon, rutile, and opaque minerals, occur as accessory minerals. A comprehensive description of the petrography analysis of the Surma group of Bhuban sandstones in the study area is discussed in the following paragraphs. The Bhuban sandstone of the study area has been classified into two formations Upper Bhuban Formation (UBF) and Middle Bhuban Formation (MBF).

4.2 Petrographic Characterization and classification of Bhuban sandstones

The present work is selected for the 20 representative samples in the four exposed sections along the roadside and the think sections are petrographically examined. The rock-thin section is examined using a Leica DM750P Petrological microscope and the image analyzer. The petrographic investigation indicates that the Bhuban sandstones are medium to fine grained along with moderate to poorly sorted

texture. A detailed account and description of the observed minerals during the petrographic analysis of the Bhuban sandstones is discussed below.

4.2.1 Quartz

In the Bhuban Sandstone, quartz is the most dominant detrital constituent among all the mineral grains of the study area, both the Upper Bhuban Formation and Middle Bhuban Formation constituting an average of 83.59% of the total framework composition. The grains are mostly sub-angular to sub-round in shape. In the upper Bhuban formation, monocrystalline quartz forms about 48.38% whereas polycrystalline quartz forms an average of 10.04% of the mineralogical composition. The monocrystalline quartz grains comprise both undulatory quartz as well as non-undulatory Quartz varieties. Overgrowths of quartz are also observed in some of the grains (Fig. 4.7F). Some polycrystalline quartz grains exhibit internal constituents that are slightly sutured. Again, in the Middle Bhuban Formation, monocrystalline quartz forms about 41.61% whereas polycrystalline quartz forms an average of 10.78% of the mineralogical composition. The detrital quartz grains in the studied samples are characterized by point contacts, concavo-convex contacts as well as straight contacts (Fig. 4.7E). Fractured monocrystalline quartz is also observed (Fig. 4.8E). It is also observed that monocrystalline non-undulose quartz occurs in greater amounts than the undulose variety. Overgrowths of silica are also observed in some of the quartz grains in the MBF.

4.2.2 Feldspars

The feldspars constitute an average of 7.66% in UBF and 8.35% in MBF in the total framework composition. In the studied sandstones two varieties of feldspars are present. Plagioclase feldspar and microcline grains are recognized through their distinctive lamellar twinning and cross-hatch twining, with average abundances of 4.29% and 1.01%, respectively, in both formations. Feldspar grains were observed as sub-angular and sub-rounded shapes, appearing colorless, however, some grains are showing cloudy, or dusty due to alteration (Fig. 4.7B).

4.2.3 Lithic fragments

The lithic fragments are also significant components of the framework in the Bhuban Sandstone, mainly comprising metamorphic and sedimentary lithic fragments, with a few amounts of igneous lithic fragments also present. These fragments

constitute an average of about 7.86% in UBF and 9.38% in MBF of the total framework composition of the sandstones. The lithic fragments are mostly variable in size and shape with prominent grain boundaries such as medium to coarse-grained and angular to sub-round in shape. In metamorphic lithic fragments are mainly schist and gneiss present in the studied Sandstones. Conversely, Sedimentary lithic fragment includes shale and chert (Fig. 4.7E and 4.8B).

4.2.4 Mica

The detrital grains of micas including muscovite and biotite (Fig. 4.7A) are consistently present in all studied sandstones with an average of 5.32% in UBF and 4.5% in MBF of the total framework composition. Both types can be easily identified by their distinctive characteristics, such as their flaky nature and parallel extinction. In general, muscovite is chemically more stable, attributed to the greater resistance of muscovite to weathering resulting in its higher abundance compared to biotite in all samples. The muscovite exhibits deformation in the form of kink bands, observed in most of the samples. This bending is a result of mechanical compaction during diagenetic evolution.

4.2.5 Cement

The cement is the common binding material for the framework grains. There are mainly four types of cement have been observed in both the formation (UBF and MBF) of examined sandstones calcite, siliceous, ferruginous, and argillaceous with an average of (3.34) %. The silica cement is in the form of overgrowths on the surface of detrital grains whereas the calcite cement tends to fill up the pore spaces within the detrital sandstone grains. The ferruginous cement is also present in some of the samples (Fig. 4.7C). Apart from the framework grains few accessory minerals are also present in the examined sandstone samples both in the form of opaque and non-opaque varieties. Non-opaque minerals include zircon, andalusite, hornblendes, garnet, sphene, tourmaline, mica, and epidote and are generally sub-angular to sub-rounded in shape. Opaque minerals include iron oxides and their alteration products.

4.3 Classification of Sandstones

As per analysis of the modal counting data using the point counting method (as shown in Tables 4.1,4.2, and 4.3) followed by the Gazzi-Dickinson method (Dickinson 1970; Ingersoll et al. 1984) the Upper Bhuban Formation and Middle Bhuban Formation for sandstones are classified as sub-litharenite and arkosic-wacke varieties while plotted in the Q-F-L ternary plot (Fig. 4.1 and Fig. 4.2) proposed by Pettijohn et al. (1972) and Folk (1974).

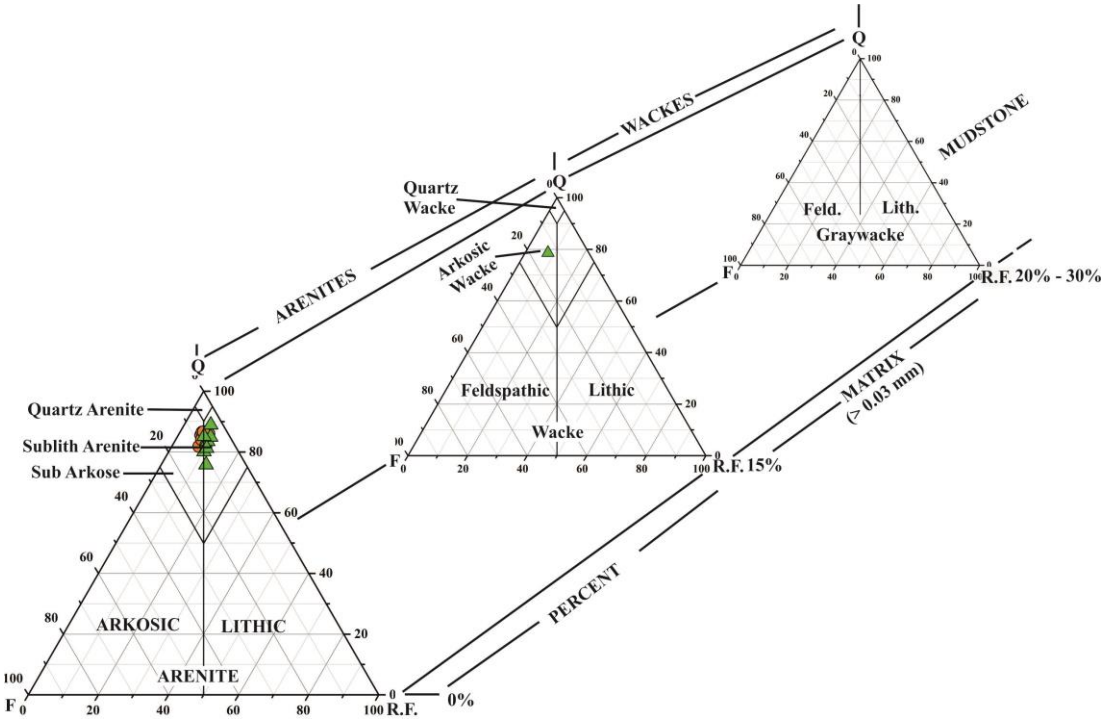

Figure 4.1. Petrographic classification of sandstones in the study area (After Pettijohn, et al. 1972). The green triangle indicates the Upper Bhuban sandstone samples and the orange circle shows the Middle Bhuban sandstone samples.

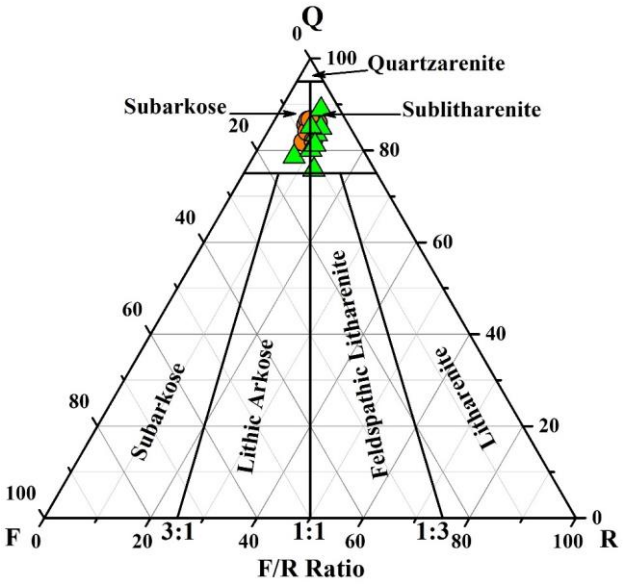

Figure 4.2. Petrographic classification of sandstones in the study area (After Folk, et al. 1980). The green triangles indicate the Upper Bhuban sandstone samples and the orange circles indicate the Middle Bhuban sandstone samples.

4.4 Source rock composition of Bhuban sandstones

The quartz types, such as monocrystalline and polycrystalline quartz, can be used to determine the provenance of sandstones. The recalculated modal counting data of the studied samples reveals that among detrital quartz varieties, monocrystalline non-undulatory quartz has the highest percentage, with an average of 25.29% followed by monocrystalline undulatory quartz, with an average percentage of 20.39%. Conversely, an average percentage of 5.77% of polycrystalline quartz >3, while polycrystalline quartz 2-3 units with an average of 4.57% for both Upper and Middle Bhuban Formations. Consequently, the predominance of non-undulatory monocrystalline quartz, accompanied by a relatively smaller amount of polycrystalline quartz in the Bhuban sandstone of the examined area indicates that the sediments are derived from igneous and metamorphic source (Basu et al. 1975; Basu, 1985; Tortosa et al. 1991; Javed et al. 2023). Basu et al. (1975) introduced the diamond plot to distinguish different rock sources, including plutonic, low, middle, and upper-rank metamorphic types, to determine the provenance. While the recalculated values of quartz varieties from the Upper and Middle Bhuban sandstones are depicted in the diamond diagram. It is observed that the majority of the sandstones fall within the category of middle and upper-rank metamorphic rocks with a minor contribution from

Table 4.1. The modal count for the Upper Bhuban sandstone samples through the petrographic study of thin sections with the help of Gazzi-Dickinson's point-counting technique for the selected samples.

Sample No.	Quartz				Feldspar		Rock Fragments			Cement				Matrix	Mica	Chert	Opaque	Sum (%)
	Q_{Mu}	Q_{Mnu}	$Q_{P\ 2-3}$	$Q_{P>3}$	F_K	$P_{Ca/Na}$	$RF_{Ig.}$	$RF_{Sed.}$	$RF_{Met.}$	C_{Cal}	C_{Fer}	Carg	C_{Sil}					
AR#4	18.80	31.58	2.82	1.32	0.75	4.32	0.00	1.88	2.26	11.09	1.13	0.00	0.94	14.10	5.83	2.26	0.94	100
AR#5	25.62	17.97	10.52	2.87	0.57	4.59	0.00	2.49	3.25	0.76	0.00	0.00	4.78	14.91	6.88	3.44	1.34	100
AR#7	19.02	34.03	4.01	6.11	1.05	4.71	0.00	1.92	4.01	5.58	0.00	0.00	1.22	8.20	4.71	4.01	1.40	100
PK#7A	26.00	11.09	3.64	9.27	0.91	5.45	0.91	2.55	1.27	17.27	0.00	0.00	5.64	6.55	5.27	1.82	2.36	100
PK#7C	30.14	17.42	4.50	10.57	0.59	4.89	0.39	0.00	5.09	6.07	0.00	0.98	0.00	5.68	6.85	4.70	2.15	100
PK#8A	25.05	22.27	3.78	6.56	0.80	4.57	0.00	2.39	3.78	8.95	0.80	0.00	2.39	8.95	4.77	1.99	2.98	100
SS#1A	19.12	35.66	2.99	4.78	1.00	4.18	0.60	1.59	2.39	7.57	0.40	0.00	1.79	7.97	5.58	3.19	1.20	100
SS#2A	23.02	25.99	6.75	4.96	0.00	4.96	0.00	3.37	2.98	8.53	0.60	0.00	1.39	6.55	5.75	3.57	1.59	100
SS#3A	15.06	36.49	3.28	5.60	0.58	3.28	0.00	2.70	3.28	6.56	0.00	0.58	2.12	9.65	5.21	4.25	1.35	100
ZT#6A	16.70	35.76	8.25	1.57	1.38	4.91	0.59	3.34	1.57	5.70	0.00	0.00	0.00	8.25	5.70	5.30	0.98	100
ZT#6B	13.56	41.41	3.44	2.53	1.63	3.07	0.00	2.17	2.53	0.00	13.92	0.00	6.87	1.99	4.16	2.17	0.54	100
ZT#7	22.69	16.15	7.50	2.88	0.96	4.04	0.00	3.65	2.12	3.27	18.08	0.00	7.12	4.42	3.08	3.65	0.38	100

Note. Q_{Mu}: monocrystalline undulatory quartz, Q_{Mnu}: monocrystalline non-undulatory quartz, Q_{P2-3}: polycrystalline quartz with 2-3 grains per quartz, $Q_{P>3}$: polycrystalline quartz with >3 grains per quartz, $P_{Ca/Na}$: plagioclase, F_K: potash feldspar, R_{FIg}: igneous rock fragment, RF_{Sed}: sedimentary rock fragment, RF_{Met}: metamorphic rock fragment, C_{Sil}: siliceous cement, $C_{arg:}$ argillaceous cement, C_{Fer}: ferruginous cement, C_{Cal}: carbonaceous/calcite cement, AR= Aizawl- Reiek road section, PK= Paikhai road section, SS= Sakawrtuichhuan- Sairang road Section (SS), ZT= Zemabawk-Tuirial road Section.

Table 4.2. The modal count for the Middle Bhuban sandstone samples through the petrographic study of thin sections with the help of Gazzi-Dickinson's point-counting technique for the selected samples

Sample No.	Quartz				Feldspar		Rock Fragments			Cement				Matrix	Mica	Chert	Opaque	Sum
	Q_{Mu}	Q_{Mnu}	$Q_{P\ 2-3}$	$Q_{P>3}$	F_K	$P_{Ca/Na}$	$RF_{Ig.}$	$RF_{Sed.}$	$RF_{Met.}$	C_{Cal}	C_{Fer}	C_{arg}	C_{Sil}					
AR#1	26.71	12.84	7.02	1.88	0.00	4.11	0.00	2.23	3.25	1.71	19.52	0.00	0.00	9.93	4.62	5.48	0.68	100
PK#1B	9.77	24.62	2.44	13.16	0.94	6.58	0.38	2.82	5.26	8.08	0.00	0.00	0.94	12.78	5.08	4.32	2.82	100
PK#1C	14.39	26.89	2.08	8.90	3.79	5.30	0.00	0.57	4.55	3.41	0.00	0.00	0.95	17.99	3.79	3.41	3.98	100
PK#2	28.07	12.98	2.63	10.70	3.16	3.51	0.00	3.16	3.68	8.60	0.00	0.00	6.49	10.53	2.11	3.16	1.23	100
PK#3	14.67	31.70	3.62	11.05	0.54	3.44	0.00	3.44	3.44	7.97	0.54	0.00	0.72	9.78	4.53	3.44	1.09	100
PK#4	25.85	15.86	6.24	6.06	0.53	4.10	0.00	1.07	3.74	20.14	0.00	0.00	0.00	7.66	3.92	2.50	2.32	100
ZT#1	21.81	27.70	3.54	2.16	0.00	2.16	0.00	2.55	2.16	6.68	1.18	0.00	1.96	14.73	5.50	6.48	1.38	100
ZT#2	11.66	27.34	2.29	2.49	0.96	3.63	0.00	2.29	3.25	25.24	0.00	0.00	0.96	12.05	2.87	3.25	1.72	100

Note. Q_{Mu}: monocrystalline undulatory quartz, Q_{Mnu}: monocrystalline non-undulatory quartz, $Q_{P2-3:}$ polycrystalline quartz with 2-3 grains per quartz, $Q_{P>3:}$ polycrystalline quartz with >3 grains per quartz, $P_{Ca/Na}$: plagioclase, $F_{K:}$ potash feldspar, RF_{Ig}: igneous rock fragment, RF_{Sed}: sedimentary rock fragment, RF_{Met}: metamorphic rock fragment, C_{Sil}: siliceous cement, $C_{arg:}$ argillaceous cement, C_{Fer}: ferruginous cement, C_{Cal}: carbonaceous/calcite cement, AR= Aizawl- Reiek road section, PK= Paikhai road section, SS= Sakawrtuichhuan- Sairang road Section (SS), ZT= Zemabawk-Tuirial road Section.

Table 4.3. Re-calculated model count from the petrographic data and the classification of Sandstone for Upper Bhuban Formation and Middle Bhuban Formation.

	Recalculated %				
	Sample No	Q	F	L	Name
Upper Bhuban Formation	AR#4	85.55	7.96	6.49	Sublitharenite
	AR#5	83.94	7.61	8.45	Sublitharenite
	AR#7	84.38	7.69	7.93	Sublitharenite
	PK#7A	81.85	10.42	7.74	Sublitharenite
	PK#7C	85.11	7.45	7.45	Sublitharenite
	PK#8A	83.33	7.76	8.91	Sublitharenite
	SS#1A	86.50	7.16	6.34	Sublitharenite
	SS#2A	84.30	6.89	8.82	Sublitharenite
	SS#3A	85.99	5.49	8.52	Sublitharenite
	ZT#6A	84.08	8.49	7.43	Sublitharenite
	ZT#6B	86.63	6.68	6.68	Sublitharenite
	ZT#7	82.05	8.33	9.62	Sublitharenite
Middle Bhuban Formation	AR#1	83.48	7.08	9.44	Sublitharenite
	PK#1B	75.78	11.40	12.82	Sublitharenite
	PK#1C	78.63	13.68	7.69	Arkosicwacke
	PK#2	80.10	9.82	10.08	Sublitharenite
	PK#3	84.89	5.54	9.57	Sublitharenite
	PK#4	85.11	7.30	7.58	Sublitharenite
	ZT#1	88.92	3.48	7.59	Sublitharenite
	ZT#2	81.21	8.51	10.28	Sublitharenite

a low-grade metamorphic source. Again, Tortosa et al. (1991) introduced a modified diamond diagram based on Basu et al. (1975), retaining the original parameters but adding new source rock fields. In this plot (Figure 4.3a & 4.3b), the majority of samples fall within the granitic field with a few in the metamorphic field. Both the plots suggest their origin from a granitic as well as Metamorphic terrain.

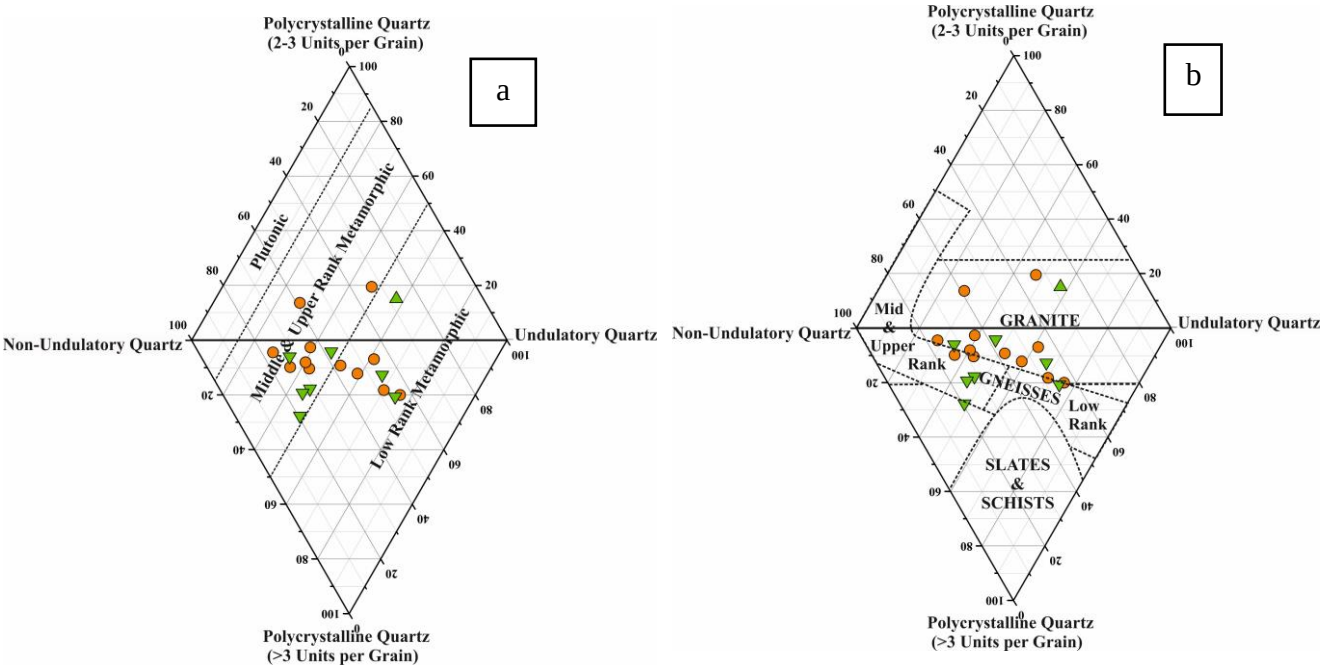

Figure 4.3. The Diamond diagram plots showing the provenance for the studied sandstone samples of (a) after Basu et al. (1975) and (b) after Tortosa et al. (1991) for the Bhuban Formation in the study area. (where green triangles indicate the Upper Bhuban sandstone samples and the orange circles indicate the Middle Bhuban sandstone samples).

4.5 Tectonic Settings

Dickinson and Suczek (1979) proposed Q-F-L and Qm-F-L_t tectonic discriminating diagrams to determine the tectonic setting of the source area for Bhuban sandstones. The recalculated modal counting data for the Upper Bhuban and Middle Bhuban Formation are as shown in Table 4.3, while plotting these data in Q-F-L and Q_m-F-L_t diagrams, following the approach proposed by Suczek's (1979) and Dickinson

et al. (1983), reveals that the Bhuban sedimentary rocks suggest a derivation from the recycled orogen field and in the quartzose recycled field (Fig. 4.4a & 4.4b). The sediments mainly come from the erosion of sedimentary and metamorphic rocks exposed by the uplift of fold-belts and thrust sheets in recycled orogens (Dickinson and Suczek, 1979; Dickinson, 1983). Conversely, the existence of non-undulatory monocrystalline quartz suggests that the sandstones likely originated from a plutonic source (Basu et al. 1975; Tortosa et al. 1991). Therefore, the detritus Bhuban sedimentary rocks strongly suggest a predominantly mixed source, including metamorphic, sedimentary, and igneous rocks, where the Q_m monocrystalline quartz, F the feldspar grains, and L_t, total polycrystalline lithic fragments, including quartz varieties.

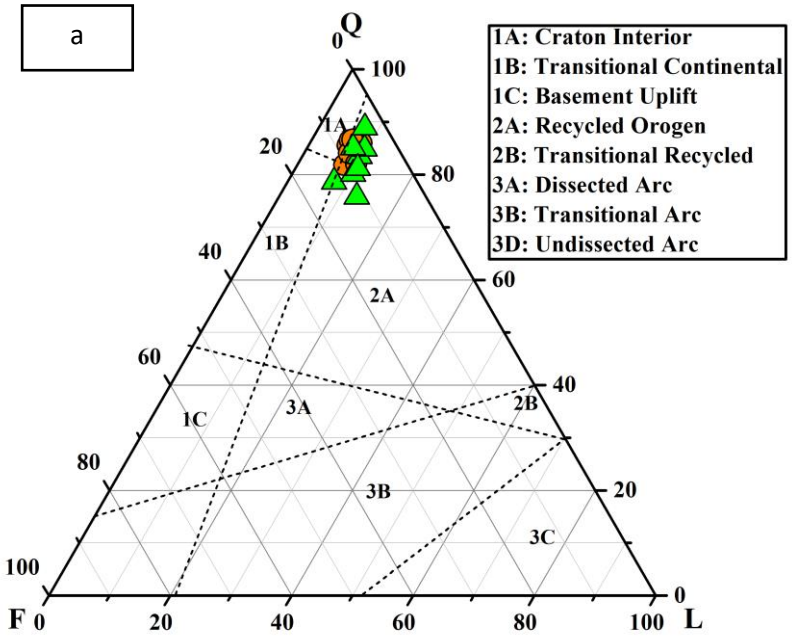

Figure 4.4a. The QFL plot (a) Bhuban Sandstones showing the dominantly recycled orogen provenance (After Dickinson and Suczek, 1979)

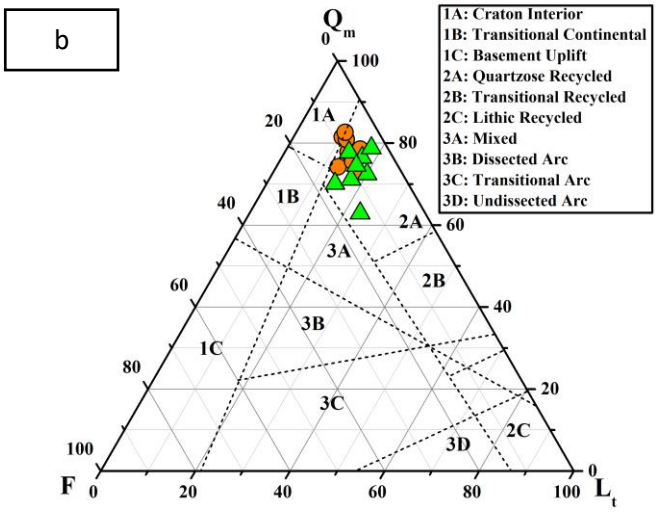

Figure 4.4b. The Q_mFL_t plot shows the quartzose recycled provenance for the Bhuban sandstones (Dickinson et al. 1983).

4.6 Paleoclimatic Conditions

Paleoclimatic conditions play a crucial role in determining the detrital framework of the Bhuban sandstone. Estimating the prevailing paleoclimatic conditions during sediment deposition is vital for understanding the mineral compositions of sandstones. While the compositions of source rocks and their associations are influenced by plate tectonics and structural evolution, the processes of weathering, production, and detrital mode composition are primarily determined by climate (Basu, 1985; Suttner and Dutta, 1986; Ahmad et al. 2019). Suttner et al. (1981) propose that a high abundance of quartz, along with a comparatively lower amount of feldspar and rock fragments, suggests sediment derivation from a metamorphic source in a humid climatic condition. Suttner et al. (1981) introduced the QFR ternary plot to interpret paleoclimatic conditions. The plot (Fig. 4.5.a) indicates a humid climatic condition with a metamorphic source during the sedimentation of the studied sandstones. Suttner and Dutta (1986) developed a bivariant log/log plot to identify paleoclimatic conditions. Employing this diagram, it can be inferred that the studied samples of the Upper and Middle Bhuban Formation were deposited under warm and humid tropical climatic conditions (Fig. 4.5b).

4.6.1 Weathering Index Diagram

Grantham and Velbel (1988) determined the paleoclimatic conditions using the weathering index, WI=C x R (WI-Weathering index, C-Climate, and R-Relief), and the bivariate plot of ln(Q/R) vs ln(Q/F) (Weltje, 1994). According to the plot, the Bhuban sandstone samples fall within the weathering indices at 2, indicating a moderate weathering relief under a tropical humid climate (Fig. 4.6).

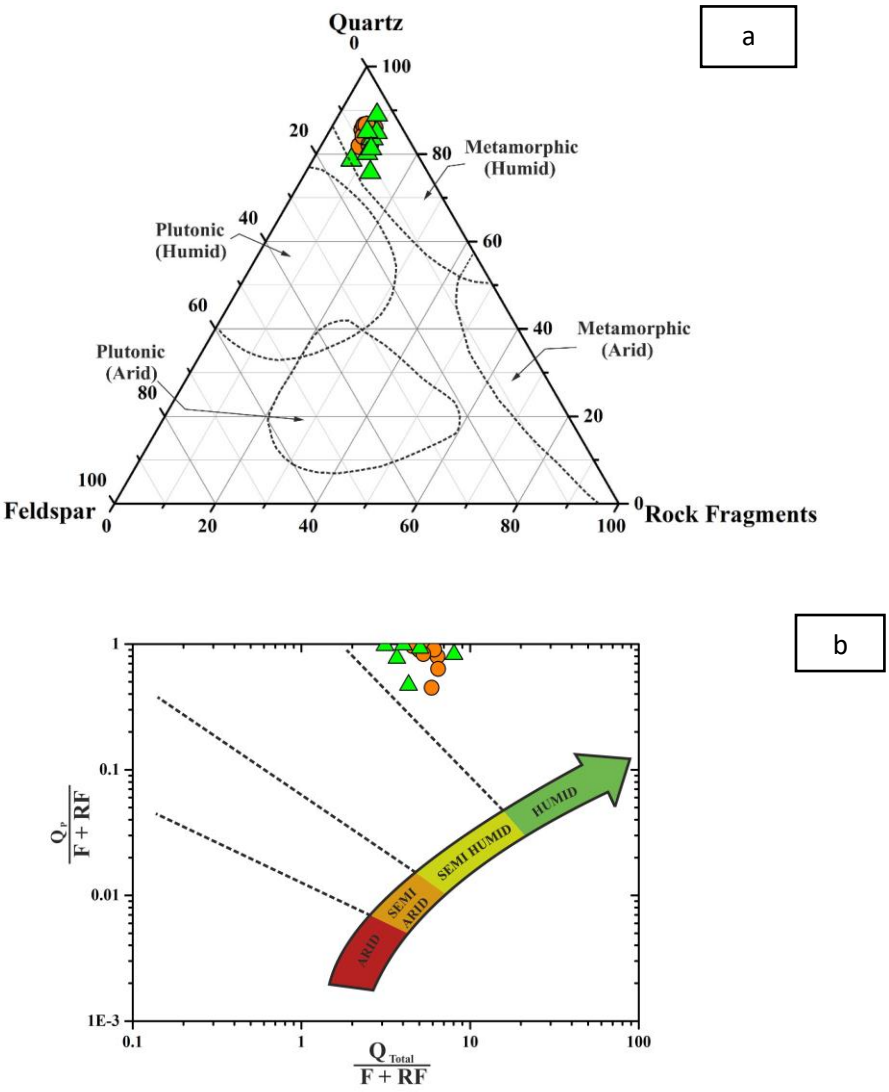

Figure 4.5. The triangular plot of QFR for (a) indicating the climatic conditions of the Bhuban Sandstones (after Suttner et al. 1981) and the bivariate log–log plot of Q_p/ (F + R) versus Qt/ (F + R) (b) showing the humid paleoclimatic conditions of the studied samples (after Suttner and Dutta 1986).

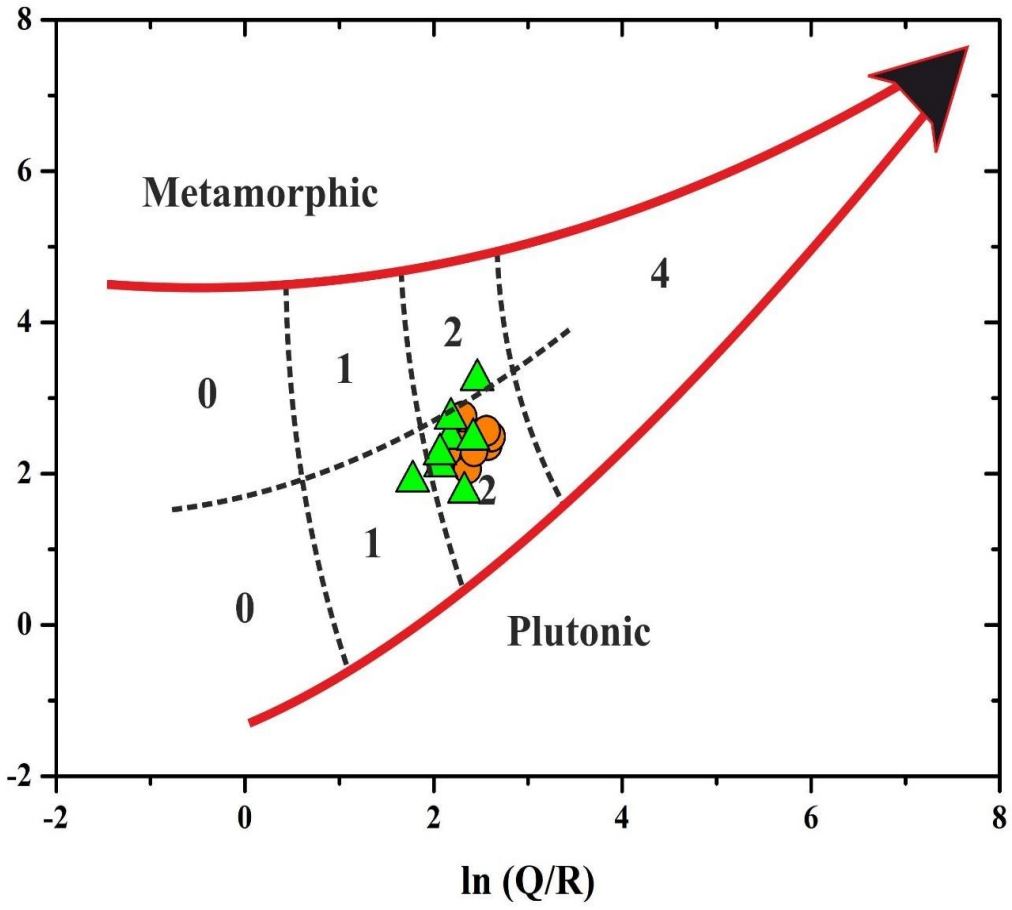

SEMI-QUANTITATIVE WEATHERING INDEX (Grantham and Velbel, 1988)			PHYSIOGRAPHY (Relief)		
			High (Mountain)	Moderate (Hills)	Low (Plains)
			0	1	2
CLIMATE (Precipitation)	(Semi-) Arid & Mediterranean	0	0	0	0
	Temperate Subhumid	1	0	1	2
	Tropical Humid	2	0	2	4

Figure 4.6. The semi-quantitative weathering index for the Bhuban sandstones (After Weltje, 1994; Grantham and Velbel, 1988) represents weathering indices of the number 2 indicating the degree of moderate weathering under the tropical Humid climate.

4.7 Diagenetic evolution of Bhuban sandstones in the Surma Group

Diagenesis encompasses various physical, biological, and geochemical processes occurring post-sediment deposition, leading to modifications in the original composition of sediments from the source area (Worden and Burley, 2003). According to Sengupta (1994), diagenesis refers to the alteration of sediments undergo between deposition and lithification under normal pressure-temperature conditions. The key diagenetic processes that occurred in both the Upper and Middle Bhuban Formations are cementation, mechanical compaction, dissolution, grain replacement, recrystallization, grain deformation, grain fracturing, and quartz overgrowth, and also have notably influenced the reservoir quality of the sandstones, as observed from the thin section study (Figs. 4.7 and 4.8).

4.7.1 Cementation

Cementation is a crucial diagenetic process where authigenic minerals precipitate in the pore spaces, causing loose sediments to consolidate into rock and reduce porosity. There are four types of cement were identified in the studied thin Section such as calcite cement, feldspar cement hematite cement, and quartz cement, as shown in Figures 4.7C, 4.8D, and 4.8E.

4.7.1.1 Silica cement

In siliciclastic sequences, silica cement plays a significant role, as noted by Rezaee and Tingate (1997). Silica cements are present in significant amounts in the study area. This cement is formed through the precipitation of silica in pore spaces (Baiyegunhi et al. 2017). Quartz cement is typically found as both pore-filling material and overgrowths on the surfaces of detrital quartz grains. In the mineralogical composition of the studied framework, silica cement develops in a shallow marine diagenetic environment as well as during early diagenetic stages (Baiyegunhi et al. 2017). Quartz overgrowth is the most prevalent type of silica cement observed in both the Upper and Middle Bhuban Formations (Fig. 4.8E). The result of syntaxial overgrowths (Fig. 4.7F.) usually gives the quartz grains are more euhedral crystal shapes with the syntaxial overgrowths frequently make quartz grains euhedral in shape as shown in (Fig. 4.7F.)

4.7.1.2 Calcite cementation

Calcite cementation is another prevalent type of cement found in the UBF and MBF, primarily developed during the early diagenetic stages. Detrital framework grains undergo partial or complete replacement by calcite, appearing as intergranular cement with microcrystalline and blocky to poikilotopic textures (Fig. 4.7C, & 4.7D). In the petrographic examination of framework grains, the common observation is the replacement of detrital silicate minerals by poikilotopic calcite cement (PC) (Fig. 4.7A and 4.7C). In most of the studied sandstone samples, calcite cements occupy spaces between two detrital mineral framework grains or their margins. The precipitation of calcite cement results in the occlusion of original porosity and permeability, along with the suppression of later quartz overgrowth formation and/or feldspar alteration (Fig. 4.7C).

4.7.1.3 Ferruginous cementation

Ferruginous cement is less common compared to other cement types in sandstones. It appears as reddish-brown cement that directly precipitates in the intergranular pore spaces or forms thin coatings around the boundaries of detrital grains (Fig. 4.8D). The presence of iron oxide staining on most of the clay minerals and detrital grains suggests the formation of ferruginous cement during the early diagenetic stage while oxygen was present (Christopher Baiyegunhi et al. 2017).

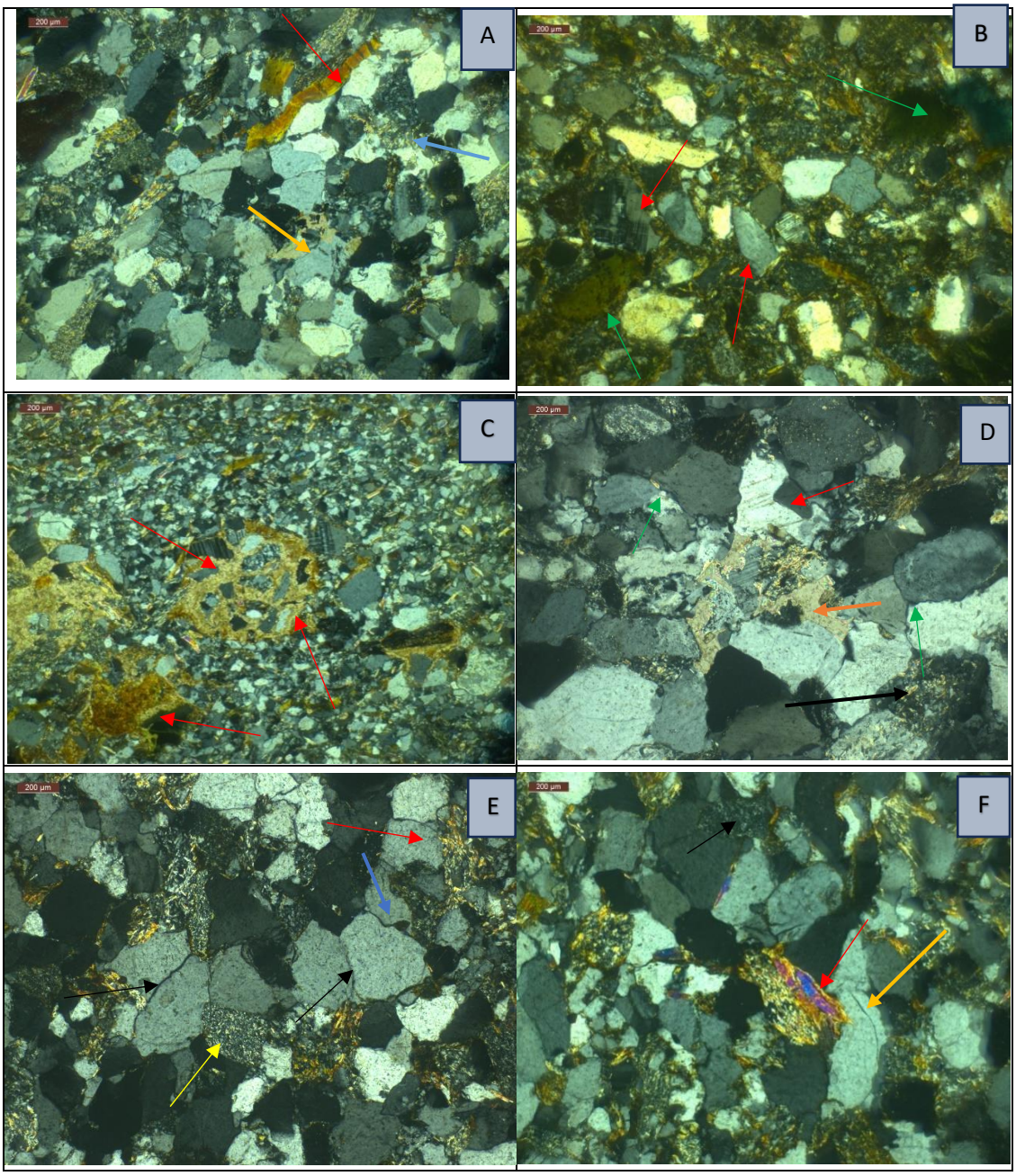

Figure 4.7. The Optical Photomicrograph of Bhuban Sandstone showing **(A)** Bending of mica flakes (red arrow), Poikilotopic calcite cement (yellow arrow), dissolution of detrital grain (blue arrow) **(B)** Glauconite cement (green arrow), albitization Feldspar overgrowth which is partially albitized (red arrow) **(C)** replacement of detrital mineral grains i.e., quartz, Feldspar (red arrow), by poikilotopic cement **(D)** Minerals replacement of calcite also replaced detrital framework grains ((yellow arrow), concave-convex quartz contacts (red arrow), mineral grains, replaced by Pseudomatrix (black arrow), suture contacts (green arrow) **(E)** Line contact (black arrow), concavo-convex (blue arrow) Metamorphic rock fragments (yellow arrow), clay matrix replaced the detrital grains(red arrow) **(F)** Sedimentary rock fragment (black arrow), syntaxial euhedral quartz overgrowth (yellow arrow), Recrystallization of clay minerals into muscovite (red arrow).

4.7.2 Mechanical compaction

Compaction represents the initial diagenetic process impacting sands immediately after deposition and burial beneath the sediment-water interface. It involves packing readjustment, plastic deformation of soft lithic grains, grain bending, and fracturing. This process leads to a rearrangement of detrital mineral grains, altering their shapes (Burley and Worden, 2009). Compaction is primarily driven by overburden loading, inducing changes in the packing density of constituent detrital framework grains. Mechanical compaction relies on the relative pressure-related solubilities of various grains and rock fragments in clastic terrigenous rocks, influenced by pressure, temperature, and water chemistry conditions during progressive burial. The results are shown in the development of various grain contacts (Fig. 4.7D and Fig. 4.7E) (Baiyegunhi et al. 2017). In the studied Bhuban sandstone samples, the number of points and long contacts decreases with increasing burial depth accompanied by an increase in the concavo-convex and sutured contacts among the grains. The grains undergo moderate to intense physical and chemical compaction during progressive burial, evident from the change in grain contacts. The contact patterns evolve from non-contact to point contacts, long contacts, and finally to concavo-convex contacts. The presence of long contacts, sutured contacts, and concavo-convex contacts indicates a moderate degree of compaction, attributed to deep burial diagenesis (Fig. 4.7D). The overburden pressure compaction in the sediments is leading to the fracturing and deformation of grains, particularly feldspar and muscovite. Some muscovite grains exhibit complete deformation, and the bending of detrital mica flakes and fracturing of quartz grains are indicative of mechanical compaction (Figs.4.7A & Fig. 4.8E). Overall, the Bhuban sandstones exhibit varying degrees of mechanical compaction, resulting in reduced porosity and permeability. Stylolite structures are also present in some sandstone samples (Fig. 4.7B, and Fig. 4.8F).

4.7.3 Dissolution

Dissolution is a process where the mineral is destroyed by interaction with fluid leaving behind a void (Burley and Worden, 2009). The diagenetic dissolution process can create the secondary porosity of authigenic minerals or sedimentary grains by the removal in a solution of all or a part of previously existing minerals, and increase the

pore spaces of sandstones (Ehrenberg, 1990; Selley, 1998; Al-Areeq et al. 2016). In the present study of Bhuban sandstones, the secondary porosity between the framework grains and the formation of sutured grain contacts by pressure solution activity along the grain boundaries by the process of dissolution is occasionally observed (Figs. 4.7A & Fig. 4.8A).

4.7.4 Replacement

Some minerals of Bhuban sandstones become weak and unstable when the temperature rises due to an increase in burial depth. Due to the change in the diagenetic environment, the minerals undergo a replacement process where they are replaced by new minerals that are more stable. Replacement is the process whereby one mineral dissolve and another mineral simultaneously forms in its place (Guilbaud et al. 2012). The present study displays the mineral grains that are involved in replacement processes are silica, feldspar, and clay minerals. The identified replacement events that are observed in the thin sections of Bhuban Sandstones are the replacement of quartz by calcite cement, the replacement of feldspars by sericite, and clay minerals replaced by mica (Figs. 4.7E 4.7F& 4.8D). In addition, albitization of feldspar probably occurred during the fracturing of the detrital K-feldspar creating the secondary porosity has been noticed within the Bhuban Sandstones unit (Aagaard *et al.*, 1990) (Fig. 4.7B). The micro-fractures within the detrital grains and cleavages of the mineral grains of studied sandstone are mostly affected by the albitization. The detrital grains and cleavages of mineral grains of studied sandstone are mostly affected by the albitization.

4.7.5 Recrystallization

Detrital grains, such as quartz and feldspar, also undergo vast recrystallization through the increase of crystalline grain size as overgrowth (Baiyegunhi et al. 2017). The process of mineral recrystallization is frequently observed in Bhuban sandstones. This process results in changes to the size and shape of mineral crystals without altering their chemical composition or mineralogy. As a result, the pore space between the detrital grains is reduced, as well as the connectivity between pores. The examined sediments display the recrystallization of clay minerals to muscovite as shown in Figure 4a, under the deep burial compaction during late diagenesis; as a result, there is a negative impact on the porosity and permeability of the sediments. The current

study reveals that sericitization has occurred in the studied sample, which is primarily formed by the recrystallization processes of detrital plagioclase minerals as depicted in Figures 4.7F& 4.8D.

4.7.6 Grain deformation and fracturing

The presence of fractures and deformation bands significantly impacts the relationship between porosity and permeability, as well as the performance of hydrocarbon reservoirs in sandstones (Cartwright, 1994; Conybeare & Shaw, 2000; Cosgrove, 2001; Cobbold et al. 2013). Although not intense, grain fracturing of detrital minerals has been observed in some quartz grains. Due to the mechanical compaction of sediments, some muscovite grains have also become deformed, as observed in this study. According to Hu and Huang (2017), sandstones have undergone chemical compaction which involves recrystallization, dissolution, and precipitation as points of contact between grains are susceptible to dissolution, which is an apparent response to overburden weight and higher stress. The present study shows grain fracturing, which provides key information about the processes of compaction, consolidation, and the patterns of fluid flow. These fractures are influenced by the dissolution process enhancing the secondary porosity of the sedimentary grains (Fig. 4.7A, 4.8E & 4.8F). The occurrence of grain fracturing in authigenic grains is primarily observed during late diagenesis, which indicates a post-depositional tectonic disturbance of the sediments. This reflects the moderate compaction of the Bhuban Sandstones.

4.8 Diagenesis of Bhuban Sandstones

The examination of thin sections revealed that the Bhuban sandstones contain a variety of detrital minerals, such as quartz, plagioclase, microcline, muscovite biotite, along with some clay minerals. While authigenic minerals like silica, calcite hematite, and glauconite were formed during diagenesis, these minerals make up the rock framework grains, with some of them occurring as cement (Fig. 4.7C). The diagenesis inferred from petrographic investigations has been extensively studied by multiple researchers with varying perspectives (Baiyegunhi et al. 2017; Chima et al. 2018).

4.8.1 Early Diagenesis

The early diagenesis of sandstones is primarily influenced by time-temperature history, fundamental mineralogy and fabric, and pore water geochemistry (Worden and Burley, 2003). According to Berner (1980) and Chapelle (1993), the early

diagenesis stages include all processes that occur at or near the surface of the sediments where the chemistry of the interstitial water is controlled mainly by the depositional environment. The early diagenetic stage in the present study is distinguished by the occurrence of cementation i.e., quartz (Fig. 4.8E), the formation of authigenic clay minerals through precipitation, the emergence of minor quartz and hematite coating, as well as consolidation (Fig. 4.8D). The presence of different types of grain contacts, such as point and long contacts, are observed in Bhuban sandstone, which indicates an early stage of diagenesis. As the depth of burial increases, the compaction caused by the overlying loads intensifies, resulting in a continuous reduction in primary porosity. This reduction in primary porosity leads to a decrease in both long and point contacts in the present study. In addition, cement precipitation, matrix, authigenic mineral formation, and mild cementation are the characteristic features of the early diagenetic processes. According to Harder (1980) the process of glauconite precipitation must have occurred at the interface between reducing and oxidizing zones in muddy sediments and the presence of Si, Fe, Al, and K-containing pore fluids. In the present study, glauconite occurred as cement, which is likely precipitated at the early diagenetic stage (Fig. 4.7B).

4.8.2 Late Diagenesis

The late diagenetic stage starts with increasing pressure and changes in pore-water chemistry with increasing depth (Boggs, 2014), which helps with physical (compaction and porosity loss), mineralogical or chemical changes (mineral replacement, dissolution of minerals, and precipitation of new cement) of framework grains. The physical and chemical compaction of mineral grains, replacement of minerals, grain deformation, and cementation are the primary factors that significantly impact the late stage of diagenesis. At these stages, the physical and chemical compaction became more significant due to an increase in overlying pressure which led to more compactness of framework grain packing as a result of partial loss of pore spaces. Mineral replacements, such as albitization (where Ca-plagioclase and K-feldspar are converted to albite and muscovite), provide indications of late diagenetic stages in the Bhuban sandstones. At the end of the late diagenetic stage, due to an increase in overburden pressure, the compaction became more prominent. Consequently, the grain contact patterns change progressively from point to long

contact, then to concavo-convex contact, and finally to sutured contacts as shown in Figure 4.7D. Additionally, bending of muscovite flakes due to over-compaction of sediments and diagenetic replacement, such as detrital feldspar and quartz replaced by calcite, clay matrix composed by new minerals are frequently observed in the studied thin section, which is likely formed during the late stage of diagenesis (Fig. 4.7A, 4.7C). Calcite commonly occurs as cement in the early and late stages of diagenesis in mineral grain-supported sandstones (Worden & Burley, 2003). In the present study, the replacement of mineral grains by calcite cement has been noticed in some samples (Fig. 4.7C, and 4.7D).

4.8.3 Uplift-related Diagenesis

Due to the uplift and consequent exposure of Bhuban sandstones, the influx of surface water into the rocks results in an uplift-related diagenetic environment. Large amounts of meteoric or surface waters never enter marine sediment deposits unless they are uplifted and subjected to weathering (Hurst and Irwin, 1982). Mineral assemblages formed during the late diagenetic stage under high pressure and temperature conditions become unstable during the uplift-related diagenetic stage which can be resulted in the alteration or dissolution of unstable minerals. In the uplifted related diagenetic stages, early feldspar dissolution resulted in the formation of some secondary porosity that has been noted in the present samples (Fig. 4.8A). The higher degree of compaction due to high pressure and high-temperature environment at a greater depth highlights the grain deformation and fracturing in the present study (Fig. 4.7A and 4.8E). The grain fractures are influenced by the dissolution process, which enhances the secondary porosity of the sedimentary grains, during the uplift-related stage of diagenesis.

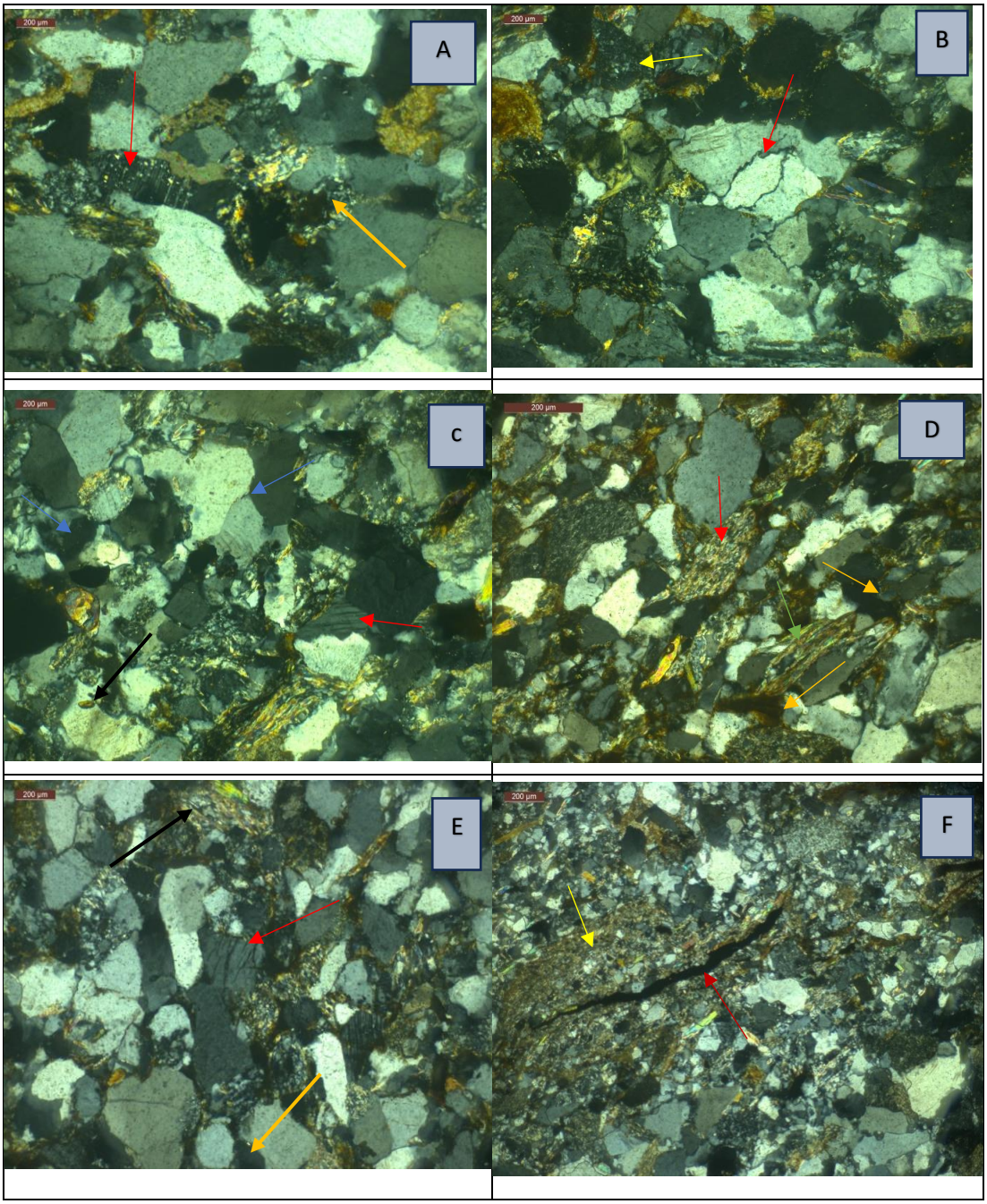

Figure 4.8. The Optical Photomicrographs of Bhuban sandstone showing **A.** Feldspar dissolution by calcite cement (red arrow), Quartz dissolution (yellow arrow); **B.** Stylolite due to strong compaction (red arrow), Sedimentary Rock fragment (yellow arrow); **C.** Feldspar overgrowth (red arrow), heavy minerals (black arrow), suture contact (blue arrow); **D.** Hematite cement (yellow arrow), metamorphic lithic fragment (red arrow), recrystallization of clay minerals to muscovite (green arrow); **E.** Monocrystalline Quartz Grain fracture (red arrow), silica cement (yellow arrow) sericitization (black arrow); **F.** Psuedomatrix (yellow arrow), Secondary stylolite fracture or microfracture (red arrow).

4.9 Implications of Diagenesis on Reservoir Properties

Porosity and permeability have a direct correlation with the accumulation and extraction of oil from a reservoir. Greater porosity leads to a higher accumulation of hydrocarbons within the reservoir, while greater permeability results in increased recovery of hydrocarbons. The diagenesis of sediments modifies the original pore spaces and geometry of sandstones and hence controls their overall porosity and permeability (Baiyegunhi, 2020). Through thin-section observations, the porosity and permeability of the Bhuban sandstone reservoirs are strongly influenced by diagenetic processes that either reduce or enhance. Porosity and permeability are the main factors responsible for the quality of the reservoir. The greater the porosity, the more hydrocarbons will accumulate in the reservoir and the greater the permeability, the greater the recovery of hydrocarbons. In addition, the flow of fluids through rocks is regulated by porosity and permeability, which are essential factors in sediment diagenesis. The fluid flowing through the rock causes cementation, authigenesis and dissolution of minerals. A petrographic examination of the Bhuban sandstones revealed both primary and secondary porosity. Primary porosity refers to the intergranular pore space and microporosity (matrix micro pores) that are present within sediment immediately following deposition and before diagenetic modification. The Bhuban sandstone undergoes crucial diagenetic processes, including cementation (involving calcite, quartz, feldspars, clays, and iron oxide), compaction, albitization, mineral replacement, dissolution, and grain fracturing or deformation. These processes either can reduce or enhance the porosity while simultaneously impacting the reservoir properties of the studied sandstones (Baiyegunhi et al. 2017). The compaction of mineral grains under overburden pressure caused changes in grain contacts, which in turn resulted from progressive burial and ultimately led to a decrease in primary intergranular porosity and pore radii of the Bhuban sandstone. The presence of high concentration of carbonate cement affected the reservoir porosity, which significantly controlled the reservoir quality of sandstones. The reservoir quality in the study area is typically improved by the existence of fractured and dissolution pores, where dissolution of mineral grains had a great influence on the development degree of secondary pores (Zhang et al. 2017; Yuan et al. 2019; Zhang et al. 2022; Cui, 2022). In the present study, although secondary porosity resulting from framework grain

dissolution (mainly feldspars) is typically always present, it may only account for a small part of total porosity. In summary, it can be inferred that the diagenetic processes of the Bhuban sandstone have resulted in the reduction of porosity and the isolated nature of the pores (reduced permeability), which makes them unfavorable for the production of hydrocarbons.

CHAPTER 5
GRANULOMETRIC STUDY OF SANDSTONES

5.1 Introduction

Grain size analysis is a valuable tool for identifying the textural properties of sediments, describing sedimentary rocks, and determining the conditions under which the sediment was deposited. The grain size is an essential physical property of sediments, which provides information on the properties and forces operative at the time of deposition. Also, it helps to understand the nature of the transporting medium, the energy flow of the sediments, and the depositional environments in which the sedimentation has occurred. Grain size is a vital characteristic of siliciclastic sediments; as a result, it is one of the most significant qualities that may be used to describe sedimentary rocks. Extensive use of grain-size features is carried out to gain insight into depositional processes, hydrodynamic conditions, and depositional environment (Boggs, 2009). The components of sediments are connected to their provenance since they are products of the source composition, weathering, and transportation (Dickinson et al. 1983). To acquire a comprehensive understanding of the hydrodynamic condition of siliciclastic sedimentary rocks, sediment provenance, paleo-environmental features, and reconstruction of ancient sediment transport histories through the grain size analysis is a more useful tool (Srivastava et al. 2012; Baiyegunhi et al. 2017). The grain size parameters such as graphic mean size, graphic skewness, graphic kurtosis, and their statistical relationships represented by different plots namely bivariate plots, linear discriminate functions, log probability curves, and C-M plots have been more useful for determining the depositional processes, transportation mechanism, hydrodynamic conditions, and depositional environments (Folk and Ward, 1957; Friedman, 1979; Baiyegunhi et al. 2017). The most commonly used statistical methods in a grain size analysis include mean, median, mode, kurtosis, sorting, and skewness, which are the most useful approaches for describing sediments and promoting the interpretation of depositional settings and identification of net sediment transit paths. The bivariate scatter plots are interrelated with the grain size parameters for comparing different depositional settings (Srivastava and Mankar, 2009). The shapes of grain-size cumulative curves are environmentally significant as they convey information about the log probability curves. These segments of the

curves illustrate various grain transportation methods, including traction, saltation, and suspension. Friedman (1961) suggested that a bivariate plot of skewness vs. mean size in sediment plots has been useful for discriminating dune, fluvial, and beach environments. The sediment bivariate plots of sorting against skewness are a very valuable method to distinguish between river sands from beach sands (Friedman, 1961). Duane (1964) explained the importance of the kurtosis parameters to distinguish various environments of deposition of sediments. Passega (1957) first introduced the C-M plot to evaluate the hydrodynamic processes during the deposition of the sediments.

5.2 Grain Size Analysis

Sedimentologists have extensively employed grain size distribution analysis as a means of classifying sedimentary environments and understanding sediment transport dynamics. This technique has been utilized in several studies by various researchers (Udden, 1914; Wentworth, 1922; Keller, 1949; Folk and Ward, 1957; Friedman, 1961; Sahu, 1964; Moiola and Weiser, 1968; Vincent, 1998; Srivastava and Mankar, 2009). It can also be referred to as a technique for figuring out the proportions of various-size particles in sediments, based on the statistical treatment of the grain size data. In the present work, the graphic mean (Mz), graphic standard deviations (σ_1), graphic skewness (S_{KI}), and graphic kurtosis (K_G) are used to depict the various textural characteristics of the Bhuban sediments discussed below.

5.2.1 Grain Size Statistics

In this study, the modal characteristics of a sediment population are determined by the highest points on the frequency curves, which are based on weight percentage values. The volume percentage frequency distribution curves are utilized to indicate the modal properties of the sediment population. The sediments show both unimodal and bimodal in nature (Fig. 5.1 & Fig. 5.2). This bimodality is probably due to the medium to low energy of the marine setting, whereas unimodality indicates the consistent depositional process during which the sediments were deposited (Baiyegunhi et al. 2020). The volume percent frequency curves reveal that the majority of the Bhuban sandstones are bimodal in nature (Figs. 5.1 & 5.2), with peaks of 1.0Ø, 3.5Ø, and 4.0Ø resulting in medium to low energy conditions of the marine setting with a strong fluvial influence during the deposition of the sediments.

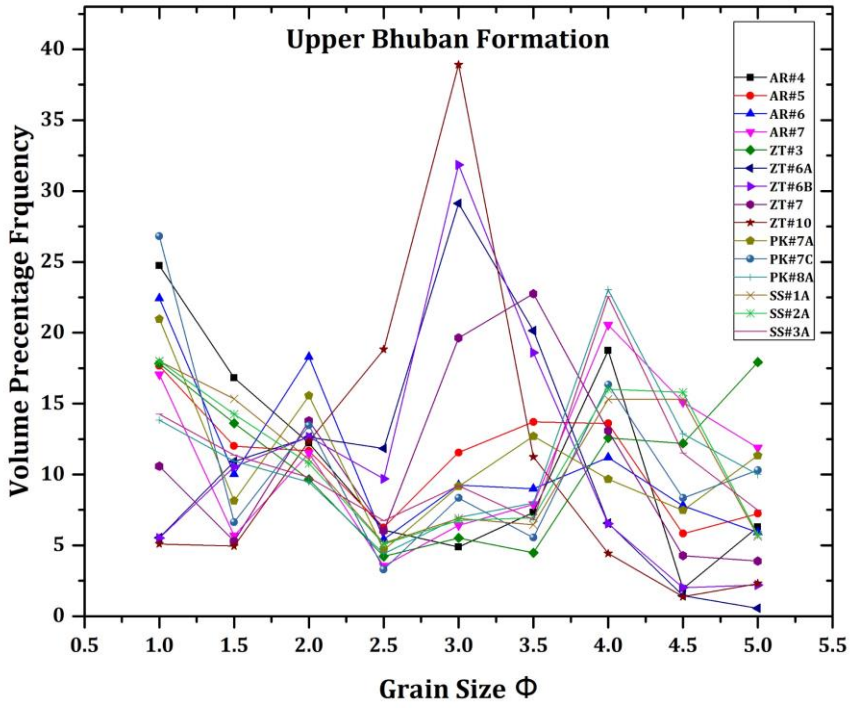

Figure 5.1. Relationship between volume percentage frequency and grain size for Upper Bhuban Formation (UBF) of Surma Group. Note: - AR, ZT, SS, and PK are sample numbers as referred to in Table 5.1.

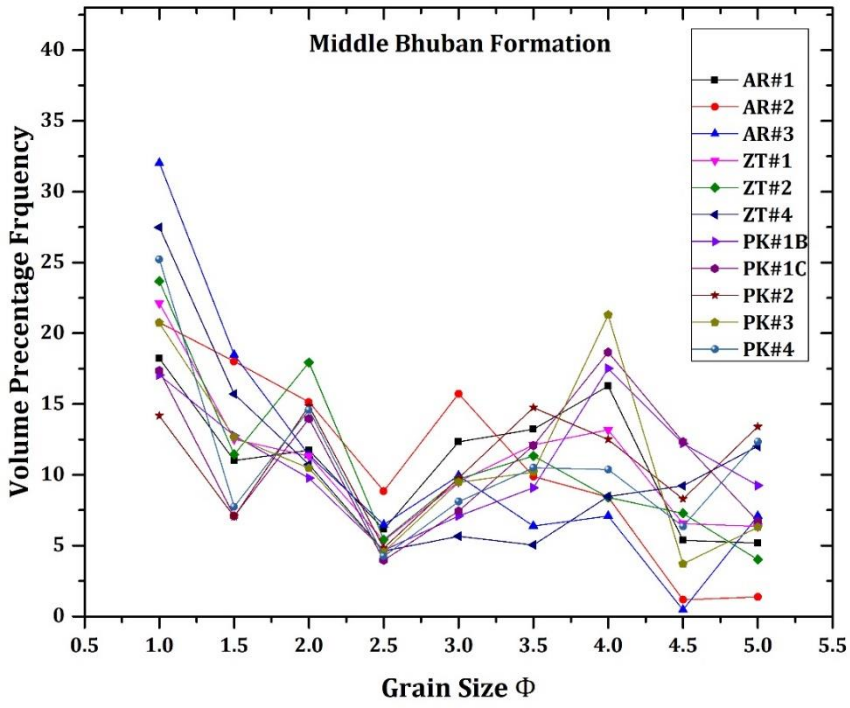

Figure 5.2. Relationship between volume percentage frequency and grain size for Upper Bhuban Formation (UBF) of Surma Group. Note: - AR, ZT, SS, and PK are sample numbers as referred in Table 5.1.

5.2.2 Study of Cumulative Curves

The grain size analysis data from representative sandstone samples were used to prepare cumulative curves, where the arithmetic scale was employed with cumulative weight percentage (wt.%) at the Y-axis and grain size data (in Φ units) at the X-axis. The cumulative curve of the Bhuban sandstone is characterized by initially (fine size) moderately steep, with a concave middle part and gentle (fine size) end portion (Fig. 5.3 & 5.4). The cumulative curve generally indicates the sorting characteristics of the grain size samples where a very gentle slope shows poor sorting and a very steep slope means good sorting. Most of the Bhuban samples of both the Upper Bhuban Formation and Middle Bhuban Formation show the S-type of the slope curves as represented in figures 5.3 and 5.4.

5.2.3 Univariate Grain Size Parameters

Grain size statistical parameters (graphic mean, standard deviation, skewness, and kurtosis) are employed to make numerical comparisons between grain size and depositional conditions. These parameters are calculated from the grain-size cumulative curves by deriving the Ø5, Ø16, Ø50, Ø75, Ø84, and Ø95 values (Folk and Ward, 1957). In the present study, a variety of univariate grain size parameters were calculated using the mathematical techniques introduced by Folk and Ward (1957). The following mathematical equations (Folk and Ward, 1957) were used to calculate the various univariate grain size parameters which are presented in Table 5.1 & Fig. 5.5

Graphic mean M_Z = (Ø16+Ø50+Ø84)/3

Standard deviation (sorting) σ1 = (Ø84-Ø16)/4+ (Ø95-Ø5)/6.6

Graphic skewness SK_I = [Ø84+Ø16-2(Ø50)]/[2(Ø84-Ø16)] +[Ø95+Ø5-2(Ø50)]/[2(Ø95-Ø5)]

Graphic kurtosis K_G = (Ø95-Ø5)/[2.44(Ø75-Ø25)]

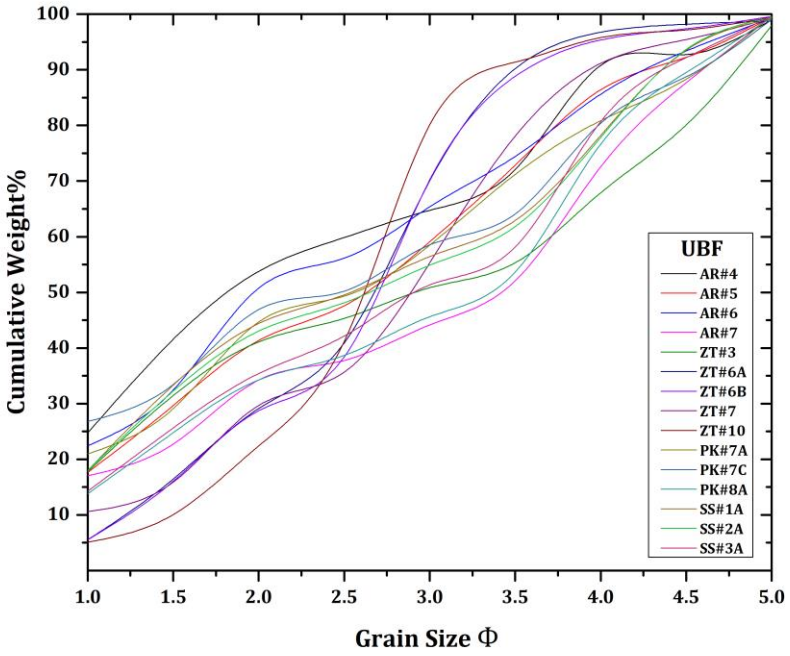

Figure 5.3. The cumulative curves of sediments in the Upper Bhuban Formation

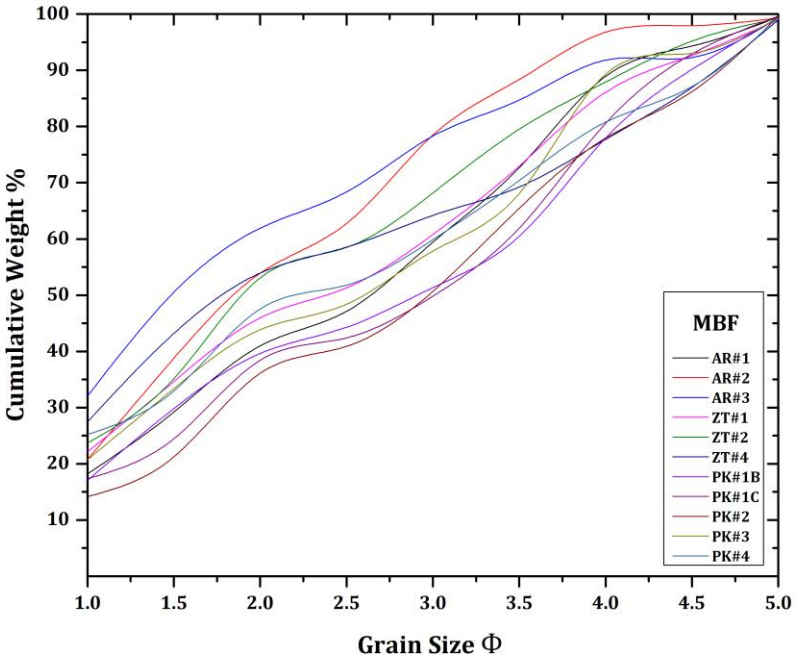

Figure 5.4. The cumulative curve of sediments in the Middle Bhuban Formation.

5.2.4 Graphic mean (M_Z)

The graphic mean size is a parameter that pertains to the entire (overall) grain size of sediment. It represents the average size of the sediment and is denoted by the ∅ mean size. This parameter indicates the level of energy conditions within the environment. It is the average size of the sediment represented by ∅ the mean size and connotes the index of energy conditions (Passega, 1964). The graphic mean size of the studied sediments suggests low to moderate energy conditions of deposition. According to Folk, (1980), sediments become finer when the energy of the transporting medium decreases throughout their depositional pathways. The calculated graphic mean values range from 1.98∅ to 2.88∅, which indicates that the sediments are characterized by fine to very fine grain size with low energy conditions of deposition as shown in Table 5.1, and Fig. 5.5.

5.2.5 Inclusive Graphic Standard Deviation (σ_1)

The standard deviation is an indicator of sediment sorting and reflects changes in the kinetic energy or velocity conditions of the sandstone depositional environment (Ramanathan et al. 2009). The inclusive standard deviation assesses the sorting or

uniformity distribution of the grain size. Also, it shows changes in the hydrodynamic energy levels in the depositional environment (Sahu, 1964). The sorting values of the sediments range from 0.79ø to 1.62ø (Table 5.1 & Fig. 5.5). These values indicate that the sediments of the study area are mainly poorly sorted, with some being moderately sorted in nature (Fig. 5.6A). The predominance of poorly sorted sediments is due to the short to moderate distance of sediment transportation, and their characteristics indicate that they were deposited in shallow marine environments under the influence of river dominance (Kasim et al. 2023).

5.2.6 Inclusive graphic skewness (S_{KI})

The graphic skewness is useful for evaluating the grain-size distribution and it indicates the spread of grain size in the tail ends of the distribution. A distribution with an asymmetrical curve that contains an abundance of fine particles will have a fine-size tail and yield a positive phi (ø) value. Conversely, a distribution with an excess of coarse particles will have a coarse-size tail and result in a negative phi (ø) value. When the phi (ø) value is zero, it indicates that the curve is symmetrical. The SKI values in Bhuban Formation sandstones range from -0.04Φ to 0.47Φ with an average of -0.03Φ, indicating that most of the samples had a coarse skewness, followed by near symmetrical, fine skewness, strongly fine skewness and strongly coarse-skewed (Table 5.1 & Fig. 5.5). This suggests that during the deposition of studied sediments, there was a high-energy condition with some riverine input, as negatively skewed sediments dominated over positively skewed sediments. This conclusion was drawn based on works by Mason and Folk (1958), Friedman (1961), and Duane (1964).

5.2.7 Graphic kurtosis (K_G)

The degree of peakedness of the grain-size distribution is conveyed by the kurtosis. The average value of Bhuban sediments indicates a platykurtic condition (average 0.77 Φ) which is followed by mesokurtic, very platykurtic, and leptokurtic distribution (Table 5.1 & Fig. 5.5). This suggests that most of the sediments are reflections of the maturity of sand (Ramanathan et al. 2009).

Table 5.1. The calculated statistical parameters for grain size analyses of the Bhuban sandstones for the Upper Bhuban and Middle Bhuban Formations in the study area (after Folk and Word, 1957).

Litho-Unit	Sample Id	M_Z	σ_1	SKI	K_G	σ_1	S_{KI}	K_G
Upper Bhuban Formation	AR#4	2.17	1.39	0.33	0.68	Poorly sorted	Strongly fine skewed	Platykurtic
	AR#5	2.50	1.36	-0.06	0.74	Poorly sorted	Near symmetrical	Platykurtic
	AR#6	2.26	1.41	0.25	0.72	Poorly sorted	Fine skewed	Platykurtic
	AR#7	2.88	1.49	-0.32	0.70	Poorly sorted	Strongly coarse skewed	Platykurtic
	ZT#3	2.67	1.59	0.10	0.60	Poorly sorted	Fine skewed	Very platykurtic
	ZT#6A	2.50	0.90	-0.26	0.94	Moderately sorted	Coarse-skewed	Mesokurtic
	ZT#6B	2.43	1.00	-0.32	0.99	Moderately sorted	Strongly coarse- skewed	Mesokurtic
	ZT#7	2.71	1.10	-0.22	0.98	Poorly sorted	Coarse-skewed	Mesokurtic
	ZT#10	2.54	0.79	-0.20	1.41	Moderately sorted	Coarse-skewed	Leptokurtic
	PK#7A	2.58	1.54	-0.05	0.73	Poorly sorted	Near symmetrical	Platykurtic
	PK#7C	2.47	1.61	0.00	0.66	Poorly sorted	Near symmetrical	Very platykurtic
	PK#8A	2.95	1.42	-0.41	0.69	Poorly sorted	Strongly coarse skewed	Platykurtic
	SS#1A	2.56	1.45	-0.01	0.65	Poorly sorted	Near symmetrical	Very platykurtic
	SS#2A	2.56	1.43	0.00	0.64	Poorly sorted	Near symmetrical	Very platykurtic
	SS#3A	2.73	1.37	-0.20	0.68	Poorly sorted	Coarse skewed	Platykurtic

Table 5.1.cont.

Litho-Unit	Sample Id	M_Z	$б_I$	S_{KI}	K_G	$б_I$	S_{KI}	K_G
Middle Bhuban Formation	AR#1	2.44	1.36	-0.10	0.77	Poorly sorted	coarse-skewed	Platykurtic
	AR#2	1.98	1.12	0.12	0.84	Poorly sorted	Fine skewed	Platykurtic
	AR#3	1.99	1.48	0.47	0.94	Poorly sorted	Strongly fine skewed	Mesokurtic
	ZT#1	2.39	1.45	-0.04	0.72	Poorly sorted	Nearly symmetrical	Platykurtic
	ZT#2	2.16	1.37	0.22	0.75	Poorly sorted	Fine skewed	Platykurtic
	ZT#4	2.27	1.62	0.36	0.66	Poorly sorted	Strongly fine skewed	Very platykurtic
	PK#1B	2.71	1.46	-0.18	0.66	Poorly sorted	Coarse-skewed	Very platykurtic
	PK#1C	2.71	1.44	-0.26	0.75	Poorly sorted	Coarse-skewed	Platykurtic
	PK#2	2.84	1.45	-0.17	0.75	Poorly sorted	Coarse-skewed	Platykurtic
	PK#3	2.48	1.40	-0.04	0.70	Poorly sorted	Nearly symmetrical	Platykurtic
	PK#4	2.40	1.59	0.13	0.69	Poorly sorted	Fine skewed	Platykurtic

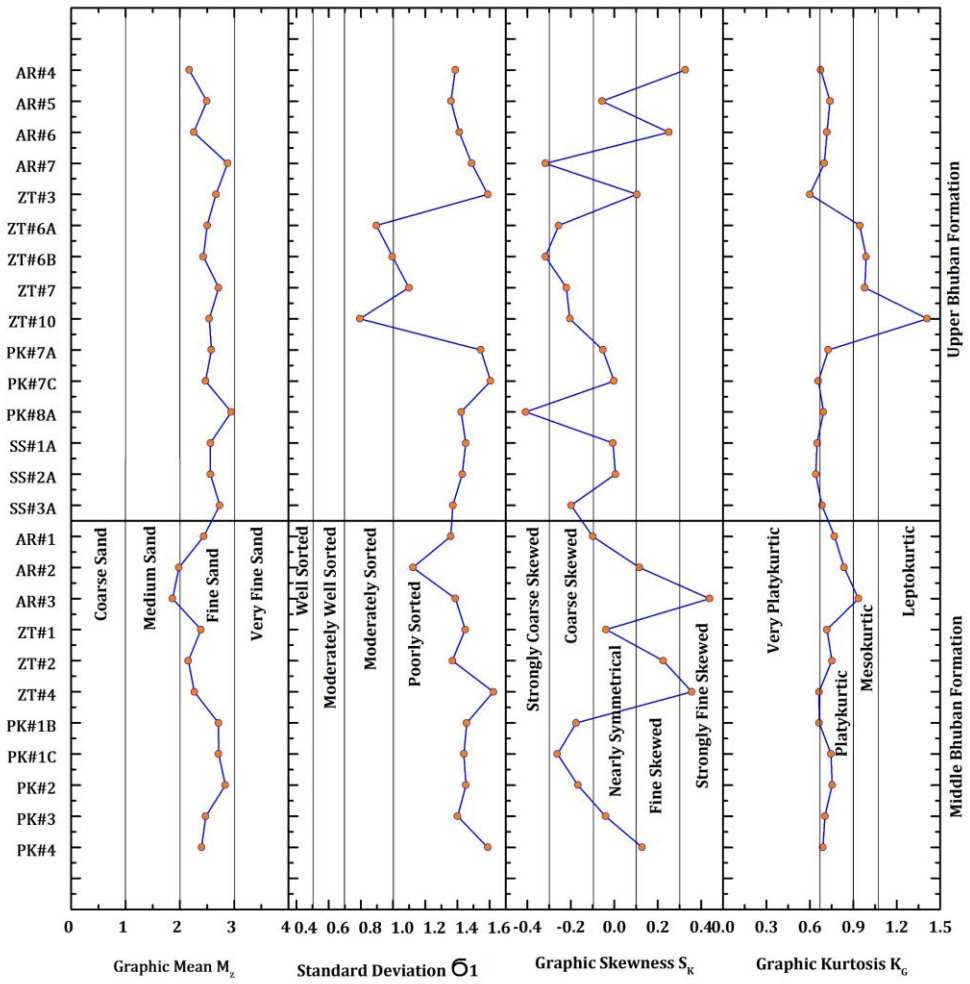

Figure 5.5. The statistical variations of sandstones in the Upper and Middle Bhuban Formations.

5.2.8 Bivariate plots of statistical parameters

The bivariate plots through the multiple textural parameters have been employed to recognize the depositional setting (Friedman, 1967). It depends on the presumption that statistical parameters, accurately indicate that variations in the fluid-flow mechanisms responsible for sediment transportation and deposition (Sutherland and Lee, 1994). Previous studies conducted by some researchers (Khalaf et al. 1982; Srivastava and Mankar, 2009) have established the effectiveness and documented the usefulness of bivariate plots in identifying the mechanisms of various sedimentary

environments. Additionally, they have highlighted that bivariate plots are the most vital and commonly used types of plots (Folk and Ward, 1957; Friedman, 1967; Moiola and Weiser, 1968). Bivariate plots have also been utilized to distinguish between marine and fluvial sands. The bivariate plots that were employed to differentiate between various depositional environments included the standard deviation vs. graphic mean, skewness vs. kurtosis, and skewness vs. standard deviation.

5.2.9 Graphic standard deviation (sorting) (σ_1) versus graphic mean size (M_Z)

According to the bivariate plot of mean versus graphic standard deviation (sorting), the Bhuban samples consist of fine to very fine sand that is poorly to very poorly sorted (Fig. 5.6A). The presence of fine-grained sediments in the basin during deposition suggests that the energy conditions were moderately low (Baiyegunhi et al. 2017). Sediments that are effectively sorted during extended transportation typically have similar grain sizes, and if there are any variations, the sediment is likely either deposited quickly or near its source (Rajganapathi et al. 2013). Baiyegunhi et al. 2017) reported that the majority of Bhuban sandstones are fine grained and poorly sorted, it's plausible that sediment grains spent a significant amount of time in the transporting medium, and as a result of grain-to-grain interactions, their sizes may have been reduced. As per Ramanathan et al. (2009), the standard deviation is an indicator of sediment sorting and reflects changes in the kinetic energy or velocity conditions of the depositing agent. In terms of the depositional environment, the binary plots of mean vs. standard deviation of analyzed sandstone samples (Fig. 5.6A, B) show the influence of the riverine environment (after Friedman1967; Moiola and Weiser, 1968).

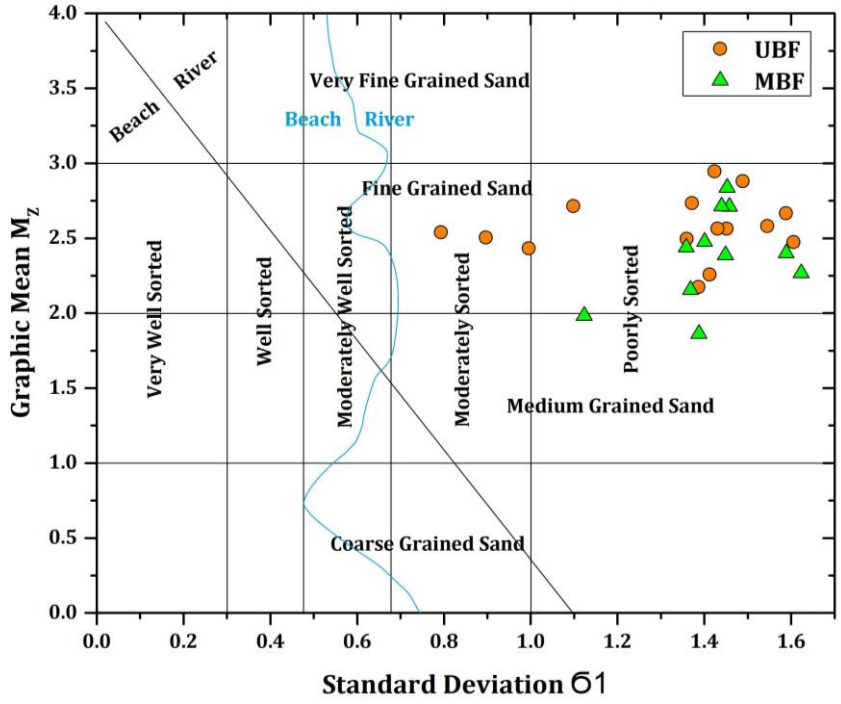

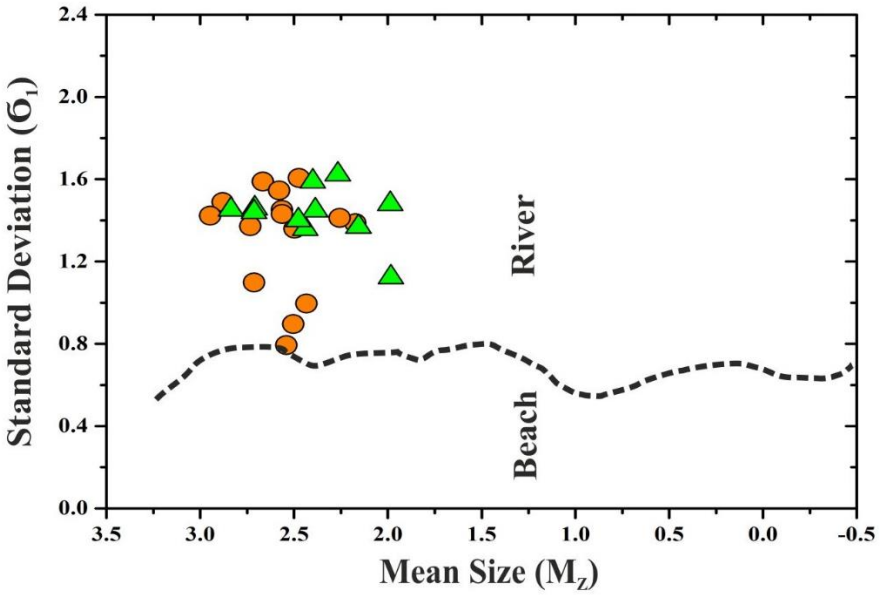

Figure 5.6 (A). The binary plot of graphic mean vs standard deviation (After Friedman 1967; Moiola and Weiser, 1968) for Upper Bhuban Formation (UBF) and Middle Bhuban Formation (MBF). (B) The binary plot of graphic mean size vs standard deviation (After Friedman, 1967) shows the deposition environment for Upper Bhuban Formation (orange circle) and Middle Bhuban Formation (green triangle).

5.2.10 Graphic skewness (S_{KI}) versus graphic kurtosis (K_G)

Friedman (1967) and Thomas et al. (1972) used a bivariate plot of SK_I (graphic skewness) against K_G (kurtosis) to identify the energy condition and depositional medium as well as particle size during deposition. The bivariate plot of graphic kurtosis versus skewness shows that the Bhuban samples are platykurtic to mesokurtic and are mostly coarse skewed to near symmetrical. According to the bivariate plot of graphic skewness (S_{KI}) vs. graphic kurtosis (K_G) (after Friedman, 1967), it can be incidental that samples were deposited in a riverine setting (Fig. 5.7). Figure 5.8 also shows that the sandstone samples were a combination of fine to medium-grained particles, which suggests that they were deposited in a medium to high energy fluvial setting (Thomas et al. 1972).

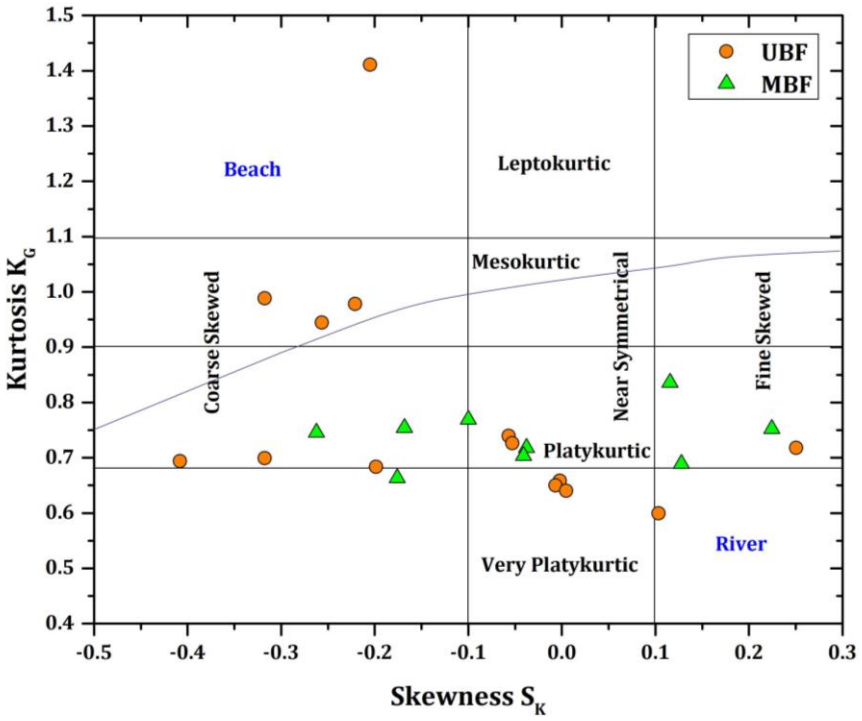

Figure 5.7. The bivariate plot of kurtosis vs. skewness (after Friedman, 1967) showing skewness, kurtosis category, and depositional environment for the Upper Bhuban Formation (UBF) and Middle Bhuban Formation (MBF) of the Surma Group of sediment in the study area.

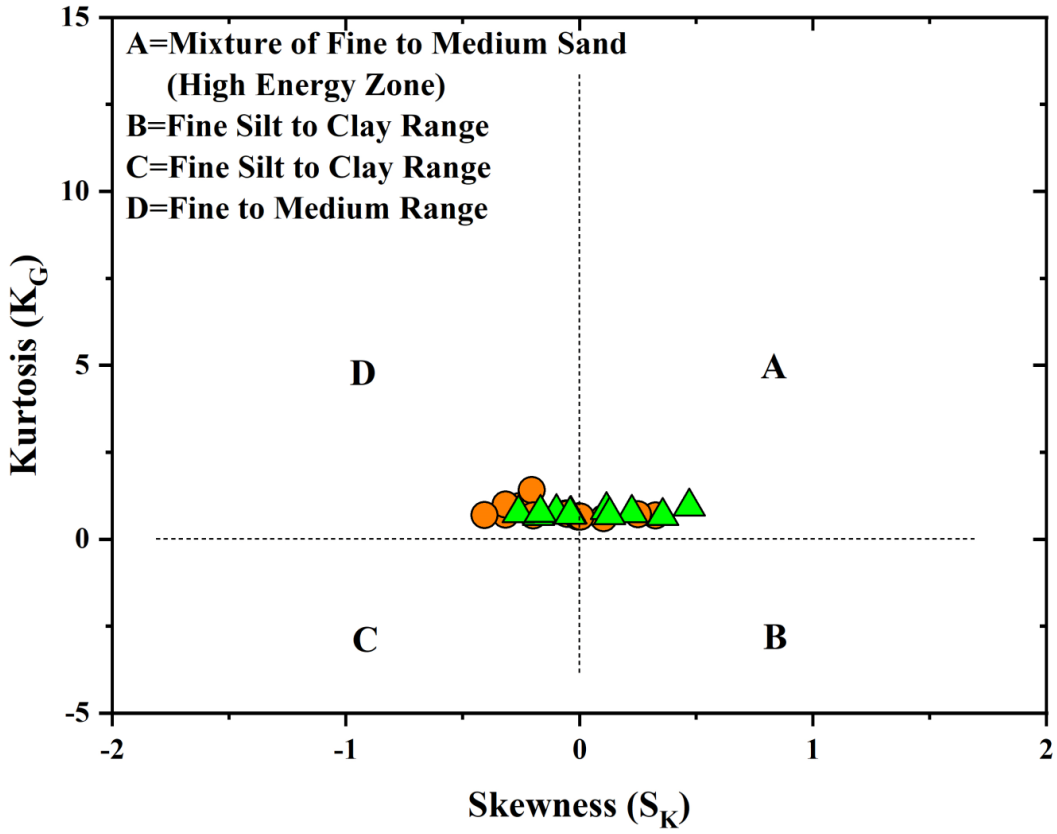

Figure 5.8. The bivariate plot of the kurtosis vs skewness (after Thomas et al. 1972) shows a fine to medium grain size range for the Upper Bhuban Formation (orange circle) and Middle Bhuban Formation (green triangle) of the Surma Group of sediment in the study area.

5.2.11 Graphic skewness (SK_I) vs standard deviation (σ_1)

The binary plot of the graphic skewness vs standard deviation (Friedman, 1967; Folk, 1974) indicates that the Bhuban sandstones are mostly poorly sorted to moderately sorted and have coarse skewed to nearly symmetrical in character (Fig. 5.9). Furthermore, the aforementioned relationship also reveals that the sediments were deposited under the influence of river environment.

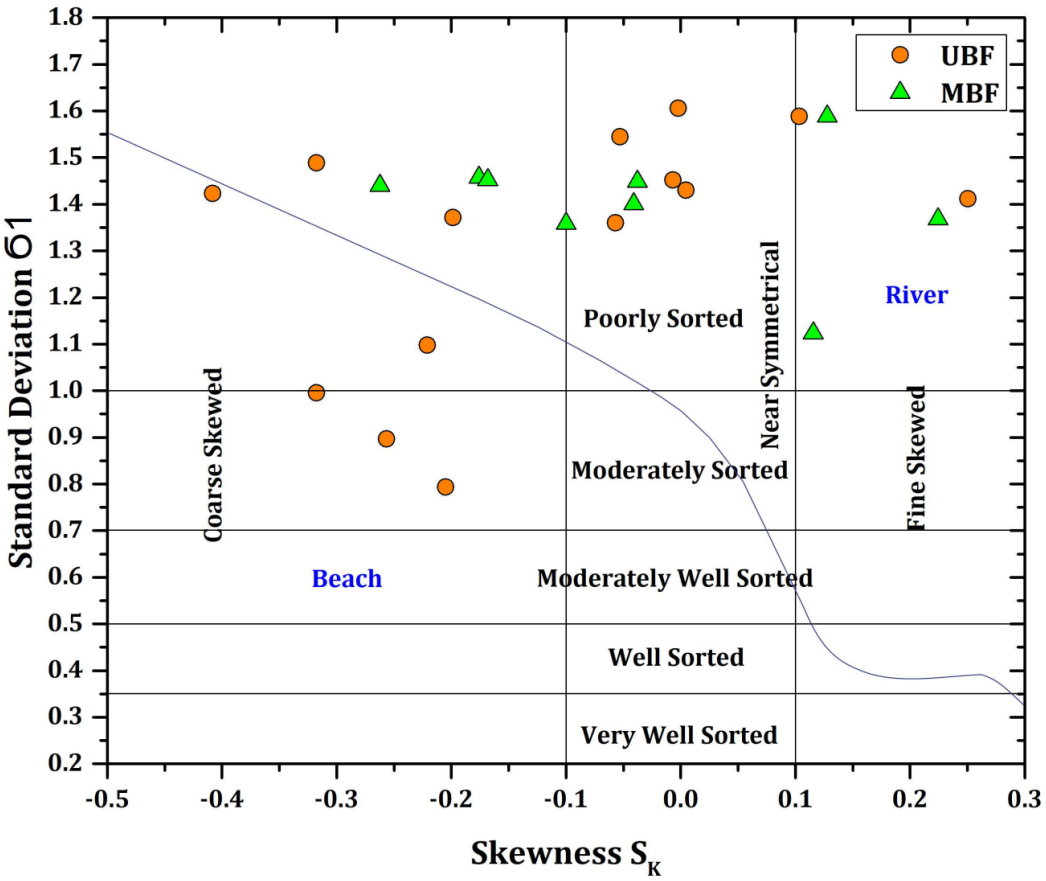

Figure 5.9. The bivariate plot of sandstones standard deviation vs skewness showing the sorting, skewness category, and depositional environment for the Upper Bhuban Formation (UBF) and Middle Bhuban Formation (MBF) of the Surma Group of sediment in the study area. (after Friedman, 1967; Folk, 1974).

5.2.12 Log-Log plot

Sahu (1964) developed a method to interpret the depositional environment by analyzing the grain size values using a bivariate plot of $\sqrt{\sigma 1\text{-}2}$ versus $(K_G/M_Z) \times \sigma 12$. The Log-Log plot (Fig. 5.10) indicates that the sediments have undergone deposition in a shallow marine basinal part which is characterized by deltaic conditions with the strong influence of rivers.

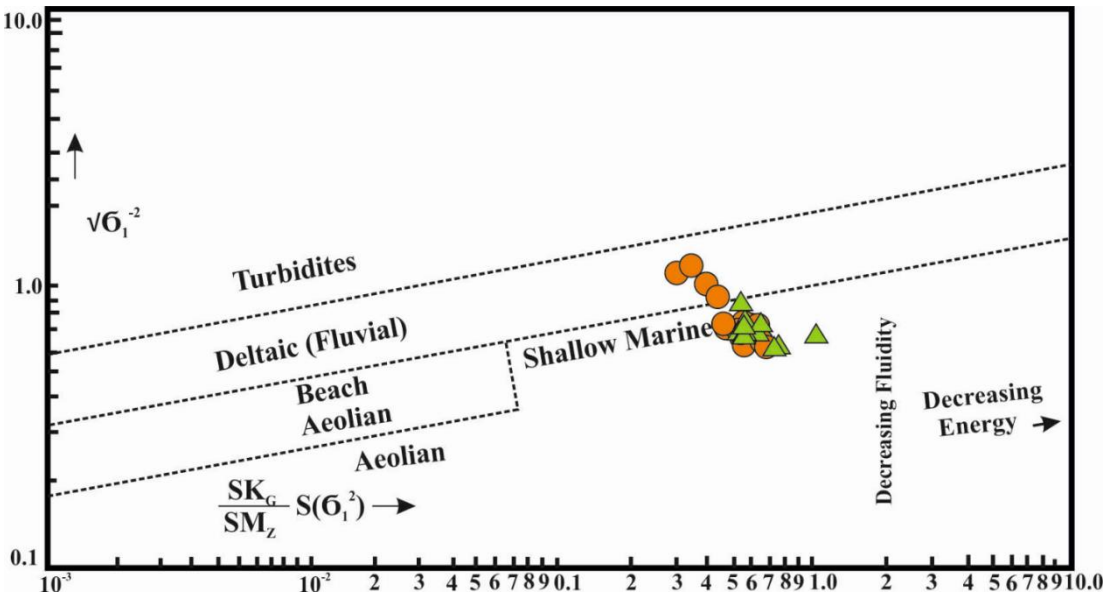

Figure 5.10. The Log-log plot for the sandstones of the Upper Bhuban Formation (orange circle) and Middle Bhuban Formation (green triangle) of the Surma Group of sediment in the study area. (after Sahu, 1964).

5.3 Linear discriminant function (LDF)

Based on grain size, the linear discriminant function (LDF) was employed to understand energy variations. The results of fluidity factors also show a strong correlation between the various processes and the depositional environment (Sahu, 1964; Rajganapathi et al. 2013; Kulkarni et al. 2015) (Table 5.2 and Table 5.3). To distinguish between the various processes and depositional environments, the modified versions of Sahu (1964) linear discriminant functions of Y1 (aeolian and beach), Y2 (beach and shallow marine), Y3 (shallow marine and deltaic or lacustrine) and Y4 (turbidity and deltaic) were used. The sediments grain size statistical parameters that are utilized to differentiate between beach (b) and aeolian (aeol) below equation was applied:

$Y1_{(aeol:\ b)} = -3.5688M_Z + 3.7016\sigma_I 2 - 2.0766\ SK_I + 3.1135K_G$

Where, the environment is "aeolian " if Y1 is < -2.7411, and "beach" if Y1 is >-2.7411

Again, in order to distinguish between beach (B) and shallow marine (SM) environments the following equation is applied.

$Y2(B:SM) == 15.6534\ M_Z + 65.7091\ \sigma_1 2 + 18.1071\ SK_I + 18.5043\ K_G$

The environment is "beach (B)" if Y2 is < −63.3650, and the environment is "shallow marine" (SM) if Y2 is > −63.3650,

To distinguish the environment of deposition between shallow marine (SM) and deltaic or lacustrine (L), the following equation was applied:

$Y3(SM: F) = 0.2852\ M_Z - 8.7604\ \sigma_1 2 - 4.8932\ SK_I + 0.0482\ K_G$

Where the environment is shallow marine if Y3 is > −7.4190, and the environment is deltaic or lacustrine if Y3 is < −7.4190. Another LDF equation that differentiates between deltaic (D) and turbidity current deposits (T) can be written as

$Y4(F: T) = 0.7215\ M_Z - 0.4030\ \sigma_1 2 + 6.7322\ SK_I + 5.2927\ K_G$

If Y4 is < 9.8433, it implies turbidity current deposition; if Y4 is > 9.8433, it suggests deltaic deposition. Where M_Z, σ_1, S_{KI}, and K_G respectively represent mean grain size, standard deviation, skewness, and kurtosis.

Table 5.2. The classification of depositional environments by Sahu (1964) for the Upper Bhuban Formation.

Discriminate functions					**Depositional Environments**			
Sample No.	Y1	Y2	Y3	Y4	Y1	Y2	Y3	Y4
AR#4	0.78	178.70	-17.78	6.56	Beach	Shallow agitated marine	Fluvial	Turbidity current
AR#5	0.35	173.20	-15.17	4.59	Beach	Shallow agitated marine	Fluvial	Turbidity current
AR#6	-4.13	92.36	-5.78	6.87	Aeolian	Shallow agitated marine	Shallow agitated marine	Turbidity current
AR#7	0.76	197.83	-17.00	2.75	Beach	Shallow agitated marine	Fluvial	Turbidity current
ZT#3	1.47	220.44	-21.81	4.78	Beach	Shallow agitated marine	Fluvial	Turbidity current
ZT#6A	-2.49	104.81	-5.02	4.75	Beach	Shallow agitated marine	Shallow agitated marine	Turbidity current
ZT#6B	-1.28	115.75	-6.39	4.45	Beach	Shallow agitated Marine	Shallow agitated marine	Turbidity current
ZT#7	-1.71	135.81	-8.66	5.16	Beach	Shallow agitated marine	Fluvial	Turbidity current
ZT#10	-1.92	103.53	-3.72	7.67	Beach	Shallow agitated marine	Shallow agitated marine	Turbidity current
PK#7A	2.00	209.69	-19.88	4.39	Beach	Shallow agitated marine	Fluvial	Turbidity current
PK#7C	2.77	220.26	-21.84	4.22	Beach	Shallow agitated marine	Fluvial	Turbidity current
PK#8A	-0.01	184.68	-14.88	2.23	Beach	Shallow agitated marine	Fluvial	Turbidity current
SS#1A	0.69	190.46	-17.66	4.39	Beach	Shallow agitated marine	Fluvial	Turbidity current
SS#2A	0.41	186.47	-17.18	4.45	Beach	Shallow agitated marine	Fluvial	Turbidity current
SS#3A	-0.25	175.46	-14.70	3.50	Beach	Shallow agitated marine	Fluvial	Turbidity current

Table. 5.3. The classification of depositional environments by Sahu (1964) for the Middle Bhuban Formation

AR#1	0.72	171.85	-14.94	4.42	Beach	Shallow agitated marine	Fluvial	Turbidity current
AR#2	-0.04	131.54	-11.02	6.13	Beach	Shallow agitated marine	Fluvial	Turbidity current
AR#3	2.48	180.89	-18.43	8.47	Beach	Shallow agitated marine	Fluvial	Turbidity current
ZT#1	1.56	187.86	-17.48	4.42	Beach	Shallow agitated marine	Fluvial	Turbidity current
ZT#2	1.11	174.76	-16.85	6.29	Beach	Shallow agitated marine	Fluvial	Turbidity current
ZT#4	2.99	227.31	-24.14	6.48	Beach	Shallow agitated marine	Fluvial	Turbidity current
PK#1B	0.63	191.18	-16.95	3.43	Beach	Shallow agitated marine	Fluvial	Turbidity current
PK#1C	0.86	187.77	-16.07	3.30	Beach	Shallow agitated marine	Fluvial	Turbidity current
PK#2	0.38	193.90	-16.81	4.06	Beach	Shallow agitated marine	Fluvial	Turbidity current
PK#3	0.70	179.95	-16.25	4.45	Beach	Shallow agitated marine	Fluvial	Turbidity current
PK#4	2.66	218.46	-22.02	5.23	Beach	Shallow agitated marine	Fluvial	Turbidity current

The linear Discriminant Function (LDF) of the Y1 equation suggests that the sediments have been deposited in a beach environment, where Y2 values show shallow agitated marine deposits. Based on Y3 values, the majority of the samples are classified as belonging to the fluvial environment, while only a few samples are lying in the shallow agitated marine deposits, and Y4 values indicate that the samples were deposited under the influence of fluvial turbidity action. The binary plot of Y2 versus Y1 (Sahu, 1964) showed that most of the Bhuban samples lie in the beach/shallow marine environment (Fig. 5.11). Another binary plot of Y3 versus Y2 indicates that the samples were deposited in a field of fluvial/agitated environment (Fig. 5.12). Furthermore, the plot of Y4 against Y3 (Fig. 5.13), directly reflects that all the samples from the Bhuban Formation are turbidity current deposits under the fluvial influence. Thus, based on different parameters of LDF suggested that the sediments have been deposited in shallow marine conditions under the strong influence of fluvial characteristics.

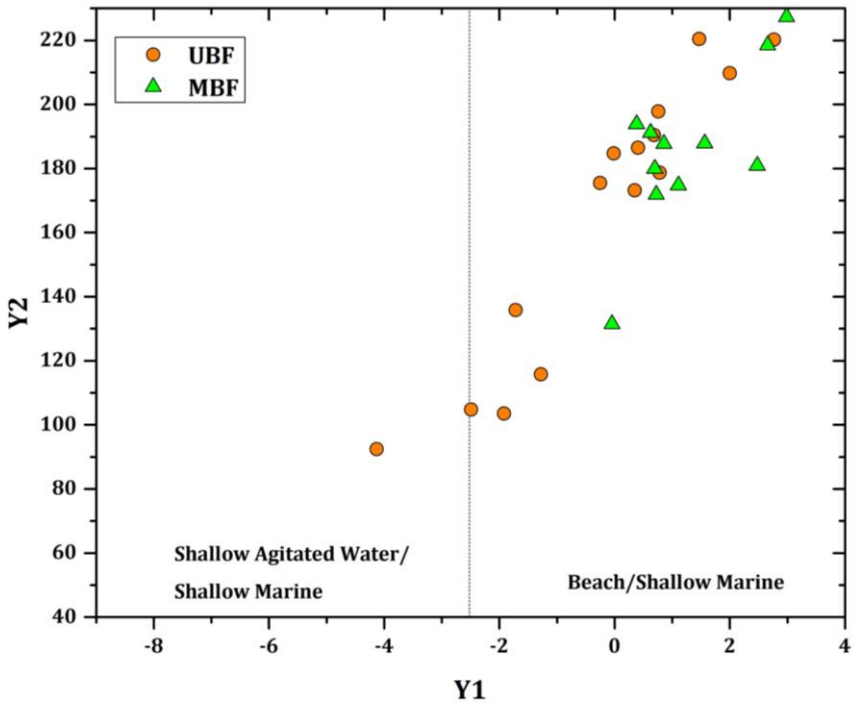

Figure 5.11. Linear discrimination function (LDF) (after Sahu, 1964), showing the relationship between Y1 vs Y2, indicating the depositional environments and processes for Upper Bhuban Formation (UBF) and Middle Bhuban Formation (MBF).

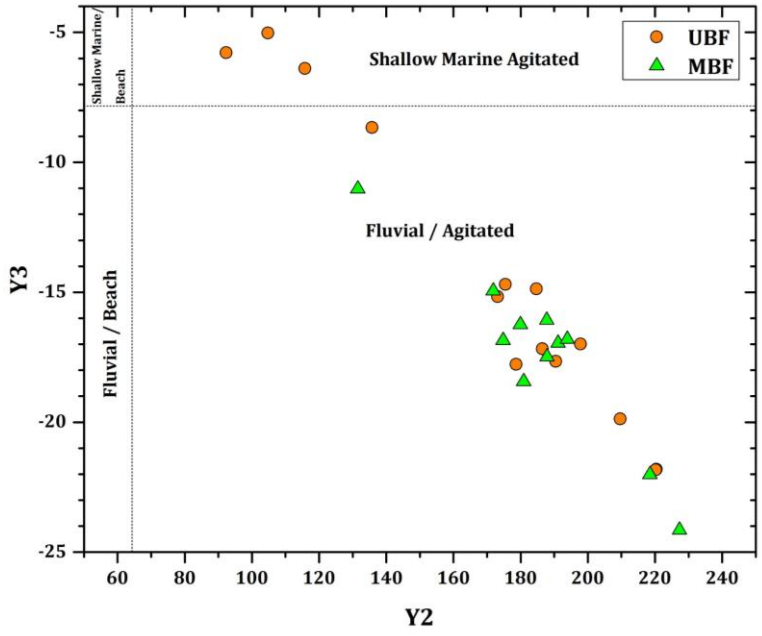

Figure 5.12. Linear discrimination function (LDF) (after Sahu, 1964), showing the relationship between Y2 vs Y3, indicating the depositional environments and processes for Upper Bhuban Formation (UBF) and Middle Bhuban Formation (MBF).

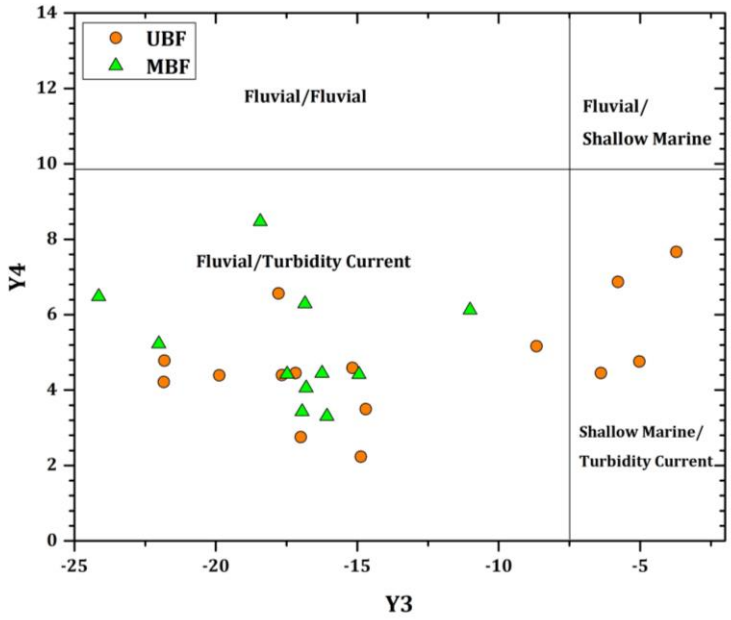

Figure 5.13. Linear discrimination function (LDF) (after Sahu, 1964), showing the relationship between Y3 vs Y4, indicating the depositional environments and processes for Upper Bhuban Formation (UBF) and Middle Bhuban Formation (MBF).

5.4 Passega diagram (C-M Pattern)

Passega (1957) developed a C-M plot which helps to understand the role of hydrodynamic forces in sediment deposition. The C-M is a bivariate plot of the median values (M) in microns versus the coarser one-percentile value (C) in microns on a log-probability scale. According to Visher, (1969), the relationship between C and M depends on the sediment type, as well as the energy of the transport medium. On the C-M diagram of Passega (1957), the majority of the analyzed samples are clustered towards the fields between the P-Q region (Fig. 5.14), which illustrates that the transport mechanisms of Bhuban sediments were deposited by suspension with some rolling nature. As a result, the transportation of sediments mostly finer and medium fractions deposited in a fluvial-dominated condition.

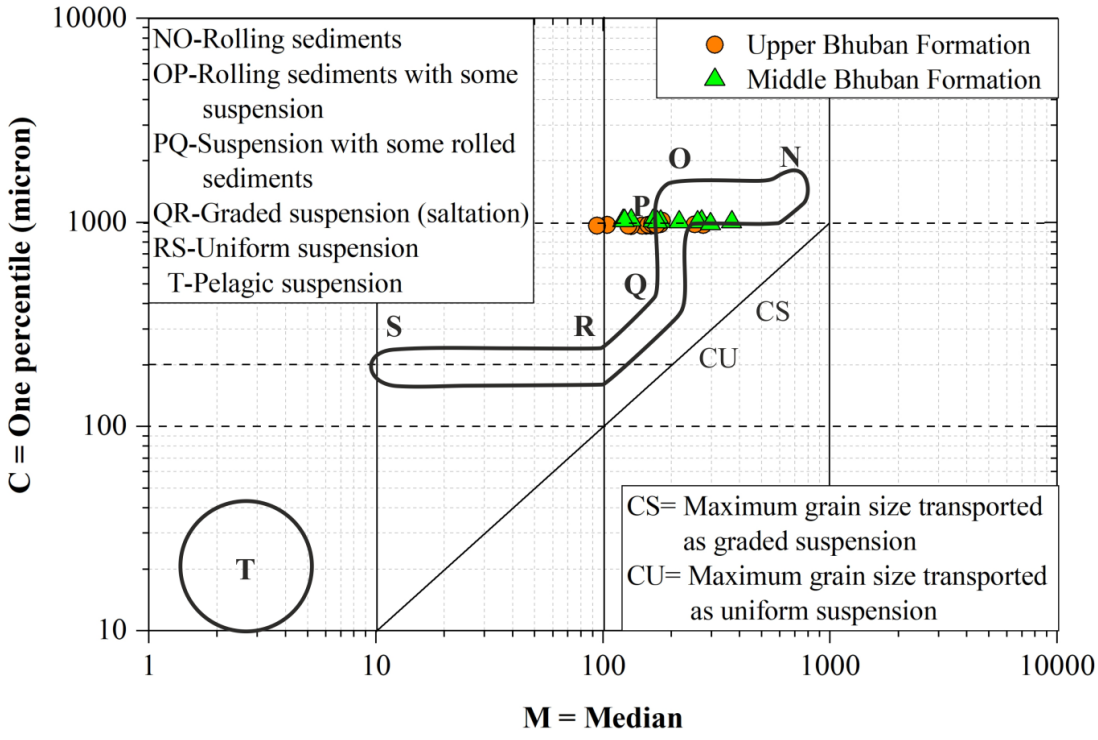

Figure 5.14. The C-M plot shows the transporting mechanism for the sandstones in the study area (after Passega, 1964).

5.5 Discussion and Interpretation

The Bhuban sandstones have been interpreted based mostly on univariate grain size parameters, bivariate plots, linear discriminant function, and log–log probability curves, and the C–M pattern. According to the grain size distribution,

Bhuban sediments are predominantly fine-grained, poorly sorted to moderately sorted, platykurtic to mesokurtic, and mainly coarse-skewed. The nature of fine-grained sediments points to the fact that moderately low-energy conditions dominated in the study area. The poorly to moderately sorted nature of the sediments is due to the short to moderate distance of sediment transportation, and their characteristics indicate that they were deposited in a shallow marine condition with the influence of fluvial characteristics. The dominance of the coarse skewed category indicates that during the deposition of sediments, there was moderate to high-energy condition with some riverine input. The univariate grain size parameters of volume percent frequency curves show that most of the Bhuban sediments are bimodal with peaks of 1.0, 3.5, and 4.0 due to low to medium energy conditions of the marine setting at the time of deposition. Various linear discriminant functions also suggest that sediments have been deposited in a shallow marine setup with the influence of fluvial process and turbidity action. The C–M pattern signifies that the transport mechanisms of the analysed sediments were mostly deposited by suspension with some rolling sediments, which resulted in finer to medium fractions under the influence of fluvial action in marine conditions.

CHAPTER-6

HEAVY MINERAL STUDY

6.1 Introduction

The analysis of heavy minerals and their properties in sedimentary rock is one of the oldest endeavors in sedimentary petrology. It is extensively used as a reference for source-rock characterization, assessments of lithological variation, heavy mineral zonation, and dispersal pattern, and it also aids in giving a mineralogical basis by which two source locations may be separated from one another (Morton et al. 1992). Heavy minerals are accessory minerals with a concentration of less than 1 percent and a specific gravity of greater than 2.89 g/cm^3, as well as a volumetric weight of fewer than 1 percent of terrigenous rocks (Folk, R.L. 1980). Heavy mineral composition of sandstones is commonly employed in provenance investigations in sedimentary petrology. The detrital sediments that contain accessory minerals are comprised of several distinct mineral species, each with its unique history. As a result of their deposition nature, transportation behaviors, and alteration of physical and chemical properties which could lead to reveal their provenance. The mineral assemblage can be a direct indication of the supply of sediments from their parent rocks such as igneous, metamorphic, or even sedimentary (Sengupta, 1996). The heavy mineral assemblage in sediment is mainly governed by the provenance, source area weathering, transport mechanism, deposition, and post-depositional modification (Morton, and Hallsworth. 1994).

6.2 Heavy Mineral Descriptions

The heavy mineral assemblages of Bhuban sandstone included Zircon, Tourmaline, Rutile, Garnet, Apatite, Chlorite, Epidote, Diopside, Augite, Kyanite, Staurolite, Sillimanite, and non-opaque minerals which are presented in the Table 6.1 & 6.2. The identified heavy minerals and their characteristics are discussed below.

6.2.1 Zircon

Zircon grains, the most stable non-opaque heavy mineral observed in the studied sediments (Figure 6.1.D-E-F), exhibit subangular to subrounded edges, usually colorless with parallel extinction. Dominating the heavy mineral assemblage, Zircon constitutes an average of 29.93%, followed by tourmaline and rutile for the Bhuban

Formation including the Upper and Middle Bhuban Formations (UBF is 21.36% and MBF 22.38%). The sub-rounded edge of Zircon, as suggested by Krumbein et al. 1938 indicates its origin from reworked sediments with a significant amount of transportation through the depositional medium.

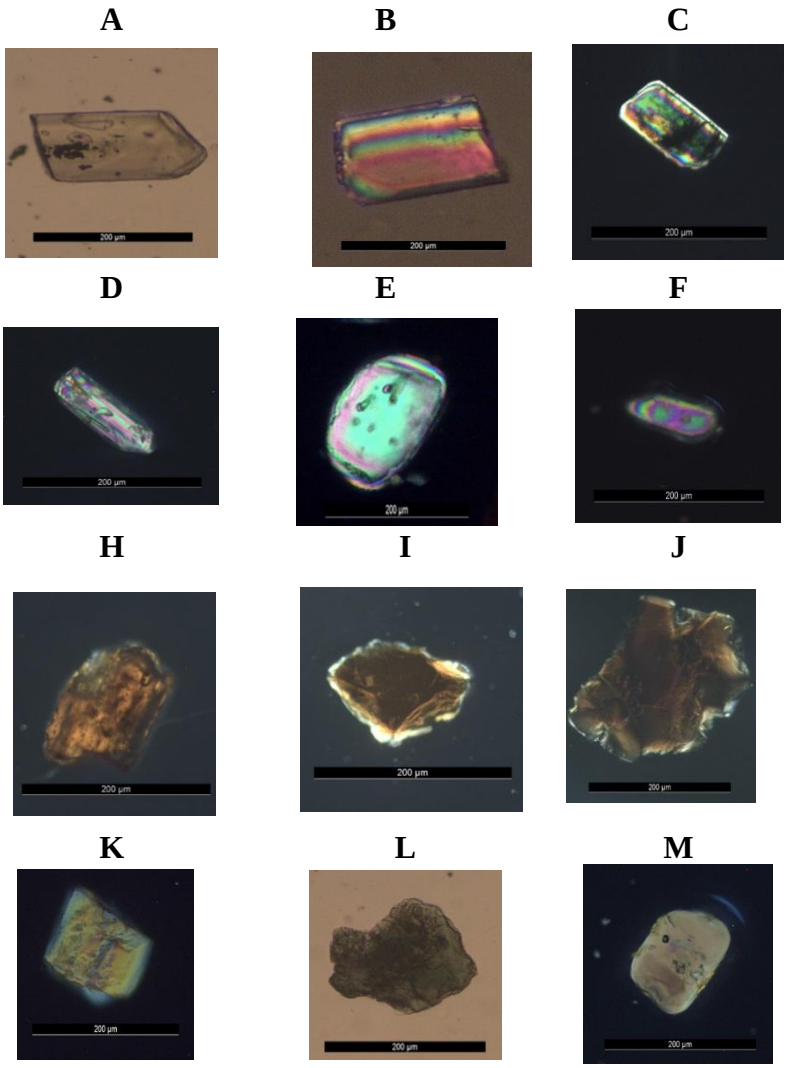

Figure 6.1. Photomicrographs of heavy minerals from Bhuban sandstone Tourmaline (A-C), Zircon (D-F), Rutile (H-J), Sillimanite (K), Chlorite (L), Epidote (M).

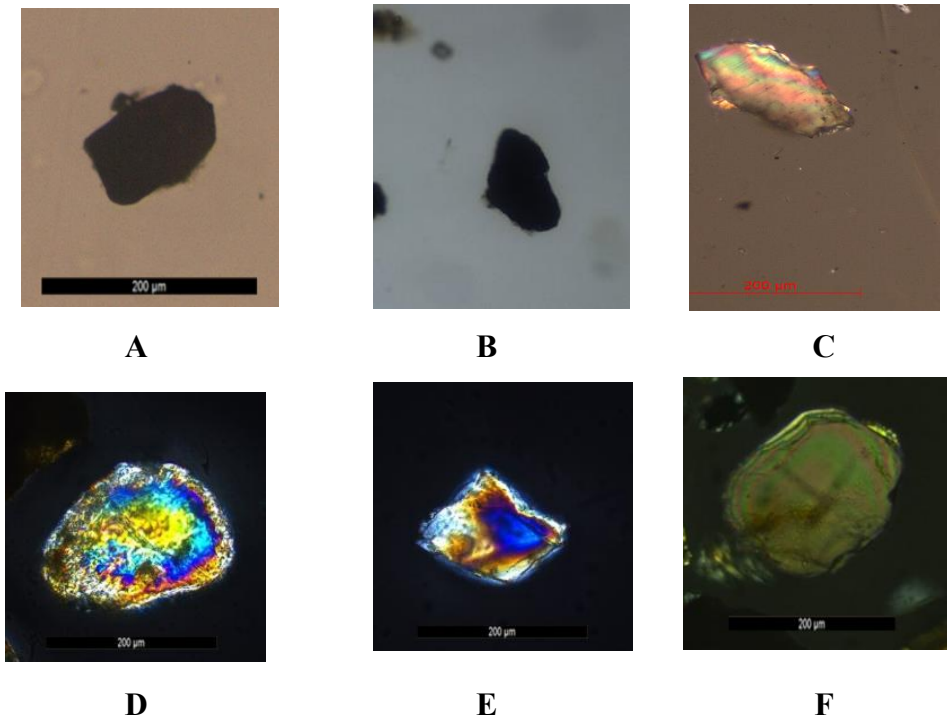

Figure 6.2. Photomicrographs of heavy minerals from Bhuban sandstone Garnet (A) opaque Mineral (B) Kyanite (C), Diopside (D) Augite (E) Staurolite (F)

6.2.2 Tourmaline

The grains exhibit pleochroism, and prismatic shapes, as well as range in color from pale green to grayish, comprising an average of 15.34% of the total heavy mineral assemblage for both Formations where UBF is 15.25% and MBF 15.70%. They are predominantly subhedral to subrounded in shape, with some grains displaying a rounded form. Extinction is generally parallel (Figure 6.1. A, B, C).

6.2.3 Rutile

Rutile stands out among other heavy minerals with its distinctive rich blood red, brownish red, or yellowish-brown color. Characterized by a high refractive index, no cleavage, and the presence of both euhedral and subhedral forms, as well as a short prismatic form, it makes up an average of 10.84% of the total heavy mineral assemblage for both the Formation where UBF is 13.65% and MBF 13.17% (Figure 6.1 H, I, J).

6.2.4 Garnet

In the heavy mineral assemblage, detrital garnets appear as euhedral, sharp irregular fragments, and sub-rounded to rounded grains. They typically exhibit colors ranging from colorless to light pale pink or pale brown. The mineral is easily identifiable due to its high relief and isotropic nature. Garnets make up an average of 6.22% of the total heavy mineral assemblage (Figure. 6.2A).

Table 6.1. The percentages of Heavy minerals and ZTR Index of Bhuban sandstones for the Upper Bhuban Formation in the study area (where, Zr=Zircon, Tr=Tourmaline, Rt=Rutile, Ky=Kyanite, Si=Sillimanite, Ep=Epidote, Cl= Chlorite, Hornblende, Bt=Biotite, Gr=Garnet, Ap=Apatite, Au= Augite, St=Staurolite, Di=Diopside, Op=Opaque minerals,

Sample No.	Zr	Tr	Rt	Ky	Si	Ep	Cl	Hb	Bt	Gr	Ap	Au	St	Di	Op	ZTR
AR#4	23.53	16.81	14.29	5.88	3.36	1.68	1.68	2.52	3.36	4.20	2.52	1.68	0.84	1.68	14.29	54.62
AR#5	23.01	16.81	13.27	5.31	7.08	2.65	0.00	0.88	2.65	3.54	1.77	0.00	2.65	1.77	18.58	53.10
AR#6	19.13	14.78	11.30	7.83	2.61	0.87	2.61	3.48	5.22	4.35	3.48	0.87	5.22	1.74	16.52	45.22
AR#7	20.65	11.96	15.22	7.61	6.52	5.43	0.00	2.17	2.17	1.09	2.17	2.17	3.26	2.17	17.39	47.83
ZT#3	22.12	15.38	12.50	8.65	6.73	1.92	0.96	2.88	0.96	3.85	1.92	0.96	0.96	1.92	17.31	50.00
ZT#6A	23.58	19.81	16.04	7.55	8.49	0.94	0.00	0.00	1.89	2.83	0.94	2.83	0.00	1.89	14.15	59.43
ZT#6B	23.20	15.20	17.60	8.00	6.40	0.00	2.40	1.60	2.40	4.00	1.60	0.00	1.60	1.60	15.20	56.00
ZT#7	21.52	13.92	11.39	6.33	7.59	3.80	2.53	0.00	2.53	3.80	0.00	1.27	2.53	2.53	18.99	46.84
ZT#10	25.24	17.48	12.62	6.80	4.85	0.97	2.91	0.97	0.00	4.85	1.94	1.94	2.91	1.94	16.50	55.34
PK#7A	22.86	18.10	13.33	8.57	6.67	0.00	1.90	2.86	2.86	0.95	2.86	0.00	2.86	1.90	14.29	54.29
PK#7C	16.50	10.68	12.62	5.83	5.83	1.94	4.85	0.97	3.88	4.85	2.91	1.94	1.94	1.94	20.39	39.81
PK#8A	22.50	11.67	15.00	6.67	3.33	3.33	2.50	0.00	1.67	0.00	1.67	3.33	2.50	1.67	22.50	49.17
SS#1A	21.25	18.75	13.75	8.75	3.75	1.25	0.00	3.75	1.25	2.50	0.00	3.75	5.00	2.50	13.75	53.75
SS#2A	19.81	15.09	12.26	8.49	6.60	2.83	0.94	1.89	1.89	3.77	0.94	3.77	0.00	1.89	18.87	47.17
SS#3A	16.05	12.35	13.58	4.94	9.88	0.00	2.47	0.00	3.70	3.70	1.23	2.47	3.70	2.47	25.93	41.98
Avg	21.36	15.25	13.65	7.14	5.97	1.84	1.71	1.59	2.42	3.21	1.73	1.79	2.39	1.97	17.64	50.30

Table 6.2. The percentages of Heavy minerals and ZTR Index of Bhuban sandstones for the Middle Bhuban Formation in the study area (where, Zr=Zircon, Tr=Tourmaline, Rt=Rutile, Ky=Kyanite, Si=Sillimanite, Ep=Epidote, Cl= Chlorite, Hornblende, Bt=Biotite, Gr=Garnet, Ap=Apatite, Au= Augite, St=Staurolite, Di=Diopside, Op=Opaque minerals

Sample No.	Zr	Tr	Rt	Ky	Si	Ep	Cl	Hb	Bt	Gr	Ap	Au	St	Di	Op	ZTR
AR#1	21.69	14.46	18.07	8.43	4.82	0.00	2.41	0.00	2.41	6.02	2.41	0.00	0.00	2.41	18.07	54.22
AR#2	25.22	14.78	12.17	7.83	6.09	2.61	0.87	1.74	2.61	2.61	0.87	0.00	2.61	1.74	19.13	52.17
AR#3	26.74	16.28	13.95	6.98	4.65	1.16	0.00	3.49	1.16	0.00	0.00	2.33	3.49	2.33	19.77	56.98
ZT#1	19.18	13.70	12.33	6.85	4.11	1.37	0.00	2.74	2.74	4.11	1.37	1.37	2.74	2.74	27.40	45.21
ZT#2	24.37	15.13	12.61	5.88	6.72	3.36	2.52	0.00	3.36	0.84	1.68	2.52	1.68	1.68	19.33	52.10
ZT#4	24.11	15.18	11.61	8.04	5.36	2.68	0.00	1.79	2.68	1.79	0.89	4.46	2.68	1.79	16.96	50.89
PK#1B	22.33	14.56	10.68	6.80	3.88	4.85	1.94	0.97	2.91	3.88	1.94	0.00	1.94	1.94	20.39	47.57
PK#1C	22.02	15.60	11.93	5.50	7.34	2.75	0.92	2.75	0.00	0.92	2.75	4.59	1.83	1.83	20.18	49.54
PK#2	13.98	18.28	13.98	7.53	4.30	2.15	5.38	0.00	3.23	2.15	1.08	2.15	1.08	2.15	24.73	46.24
PK#3	22.22	14.81	11.11	4.94	7.41	0.00	2.47	1.23	1.23	4.94	6.17	2.47	3.70	2.47	17.28	48.15
PK#4	24.35	20.00	16.52	2.61	6.09	0.00	0.87	1.74	0.00	0.87	1.74	3.48	0.87	1.74	18.26	60.87
Avg	22.38	15.70	13.17	6.49	5.52	1.90	1.58	1.49	2.03	2.55	1.90	2.12	2.05	2.07	20.13	51.26

6.2.5 Chlorite

The detrital chlorite presents as greenish in color, displaying in the form of thin, flaky, oval, or irregular shapes, with no pleochroism observed. On average, they constitute about 1.74% of the total heavy mineral assemblage for both the Upper and Middle Bhuban Formations. (Figure 6.1 L).

6.2.6 Sillimanite

The sillimanite develops as a thin elongated prismatic habit with colorless grains showing parallel extinction and distinct cleavage. Sillimanite comprises an average of 3.38% of total heavy mineral assemblages for Upper and Middle Bhuban Formations. (Figure 6.1K).

6.2.7 Kyanite

The kyanite has angular to bladed or even prismatic grain texture is usually is colorless, weakly pleochroic, and has cross-fractures and step-like features. Kyanite constitutes an average of 4.77% of the total heavy mineral assemblage (Figure 6.2C).

6.2.8 Epidote

The mineral grains of epidote are commonly greenish-yellow and pleochroic, displaying a subrounded to rounded shape. Epidote minerals have a low extinction angle and constitute approximately 2.19% of the total heavy mineral assemblage for both the Upper and Middle Bhuban Formations. (Figure 6.1M).

6.2.9 Opaque Minerals

The opaque minerals cannot be adequately described due to their lack of distinct optical properties. The opaque minerals show diverse habits with forms being cubic or rhombohedral. However, some are distinct as hematite and magnetite. On average, opaque minerals make up about 20.61% of total heavy mineral assemblages for both the Upper and Middle Bhuban Formations (Figures 6.2.B)

6.3 ZTR Maturity Index and Provenance

According to Hubert (1962), the Zircon-Tourmaline-Rutile (ZTR) index aids in evaluating the mineralogical maturity of sedimentary rocks. When the ZTR index is below 75%, sediments are classified as mineralogically immature or sub-mature. The present work on the ZTR index of the Bhuban Formation ranges from 39.81% to 60.81%, with an average of approximately 50.71%. Where the Upper Bhuban

Formation's average ZTR maturity index is 50.30% and in the Middle Bhuban Formation the average maturity index is 51.26% This result reveals that the Bhuban sediments are mineralogically immature. Subsequently, the ZTR triangular diagram reveals that all samples fall within the A1 tier of the A block (Figure 6.3). This suggests that the zircon proportion is the highest, followed by tourmaline and rutile. The presence of kyanite, staurolite, sillimanite, tourmaline, etc., indicates a derivation from acid igneous and crystalline metamorphic rocks (Ramamoorthy et al. 2015). Additionally, the presence of prismatic and angular zircon grains, along with a high percentage of opaque minerals, further supports the indication of an igneous source.

The subhedral and rounded zircon grains, as shown in (Figure 6.1.D-E-F), suggest their derivation from reworked sedimentary sources. The presence of kyanite in the samples indicates a metamorphic source for the sediments, possibly from a region with a higher degree of metamorphism, such as the Higher Himalaya where kyanite-grade metamorphism is commonly found. This suggests that the sediments for both the Upper and Middle Bhuban Formations may have originated from the Himalayan terrain.

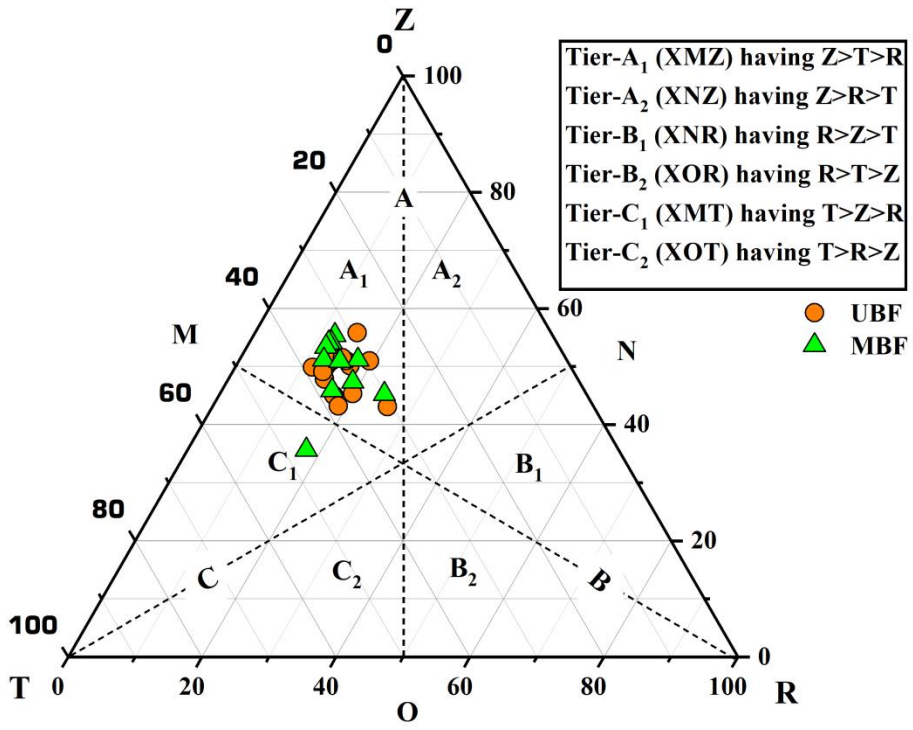

Figure 6.3. The ZTR maturity index of Bhuban sandstones in the study area (After Hubert, 1962).

6.4 Conclusion

The abundance of euhedral zircon and rutile in the rocks suggests an origin from acidic igneous and crystalline metamorphic rocks, with sediment transportation over a short to moderate distance. Prismatic and angular zircon grains, along with a notable proportion of opaque minerals, further indicate an igneous rock source. However, the presence of rounded zircons, tourmalines, and rutile's suggests that sedimentary rocks might have been recycled and transported over a considerable distance. The zircon fragments imply a short to moderate transportation distance, and the low ZTR index for Bhuban sediments indicates mineralogical immaturity. Additionally, the presence of kyanite, staurolite, sillimanite, tourmaline, and rutile in the examined Bhuban sandstones points to a high-rank metamorphic source.

CHAPTER-7

SANDSTONE GEOCHEMISTRY

7.1 Introduction

Sandstone geochemistry has been widely employed in worldwide studies to elucidate the sedimentological evolution of a sedimentary basin over geological time. This geochemical analysis, which is closely linked to the mineral composition of the rocks, helps understand processes like weathering, diagenesis, and provenance. Furthermore, rare earth geochemistry serves as a valuable tool in comprehending sediment recycling and maturation, offering insights into ancient sedimentary histories. Trace and rare earth elements (REE) play a crucial role in identifying provenance, tectonic settings, and discerning between felsic and mafic contributions in the source region (Pettijohn et al. 1972; Taylor and McLennan 1985; Lindsey1999; Bhatia and Crook 1986, McLennan et al. 1993). Tectonism has been proposed as the primary influence on sedimentary composition (Pettijohn et al. 1972; Blatt et al. 1980). The chemical composition of clastic sedimentary rocks is determined by the relationships between plate tectonic features (e.g., plate instability, plate interaction, geothermal, burial depth, and pressure gradients) and variables including origin, relief, physical sorting, and diagenesis. Therefore, to identify signatures of source rocks and tectonic settings in the compositions of various modern and ancient sandstone suites, it is essential to have a thorough understanding of the geochemical characteristics of these suites. Moreover, it allows for inferring how elements were redistributed both during and after deposition.

In this study, 20 representative samples from the Surma Group of Bhuban Formation both Upper Bhuban and Middle Bhuban Formations were chosen for whole-rock geochemical analysis to ascertain the source area characteristics, framework of the tectonic setting, provenance, paleo weathering, and paleoclimate of sandstone.

7.2 Major Oxides

Bhuban sandstones (hereafter, UBF: Upper Bhuban Formation; MBF: Middle Bhuban Formation) are enriched in SiO_2 (UBF: 63.17; MBF: 66.11 wt.%), moderately

enriched in Al_2O_3 (UBF: 12.55; MBF: 13.11 wt.%), Fe_2O_3 (UBF: 6.82; MBF: 6.23 wt.%), MgO (UBF: 3.44; MBF: 2.07 wt.%), Na_2O (UBF: 1.33; MBF: 1.54 wt.%) and K_2O (UBF: 2.81; MBF: 2.72 wt.%), while depleted in MnO (UBF: 0.09; MBF: 0.13 wt.%), CaO (UBF: 2.08; MBF: 1.61 wt.%), TiO_2 (UBF: 0.98; MBF: 1.00 wt.%) and P_2O_5 (UBF: 0.17; MBF: 0.18 wt.%). The major element contents of Bhuban sandstones are presented in Table 7.1. In the studied area, the Upper Bhuban Formation exhibits a moderate to weak positive correlation of SiO2 (r=0.03), Fe2O3 (r=0.36), Na2O (r=0.07), TiO2 (r=0.53), and P2O5 (r=0.12) with Al2O3, where "r" represents the correlation coefficient. Conversely, MnO (r=-0.30), MgO (r=-0.04), K2O (r=-0.28), and CaO (r=-0.51) show negative correlations with Al2O3. On the other hand, the Middle Bhuban Formation show a moderate positive correlation of SiO2 (r=0.52), Na2O (r=0.38), TiO2 (r=0), P2O5 (r=0.61), and K2O (r=0.36) with Al2O3. While negative correlations are observed for Fe2O3 (r=-0.59), MnO (r=-0.71), MgO (r=-0.79), and CaO (r=-0.61) with Al2O3 (Figure 7.1 and Table 7.1). A positive correlation of these oxides indicates their enrichment possibly due to their association with rock fragments of sandstones and/or clay minerals while a negative correlation indicates either alteration and/or leaching during sedimentation processes. The correlation between Fe_2O_3 and TiO_2 is positive (r=UBF: 0.30; MBF: 0.60) and enrichment of both elements in the sediments implies the presence of Fe and Ti-bearing heavy minerals. Occasionally, Fe_2O_3 (UBF: 6.82 wt.%; MBF: 6.22 wt.%) gets enriched due to diagenesis, this is also supported by the lower concentrations of Ni, Cr, and V which represents syngenetic and early diagenetic precipitation of Fe oxides. The variation in SiO_2/Al_2O_3 (UBF: 5.06; MBF: 5.07) is higher, so it can be assumed that the ratio increases concerning weathering, recycling, and sediment transport. The population of quartz grains increases with the process that causes the leaching of less resistant minerals. Fyffe and Pickerill (1993) suggested that the higher ratio of Al_2O_3/TiO_2 indicates probable continental derivation of sediments, for Bhuban sandstones this ratio is UBF: 13.07; MBF: 13.66. In Figure 7.1 the correlation between various oxides is represented while Figure 7.2 shows the UCC normalized patterns of the samples representing a depletion of CaO and Na_2O concentrations and an enrichment of TiO_2, Fe_2O_3, and MgO.

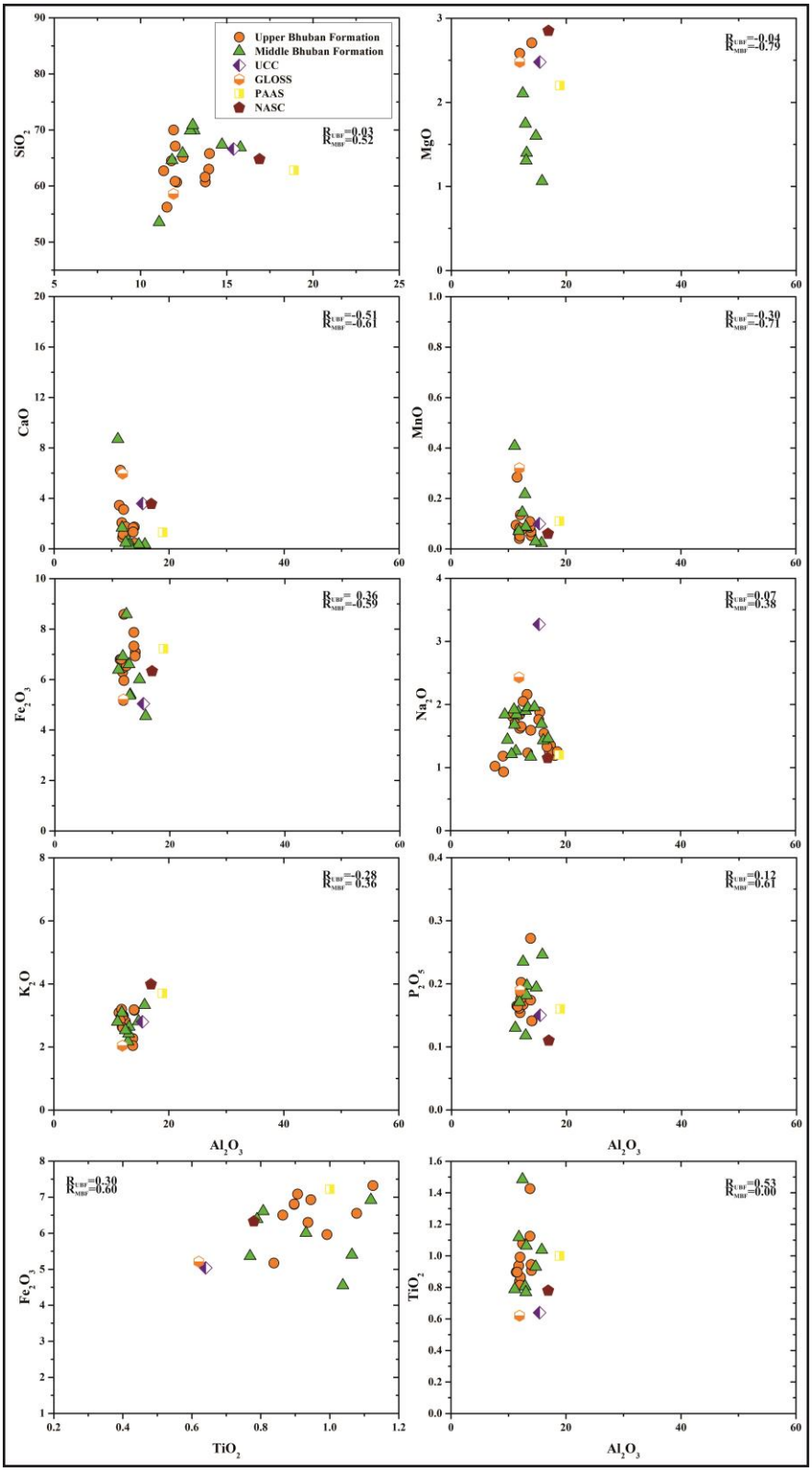

Figure. 7.1: Variation diagram / Harkar Plot for correlation between wt.% of SiO_2 vs major oxides.

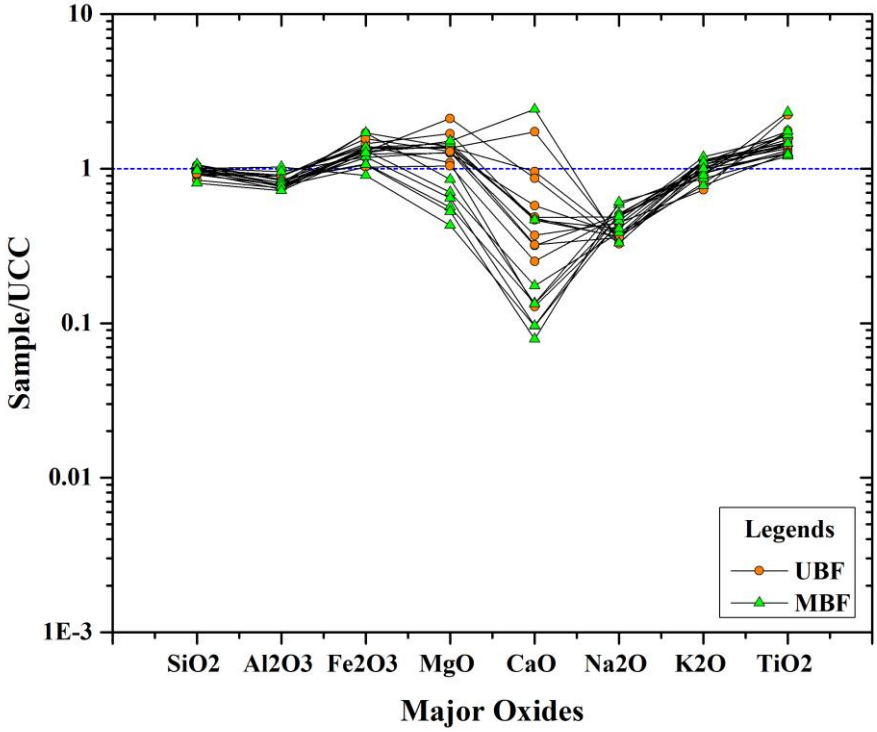

Figure 7.2. The UCC normalized plot for major oxides of the Upper Bhuban Formation and Middle Bhuban Formation.

7.3 Sandstone classification

The classification schemes of Pettijohn et al. (1973) and Blatt and Murray (1980) are frequently used to classify sandstones. Figure 7.3A represents the classification of Pettijohn *et al.* (1973) using the logarithmic values of the ratio of (SiO_2/Al_2O_3) vs (Na_2O/K_2O) which predicts that most of the Bhuban samples are litharenite followed by a few arkoses. Again, the ternary plot of Blatt *et al.* 1980), uses the wt.% values of Na_2O, (Fe_2O_3+MgO), and K_2O to classify the sandstones into greywacke, arkose, and lithic sandstone. Figure 7.3B shows that the samples are confined to the field of lithic sandstone. By integrating different geochemical schemes of classification, Bhuban sandstones are primarily identified as litharenite, with arkose and wacke types.

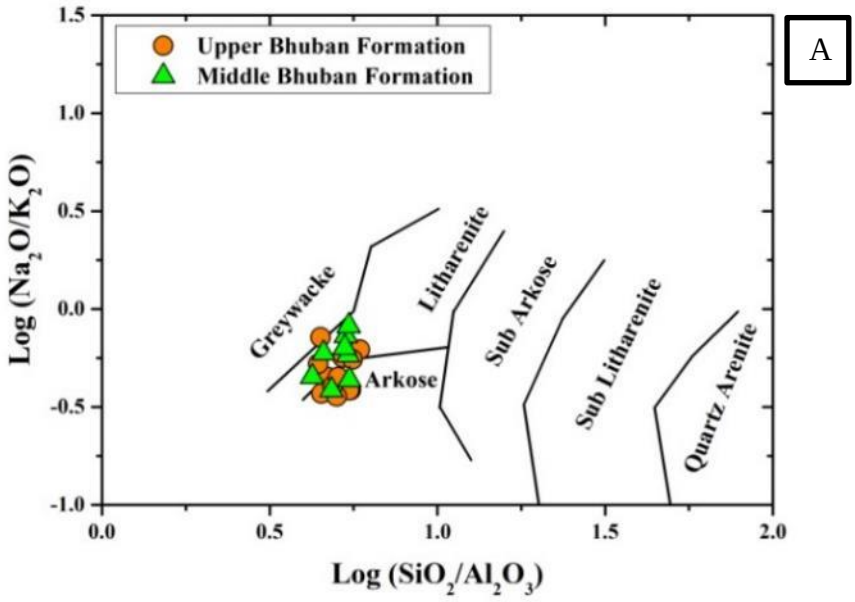

Figure. 7.3 A. Log (SiO_2/ Al_2O_3) vs Log (Na_2O_3/K_2O) classification of Bhuban sandstones, Mizoram (Pettijohn et al.1972).

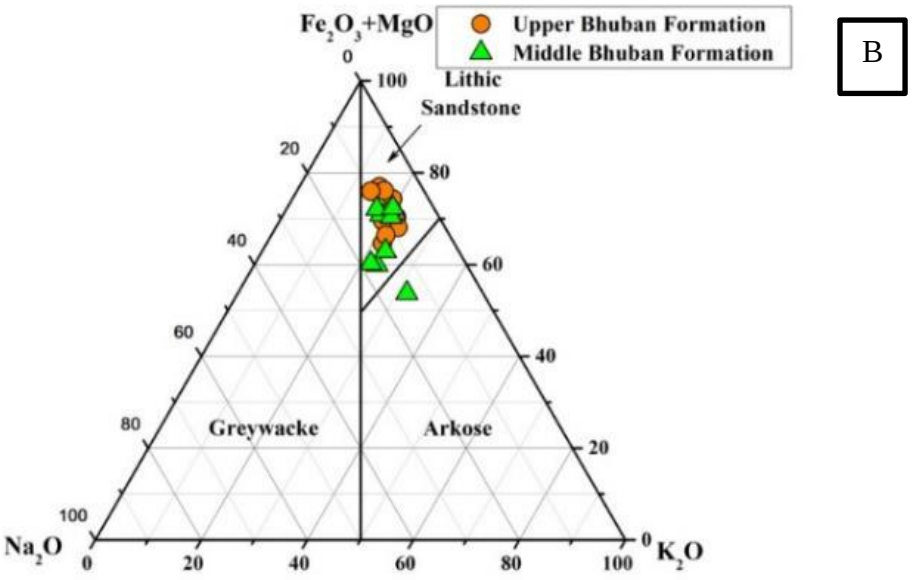

Figure.7.3B. Na_2O-(Fe_2O_3+MgO)-K_2O ternary plot for Bhuban sandstone classification (Blatt et al. 1980).

Table 7.1. Major elements in terms of wt.% and their corresponding elemental ratio of Upper Bhuban Formation and Middle Bhuban Formation.

Lithounit	**Upper Bhuban Formation (UBF)**											
Sample No.	**AR#4**	**AR#5**	**AR#7**	**PK#7A**	**PK#7C**	**PK#8A**	**SS#1A**	**SS#2A**	**SS#3A**	**ZT#6A**	**ZT#6B**	**ZT#7**
Major Oxides												
SiO_2	65.78	62.99	69.99	62.69	64.48	60.65	65.11	67.11	56.21	60.72	60.81	61.59
TiO_2	0.91	0.95	0.84	0.90	0.94	0.86	1.08	0.99	0.90	1.13	0.81	1.43
Al_2O_3	14.00	13.96	11.92	11.35	11.80	12.10	12.47	12.02	11.54	13.76	12.01	13.74
Fe_2O_3	7.08	6.93	5.17	6.80	6.30	6.50	6.55	5.96	6.81	7.32	8.58	7.87
MnO	0.05	0.07	0.04	0.09	0.06	0.14	0.08	0.05	0.28	0.09	0.08	0.11
MgO	2.71	3.39	2.58	3.41	3.12	5.24	3.48	3.17	3.37	4.18	3.42	3.20
CaO	0.46	1.72	0.90	3.44	2.07	3.12	1.74	1.14	6.22	1.67	1.15	1.33
Na_2O	1.42	1.18	1.63	1.19	1.23	1.07	1.59	1.64	1.15	1.19	1.17	1.46
K_2O	3.16	3.18	2.63	3.09	3.19	2.99	2.81	2.98	2.85	2.27	2.60	2.04
P_2O_5	0.14	0.14	0.15	0.17	0.16	0.20	0.17	0.18	0.16	0.17	0.19	0.27
SiO_2/Al_2O_3	4.70	4.51	5.87	5.52	5.47	5.01	5.22	5.58	4.87	4.41	5.06	4.48
Al_2O_3/TiO_2	15.43	14.77	14.23	12.65	12.59	14.01	11.56	12.11	12.86	12.23	14.76	9.64
K_2O/Al_2O_3	0.23	0.23	0.22	0.27	0.27	0.25	0.23	0.25	0.25	0.16	0.22	0.15
K_2O/Na_2O	2.22	2.70	1.62	2.60	2.60	2.80	1.77	1.81	2.47	1.91	2.23	1.39

Table 7.1. Cont...

Lithounit	**Middle Bhuban Formation (MBF)**							
Sample No.	**AR#1**	**PK#1B**	**PK#1C**	**PK#2**	**PK#3**	**PK#4**	**ZT#1**	**ZT#2**
Major Oxides								
SiO_2	66.87	69.91	69.87	67.38	70.87	65.82	64.62	53.54
TiO_2	1.04	1.06	0.81	0.93	0.77	1.49	1.12	0.79
Al_2O_3	15.80	13.11	12.89	14.72	13.03	12.44	11.82	11.08
Fe_2O_3	4.55	5.40	6.61	6.01	5.36	8.59	6.92	6.39
MnO	0.02	0.09	0.22	0.03	0.09	0.14	0.07	0.41
MgO	1.06	1.40	1.75	1.60	1.31	2.11	3.61	3.75
CaO	0.34	0.48	0.63	0.35	0.28	0.48	1.67	8.69
Na_2O	1.50	1.92	1.26	1.67	1.98	1.61	1.34	1.08
K_2O	3.33	2.64	2.17	2.81	2.42	2.53	3.09	2.80
P_2O_5	0.25	0.20	0.12	0.19	0.18	0.24	0.17	0.13
SiO_2/Al_2O_3	4.23	5.33	5.42	4.58	5.44	5.29	5.47	4.83
Al_2O_3/TiO_2	15.22	12.32	15.97	15.81	16.94	8.38	10.57	14.05
K_2O/Al_2O_3	0.21	0.20	0.17	0.19	0.19	0.20	0.26	0.25
K_2O/Na_2O	2.22	1.37	1.72	1.68	1.22	1.57	2.30	2.60

7.4 Trace Elements

The trace element concentrations of the Bhuban sandstones are presented in Table 7.2. Among the various trace elements, Large Ion Lithophile Elements (LILE) are enriched: Rb (UBF: 101.99, MBF: 92.32 ppm), Sr (UBF: 116.14, MBF: 94.47 ppm), Ba (UBF: 327.95, MBF: 350.51 ppm). While the High Field Strength Elements (HFSE) are depleted: Th (UBF: 20.29, MBF: 20.57 ppm), U (UBF: 3.05, MBF: 3.04 ppm), Hf (UBF: 7.41, MBF: 8.59 ppm), except Zr (UBF: 227.71, MBF: 264.07 ppm). Most Transitional elements are also depleted: Sc (UBF: 12.26, MBF: 11.18 ppm), Co (UBF: 12.48, MBF: 11.09 ppm), Ni (UBF: 26.15, MBF: 21.14 ppm), Cu (UBF: 25.63, MBF: 28.41 ppm), Zn (UBF: 39, MBF: 40.64 ppm), and Cr (UBF: 30.29, MBF: 28.58

ppm) except V (UBF: 82.62, MBF: 74.24 ppm) as compared to the UCC (Taylor and McLennan 1985). Due to the detrital association of zircons, Zr has a high concentration (UBF: 227.71, MBF: 264.07 ppm), while V enrichment is probably due to some intermediate/mafic input. Upper Continental Crust (UCC) normalized values of all the trace elements are plotted as shown in Figure 7.4 (Taylor and McLennan 1985), which shows the depletion of elements like Ba, Sr, Co, and Ni in comparison to UCC (Taylor and McLennan 1985). Some trace elements viz. Nb (R_{UBF}:0.61) Th (R_{UBF}:049, R_{MBF}:0.29), Zr (R_{UBF}:0.41, R_{MBF}:29), and V (R_{UBF}:0.11), are showing moderate to weak positive correlation with Al_2O_3. Similarly, Cr is positively correlated with Ni (R_{UBF}:0.48, R_{MBF}:0.17) and Rb also shows a strong positive correlation with K_2O (R_{UBF}:0.97, R_{MBF}:0.79). while Rb (R_{UBF}: -0.31, R_{MBF}: -0.21), Sr (R_{UBF}: -0.31, R_{MBF}:0.19), Nb (R_{MBF}: -0.21), and V (R_{MBF}: -0.71) are showing a negative correlation with Al_2O_3 of the studied Bhuban sandstones are shown in Figure 7.5.

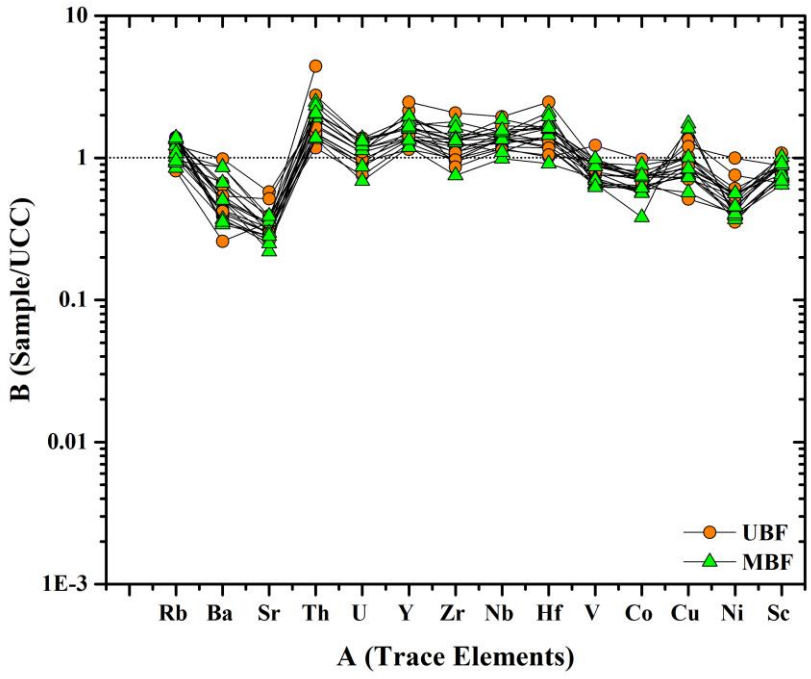

Figure 7.4. The UCC normalized the multi-element plot of Bhuban Sandstone (After Taylor and McLennan 1985).

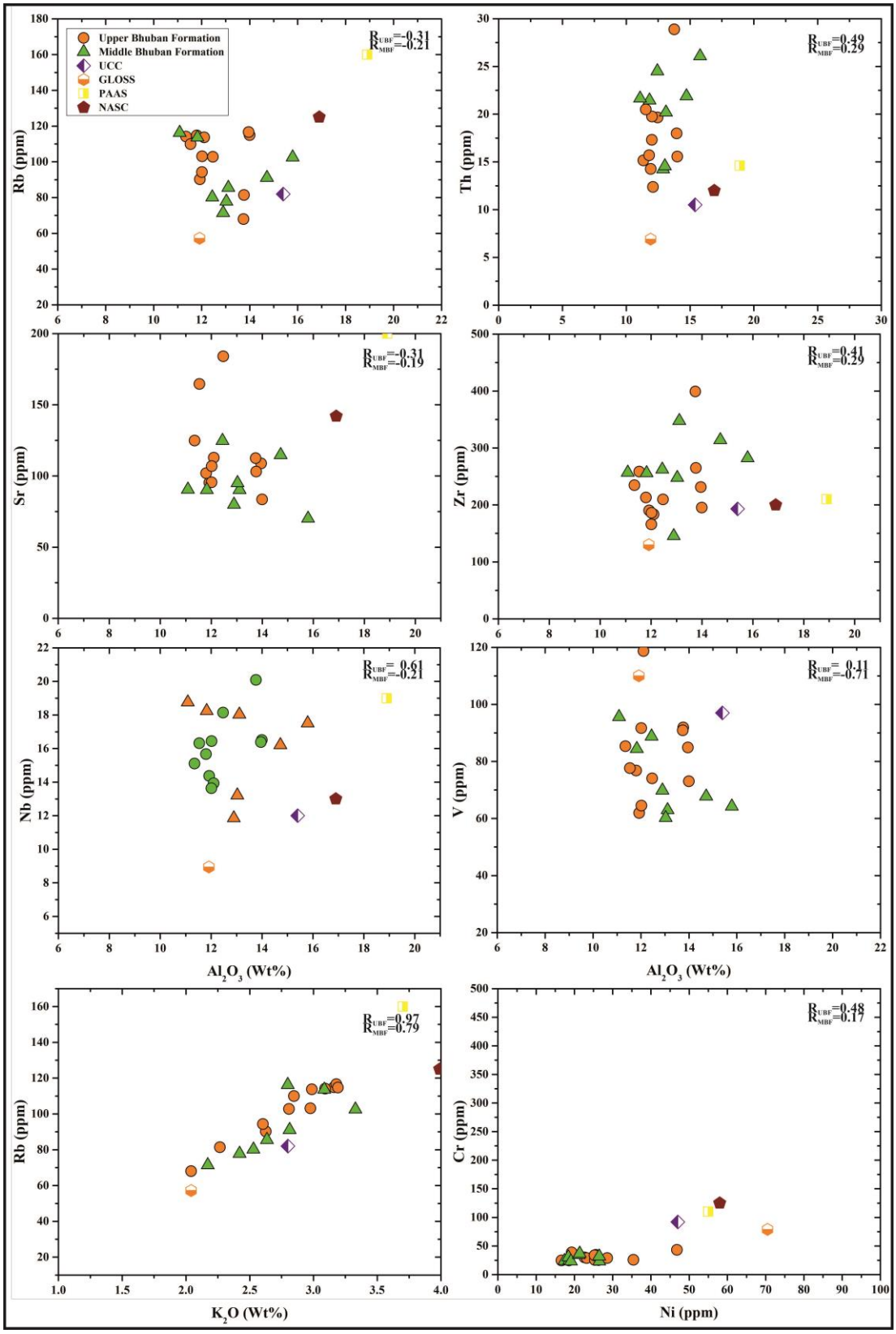

Figure 7.5. The Variation diagram / Harkar Plot for correlation between various trace elements.

Table 7.2. Trace Element compositions (ppm) of the Upper Bhuban Formation and Middle Bhuban Formation.

Lithounit	Upper Bhuban Formation (UBF)											
Sample No.	AR#4	AR#5	AR#7	PK#7A	PK#7C	PK#8A	SS#1A	SS#2A	SS#3A	ZT#6A	ZT#6B	ZT#7
Trace Elements												
Sc	11.78	12.52	9.29	12.82	10.96	14.82	11.94	10.67	12.07	12.34	12.79	15.1
V	73.07	84.91	61.91	85.32	76.8	118.7	74.05	64.51	77.68	91.9	91.69	90.92
Cr	25.09	28.85	25.8	30.09	24.77	28.94	34.49	24.57	25.53	43.12	33.66	38.61
Co	12.99	13.81	10.36	12.88	10.11	16.85	12.49	11.03	12.06	12.16	13.26	11.71
Ni	26.33	28.56	35.44	22.66	16.64	23.22	25.61	18.57	25.34	46.8	25.29	19.29
Cu	21.76	28.37	37.79	28.44	25.3	26.75	26.23	20.67	24.35	33.67	19.81	14.36
Zn	37.07	44.54	46.89	52.68	27.53	36.97	60.96	25.71	48.91	34.17	30.13	22.47
Ga	16.11	16	12.64	15.98	15.82	17.23	14.98	14.99	15.12	14.79	16.21	15.46
Rb	114.92	116.6	90.19	114.13	114.76	113.72	102.77	103.11	109.94	81.44	94.31	67.98
Sr	83.48	108.73	95.26	124.82	101.88	112.88	184.01	106.92	164.62	103.11	95.5	112.49
Y	28.68	28.69	24.12	32.85	28.47	26.51	30.76	29.14	29.87	39.93	45.16	51.89
Zr	195.37	231.17	190.39	234.55	213.13	183.66	209.55	186.17	258.49	265.05	165.96	399.07
Nb	16.51	16.39	14.37	15.11	15.67	13.93	18.14	16.44	16.32	20.09	13.64	23.36
Cs	7.03	8.15	5.38	7.72	8.02	8.46	7.24	6.54	8.27	5.27	5.39	3.64
Ba	244.24	309.4	253.34	418.71	402.65	315.85	617.8	339.05	338.84	268.97	263.78	162.78
Hf	6.38	7.31	6.21	7.46	7.13	5.37	6.88	6.21	8.53	8.8	5.54	13.07
Ta	1.39	1.29	1.21	1.06	1.24	1.05	1.52	1.18	1.4	1.42	1.03	1.96
Pb	15.53	18.34	22.49	20.53	16.71	19.93	246.99	19.04	24.27	30.33	12.62	11.05
Th	15.55	17.98	14.26	15.16	15.69	12.38	19.65	19.76	20.49	28.88	17.31	46.43
U	2.64	2.95	2.5	2.4	2.65	2.03	3.12	3.15	3.3	3.71	2.97	5.13

Table 7.2. Cont..

Lithounit	Middle Bhuban Formation (MBF)							
Sample No.	AR#1	PK#1B	PK#1C	PK#2	PK#3	PK#4	ZT#1	ZT#2
Trace Elements								
Sc	10.12	10.45	9.09	10.70	9.69	14.21	12.38	12.80
V	64.25	62.98	69.86	67.74	60.23	88.78	84.43	95.64
Cr	24.02	25.01	30.25	23.12	23.17	31.91	34.42	36.72
Co	6.61	10.79	9.95	9.76	10.67	15.37	12.64	12.95
Ni	17.40	18.68	18.43	26.51	19.07	26.47	21.16	21.38
Cu	48.95	15.99	45.21	23.49	21.35	28.23	20.50	23.57
Zn	33.36	27.36	40.26	81.10	33.09	49.87	29.25	30.83
Ga	14.86	14.00	12.31	14.79	13.08	15.21	15.90	16.40
Rb	102.56	85.53	71.43	91.13	77.83	80.19	113.64	116.29
Sr	70.14	90.28	79.95	114.76	95.09	124.79	90.22	90.50
Y	33.47	35.75	25.07	37.57	28.05	41.37	33.80	34.90
Zr	282.33	347.73	145.54	314.01	247.74	262.30	256.00	256.92
Nb	17.52	18.03	11.86	16.21	13.22	22.43	18.24	18.76
Cs	4.71	3.89	3.74	4.27	3.56	3.80	7.28	7.25
Ba	319.65	317.83	232.14	541.16	418.69	538.90	213.29	222.41
Hf	9.13	11.11	4.83	10.38	7.70	8.46	8.52	8.63
Ta	1.37	1.34	0.76	1.23	0.83	1.79	1.44	1.48
Pb	21.88	13.42	16.82	27.06	15.72	37.10	13.41	13.85
Th	26.08	20.19	14.24	21.89	14.56	24.51	21.46	21.65
U	3.70	2.95	1.86	3.06	2.34	3.29	3.54	3.56

7.5 Rare Earth Elements

The concentration of REE, along with certain elemental ratios of Bhuban sandstones, is represented in Table 7. 3 and Table 7.4. The Chondrite normalized patterns of REE concentration are shown in (Figure 7.6**)**, which shows the Light Rare Earth Elements (LREE: La-Gd) are enriched over Heavy Rare Earth Elements (HREE: Tb-Lu), with LREE/HREE ratio UBF: 4.33; MBF: 4.55. Bhuban sediments showed a negative Eu anomaly (i.e., Eu/Eu* <1) with an average of UBF: 0.62, MBF: 0.64. The $(La/Yb)_N$ ratio: UBF: 9.66 and MBF: 10.27 which are comparable with the UCC: 10.47 (Taylor and McLennan 1985). Similarly, Chondrite normalized $(La/Sm)_N$ = UBF: 3.68, MBF: 3.58 and $(Gd/Yb)_N$ = UBF: 1.66, MBF: 1.80 ratio bears a resemblance with the UCC (Taylor and McLennan 1985).

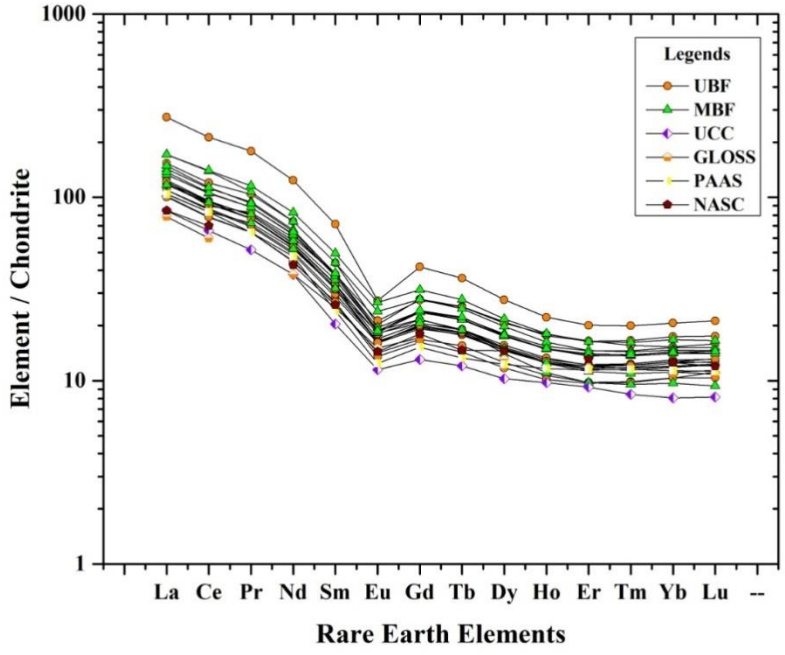

Figure 7.6. The Chondrite normalized REE patterns of Bhuban sandstones. (Taylor and McLennan, 1985).

Table 7. 3: Rare Earth Elements (REE) compositions (ppm) of the Upper Bhuban Formation and Middle Bhuban Formation.

Lithounit	**Upper Bhuban Formation**											
Sample No	**AR#4**	**AR#5**	**AR#7**	**PK#7A**	**PK#7C**	**PK#8A**	**SS#1A**	**SS#2A**	**SS#3A**	**ZT#6A**	**ZT#6B**	**ZT#7**
Rare Earth Elements												
La	40.23	40.28	37.20	44.37	43.22	36.86	45.64	43.62	44.47	56.35	44.83	100.34
Ce	81.79	83.16	75.10	91.26	87.80	74.51	91.57	88.27	90.44	114.89	85.97	203.62
Pr	9.46	9.65	8.84	10.94	10.59	8.83	10.91	10.50	10.50	14.26	11.31	24.50
Nd	34.84	35.69	31.88	39.66	38.58	31.65	39.98	38.51	38.07	52.50	42.82	88.10
Sm	6.61	6.86	6.12	7.72	7.48	6.20	7.76	7.27	7.30	10.16	8.80	16.49
Eu	1.40	1.43	1.23	1.48	1.42	1.18	1.57	1.40	1.40	1.76	1.85	2.38
Gd	5.86	5.97	5.15	6.27	6.04	4.95	6.58	6.18	6.14	8.51	8.40	12.77
Tb	1.04	1.03	0.90	1.11	1.05	0.83	1.10	1.05	1.07	1.47	1.46	2.10
Dy	5.59	5.58	4.80	5.79	5.54	4.47	5.95	5.60	5.70	7.97	7.84	10.52
Ho	1.09	1.07	0.91	1.11	1.07	0.86	1.13	1.07	1.09	1.50	1.52	1.89
Er	2.96	2.97	2.44	3.05	2.87	2.41	3.02	2.91	2.98	4.09	4.10	5.00
Tm	0.42	0.42	0.35	0.44	0.41	0.35	0.43	0.42	0.43	0.59	0.55	0.71
Yb	2.97	2.98	2.57	3.22	2.94	2.56	3.15	3.09	3.16	4.31	3.80	5.12
Lu	0.46	0.47	0.40	0.50	0.46	0.42	0.48	0.49	0.50	0.67	0.61	0.81

Table 7. 3. Cont.…

Lithounit	Middle Bhuban Formation							
Sample No.	AR#1	PK#1B	PK#1C	PK#2	PK#3	PK#4	ZT#1	ZT#2
Rare Earth Elements								
La	66.87	69.91	69.87	67.38	70.87	65.82	64.62	53.54
Ce	1.04	1.06	0.81	0.93	0.77	1.49	1.12	0.79
Pr	15.80	13.11	12.89	14.72	13.03	12.44	11.82	11.08
Nd	4.55	5.40	6.61	6.01	5.36	8.59	6.92	6.39
Sm	0.02	0.09	0.22	0.03	0.09	0.14	0.07	0.41
Eu	1.06	1.40	1.75	1.60	1.31	2.11	3.61	3.75
Gd	0.34	0.48	0.63	0.35	0.28	0.48	1.67	8.69
Tb	1.50	1.92	1.26	1.67	1.98	1.61	1.34	1.08
Dy	3.33	2.64	2.17	2.81	2.42	2.53	3.09	2.80
Ho	0.25	0.20	0.12	0.19	0.18	0.24	0.17	0.13
Er	4.23	5.33	5.42	4.58	5.44	5.29	5.47	4.83
Tm	15.22	12.32	15.97	15.81	16.94	8.38	10.57	14.05
Yb	0.21	0.20	0.17	0.19	0.19	0.20	0.26	0.25
Lu	2.22	1.37	1.72	1.68	1.22	1.57	2.30	2.60

Table 7. 4. Elemental ratios of Trace and REE elements of Upper and Middle Bhuban Formations

Lithounit	Upper Bhuban Formation											
Sample No	AR#4	AR#5	AR#7	PK#7A	PK#7C	PK#8A	SS#1A	SS#2A	SS#3A	ZT#6A	ZT#6B	ZT#7
Elemental Ratio												
ΣLREE	376.97	382.92	346.66	422.77	409.49	343.85	429.10	409.71	413.71	543.52	441.55	929.33
ΣHREE	93.04	92.87	79.21	98.02	92.18	77.17	97.54	94.05	96.05	131.77	126.91	167.94
LREE/HREE	4.05	4.12	4.38	4.31	4.44	4.46	4.40	4.36	4.31	4.12	3.48	5.53
$(La/Lu)_N$	9.04	8.91	9.76	9.27	9.66	9.02	9.89	9.33	9.23	8.78	7.69	12.88
Eu/Eu*	0.67	0.67	0.65	0.63	0.63	0.63	0.65	0.62	0.62	0.56	0.65	0.48
Ce/Ce*	0.98	0.99	0.97	0.97	0.96	0.97	0.96	0.97	0.98	0.95	0.89	0.96
$(La/Sm)_N$	3.83	3.70	3.82	3.62	3.64	3.74	3.70	3.78	3.83	3.49	3.21	3.83
$(Gd/Yb)_N$	1.60	1.62	1.63	1.58	1.67	1.57	1.69	1.62	1.58	1.60	1.79	2.02
$(La/Yb)_N$	9.16	9.14	9.79	9.31	9.95	9.72	9.78	9.53	9.52	8.83	7.98	13.25
$(La/Nd)_N$	2.24	2.19	2.26	2.17	2.17	2.26	2.21	2.19	2.26	2.08	2.03	2.21
La/Th	2.59	2.24	2.61	2.93	2.75	2.98	2.32	2.21	2.17	1.95	2.59	2.16
La/Sc	3.42	3.22	4.01	3.46	3.94	2.49	3.82	4.09	3.68	4.57	3.51	6.65
La/Co	3.10	2.92	3.59	3.45	4.27	2.19	3.66	3.96	3.69	4.63	3.38	8.57
Th/Sc	1.32	1.44	1.54	1.18	1.43	0.84	1.65	1.85	1.70	2.34	1.35	3.08
Th/Co	1.20	1.30	1.38	1.18	1.55	0.73	1.57	1.79	1.70	2.37	1.31	3.96
Th/U	5.90	6.10	5.71	6.14	5.93	6.08	6.29	6.28	6.21	7.78	5.83	9.04
Th/Cr	0.62	0.62	0.55	0.50	0.63	0.43	0.57	0.80	0.80	0.67	0.51	1.20

Table 4 cont.

Lithounit	Upper Bhuban Formation											
Sample No	AR#4	AR#5	AR#7	PK#7A	PK#7C	PK#8A	SS#1A	SS#2A	SS#3A	ZT#6A	ZT#6B	ZT#7
Elemental Ratio												
Cr/Th	1.61	1.60	1.81	1.99	1.58	2.34	1.76	1.24	1.25	1.49	1.94	0.83
Cr/V	0.34	0.34	0.42	0.35	0.32	0.24	0.47	0.38	0.33	0.47	0.37	0.42
Cr/Ni	0.95	1.01	0.73	1.33	1.49	1.25	1.35	1.32	1.01	0.92	1.33	2.00
V/Ni	2.78	2.97	1.75	3.77	4.61	5.11	2.89	3.47	3.06	1.96	3.63	4.71
V/Y	2.55	2.96	2.57	2.60	2.70	4.48	2.41	2.21	2.60	2.30	2.03	1.75
Y/Ni	1.09	1.00	0.68	1.45	1.71	1.14	1.20	1.57	1.18	0.85	1.79	2.69
Zr/Zn	5.27	5.19	4.06	4.45	7.74	4.97	3.44	7.24	5.29	7.76	5.51	17.76
Zr/Cr	7.79	8.01	7.38	7.80	8.61	6.35	6.08	7.58	10.12	6.15	4.93	10.34
Zr/Sc	16.59	18.47	20.50	18.29	19.45	12.40	17.54	17.45	21.41	21.47	12.97	26.44
Sr/Cu	3.84	3.83	2.52	4.39	4.03	4.22	7.01	5.17	6.76	3.06	4.82	7.83
Rb/Sr	1.38	1.07	0.95	0.91	1.13	1.01	0.56	0.96	0.67	0.79	0.99	0.60
Ga/Rb	0.14	0.14	0.14	0.14	0.14	0.15	0.15	0.15	0.14	0.18	0.17	0.23
K/Rb	227.33	225.39	240.73	223.91	229.88	217.15	225.89	238.52	214.01	229.96	228.20	248.02
Zr/Hf	30.63	31.63	30.68	31.42	29.91	34.17	30.44	29.99	30.31	30.11	29.95	30.54
Zr/Th	12.56	12.85	13.35	15.48	13.58	14.84	10.66	9.42	12.62	9.18	9.59	8.60
Ti/Zr	27.80	24.48	26.36	22.90	26.33	28.17	30.80	31.91	20.78	25.42	29.37	21.40

.

Table 7.4. Cont…

Middle Bhuban formation								
Sample No	AR#1	PK#1B	PK#1C	PK#2	PK#3	PK#4	ZT#1	ZT#2
Elemental Ratio								
ΣLREE	496.59	470.72	425.60	587.06	383.18	617.08	473.52	501.47
ΣHREE	109.61	114.97	82.25	119.03	90.95	133.21	109.67	111.56
LREE/HREE	4.53	4.09	5.17	4.93	4.21	4.63	4.32	4.50
$(La/Lu)_N$	10.14	8.75	12.49	11.73	9.16	10.33	9.75	10.25
Eu/Eu*	0.60	0.63	0.66	0.67	0.69	0.66	0.60	0.59
Ce/Ce*	0.97	0.97	0.96	1.03	0.96	1.00	0.96	0.97
$(La/Sm)_N$	3.73	3.48	3.29	3.90	3.27	3.46	3.69	3.85
$(Gd/Yb)_N$	1.69	1.57	2.23	1.89	1.85	1.87	1.64	1.69
$(La/Yb)_N$	10.16	8.75	12.07	11.67	9.39	10.20	9.53	10.39
$(La/Nd)_N$	2.15	2.10	2.02	2.33	2.00	2.07	2.20	2.29
La/Th	2.01	2.41	3.01	2.87	2.63	2.56	2.35	2.52
La/Sc	5.18	4.66	4.72	5.88	3.96	4.41	4.07	4.26
La/Co	7.93	4.51	4.31	6.44	3.59	4.08	3.99	4.21
Th/Sc	2.58	1.93	1.57	2.05	1.50	1.72	1.73	1.69
Th/Co	3.95	1.87	1.43	2.24	1.36	1.59	1.70	1.67
Th/U	7.05	6.85	7.65	7.16	6.23	7.45	6.06	6.08
Th/Cr	1.09	0.81	0.47	0.95	0.63	0.77	0.62	0.59

Table 7.4. Cont.

Middle Bhuban Formation								
Sample No	**AR#1**	**PK#1B**	**PK#1C**	**PK#2**	**PK#3**	**PK#4**	**ZT#1**	**ZT#2**
Elemental Ratio								
Cr/Th	0.92	1.24	2.12	1.06	1.59	1.30	1.60	1.70
Cr/V	0.37	0.40	0.43	0.34	0.38	0.36	0.41	0.38
Cr/Ni	1.38	1.34	1.64	0.87	1.21	1.21	1.63	1.72
V/Ni	3.69	3.37	3.79	2.56	3.16	3.35	3.99	4.47
V/Y	1.92	1.76	2.79	1.80	2.15	2.15	2.50	2.74
Y/Ni	1.92	1.91	1.36	1.42	1.47	1.56	1.60	1.63
Zr/Zn	8.46	12.71	3.61	3.87	7.49	5.26	8.75	8.33
Zr/Cr	11.75	13.90	4.81	13.58	10.69	8.22	7.44	7.00
Zr/Sc	27.90	33.27	16.01	29.34	25.58	18.46	20.68	20.07
Sr/Cu	1.43	5.65	1.77	4.89	4.45	4.42	4.40	3.84
Rb/Sr	1.46	0.95	0.89	0.79	0.82	0.64	1.26	1.29
Ga/Rb	0.14	0.16	0.17	0.16	0.17	0.19	0.14	0.14
K/Rb	268.26	254.70	251.18	255.12	256.97	260.65	224.35	198.91
Zr/Hf	30.92	31.29	30.11	30.26	32.19	31.00	30.05	29.77
Zr/Th	10.83	17.23	10.22	14.34	17.02	10.70	11.93	11.87
Ti/Zr	22.02	18.32	33.20	17.75	18.59	33.90	26.17	18.39

7.6 Geochemical Characteristics of the Provenance

Trace and REE are widely used to characterize the geochemical signature of clastic sedimentary rocks, usually for the identification of various tectonic domains that contribute to sediments. More commonly the use of elemental ratios gives a proper identification of source rocks, which has been used for various discriminant plots by various workers in the recent past (Taylor and McLennan, 1985; Bhatia and Crook, 1986; McLennan *et al.,* 1993). Trace elements like Th, Sc, Zr, Cr, Co, and Rare Earth Elements (La-Lu) are insensitive against the various processes involved during the sedimentation like transportation, diagenesis, lithification, etc. (Taylor and McLennan, 1985; Bhatia and Crook, 1986; McLennan and Hanson, 1993) make them in the use of excellent provenance proxy. To understand the characteristics of the source rocks for the different Bhuban sandstones we are using various plots Bracciali *et al.* (2007); Floyd *et al.* (1989); McLennan and Hanson (1993); Schoenborn and Fedo (2011); Jinliang and Xin (2008)] and certain elemental ratios as suggested by Cullers (1994, 2000) and Cullers & Podkovyrov (2002). An important parameter is the ratio between Al_2O_3 and TiO_2 proposed by Girty *et al.* (1996) indicating Al_2O_3/TiO_2 ratios <14 are typical for a probable mafic source rock, whereas 19–28 indicate a felsic source. Studied Bhuban Sandstone are having average ratio of 13.07 for UBF and 13.66 for MBF which represents a probable intermediate to felsic provenance that is identical in terms of source rock composition. Cullers (1994, 2000) and Cullers & Podkovyrov (2002) proposed a range of different source rock compositions in terms of various trace and REE ratios, for the present studied samples are listed in Table 7.5. We observed that the range of certain elemental ratios including Eu/Eu* (UBF: 0.48-0.67; MBF: 0.59-0.69), La_N/Lu_N (UBF: 7.69-12.88; MBF: 8.74-12.49), La/Sc (UBF: 2.49-6.65; MBF: 3.96-5.88), La/Co (UBF: 2.19-8.57; MBF: 3.59-7.93), Th/Sc (UBF: 0.83-3.07; MBF: 1.50-2.58), Th/Co (UBF: 0.73-3.96; MBF: 1.36-3.95), Cr/Th (UBF: 0.83-2.34; MBF: 0.92-2.12) and Th/Cr (UBF: 0.43-1.20; MBF: 0.47-1.08) strongly signifies the influx of sediments from a probable felsic source rocks.

Table 7.5. Trace and REE elemental ratios of the Bhuban Sandstones representing provenance (Felsic and Mafic Sources are after Cullers 1994,2000; Cullers and Podkovyrov 2002).

Elemental Ratio	Range of Upper Bhuban Formation	Range of Middle Bhuban Formation	Felsic Sources	Mafic Sources	UCC	GLOSS	PAAS	NASC
Eu/Eu*	0.48-0.67	0.59-0.69	0.32-0.83	0.70-1.02	0.69	0.71	0.63	0.65
La/Lu	7.68-12.88	8.74-12.48	3.00-27.0	1.10-7.00	10.38	7.24	9.22	7.08
La/Sc	2.48-6.64	3.95-5.87	0.70-27.7	0.40-1.1	2.21	2.2	2.39	2.09
La/Co	2.18-8.56	3.59-7.93	1.4-22.4	0.14-0.38	1.79	1.31	1.66	1.21
Th/Sc	0.83-3.07	1.50-2.57	0.64-18.1	0.05-0.4	0.75	0.53	0.91	0.8
Th/Co	0.73-3.96	1.36-3.94	0.30-7.5	0.04-1.40	0.6	0.31	0.63	0.46
Cr/Th	0.83-2.33	0.92-2.12	4.00-15.0	25-500	8.76	11.42	7.53	10.41
Th/Cr	0.42-1.20	0.47-1.08	0.06-4.0	0.002-0.045	0.11	0.09	0.13	0.1

Felsic Sources	**Cullers (1994, 2000); Cullers & Podkovyrov (2000)**
Mafic Sources	
UCC	**Upper continental crust from Rudnick and Gao, 2003, 2005***
GLOSS	**Global Subducting Sediment from Plank and Langmuir, 1998**
PAAS	**Post-Archean Australian Shales, from Taylor and McLennan, 1985**
NASC	**North American Shale Composite from Gromet *et al.*, 1984**

In sediment geochemistry, the immobile characteristics of trace elements permit us to use them in a variety of graphical plots to decipher the various types of source rocks. As suggested by Bracciali *et al.*, 2007, V and Ni are enriched in basic and ultrabasic rocks while Th enrichment represents an acidic source. This combination is well represented in a ternary plot of (V-Ni-Th×10) after Bracciali *et al.* (2007), where Bhuban sands show an enrichment of Th rather than V and Ni, and samples are clustered near the felsic field (Figure 7.7).

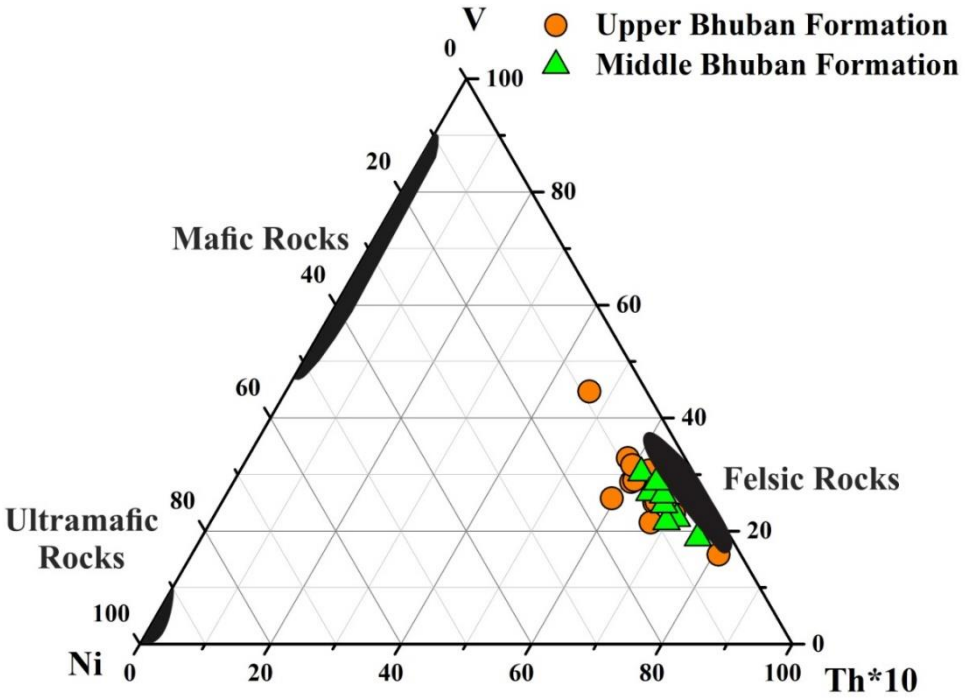

Figure. 7.7. The ternary plot of Th×10-V-Ni (After Bracciali *et al.* 2007).

Similar observations are also given by the binary plot of TiO_2 vs Ni (Figure 7.8) after Floyd *et al.* (1989) as we samples represent a felsic source.

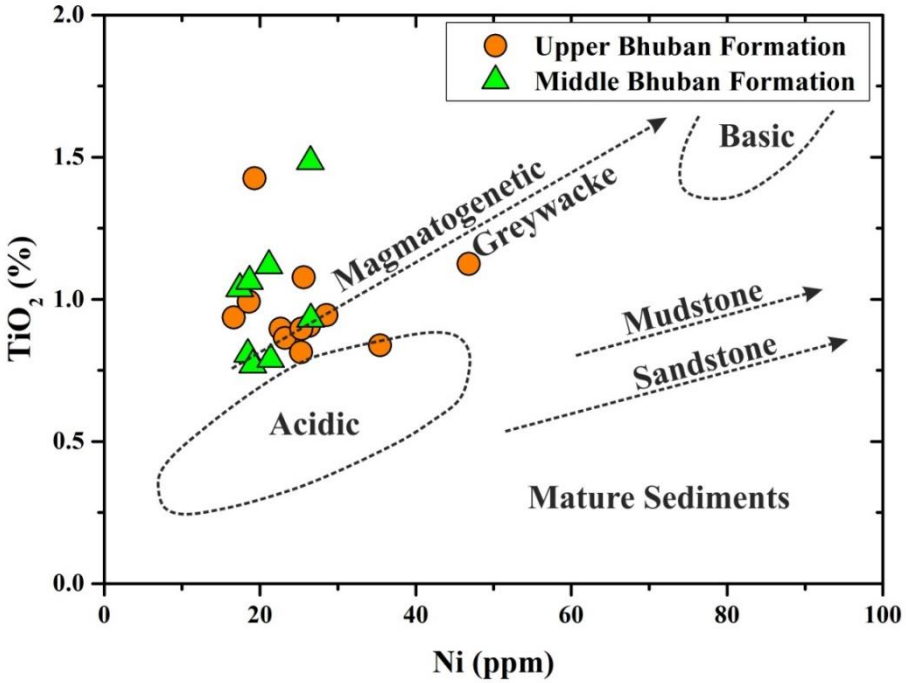

Figure. 7.8. The provenance discriminating plot of Ni vs TiO_2 (After Floyd *et al.*, 1989).

Hayashi *et al.*, 1997 use a provenance parameter based on the ratio of TiO_2/Zr that is ≥200 for a mafic source, 195-55 for an intermediate source, and ≤55 for a probable felsic source rock indicator for clastic sediments. As calculated the Bhuban samples are showing a range of UBF: 34.70-53.28; MBF: 29.65-56.61 with an average value of UBF: 43.94; MBF: 39.32, which supports the earlier observations which is shown in Figure 7.9. McLennan and Hanson (1993) proposed a binary plot by using 2 distinctive parameters i.e. the source composition as Th/Sc and a sediment recycling parameter as Zr/Sc. As plotted in Figure 7.10 we observed that both units of Bhuban sediments (UBF and MBF) are identical while comparing with the parameters. For a quantitative estimation of contribution from the various source rocks, several trace and REE plots can be used, out of which ternary plot of La-Th-Sc (Jinliang and Xin, 2008) and Sc vs Th/Sc binary plot after Schoenborn and Fedo, 2011 usually follows.

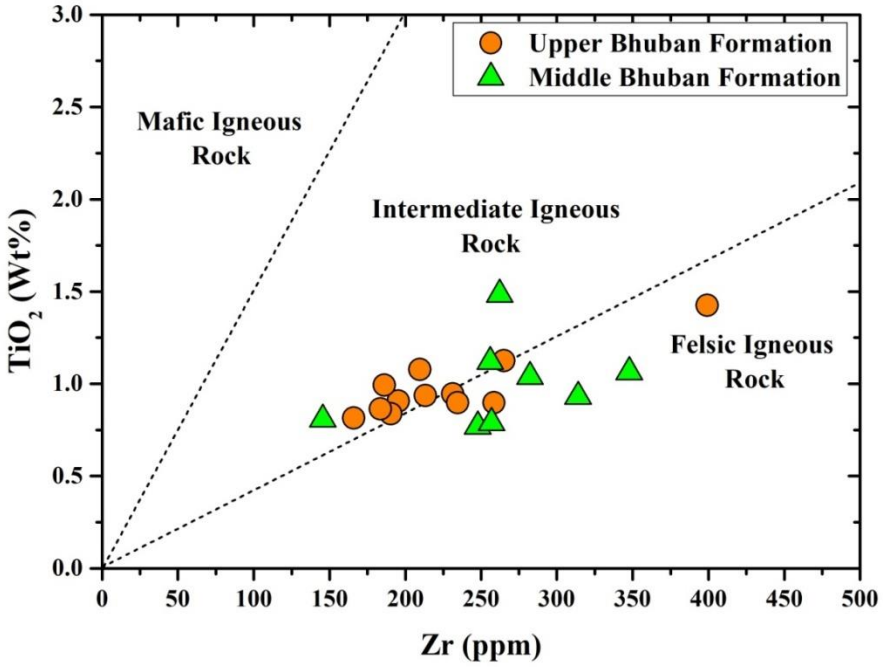

Figure 7.9. The provenance plot of Zr vs TiO_2 (After Hayashi *et al.*, 1997).

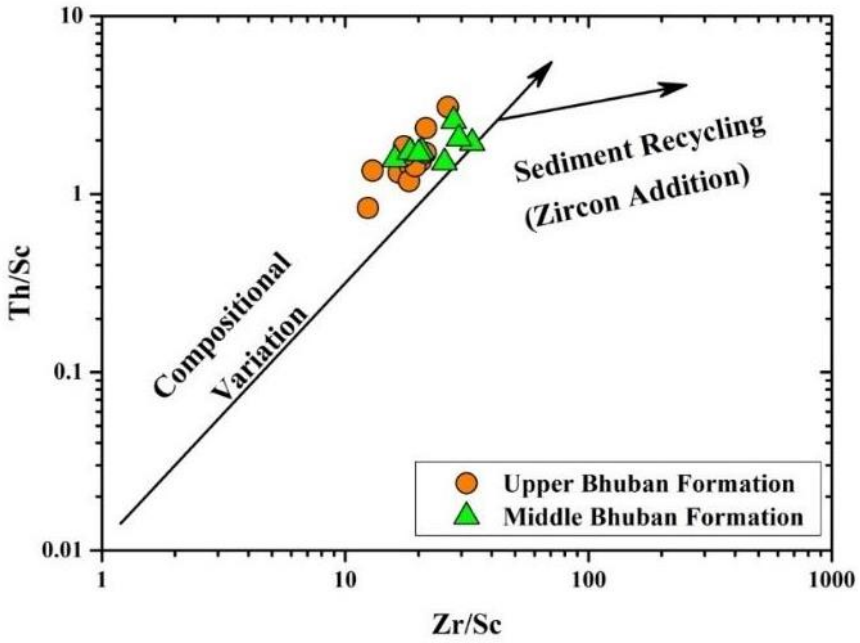

Figure 7.10. The Zr/Sc vs Th/Sc bivariate plot represents source rock composition and extent of sediment recycling (McLennan and Hanson 1993).

Jinliang and Xin (2008) represent the contribution of source sediments from the intermixing of Granite (with Eu/Eu*: 0.5 and Th/Sc: 1.18) and Granodiorite (with Eu/Eu*: 0.7 and Th/Sc: 0.5) with the help of La-Th-Sc ternary plot. While comparing the Upper and Middle Bhuban Formation we observed that the elemental ratios of Eu/Eu* (UBF: 0.62; MBF: 0.64) and Th/Sc (UBF: 1.64; MBF: 1.85) support the contributions from both Granodioritic and Granitic sources which is portrayed in Figure 7. 11.

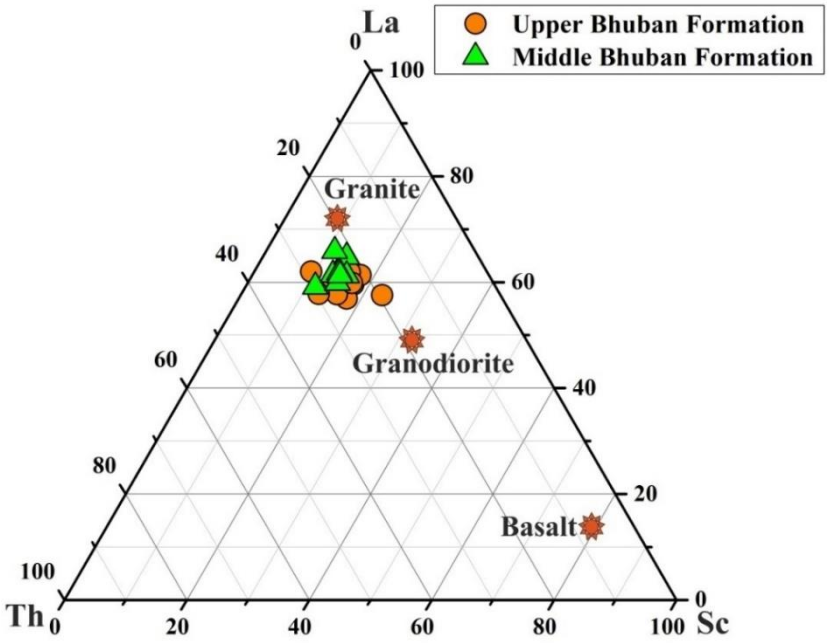

Figure 7.11. The Ternary plot of La-Th-Sc for compositional variations in the analyzed samples of Bhuban formation (After Jinliang and Xin, 2008).

This observation is also supported by the provenance mixing plot of Sc vs Th/Sc after Schoenborn and Fedo (2011) where the majority of the samples are indicative of intermixing between Granodiorite and Granite (90% Granodiorite + 10% high K-Granite) (Figure 7.12).

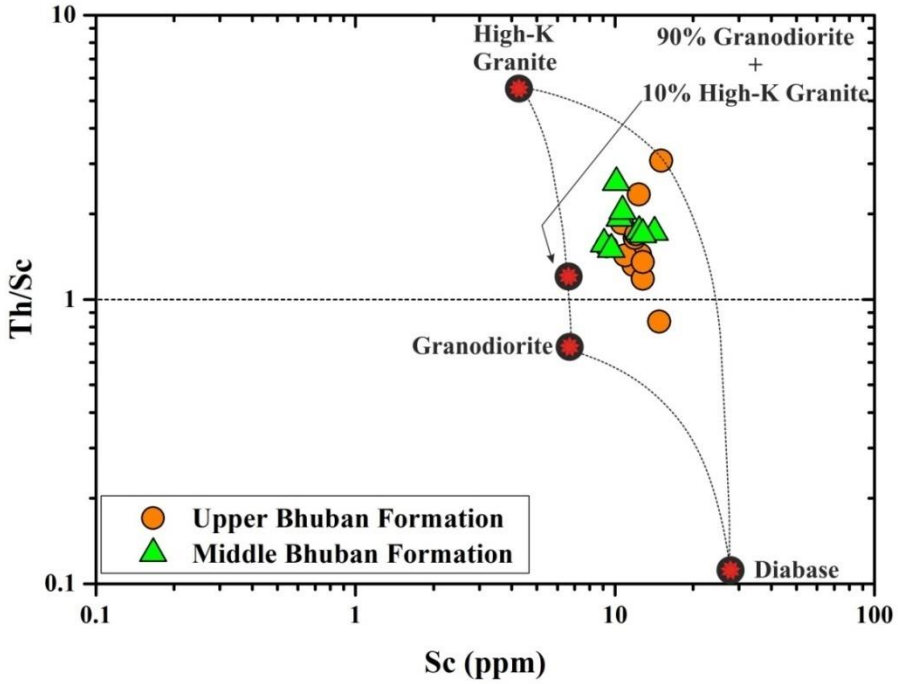

Figure 7.12. The Bivariate plot of Sc vs Th/Sc indicating the studied samples source rock

composition for the Bhuban sandstones (After Schoenborn and Fedo, 2011).

Again, from the binary plot of Y/Ni vs Cr/V after Mongelli *et al.* (2006) we can understand the nature of source rocks based on the mixing model between granite and ultramafic end members by using ratios of Y/Ni vs Cr/V (Figure 7.13). Mongelli *et al.* (2006) proposed that the higher Cr/V ratio represents a probable mafic source and for a granitic rock this ratio is low. While plotting the Bhuban sandstones are representing the source more towards the granitic field (Cr/V: avg. UBF: 0.37, MBF: 0.39). Floyd and Leveridge (1987) proposed that the sediments primarily supplied from the acidic arcs generally exhibits low ratio of La/Th and a moderate range of Hf (3–7 ppm). In the binary plot of Hf vs. La/Th after Floyd and Leveridge (1987) (Figure 7.14), Bhuban sandstones show moderate ratio of La/Th (UBF: 2.46; MBF: 2.55) with the enrichment of Hf (UBF: 7.41; MBF: 8.60 ppm) suggesting the sediments were sourced from recycled sediments which were originally derived from arc-related acidic source rocks.

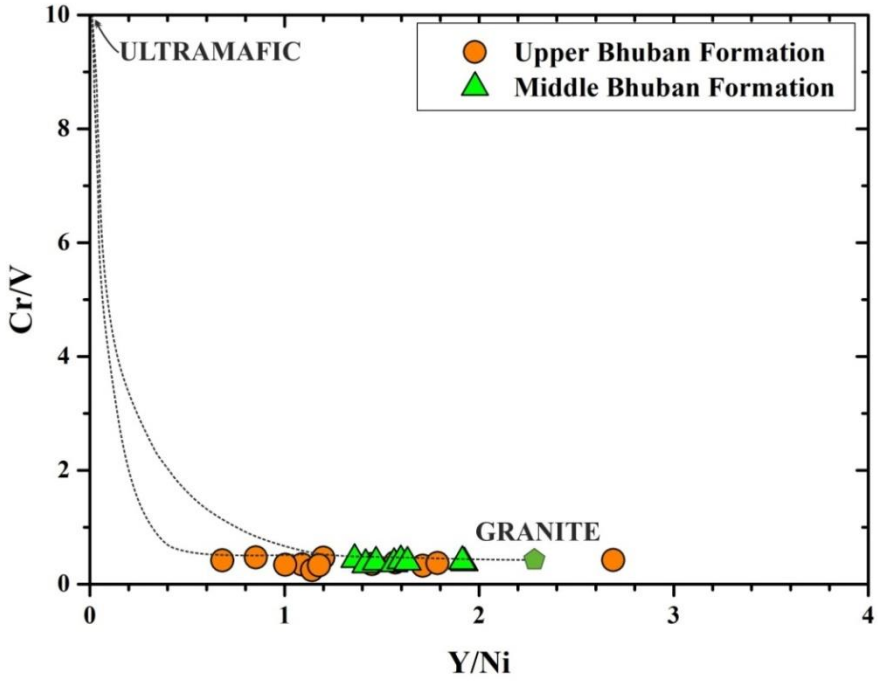

Figure 7.13. The Y/Ni vs. Cr/V binary plot for the study of Bhuban sandstone provenance
mixing model (After Mongelli *et al.* 2006).

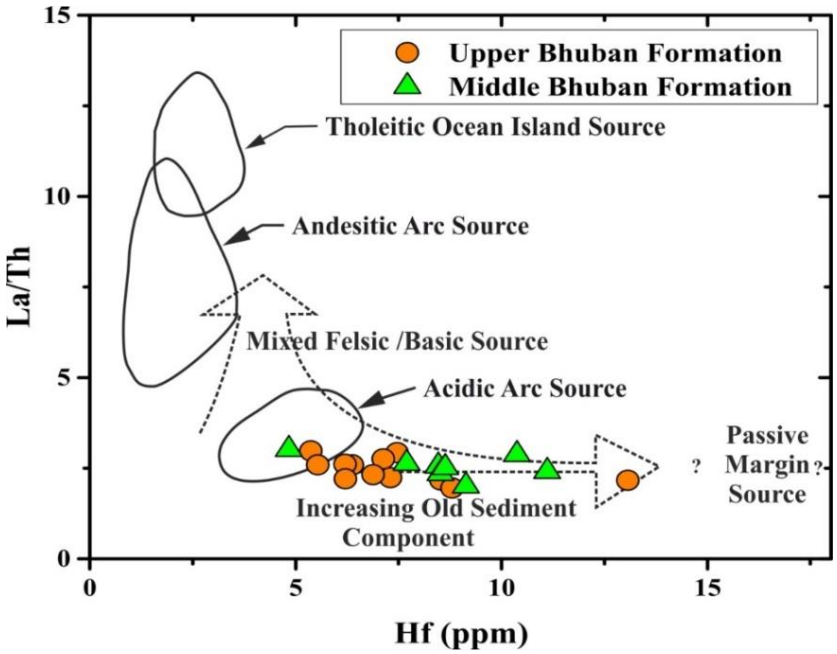

Figure 7.14. The Binary tectonic discriminating plot of Hf vs. La/Th (After Floyd and Leveridge 1987).

The normalized REE pattern and Eu anomaly are commonly used to understand the nature of possible source rocks as they don't have any differentiation during the sedimentation processes (Basu *et al.,* 1975; Armstrong-Altrin, 2009). Derivation of sediments from felsic source rock is indicated by a higher LREE/HREE ratio with negative Eu anomalies (Cullers, 1994, 2000) that also represents a fractionated behavior of primary rocks. Figure 7.6 represents the REE plot that signifies the higher concentration of LREE than the HREE which can also be understood from the ratio of $(La/Lu)_N$: (UBF: 7.69-12.88; MBF: 8.74-12.49) along with a high concentration of K as indicated by the avg. ratio of K_2O/Na_2O: UBF: 2.18; MBF: 1.84. Therefore, contributions from the fractionated granitic sources are represented by the higher ratio of LREE/HREE, this is also supported by the sharp Eu negative anomaly due to the removal of Ca-rich plagioclase from the source rocks.

7.7 Paleo-climate & Paleo-weathering

The geochemical signature of sediments in terms of distribution and concentration of certain major and trace elements provides vital information regarding the paleoclimate and paleoenvironmental conditions during the sedimentation processes (Getaneh, 2002; Moradi *et al.,* 2016). Based on the elemental concentration of sediments, Zhao *et al.* 2007; Cao *et al.* 2012 and Moradi *et al.* 2006 proposed the C-value as an indicator of paleoclimate, which is defined as,

$$\text{C-Value}=\sum(Fe+Mn+Cr+Ni+V+Co)/\sum(Ca+Mg+Sr+Ba+K+Na)$$

C-Value provides important clues about the changes in paleoclimatic conditions from warm and humid to hot and arid primarily based on the generally accepted hypotheses suggesting that Fe, Mn, Cr, Ni, V, and Co are relatively enriched under moist conditions, whereas Ca, Mg, Sr, Ba, K, and Na are concentrated under arid conditions due to the precipitation of saline minerals as a result of evaporation (Zhao *et al.,* 2007; Cao *et al.,* 2012). The C-value of clastic sediments has been widely used as a powerful tool to represent the paleoclimate in the last decade (Moradi *et al.,* 2016; Tao *et al.,* 2017; Fathy *et al.,* 2018; Li *et al.,* 2019; Zhao *et al.,* 2021; Wu *et al.,* 2022; Ma *et al.,* 2023).

A modified version of the C-value known as the Paleoclimatic Factor (PF) is proposed by Samad *et al.* 2020 with the incorporation of Rb and Ti instead of Mn, Cr, and Co:

$$PF=\sum(Fe+V+Ni+Rb+Ti)/\sum(Ca+Mg+Sr+Ba+K+Na).$$

While calculating the C-Value for Bhuban Sandstones showed a range of UBF: 0.51-1.02; MBF: 0.41-1.23 with an average of UBF: 0.72; MBF: 0.86. Palaeoclimatic Factor (PF) is also showing consistent with the C-Value, showing a range of UBF: 0.55-1.12; MBF: 0.43-1.39 with an average of UBF: 0.80; MBF: 0.95. This indicates during the sedimentation of Bhuban sandstones, the prevailing paleoclimatic condition was under warm and sub-humid to humid conditions. This observation is also substantiated by the Sr/Cu (Lerman and Gat, 1989) and Rb/Sr (Jin and Zhang, 2002; Bai *et al.,* 2015) ratios which are considered paleoclimatic indicators. Bhuban sediments are showing an average of Sr/Cu: UBF: 2.52-7.83 (avg. 4.79), MBF: 1.43-5.64 (avg. 3.86) indicating warm and humid climatic conditions (>5 for hot arid, 1.3 – 5.0 for warm and humid) prevailing at the time of sedimentation. Similarly, the Rb/Sr ratio of Bhuban sediments are: UBF: 0.56-1.38 (avg. 0.92) and MBF: 0.64-1.46 (avg. 1.01) indicating a moderate value representing humid and warm conditions during the sedimentation (high ratios for cold while low ratios reflect warm conditions). Hence both Sr/Cu and Rb/Sr ratios support the C-Value and PF as well as the petrographical bivariate plots that during the deposition of the Surma Group of Bhuban Formation rocks, the sedimentation occurred under warm and sub-humid to humid climatic conditions. The change in the mineralogical and chemical composition of clastic rocks is influenced by chemical weathering in the source area (Nesbitt *et al.* 1996). Several geochemical weathering indices have been proposed in recent decades, including the Chemical Index of Alteration (CIA) (Nesbitt and Young 1982), Chemical Index of Weathering (CIW) (Harnois 1988), Weathering Index of Parker (WIP) (Parker 1970), Plagioclase Index of Alteration (PIA) (Fedo *et al.* 1995), and Index of Chemical Variability (ICV) (after Cox *et al.* 1995) are widely used to deduce the paleoclimatic conditions of clastic sedimentary rocks, including the extent to which the source rocks have been weathered by using the major element concentrations. The mathematical derivations of these parameters are given below: (where, CaO* indicates Ca

incorporated from the silicate-bearing minerals, # indicates by using Molecular Proportions, and ^ indicates by using Weight Percentage).

$$CIA^{\#} = [Al_2O_3 / (Al_2O_3 + CaO^* + Na_2O + K_2O)] \times 100$$

$$CIW^{\#} = [Al_2O_3 / \{Al_2O_3 + CaO^* + Na_2O\}] \times 100$$

$$WIP^{\#} = [\{2(Na_2O) / 0.35\} + \{MgO / 0.9\} + \{2(K_2O) / 0.25\} + (CaO^*/0.7)] \times 100$$

$$PIA^{\#} = [\{Al_2O_3 – K_2O\} / \{Al_2O_3 + CaO^* + Na_2O – K_2O\}] \times 100$$

$$ICV^{\wedge} = [\{Fe_2O_3 + K_2O + Na_2O + CaO^* + MgO + MnO + TiO_2\} / Al_2O_3]$$

The present study shows that Bhuban sandstones (Table 7.6) have low to moderate values of the Chemical Index of Alteration (avg. UBF: 58.85, MBF: 62.72). The low to moderate values of CIA indicate that the sediments traveled for a short distance with less mechanical breakdown and/or chemical change. Although the CIA is often used to evaluate weathering, the remobilization of K during sedimentation and metamorphic processes is a considerable disadvantage. Another parameter known as the CIW (Harnois, 1988) is commonly used to minimize such problems. The average CIW value (UBF: 68.68, MBF: 73.11) indicates a moderate extent of weathering of the Bhuban sediments. The chemical weathering intensity can also be estimated using the Plagioclase Index of Alteration (PIA, Fedo *et al.* 1995). Unweathered plagioclase has a PIA value of 50. The PIA values for the studied samples (UBF: 62.52, MBF: 68.22) (Table 7.6), also justify the other parameters indicating that the source area supplied almost fresh feldspars. The WIP values of the Bhuban sandstones (UBF: 50.92, MBF: 47.20) indicate less weathered source rocks. In the A-CN-K ternary diagram (Nesbitt and Young 1984), the samples are almost clustered in the mild to moderate field indicating less weathered source rocks (Figure 7.15). When the weathering is low, the line follows a pattern parallel to the A-CN line. Intense weathering leaches alkalis such as CaO and Na_2O, which might cause the trend to shift towards the A-K line, suggesting K enrichment. High weathering signifies that the K has been removed and redirected the trend towards the Al_2O_3 apex. The lower values of PIA [(UBF: 62.52, MBF: 68.22)] imply a supply of less weathered and/or altered detritus of feldspars from the source areas as depicted in the AK-C-N plot (Fedo *et al.*

1995) (Figure 7.16) where samples are following A-CN line. Maximum PIA value i.e. 100 indicates weathered products like kaolinite, gibbsite, etc., and 50 for un-weathered plagioclase.

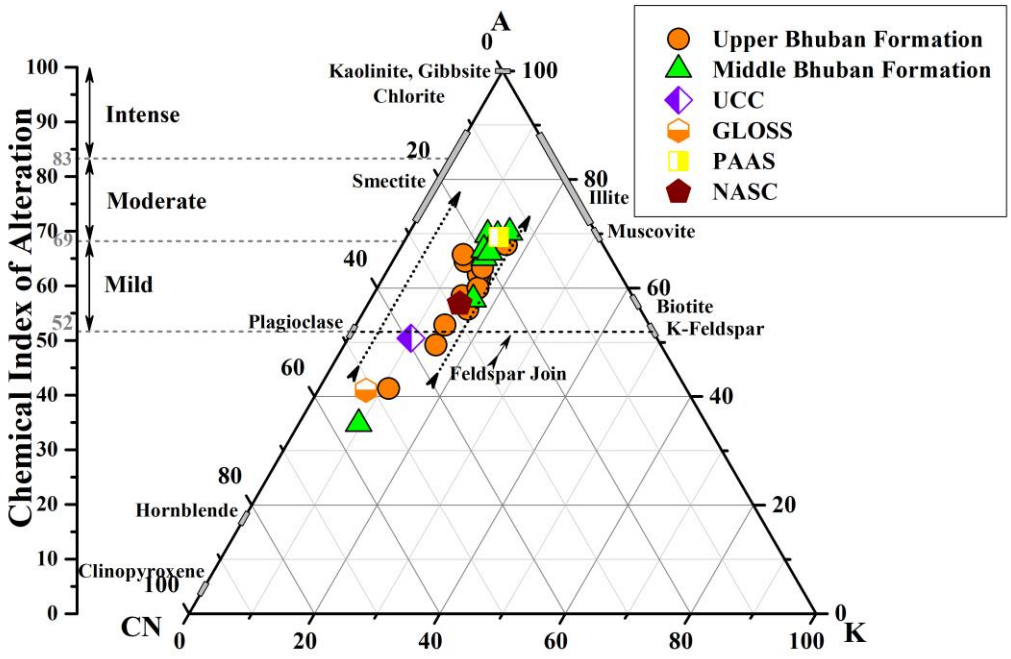

Figure 7.15. The A-CN-K ternary plot represents a moderate to intense nature of weathering of source rocks (Nesbitt and Young 1984).

The plot of CIA vs. ICV (Long et al. 2012) represents that the source rock of the Bhuban sediments had matured and had undergone low to moderate weathering (Figure 7.17). The binary plot of Th vs Th/U (McLennan and Hanson, 1993) is shown in (Figure 7.18) representing a weathering trend of the source rocks. The average value of Th/U [UBF: 6.44, MBF: 6.82] in the Bhuban sandstones shows a comparable characteristic of the upper crust that has experienced a general trend of weathering for the source rocks.

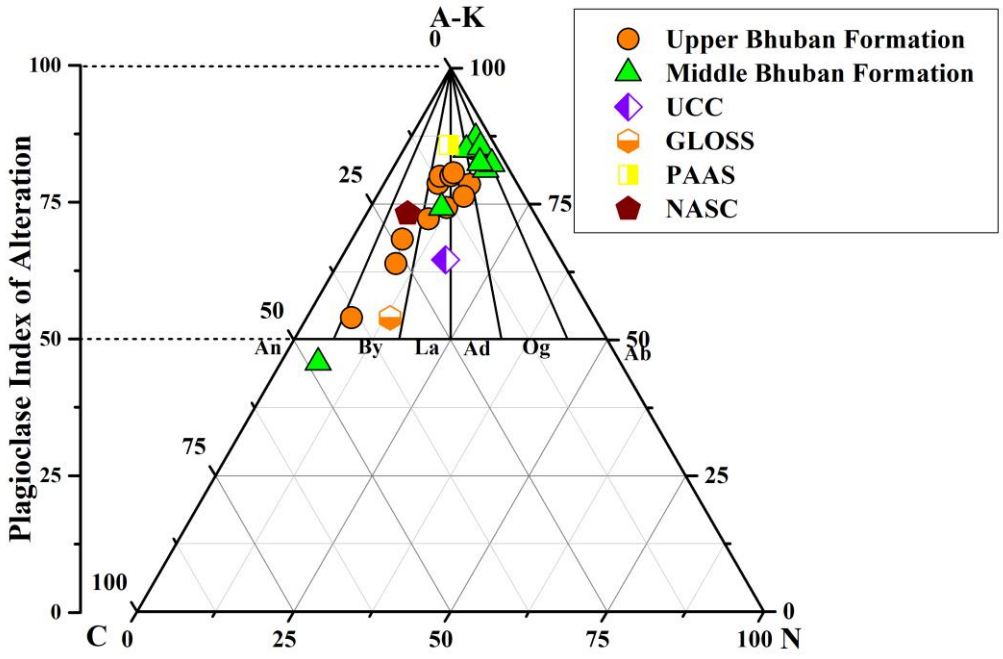

Figure 7.16. The AK–C–N plot for Bhuban sandstones (After Fedo et al. 1995).

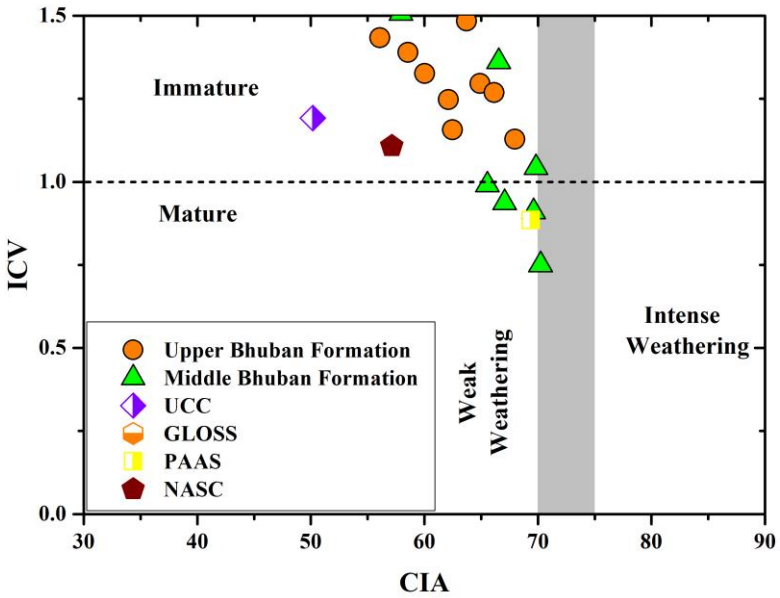

Figure 7.17. The Binary plot of CIA vs. ICV represents the maturity and weathering nature of the Bhuban sediments (Long et al. 2012).

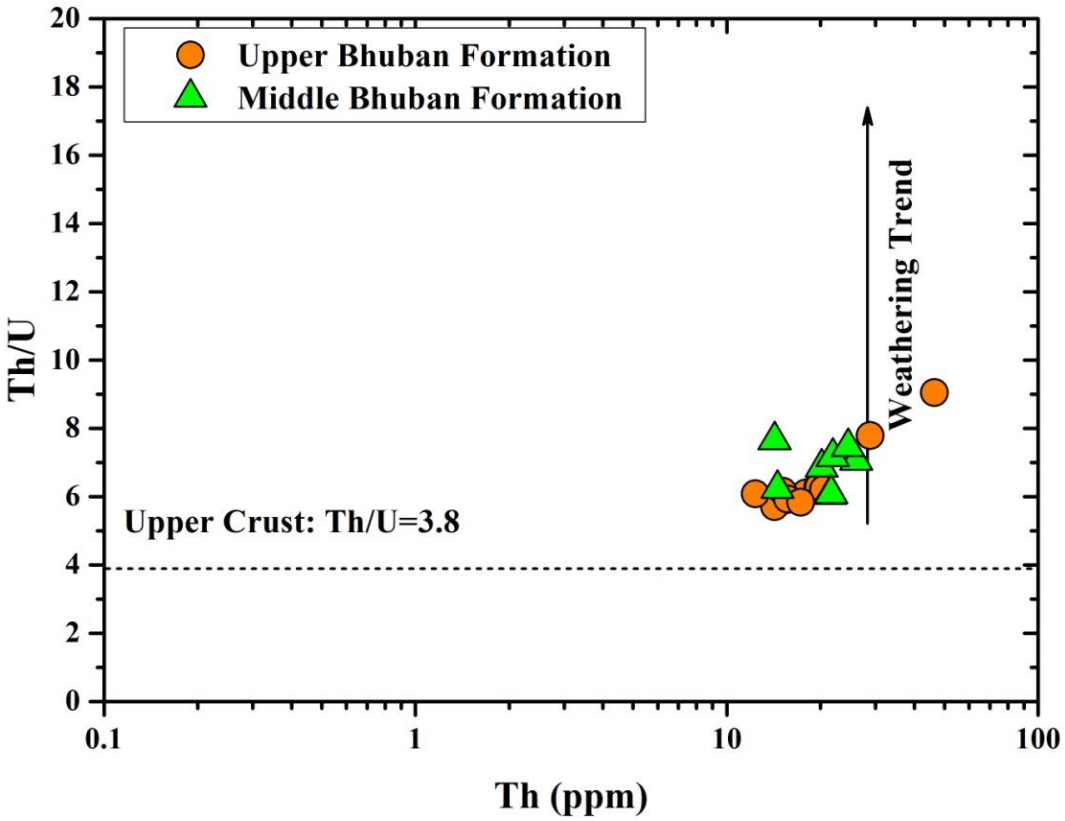

Figure 7.18. The binary plot of Th vs Th/U shows the Upper Crustal signature for the Bhuban sediments and also shows the weathering trend (McLennan and Hanson, 1993).

Table 7.6. Weathering indices and Paleo-climatic Factors of the Bhuban Sandstones: Chemical Index of Alteration (CIA) (after Nesbitt and Young 1982), Plagioclase Index of Alteration (PIA) (after Fedo *et al.* 1995), Chemical Index of Weathering (CIW) (after Harnois 1988), Weathering Index of Parker (WIP) (after Parker 1970), Index of Chemical Variability (ICV) (after Cox *et al.* 1995), C-Value (after Zhao *et al.*, 2007) and Paleoclimatic Factor (PF) (After Samad *et al.*, 2020)

Lithounit	**Sample No.**	**Weathering Indices**					**Paleoclimatic Factors**	
		CIA	**PIA**	**CIW**	**WIP**	**ICV**	**C-Value**	**PF Value**
Upper Bhuban Formation	AR#4	67.97	76.91	81.51	48.59	1.13	0.88	0.97
	AR#5	62.11	67.46	73.35	51.58	1.25	0.72	0.80
	AR#7	62.48	67.77	73.42	46.72	1.16	0.65	0.74
	PK#7A	49.54	49.35	58.01	55.40	1.67	0.60	0.66
	PK#7C	56.06	59.03	67.08	52.33	1.43	0.64	0.71
	PK#8A	53.18	54.44	61.99	57.61	1.65	0.54	0.58
	SS#1A	58.56	61.98	68.32	52.53	1.39	0.67	0.76
	SS#2A	60.03	64.79	71.54	52.09	1.33	0.65	0.74
	SS#3A	41.47	39.04	46.63	59.93	1.87	0.51	0.55
	ZT#6A	64.90	69.38	73.39	45.97	1.30	0.80	0.89
	ZT#6B	63.72	69.57	74.92	45.26	1.48	1.02	1.09
	ZT#7	66.15	70.51	74.02	43.02	1.27	0.99	1.12
Middle Bhuban Formation	AR#1	70.23	79.77	83.63	45.90	0.75	0.67	0.80
	PK#1B	65.56	71.77	76.47	45.16	0.99	0.80	0.92
	PK#1C	69.84	76.61	80.03	36.49	1.04	1.12	1.20
	PK#2	69.63	77.57	81.34	44.59	0.91	0.87	0.98
	PK#3	67.08	73.38	77.53	43.15	0.94	0.85	0.94
	PK#4	66.55	73.41	77.97	43.32	1.36	1.23	1.39
	ZT#1	57.94	61.80	69.27	52.77	1.51	0.71	0.80
	ZT#2	34.97	31.41	38.66	66.20	2.16	0.41	0.43

7.8 Tectono-provenance Settings

Sandstone geochemistry is widely used for the understanding of the paleo-tectonic setup associated with a sedimentary basin. Many workers have proposed several schemes based on the geochemical composition of clastic sediments to decipher the tectonic setting although the majority of them are not always supported in all cases. However major oxide, trace, and REE concentrations utilized for the discriminating diagrams along with their ratios can well differentiate between different tectonic configurations (Bhatia, 1983, 1985; Roser and Korsch, 1986; Bhatia and Crook, 1986; Floyd *et al.*, 1991). For the present study, we have followed ratios of certain elemental concentrations as represented in Table 7.7 and various bivariate plots: (Fe_2O_3+MgO) vs. K_2O/Na_2O (Bhatia, 1983), SiO_2 vs. K_2O/Na_2O (Roser and Korsch, 1986), La/Sc vs. Ti/Zr (Bhatia and Crook, 1986) and discriminant function plot of

[**Discriminant Function-I**: $(-0.0447\times SiO_2) - (0.972\times TiO_2) + (0.008\times Al_2O_3) - (0.267\times Fe_2O_3) + (0.208\times FeO) - (3.082\times MnO) + (0.14\times MgO) + (0.195\times CaO) + (0.719\times Na_2O) - (0.032\times K_2O) + (7.51\times P_2O_5) + 0.303$ and

Discriminant Function-II: $(-0.421\times SiO_2) + (1.988\times TiO_2) -(0.526\times Al_2O_3) - (0.551\times Fe_2O_3) - (1.61\times FeO) + (2.72\times MnO) + (0.881\times MgO) - (0.907\times CaO) - (0.177\times Na_2O) - (1.84\times K_2O) + (7.244\times P_2O_5) + 43.57$] (After Bhatia 1983).

As suggested by Bhatia, 1983 the re-calculated values of major oxides showing higher values of Fe_2O_3+MgO [UBF: 7.75-12 (10.26), MBF: 5.62-10.69 (8.30)] and TiO_2 [UBF: 0.81-1.43 (0.98), MBF: 0.77-1.48 (1)] are representing an Oceanic Island Arc tectonic setup and possible sources like calc-alkaline andesitic rocks exhibiting high concentration of TiO_2, Al_2O_3, Fe_2O_3 and Na_2O. This indicates an initial oceanic arc configuration developed at the initial phase of collision between the oceanic portions of Indian plate (Neo-Tethyan oceanic slab) with the Eurasian plate. This observation is also supported by trace and rare earth elemental ratios suggested by Bhatia, 1985 and Bhatia & Crook, 1986. Discriminating ratios like LREE/HREE [UBF: 3.48-5.53 (4.33), MBF: 4.09-5.17 (4.55)] also support similar tectonic configurations with possible magmatic arc source rocks. Based on these ratios another possible tectonic configuration i.e. Active Continental Margin is also shown by various

observations because after the formation of the magmatic arc, during the last stage of magmatism, the tectonic setup is turned into an active continental margin as a result of a collision between Indian and Eurasian plate. This setup is represented by various ratios like $Al_2O_3/SiO2$ [UBF: 0.17-0.22 (0.19); MBF: 0.18-2-0.24 (0.19)], La_N/Yb_N [UBF: 7.97-13.25 (9.66), MBF: 8.75-12.07 (10.27)], Eu/Eu* [UBF: 0.48-0.67 (0.62), MBF: 0.59-0.69 (0.64)], Zr/Th [UBF: 8.59-15.47 (11.89), MBF: 10.22-17.22 (13.01)] and La/Sc [UBF: 2.49-6.65 (3.90), MBF: 3.96-5.88 (4.64)]. ACM is characterized by higher abundances of LILE such as K [avg. (UBF: 2.33 wt.%, MBF: 2.25 wt.%)], Rb [avg. (UBF: 101.99 ppm, MBF: 92.32 ppm)], Pb [avg. (UBF: 38.15 ppm, MBF: 19.91 ppm)], Th [avg. (UBF: 20.29 ppm, MBF: 20.57 ppm)], Zr [avg. (UBF: 227.71 ppm, MBF: 264.07 ppm)] and ΣREE [(UBF: 421-1097 (558) ppm, MBF: 474-750 (603) ppm)] (Bhatia, 1985, Bhatia & Crook, 1986) indicating possible derivation of sediments from felsic/granitic source rock composition like volcanic arc granite &/or syn-collisional granite supplied from Himalayan sources (Bharali *et al.*, 2021). In addition to this high concentration of REE [avg. (UBF: 558 ppm, MBF: 603 ppm)] of marine Bhuban sandstones represent a craton interior tectonic highland supply of sediments (Bhatia, 1985) indicating supply of sediments from tectonic domains of Himalayan ranges. In addition to this Floyd *et al.,* 1991 proposed the reference value for the OIA, oceanic island arc; CAAM, continental arc + active margin; PM, passive margin; OWP, oceanic within-plate (ocean islands and seamounts) tectonic settings. Correlating with the studied data (Table 7.8) shows a strong positive correlation with the active margin, oceanic island arc, and passive margin, while a moderate positive correlation with the oceanic within-plate setting.

Through this correlation the geochemical characteristics of the Bhuban sediments are similar to the previously observed settings proposed by Bhatia, 1983; Bhatia, 1985 and Bhatia & Crook, 1986.

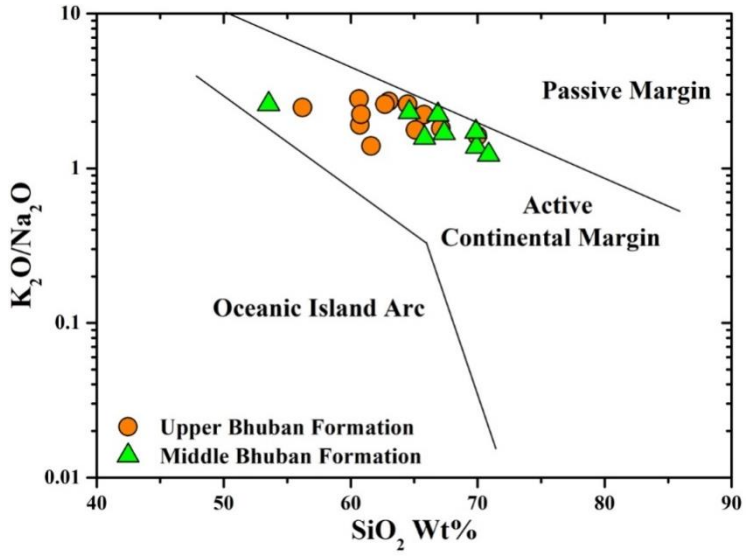

Figure 7.19. SiO_2 vs. K2O/Na_2O bivariate tectonic setting plot (After Roser and Krosch 1986).

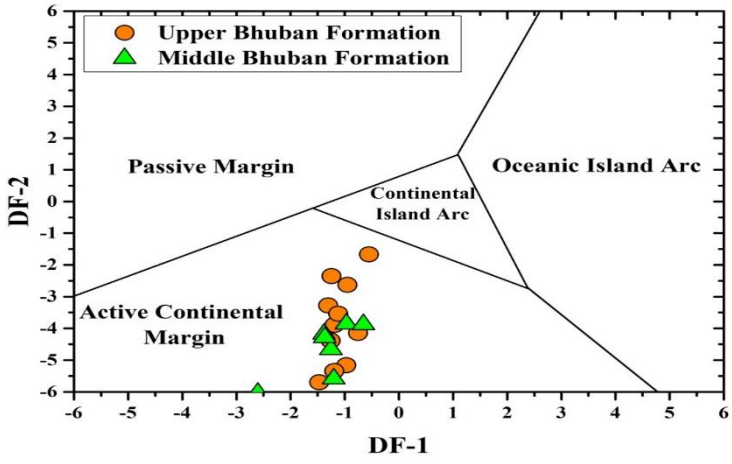

Figure 7.20. The tectonic discriminant function plots for the Bhabhan sandstones (After Bhatia, 1983).

In the binary plot of SiO_2 vs. K_2O/Na_2O (after Roser and Krosch 1986), as represented in Figure 7.19**,** most of the studied samples show clustering in the Active Continental Margin (ACM) setup. Moreover, the binary discrimination plot (Bhatia, 1983) of the studied Bhuban sandstone samples depicts the active continental margin setup (Fig. 7. 20). The trace element-based ternary diagram, i.e., Th-Co-Zr/10 and Th–Sc–Zr/10 (after Bhatia and Crook 1986), shows the Bhuban sediment clustering in the

field of active continental margin with few samples are plotted in the field of continental island arc (CIA) setting **(**Fig. 7.21). Again, in the binary plot of La/Sc vs Ti/Zr after Bhatia and crook (1986) most of the samples fall in the active continental margin field while few are clustered near ACM field (Fig. 7.22). A similar observation is also obtained from the ternary plot of La-Th-Sc after Bhatia, 1983 (Fig. 7.23).

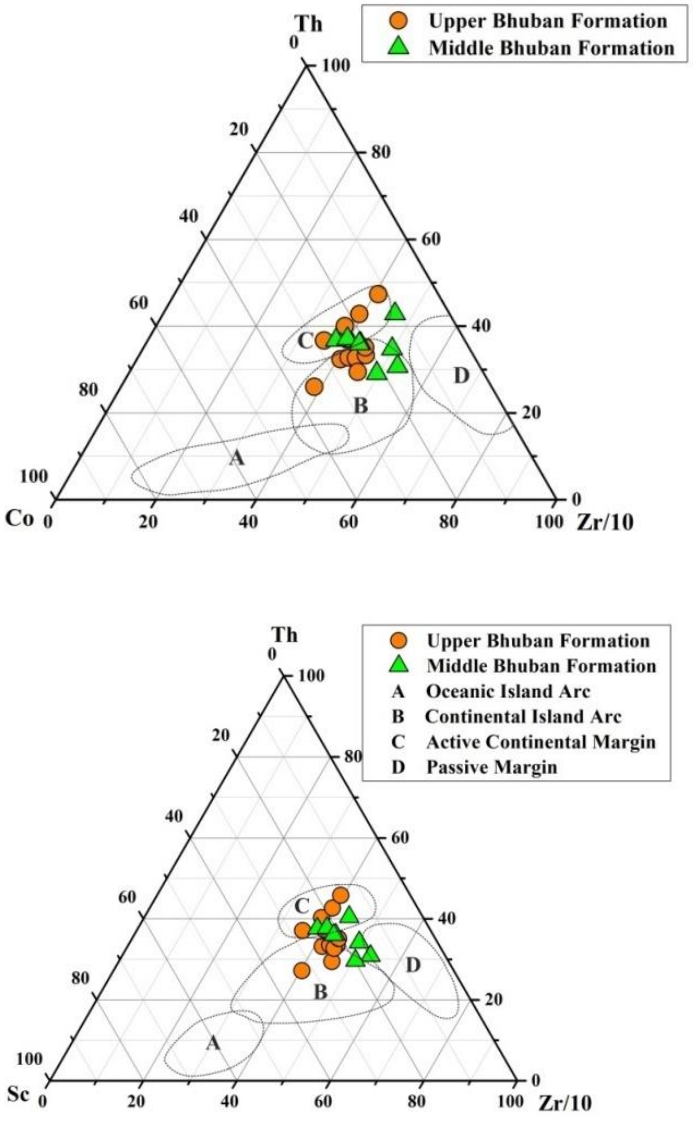

Figure 7.21. Tectonic setting plot after Bhatia and Crook (1986) of Bhuban sediments; A- oceanic island arc; B- continental island arc; C- active continental margin; D- passive margin.

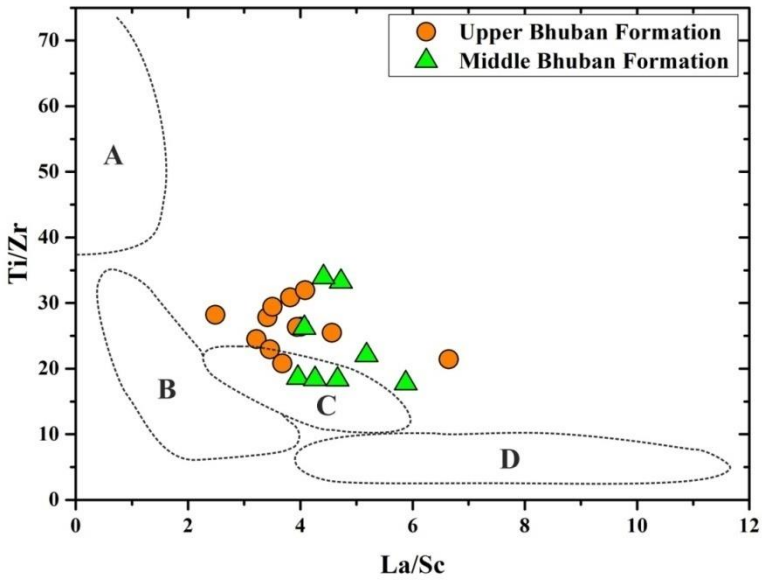

Figure 7.22. The bivariate plot of La/Sc vs Ti/Zr for the Bhuban sandstones (Bhatia and Crook, 1986); A- oceanic island arc; B- continental island arc; C- active continental margin; D-passive margin.

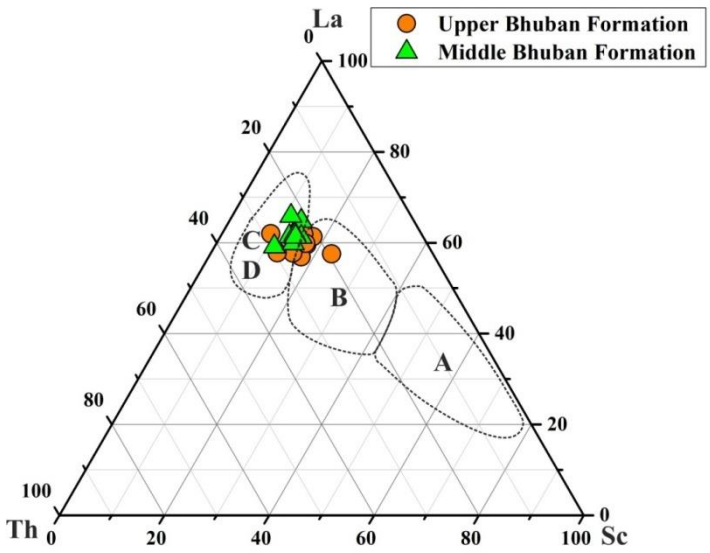

Figure 7.23. La-Th-Sc ternary plot after Bhatia, 1983; A- oceanic island arc; B- continental island arc; C- active continental margin; D-passive margin.

Previous studies on Bhuban sandstones from Surma Basin by (Bharali et al., 2018 and Bharali et al. 2021 reported that the sediments have been deposited in an active continental margin setup primarily based on the sandstone geochemistry.

Therefore based on the previous studies, various elemental ratios, and their correlations with the tectonic setting and plotting suggested an oceanic island arc to active continental margin setup that developed sequentially within the source area i.e. the Himalayan ranges which supplied the sediments from source rocks mostly various granitoid (VAG, syn-collisional Granite and Andesitic composition) derived in such settings that contributed a major portion of the studied sandstones of Upper and Middle Bhuban Formations which deposited in the central part of Surma Basin during Mio-Pliocene time.

Table 7.7. The tectonic setting parameter in comparison with Bhuban Sandstones (Bhatia, 1983; Bhatia, 1985 & Bhatia and Crook, 1986).

Elemental Parameters	Oceanic Island Arc	Continental Island Arc	Active Continental Margin	Passive Margin	Present study	
					UBF	MBF
Fe_2O_3+MgO^+	High: 8-14%	Lower: 5-8%	Low: 2-5%	Very Low: >2%	7.75-12 (10.26)	5.62-10.69 (8.30)
TiO_2^+	High: 0.8-1.4%	Lower: 0.5-0.7%	Low: 0.25-0.45%	Depleted Conc.	0.81-1.43 (0.98)	0.77-1.48 (1)
Al_2O_3/SiO_2^+	High: 0.24-0.33	Lower: 0.15-0.20	Low: 0.1-0.2	Very low: >0.1	0.17-0.22 (0.19)	0.18-0.24 (0.19)
K_2O/Na_2O^+	Low: 0.2-0.4	Higher: 0.4-0.8	High: ≃1	High: >1	1.39-2.79 (2.18)	1.22-2.59 (1.84)
$Al_2O_3/CaO+Na_2O^+$	Low: 1-2	Higher: 0.5-2.5	-	Higher (variable)	1.56-7.44 (4.20)	1.13-8.57 (5.61)
Bhatia 1983	Derived from Calc Alkaline Andesite	Derived from Felsic Volcanic	Uplifted Basement	Highly variable	-	-
	High: TiO_2, Al_2O_3, Na_2O, Fe_2O_3	High: SiO_2, K_2O	UCC Equivalent	Enriched SiO_2	-	-
	Low: SiO_2, K_2O	Low: Fe_2O_3, MgO	High: SiO_2, K_2O	Depleted Al_2O_3, TiO_2, Na_2O, CaO	-	-
		K_2O/Na_2O: ~0.6	K_2O/Na_2O: ~1	K_2O/Na_2O>1	-	-
REE[$]	58(±10)	146(±20)	186	210	421-1097 (558)	474-750 (603)

Table 7. Cont...

(Provenance)	(Undissected Magmatic Arc)	(Dissected Magmatic Arc)	(Uplifted Basement)	(Craton Interior Tectonic Highland)	-	-
$(La/Yb)_N$[$]	2.8(±0.9)	7.5(±2.5)	8.5	10.8	7.97-13.25 (9.66)	8.75-12.07 (10.27)
LREE/HREE	3.8(±0.9)	7.7(±1.7)	9.1	8.5	3.48-5.53 (4.33)	4.09-5.17 (4.55)
Eu/Eu*	1.04(±0.11)	0.79(±0.13)	0.6	0.56	0.48-0.67 (0.62)	0.59-0.69 (0.64)
K/Rb[%]	578(±92)	219(±28)	189(±20)	178(±20)	214-248 (229)	198-268 (246)
Zr/Hf[%]	45.7	36.3	26.3	29.5	29.91-34.17 (30.81)	29.77-32.19 (30.69)
Zr/Th[%]	48(±13.4)	21.5(±2.4)	9.5(±0.7)	19.1(±5.8)	8.59-15.47 (11.89)	10.22-17.22 (13.01)
La/Th[%]	4.26(±1.2)	2.36(±0.3)	1.77(±0.10)	2.2(±0.47)	1.95-2.98 (2.46)	2.01-3.01 (2.55)
La/Sc[%]	0.55(±0.22)	1.82(±0.3)	4.55(±0.8)	6.25(±1.35)	2.49-6.65 (3.90)	3.96-5.88 (4.64)
Ti/Zr[%]	56.8(±21.4)	19.7(±4.3)	15.3(±2.4)	6.47(±0.9)	20.78-31.91 (26.31)	17.75-33.90 (23.54)

Table 7.8. Reference average composition of late Proterozoic sandstones from various tectonic settings in comparison with studied Bhuban sandstones (Floyd et al. 1991).

Oxides/Elements	**Tectonic Settings**				**Present study**	
	OIA	**CAAM**	**PM**	**OWP**	**UBF**	**MBF**
SiO_2	58.25	68.73	82.59	51.42	63.17	66.11
TiO_2	0.98	0.58	0.62	2.52	0.98	1.00
Al_2O_3	15.55	13	7.16	14.66	12.55	13.11
Fe_2O_3*	7.7	5.35	3.62	13.48	6.82	6.23
MnO	0.18	0.08	0.15	0.23	0.09	0.13
MgO	3.1	2.6	1.72	6.61	3.44	2.07
CaO	5.51	2.76	0.19	9.15	2.08	1.61
Na_2O	4.13	2.41	1.02	2.86	1.32	1.54
K_2O	1.17	1.65	1.09	0.7	2.81	2.72
P_2O_5	0.23	0.14	0.11	0.28	0.17	0.18
Ba	370	481	255	209	327.95	350.51
Ce	22	48	56	24	97.37	106.87
Cr	49	55	29	230	30.29	28.58
Cu	29	22	8	77	25.63	28.41
Ga	20	15	8	--	15.44	14.57
La	10	23	22	10	48.12	51.62
Nb	5	9	7	27	16.66	17.03

Nd	10	24	39	15	42.69	46.50
Ni	22	31	15	114	26.15	21.14
Pb	15	15	11	--	38.15	19.91
Rb	30	62	50	19	101.99	92.32
Sc	27	16	8	30	12.26	11.18
Sr	362	274	72	432	116.14	94.47
V	188	106	44	400	82.62	74.24
Y	15	17	24	20	33.01	33.75
Zn	88	73	49	122	39.00	40.64
Zr	99	146	302	146	227.71	264.07
Cs	0.6	4.7	4.9	0.7	6.76	4.81
Hf	1.7	4.7	8.8	2.6	7.41	8.60
Ta	0.4	0.8	0.6	2	1.31	1.28
Th	1.9	8.5	8.1	1	20.29	20.57
U	0.8	2	3.2	0.3	3.05	3.04
Correlation Coefficient						
OIA		**CAAM**		**PM**		**OWP**	
UBF	**MBF**	**UBF**	**MBF**	**UBF**	**MBF**	**UBF**	**MBF**
0.77	**0.72**	**0.90**	**0.87**	**0.94**	**0.96**	**0.51**	**0.45**

CHAPTER -8
SUMMARY AND CONCLUSIONS

The intended research aims to investigate the sedimentary characteristics of the Bhuban Formation, situated within the Surma Group of rock formations in the Aizawl district, Mizoram. This research work involved mainly understanding the depositional environments, characteristics of the source rocks, tectonic-provenance settings, and sequence stratigraphy of the study area. This study was carried out through a combination of laboratory analysis such as petrography, heavy mineral analysis, and whole-rock geochemical analysis while field observations include lithofacies analysis and sequence stratigraphy.

The study area encompasses the Miocene Bhuban Formation, which has been subdivided into Upper and Middle units of the Bhuban Formations, ranging from Early to Middle Miocene age. Geographically, the study area extends between 23° 38′ to 23° 46′ N latitude and 92°43′ to 92° 49′ E longitude with a maximum elevation of 1159 m MSL. The analyzed sandstones mostly exhibit fine-to-medium grains and have a buff color, with only a few outcrops demonstrating massive bedding. Conversely, the shales are compact, hard, and have a dark grey color.

The field observations reveal that the Bhuban sandstones from both Upper Bhuban and Middle Formations consist of varying thicknesses of sandstone, siltstone, and shale. Shales are described as fragile and prone to crumpling, while sandstones are exhibiting massive bodies with tough, compact, and buff-colored, as well as fine to medium-grained texture. Current-bedding, ball and pillow structures, hummocky cross-stratification, planner lamination, and ripple-marked are common sedimentary structures that are frequently observed within the sandstones of the Bhuban formation. Apart from the analysis of the sequence stratigraphy, there are four types of system tracts observed, Falling Stage System Tract (FSST), Lowstand System Tract (LST), Transgressive System Tract (TST), and High stand System Tract (HST). Based on field observations and sedimentary structures present in the study area, a predominantly fluvio-tidal environment has been envisaged.

The petrographic and mineralogical studies were combined to assess the mineralogical composition, classification, tectonic-provenance settings, paleoclimatic conditions, and diagenetic changes of the Bhuban sandstones. The findings from the petrographic and modal composition studies indicate that the primary detrital components of the Bhuban sandstones consist of quartz (mainly monocrystalline and polycrystalline quartz), feldspar (predominantly K-feldspar and plagioclase feldspar), and lithic fragments (mostly met-amorphic and sedimentary). Based on the petrographical textural relationships, it can be inferred that the sandstones are primarily sub-litharenite and arkosic wacke, possessing a fine-to-medium grain size and poor to moderate sorting. The grains are sub-rounded to sub-angular in shape. Further sedimentological analysis indicates that a substantial amount of the studied sandstones are derived from a granitic source rock composition, with a significant detritus contribution from a medium- to high-rank metamorphic source. The analysis of tectono-provenance settings using petrographic ternary plots Q_mFL_t and Q_tFL revealed that the sediments were sourced from a recycled orogen, under humid climatic conditions, with minimal contributions from the craton interior. The examined area underwent a complex diagenetic process, which affected the Bhuban Sandstones in various ways, including compaction, cementation, replacement, recrystallization, dissolution, and mineral overgrowths. These diagenetic processes progressed through early, late, and uplift-related stages. This investigation concluded that the Bhuban Sandstones have low porosity and isolated pores, resulting in low permeability, making them unsuitable for hydrocarbon production.

Based on grain size analysis the Bhuban sediments have been interpreted based mostly on univariate grain size parameters, bivariate plots, linear discriminant function, and log–log probability curves, and the C–M pattern. According to the grain size distribution, Bhuban sediments are predominantly fine-grained, poorly sorted to moderately sorted, platykurtic to mesokurtic, and mainly coarse-skewed. The nature of fine-grained sediments points to the fact that moderately low-energy conditions dominated in the study area. The poorly to moderately sorted nature of the sediments is due to the short to moderate distance of sediment transportation, and their characteristics indicate that they were deposited in a shallow marine condition with the influence of fluvial characteristics. The dominance of the coarse skewed category

indicates that during the deposition of sediments, there was moderate to high-energy condition with some riverine input. The univariate grain size parameters of volume percent frequency curves show that most of the Bhuban sediments are bimodal with peaks of 1.0, 3.5, and 4.0 due to low to medium energy conditions of the marine setting at the time of deposition. Various linear discriminant functions also suggest that sediments have been deposited in a shallow marine setup with the influence of fluvial process and turbidity action. The C–M pattern signifies that the transport mechanisms of the analyzed sediments were mostly deposited by suspension with some rolling sediments, which resulted in finer to medium fractions under the influence of fluvial action in marine conditions.

Based on heavy mineral analysis reveals that the abundance of zircon and rutile in the form of euhedral suggests that these rocks originated from acidic igneous and crystalline metamorphic rocks as well as short to moderate distances of sediment transportation. In addition to this, prismatic and angular zircon grains and a significant proportion of opaque minerals also show that the sediments were sourced from igneous rock. However, rounded zircons, tourmalines, and rutile are also often found, which shows that sedimentary rock may have been recycled and transported over a considerable distance. Zircon fragments suggest a short to moderate distance of transportation as well while the ZTR index for Bhuban sediments displays a low value which suggests that the sediments are mineralogically immature. The presence of kyanite, staurolite, sillimanite, tourmaline and rutile in examined Bhuban sandstones indicates that they originated from a metamorphic source of high rank.

The whole-rock geochemical analysis reveals a higher concentration of SiO_2, followed by Al_2O_3, Fe_2O_3, MgO, K_2O, Na_2O, CaO, MnO, and P_2O_5. The SiO_2/Al_2O_3 ratio is high, averaging 5.06 for UBF and 5.07 for MBF. This suggests that the ratio increases due to weathering, recycling processes, and sediment transport processes. As a result, the population of quartz grains increases, indicating the leaching of less resistant minerals over time. The analysis of the Bhuban sandstone's Rare Earth Elements (REE) concentration, when compared to chondrite normalized patterns, reveals that the Light Rare Earth Elements (LREE: La-Gd) are enriched over Heavy Rare Earth Elements (HREE: Tb-Lu), with avg. LREE/HREE ratio of 9.803 ppm, with

a Negative Eu anomaly of 0.62. Additionally, there are relatively lower concentrations of Sr due to the fractionation of Ca-rich plagioclase from the source rocks. These findings suggest that the sandstone likely originated from fractionated felsic source rocks, such as granitoids, as indicated by the REE ratio and chondrite normalized pattern.

By integrating the different geochemical schemes of classification, Bhuban sandstones are primarily identified as litharenite, with arkose and wacke types. By assimilation, the different provenance plots based on Geochemistry analysis indicate that the sediments were derived from the felsic rocks viz. granite, granodiorite, and their metamorphic equivalents of upper to middle grade viz. schist, gneisses, etc.

The tectonic setting of Bhuban sandstones are primarily characterized by the active continental margin based on geochemical analysis with less weathered from the source rocks under the semi-humid to humid climatic conditions.

REFERENCES

Aagaard, P., Egeberg, P. K., Saigal, G. C., Morad, S., & Bjorlykke, K. (1990). Diagenetic albitization of detrital K-feldspars in Jurassic, Lower Cretaceous and Tertiary clastic reservoir rocks from offshore Norway; II, Formation water chemistry and kinetic considerations. *Journal of Sedimentary Research, 60*(4), 575-581. https://doi.org/10.1306/212F91EC-2B24-11D7-8648000102C1865D.

Ahmad, F., Amir, M., Quasim, M. A., Absar, N., & Ahmad, A. H. M. (2022). Petrography and geochemistry of the Middle Jurassic Fort Member Sandstone, Jaisalmer Formation, Western India: Implications for weathering, provenance and tectonic setting. *Geological Journal, 57*(5), 1741–1758. https://doi.org/10.1002/gj.4372.

Ahmad, F., Quasim, M. A., Ahmad, A. H. M., Ghaznavi, A. A., Khan, Z., & Albaroot, M. (2019). Factors influencing detrital mineralogy and tectono-provenance of Fort Member Sandstone, Jaisalmer Formation, Western Rajasthan, India. *Journal of the Geological Society of India, 93*, 392-398. https://doi.org/10.1007/s12594-019-1193-x.

Al Areeq, N. M., Soliman, M. A., Essa, M. A., & Al-Azazi, N. A. (2016). Diagenesis and reservoir quality analysis in the Lower Cretaceous Qishn sandstones from Masila oilfields in the Sayun–Masila Basin, eastern Yemen. *Geological Journal, 51*(3), 405-420. https://doi.org/10.1002/gj.2639.

Anithamary, I., Ramkumar, T. & Senapathi, V., (2011). Grain size characteristics of the Coleroon estuary sediments, Tamilnadu, East coast of India. *Carpathian Journal of Earth and Environmental Sciences*.151–157.

Armstrong-Altrin, J. S. (2009). Provenance of sands from Cazones, Acapulco, and Bahı´a Kino beaches, Mexico. *Revista Mexicana de Ciencias Geologicas.* 26(3): 764-782.

Armstrong-Altrin, J. S., Nagarajan, R., Madhavaraju, J., Rosalez-Hoz, L., Lee, Y. I., Balaram, V., ... & Avila-Ramírez, G. (2013). Geochemistry of the Jurassic and Upper Cretaceous shales from the Molango Region, Hidalgo, eastern Mexico: Implications for source-area weathering, provenance, and tectonic setting. *Comptes Rendus Geoscience, 345*(4), 185-202.

Badekar, A. G., Sangode, S. J., Ghosh, S. K., Tiwari, R. P., Meshram, D. C., Malsawma, J., & Lalnuntluanga, P. (2013). Petromineralogic and rock magnetic aspects of clastic sedimentation in the Surma basin, Mizoram. *Journal of the Geological Society of India, 82,* 23-37. https://doi.org/10.1007/s12594-013-0118-3.

Bai, Y., Liu, Z., Sun, P., Liu, R., Hu, X., Zhao, H., & Xu, Y. (2015). Rare earth and major element geochemistry of Eocene fine-grained sediments in oil shale-and coal-bearing layers of the Meihe Basin, Northeast China. *Journal of Asian Earth Sciences, 97,* 89-101.

Baiyegunhi, C., Liu, K. & Gwavava, O., (2017). Grain size statistics and depositional pattern of the Ecca Group sandstones, Karoo Supergroup in the Eastern Cape Province, South Africa. *Open Geosciences*, *9(1).* doi:10.1515/geo-2017-0042.

Baiyegunhi, C., Liu, K., & Gwavava, O. (2017). Diagenesis and Reservoir Properties of the Permian Ecca Group Sandstones and Mudrocks in the Eastern Cape Province, South Africa. *Minerals, 7*(6), 88. https://doi.org/10.3390/min7060088

Baiyegunhi, T. L., Liu, K., Gwavava, O. & Baiyegunhi, C., (2020). Textural characteristics, mode of transportation and depositional environment of the Cretaceous sandstone in the Bredasdorp Basin, off the south coast of South Africa: Evidence from grain size analysis. *Open Geosciences*, *12(1),* 1512–1532. doi:10.1515/geo-2020-0135.

Baiyegunhi, T. L., Liu, K., Gwavava, O., & Baiyegunhi, C. (2020). Petrography and Tectonic Provenance of the Cretaceous Sandstones of the Bredasdorp Basin, off the South Coast of South Africa: Evidence from Framework Grain Modes. *Geosciences, 10*(9), 340. https://doi.org/10.3390/geosciences10090340

Baiyegunhi, T. L., Liu, K., Gwavava, O., Wagner, N., & Baiyegunhi, C. (2020). Geochemical evaluation of the Cretaceous mudrocks and sandstones (wackes) in the Southern Bredasdorp Basin, Offshore South Africa: Implications for hydrocarbon potential. *Minerals, 10*(7), 595.

Banerjee. (1980). Palynological palaeoecology of the Tertiary sub-surface sediments of Upper Assam, India. *Proceedings IV International Palynological Conference, Lucknow* (1976-1977) 2 :708-71

Barman, B.K., & K.S., Rao. (2021). Geology of Sedimentary Formation in the state of Mizoram, NE India: A Review. In *Mizoram: Environment, development, and Climate Change*, Sati, V. P. (Ed.). Today and Tomorrow's printers and publishers New Delhi. 183-195. ISBN: 9788170197010.

Basu, A. (1985). Reading provenance from detrital quartz. *In Provenance of arenites* (pp. 231-247). Dordrecht: Springer Netherlands.

Basu, A., Young, S. W., Suttner, L. J., James, W. C., & Mack, G. H. (1975). Re-evaluation of the use of undulatory extinction and polycrystallinity in detrital quartz for provenance interpretation. *Journal of Sedimentary Research*, *45*(4), 873-882. https://doi.org/10.1306/212F6E6F-2B24-11D7-8648000102C1865D

Behra, U. K., Mohanty, B. K., Lahiri, S., Ray, J. N., Gupta, G. D., Prakash, H. S. M. & Kesari, G. K. (2011). Geology and mineral resources of Manipur, Mizoram, Nagaland and Tripura. *Geological Survey of India Miscellaneous Publications.* No. *30(4) 1(2),* 103.

Berner, R. A. (1980). *Early diagenesis: a theoretical approach* (No. 1). Princeton University Press.

Bharali, B. (2018). A Study on Tectono Provenance and Depositional Environment of The Bhuban Formation in And Around Aizawl Mizoram. PhD Thesis. Accessed from: http://hdl.handle.net/10603/250505

Bharali, B., Borgohain, P., Bezbaruah, D., Vanthangliana, V., Phukan, P. P., & Rakshit, R. (2017). A geological study on Upper Bhuban Formation in parts of Surma Basin, Aizawl, Mizoram. *Science Vision, 17*(3), 128-147.

Bharali, B., Hussain, M. F., Borgohain, P., Bezbaruah, D., Vanthangliana, V., Rakshit, R., & Phukan, P. P. (2021). Reconstruction of Middle Miocene Surma Basin as two arcs derived sedimentary model: Evidence from provenance, source rock weathering and paleo-environmental conditions. *Geochemistry International, 59,* 264–289. https://doi.org/10.1134/S0016702921030022.

Bhatia, M. R. (1983). Plate tectonics and geochemical composition of sandstones. *Journal of Geology, 91,* 611-627.

Bhatia, M. R. (1985). Rare earth element geochemistry of Australian Paleozoic graywackes and mudrocks: Provenance and tectonic controls. *Sedimentary Geology, 45,* 97-113.

Bhatia, M. R., & Crook, K. A. W. (1986). Trace element characteristics of graywackes and tectonic setting discrimination of sedimentary basins. *Contributions to Mineralogy and Petrology, 92,* 181-193.

Blatt, H. (1967). Original characteristics of clastic quartz grains. *Journal of Sedimentary Research, 37*(2), 401-424.

Blatt, H. (1967). Provenance determinations and recycling of sediments. *Journal of Sedimentary Research, 37,* 1031-1044.

Blatt, H., Middleton, G. V., & Murray, R. C. (1980). *Origin of sedimentary rocks* (2nd ed.). Prentice Hall.

Blatt, H., Middleton, G., & Murray, R. (1980). *Origin of sedimentary rocks*.

Boggs, S. (2009). *Petrology of sedimentary rocks*. Cambridge University Press.

Boggs, S. J. (2014). *Principles of sedimentology and stratigraphy* (5th ed., p. 564). Pearson Education, Inc.

Borgohain, P., Hussain, M. F., Bezbaruah, D., Vanthangliana, V., Phukan, P. P., Gogoi, M. P., & Bharali, B. (2020). Petrography and whole-rock geochemistry of Oligocene Barail Sandstones of Surma Basin: Implications for tectono-provenance and paleoclimatic condition. *Journal of Earth System Science, 129*(179). https://doi.org/10.1007/s12040-020-01431-y

Bracciali, L., Marroni, M., Pandolfi, L., & Rocchi, S. (2007). Geochemistry and petrography of Western Tethys Cretaceous sedimentary covers (Corsica and Northern Apennines): From source areas to configuration of margins. In J. Arribas, S. Critelli, & M. J. Johnsson (Eds.), *Sedimentary provenance and petrogenesis: Perspectives from petrography and geochemistry* (Vol. 420, pp. 73-93). Geological Society of America Special Paper.

Bracciali, L., Najman, Y., Parrish, R. R., Akhter, S. H., & Millar, I. (2015). The Brahmaputra tale of tectonics and erosion: Early Miocene River capture in the Eastern Himalaya. *Earth and Planetary Science Letters, 415,* 25-37.

Bruun, P., (1962). Sea-level rise as a cause of shore erosion. Proceedings of the American Society of Civil Engineers. *Journal of the Waterways and Harbors Division*, 88: 117–130.

Cantalamessa, G., & Di Celma, C. (2004). Sequence response to syndepositional regional uplift: insights from high-resolution sequence stratigraphy of late Early Pleistocene strata, Periadriatic Basin, central Italy. *Sedimentary Geology, 164* (3-4), 283-309.

Cao, J., Wu, M., Chen, Y., Hu, K., Bian, L., Wang, L., & Zhang, Y. (2012). Trace and rare earth element geochemistry of Jurassic mudstones in the northern Qaidam Basin, northwest China. *Geochemistry, 72(3),* 245-252.

Cartwright, J. A. (1994). Episodic basin-wide fluid expulsion from geopressured shale sequences in the North Sea basin. *Geology*, *22*(5), 447-450. https://doi.org/10.1130/0091-7613(1994)022<0447: EBWFEF>2.3.CO;2

Catuneanu, O. (2002). Sequence stratigraphy of clastic systems: concepts, merits, and pitfalls. *Journal of African Earth Sciences*, *35*(1), 1-43.

Catuneanu, O. (2006). Principles of Sequence Stratigraphy. Elsevier, Amsterdam, 1-375 pp.

Catuneanu, O., & Zecchin, M. (2013). High-resolution sequence stratigraphy of clastic shelves II: Controls on sequence development. *Marine and Petroleum Geology, 39*, 26–38.

Catuneanu, O., Abreu, V., Bhattacharya, J. P., Blum, M. D., Dalrymple, R. W., Eriksson, P. G., ... & Winker, C. (2009). Towards the standardization of sequence stratigraphy. *Earth-Science Reviews*, *92*(1-2), 1-33.

Catuneanu, O., Galloway, W. E., Kendall, C. G. S. C., Miall, A. D., Posamentier, H. W., Strasser, A., & Tucker, M. E. (2011). Sequence stratigraphy: methodology and nomenclature. *Newsletters on stratigraphy*, *44*, 173-245.

Catuneanu, O., Willis, A. J., & Miall, A. D. (1998). Temporal significance of sequence boundaries. *Sedimentary Geology*, *121*(3-4), 157-178.

Chapelle, F. H. (1993). *Ground-Water Microbiology and Geochemistry*. (p. 448), John Wiley and Sons: New York, NY, USA, 448.

Chaudhuri, A., Banerjee, S., & Chauhan, G. (2020). Compositional evolution of siliciclastic sediments recording the tectonic stability of a pericratonic rift:

Mesozoic Kutch Basin, western India. *Marine and Petroleum Geology*, 111, 476-495.

Chenkual, L., Kataki, T., & Sarma, J. N. (2010). Heavy minerals of Tertiary rocks exposed in Teidukhan anticline, Kolasib, Mizoram, India. *Sci Vis*, 10(1), 7-19.

Chima, P., Baiyegunhi, C., Liu, K., & Gwavava, O. (2018). Diagenesis and rock properties of sandstones from the Stormberg Group, Karoo Supergroup in the Eastern Cape Province of South Africa. *Open Geoscience, 10*, 740-771. https://doi.org/10.1515/geo-2018-0059.

Cobbold, P. R., Zanella, A., Rodrigues, N., & Løseth, H. (2013). Bedding-parallel fibrous veins (beef and cone-in-cone): Worldwide occurrence and possible significance in terms of fluid overpressure, hydrocarbon generation and mineralization. *Marine and Petroleum Geology, 43*, 1-20. https://doi.org/10.1016/j.marpetgeo.2013.01.010

Conybeare, D. M., & Shaw, H. F. (2000). Fracturing, overpressure release and carbonate cementation in the Everest Complex, North Sea. *Clay Minerals, 35*(1), 135-149.

Cosgrove, J. W. (2001). Hydraulic fracturing during the formation and deformation of a basin: A factor in the dewatering of low-permeability sediments. *American Association of Petroleum Geologists Bulletin, 85*(4), 737-748. https://doi.org/10.1306/8626C997-173B-11D7-8645000102C1865D

Cox, R., Lowe, D. R., & Cullers, R. L. (1995). The influence of sediment recycling and basement composition on evolution of mudrock chemistry in the southwestern United States. *Geochimica et Cosmochimica Acta*, *59*(14), 2919-2940.

Crook, K. A. (1974). Lithogenesis and geotectonics: the significance of compositional variation in flysch arenites (graywackes).

Cross, T. A., & Lessenger, M. A. (1988). Seismic stratigraphy. *Annual Review of Earth and Planetary Sciences, 16*, 319.

Cui, X., & Radwan, A. E. (2022). Coupling relationship between current in-situ stress and natural fractures of continental tight sandstone oil reservoirs. *Interpretation, 10*(3), SF9-SF21. https://doi.org/10.1190/INT-2021-0200.1

Cullers, R. L. (1994). The controls on the major and trace element variation of shales, siltstones and sandstones of Pennsylvanian-Permian age from uplifted continental blocks in Colorado to platform sediment in Kansas, USA. *Geochimica et Cosmochimica Acta. 58,* 4955-4972.

Cullers, R. L. (1995). The controls on the major and trace element evolution of shales, siltstones and sandstones of Ordovician to Tertiary age in the Wet Mountain region, Colorado, USA. *Chem. Geol, 123*, 107-131.

Cullers, R. L. (2000). The geochemistry of shales, siltstones and sandstones of Pennsylvanian- Permian age, Colorado, USA: Implications for provenance and metamorphic studies. *Lithos, 51,* 181-203.

Cullers, R. L. and Podkovyrov, V. N. (2000). Geochemistry of the Mesoproterozoic Lakhanda shales in southeastern Yakutia, Russia: Implications for mineralogical and provenance control, and recycling. *Precambrian Research, 104*, 77-93.

Cullers, R. L., & Podkovyrov, V. N. (2002). The source and origin of terrigenous sedimentary rocks in the Mesoproterozoic Ui Group, southeastern Russia. *Precambrian Research, 117,* 157–183. https://doi.org/10.1016/S0301-9268(02)00079-7

Dasgupta, S. (1984). Tectonic trends in Surma basin and possible genesis of folded belt. *Memoirs of the Geological Survey of India, 113*, 58- 61.

Devi, S. R., & Mondal, M. E. A. (2008). Provenance and Tectonic Setting of Barail (Oligocene) and Surma (Miocene) Group of Surma-Barak Basin, Manipur, India: Petrographic Constraints. *Geological Society of India, 71*(4), 459-467.

Devi, T. D. (2014). Textural characteristics and depositional environment of olistostromal sandstone of ukhrul, Manipur. *International Journal of Recent Development in Engineering and Technology*, *2*(1), 92-100.

Dickinson, W. R. (1970). Interpreting detrital modes of graywacke and arkose. *Journal of Sedimentary Research*, *40*(2), 695-707. https://doi.org/10.1306/74D72018-2B21-11D7-8648000102C1865D

Dickinson, W. R. (1985). Interpreting provenance relations from detrital modes of sandstones. In: Zuffa, G.G. (Ed.), Provenance of Arenites. *D. Reidel Publ. Co., Dordrecht*, New York, 333-361.

Dickinson, W. R., & Suczek, C. A. (1979). Plate tectonics and sandstone compositions. *American Association of Petroleum Geologists Bulletin*, *63*(12), 2164-2182.

Dickinson, W. R., Beard, L. S., Brakenridge, G. R., Erjavec, J. L., Ferguson, R. C., Inman, K. F., ... & Ryberg, P. T. (1983). Provenance of North American Phanerozoic sandstones in relation to tectonic setting. *Geological Society of America Bulletin*, *94*(2), 222-235.

Dickinson, W.R., & Suczek, C.A., (1979). Plate Tectonics and Sandstone Compositions. *American Association of Petroleum Geologists 63*, 2164–2182. https://doi.org/10.1306/2F9188FB-16CE-11D7-8645000102C1865D

Duane., (1964). Significance of skewness in recent sediments, western Pamlico Sound, North Carolina. *Journal of Sedimentary Petrology*, *34*(4), 864–74.

Duhawma, K.S., Rao, K., & Ch. U., Rao., (2016). Morphometry and Tectonic geomorphology of Tut watershed in Mizoram. K. Lal Duhawma, Koduru Srinivasa Rao, and Chegondi Udayabhaskara Rao (Eds.) Lap-Lambert Lap-Lambert Academic publishing, Germany. 109p. *Folded Belt. Rec. GSI* 113, 58–61.

Dutta, B. (2005). Provenance, tectonics and palaeoclimate of Protero zoic Chandarpur sandstones, Chattisgarh basin: A petrographic view. *Journal of Earth System Sciences*, *114*, 227–245. https://doi.org/10.1007/BF02702947

Ehrenberg, S. N. (1990). Relationship between diagenesis and reservoir quality in sandstones of the Garn Formation, Haltenbanken, mid-Norwegian continental shelf. *American Association of Petroleum Geologists* bulletin, *74*(10), 1538-1558. https://doi.org/10.1306/0C9B2515-1710-11D7-8645000102C1865D

Embry, A., Johannessen, E., Owen, D., Beauchamp, B., & Gianolla, P. (2007). Sequence Stratigraphy as a “Concrete” Stratigraphic.

Embry, A.F., (2002). Transgressive-Regressive (T-R) Sequence Stratigraphy, In: Armentrout, J and Rosen, N., (eds.), Sequence stratigraphic models for exploration and production: Gulf Coast SEPM Conference Proceedings, Houston 151−172.

Embry, A.F., 1993. Transgressive-regressive (T-R) sequence analysis of the Jurassic succession of the Sverdrup Basin, Canadian Arctic Archipelago. *Canadian Journal of Earth Sciences, 30,* 301−320.

Evans, P. (1964). The tectonic framework of Assam. *Geological Society of India*, *5*, 80-96.

Fathy, D., Wagreich, M., Zaki, R., Mohamed, R. S., & Gier, S. (2018). Geochemical fingerprinting of Maastrichtian oil shales from the Central Eastern Desert, Egypt: Implications for provenance, tectonic setting, and source area weathering. *Geological Journal*, *53*(6), 2597-2612.

Fedo, C. M., Wayne Nesbitt, H., & Young, G. M. (1995). Unraveling the effects of potassium metasomatism in sedimentary rocks and paleosols, with implications for paleoweathering conditions and provenance. *Geology*, *23*(10), 921-924.

Feibel, C. S. (2013). Facies analysis and plio-pleistocene paleoecology. *Early Hominin Paleoecology*, 35-58.

Floyd, P. A., & Leveridge, B. E. (1987). Tectonic environment of the Devonian Gramscatho basin, south Cornwall: framework mode and geochemical evidence from turbiditic sandstones. *Journal of the Geological Society*, *144*(4), 531-542.

Floyd, P. A., Shail, R., Leveridge, B. E., & Franke, W. (1991). Geochemistry and provenance of Rhenohercynian synorogenic sandstones: implications for tectonic environment discrimination. *Geological Society, London, Special Publications*, *57*(1), 173-188.

Floyd, P. A., Winchester, J. A., & Park, R. G. (1989). Geochemistry and tectonic setting of Lewisian clastic metasediments from the Early Proterozoic Loch Maree Group of Gairloch, NW Scotland. *Precambrian Research*, *45*(1-3), 203-214.

Folk, R. L. (1980). *Petrology of sedimentary rocks*. Hemphill Publishing Company. https://doi.org/10.1017/CBO9781107415324.004

Folk, R. L., & Ward, W. C. (1957). Brazos River bar [Texas]; a study in the significance of grain size parameters. *Journal of sedimentary research*, *27*(1), 3-26.

Folk, R.L. (1974). Petrology of Sedimentary Rocks. *Hemphill Publishing Co.,* Austin, TX.

Franklin, W. A. (1948). Photogeological map of Assam and Tripura. *Assam Oil Corporation Letter (Unpublished report)*.

Frazier, D. E. (1974). Depositional-episodes: their relationship to the Quaternary stratigraphic framework in the northwestern portion of the Gulf basin.

Friedman, G. M. (1961). Distinction between dune, beach, and river sands from their textural characteristics. *Journal of Sedimentary Research*, *31*(4), 514-529.

Friedman, G. M. (1967). Dynamic processes and statistical parameters compared for size frequency distribution of beach and river sands. *Journal of Sedimentary Research, 37*(2), 327-354.

Friedman, G. M. (1979). Differences in size distributions of populations of particles among sands of various origins: addendum to IAS Presidential Address. *Sedimentology*, *26*(6), 859-862.

Friedman, G.M., & Johnson, K.G., (1982). Exercise in Sedimentology. *John Wiley and Sons,* New York. 24-83.

Fyffe, L. R., & Pickerill, R. K. (1993). Geochemistry of Upper Cambrian-Lower Ordovician black shale along a northeastern Appalachian transect. *Geological Society of America Bulletin*, *105*(7), 897-910.

Galehouse, J.S. (1971). Point counting. In Carver R.E. (Ed.) *Procedures in Sedimentary Petrology*. New York, Wiley Inter Science, 385–407.

Galloway, W. E. (2001). The many faces of submarine erosion: theory meets reality in selection of sequence boundaries. In *AAPG Hedberg Research Conference on "Sequence Stratigraphic and Allostratigraphic Principles and Concepts", Dallas, August* (pp. 26-29).

Galloway, W. E., & Sylvia, D. A. (2002). *The many faces of erosion: Theory meets data in sequence stratigraphic analysis.*

Ganguly, S. (1975). Tectonic evolution of the Mizo Hills. *Geology Mineral and Metallurgical Society of India, 48*, 28- 40.

Ganguly, S. (1983) Geology and hydrocarbon prospects of Tripura-Cachar-Mizoram region. *Journal of Petroleum Asia, 6,* 105-109.

Ganju, J. L. (1975). Geology of Mizoram. *Geology Mineral and Metallurgical Society of India, 48,* 17–26.

Getaneh, W. (2002). Geochemistry, provenance, and depositional tectonic setting of the Adigrat Sandstone, northern Ethiopia. *Journal of African Earth Sciences, 35*(2), 185-198.

Girty, G. H., Ridge, D. L., Knaack, C., Johnson, D., & Al-Riyami, R. K. (1996). Provenance and depositional setting of Paleozoic chert and argillite, Sierra Nevada, California. *Journal of Sedimentary Research*, *66*(1), 107-118.

Glaister, R. P., & Nelson, H. W. (1974). Grain-size distributions, an aid in facies identification. *Bulletin of Canadian Petroleum Geology*, *22*(3), 203-240.

Grantham, J. H., & Velbel, M. A. (1988). The influence of climate and topography on rock fragment abundance in modern fluvial sands of the southern Blue Ridge Mountains, North Carolina. *Journal of Sedimentary Petrology, 58,* 219–227. https://doi.org/10.1306/212F8D5F-2B24-11D7-8648000102C1865D.

Guilbaud, R., Bernet, M., Huyghe, P., Erens, V., Chirouze, F., and Dupont-Nivet, G. (2012). On the influence of diagenesis on the original petrographic composition of Miocene–Pliocene fluvial sandstone in the Himalayan foreland basin of western-central Nepal. *Journal of Asian Earth Sciences, 44,* 107-116. https://doi.org/10.1016/j.jseaes.2011.04.025.

Haider, S. W. (2016). Sediments analysis of eastern makran coast line area of Pakistan by X-ray diffraction. *Journal of Biodiversity & Environmental Sciences,* 9(1), 11-19.

Harder, H. (1980). Syntheses of glauconite at surface temperatures. *Clays and Clay Minerals, 28,* 217-222.

Harnois, L. (1988). The CIW index: a new chemical index of weathering. *Sedimentary Geology*. 55:319-322.

Hayashi, K. I., Fujisawa, H., Holland, H. D., & Ohmoto, H. (1997). Geochemistry of ~1.9 Ga sedimentary rocks from northeastern Labrador, Canada. *Geochimica et*

Cosmochimica Acta, 61, 4115–4137. https://doi.org/10.1016/S0016-7037(97)00214-7.

Hayman, R. J (1937). Reconnaissance map of part of Lushai Hills. Repon R.J.H.II (Unpublished Burma Oil Company Report).

Hossain, H. M. Z., Roser, B. P., & Kimura, J. I. (2010). Petrography and whole-rock geochemistry of the Tertiary Sylhet succession, northeastern Bengal Basin, Bangladesh: Provenance and source area weathering. *Sedimentary Geology*, *228*(3-4), 171-183.

Hu, X., & Huang, S. (2017). Physical properties of reservoir rocks. *Physics of petroleum reservoirs*, 7-164.

Hubert, J. F. (1962). A zircon-tourmaline-rutile maturity index and the interdependence of the composition of heavy mineral assemblages with the gross composition and texture of sandstones. *Journal of Sedimentary Research*, *32*(3), 440-450.

Hubert, J.F. (1971). Analysis of heavy mineral assemblages. In, R.E. Carver (Ed.), Procedures in Sedimentary Petrology. *Wiley*, New York, 453-478.

Hunt, D., & Tucker, M. E. (1992). Stranded parasequences and the forced regressive wedge systems tract: deposition during base-level'fall. *Sedimentary Geology*, *81*(1-2), 1-9.

Hurst, A., & Irwin, H. (1982). Geological modelling of clay diagenesis in sandstones. *Clay minerals*, *17*(1), 5-22.

Hussain, M. F., & Bharali, B. (2019). Whole-rock geochemistry of Tertiary sediments of Mizoram Foreland Basin, NE India: Implications for source composition, tectonic setting and sedimentary processes. *Acta Geochimica*, *38*, 897-914.

Ingersoll, R. V. (1978). Petrofacies and petrologic evolution of the Late Cretaceous fore-arc basin, northern and central California. *The Journal of Geology*, *86*(3), 335-352.

Ingersoll, R. V., Bullard, T. F., Ford, R. L., Grimm, J. P., Pickle, J. D., & Sares, S. W. (1984). The effect of grain size on detrital modes: a test of the Gazzi-Dickinson point-counting method. *Journal of Sedimentary Research*, *54*(1), 103-116.

Javed, A., Khan, K. F., & Quasim, M. A. (2023). Petrography of the bajocian sandstone of joyan member, jaisalmer basin, western Rajasthan: implications for provenance and basin evolution. *Journal of the Geological Society of India*, *99*(1), 73-87.

Jervey, M. T. (1988). Quantitative geological modeling of siliciclastic rock sequences and their seismic expression.

Jinliang, Z., & Xin, Z. (2008). Composition and provenance of sandstones and siltstones in Paleogene, Huimin depression, Bohai Bay basin, eastern China. *Journal of China University of Geosciences*, *19*(3), 252-270.

Johnsson, M. J. (1993). The system controlling the composition of clastic sediments in Johnsson, M. J. and Basu, A., eds., Processes Controlling the composition of Clastic Sediments Boulder, Colorado, *Geol. Soc. Am. Special Paper,* 284.

Karunakaran, C. & Ranga Rao, A. (1979). Status of exploration for hydrocarbon in the Himalayan Region. Himalayan Geol. Seminar. New Delhi 1976. *Geological Survey of India, Miscellaneous Publishing, 41,* 1-66.

Karunakaran, C. (1974). Geology and mineral resources of the states of India. Part IV-Arunachal Pradesh, Assam, Manipur, Meghalaya, Mizoram, Nagaland and Tripura. *Geological Survey of India, Miscellaneous Publishing, 30,* 1-124.

Kasim, S. A., Ismail, M. S., & Ahmed, N. (2023). Grain size statistics and morphometric analysis of Kluang-Niyor, Layang-Layang, and Kampung Durian Chondong tertiary sediments, onshore peninsular Malaysia: implications for paleoenvironment and depositional processes. *Journal of King Saud University-Science*, *35*(2), 102481.

Keller, W. D. (1945). Size distribution of sand in some dunes, beaches, and sandstones. *AAPG bulletin*, *29*(2), 215-221.

Khalaf, F. I., Al-Ghadban, A., Al-Saleh, S., & Al-Omran, L. (1982). Sedimentology and mineralogy of Kuwait bay bottom sediments, Kuwait Arabian Gulf. *Marine Geology*, *46*(1-2), 71-99.

Krumbein, W. C., & Pettijohn, F. J. (1938). *Manual of sedimentary petrography*. Appleton-Century-Crafts Inc.Vincent, C. E., Stolk, A., & Porter, C. F. C. (1998).

Sand suspension and transport on the Middelkerke Bank (southern North Sea) by storms and tidal currents. *Marine Geology*, *150*(1-4), 113-129.

Krumbein, W. C., & Pettijohn, F. J. (1966). *Manual of sedimentary petrography*. Appleton-Century-Crofts.

Krumbein, W.C., & Pettijohn, F.J. (1938). *Manual of sedimentary petrography*. New York: Appleton-Century- Crafts Inc. 549.

Kulkarni, S. J., Deshbhandari, P. G., & Jayappa, K. S. (2015). Seasonal variation in textural characteristics and sedimentary environments of beach sediments, Karnataka Coast, India. *Aquatic Procedia*, *4*, 117-124.

Lalmuankimi, C., Kumar, S., & Tiwari, R. P. (2011). Geochemical study of upper Bhuban sandstone in Muthi, Mizoram, India. *Sci. Vis*, *11*(1), 40-46.

Lalnunmawia, J., & Lalhlimpuii, J. (2014). Classification and provenance studies of the sandstones exposed along Durtlang road section, Aizawl, Mizoram. *Sci. Vis*, *14*(3), 158-167.

Lerman, A. D. I., and Gat, J. (Eds.) (1989). Physics and chemistry of lakes. *Ber-lin: Springer*-Verlag.

Li, H., Sun, H. S., Evans, N. J., Li, J. W., Wu, J. H., Jiang, W. C., & Halassane, N. (2019). Geochemistry and geochronology of zircons from granite-hosted gold mineralization in the Jiaodong Peninsula, North China: Implications for ore genesis. *Ore Geology Reviews*, *115*, 103188.

Lindsey, D. A. (1999). *An evaluation of alternative chemical classifications of sandstones* (No. 99-346). US Geological Survey.

Long, X., Yuan, C., Sun, M., Safonova, I., Xiao, W., & Wang, Y. (2012). Geochemistry and U–Pb detrital zircon dating of Paleozoic graywackes in East Junggar, NW China: Insights into subduction–accretion processes in the southern Central Asian Orogenic Belt. *Gondwana Research*, *21*(2-3), 637-653.

Ma, Y., Yang, H., Ma, Y., Wang, Y., Wu, W., An, N., ... & Fu, D. (2023). Geochemical characteristics of shales from Upper Carboniferous Yanghugou formation in Weiningbeishan area, China: Implication for provenance, source weathering and tectonic setting. *Marine and Petroleum Geology*, *149*, 106082.

Malsawma, J., Lalnuntluanga, P., Badekar, A., Sangode, S. J., & Tiwari, R. P. (2010). Magnetic polarity stratigraphy of the Bhuban succession, Surma Group, Tripura-

Mizoram accretionary belt. *Journal of the Geological Society of India*, *76*, 119-133.

Mandaokar, B. D. (2000). Palynology and palaeoenvironment of the Bhuban formation (early Miocene) of Ramrikawn, near Aizawl, Mizoram, India. *Journal of Palaeosciences*, *49*(1-3)), 317-324.

Mason, C. C., & Folk, R. L. (1958). Differentiation of beach, dune, and aeolian flat environments by size analysis, Mustang Island, Texas. *Journal of Sedimentary Research*, *28*(2), 211-226.

McLennan, S. M., Hemming, S., McDaniel, D. K., & Hanson, G. N. (1993). Geochemical approaches to sedimentation, provenance and tectonics. *Geol. Soc. Am. Spec. Pap. 284* 295-303.

McLennan, S. M., Hemming, S., McDaniel, D. K., & Hanson, G. N. (1993). Geochemical approaches to sedimentation, provenance, and tectonics.

McLennan, S. M., Taylor, S. R., & Eriksson, K. A. (1983). Geochemistry of Archean shales from the Pilbara Supergroup, western Australia. *Geochimica et Cosmochimica Acta*, *47*(7), 1211-1222.

Moiola, R. J., & Weiser, D. A. N. I. E. L. (1968). Textural parameters; an evaluation. *Journal of Sedimentary Research*, *38*(1), 45-53.

Mongelli, G., Critelli, S., Perri, F., Sonnino, M., & Perrone, V. (2006). Sedimentary recycling, provenance and paleoweathering from chemistry and mineralogy of Mesozoic continental redbed mudrocks, Peloritani Mountains, Southern Italy. *Geochemical Journal*, *40*(2), 197-209.

Moradi, A. V., Sarı, A., & Akkaya, P. (2016). Geochemistry of the Miocene oil shale (Hançili Formation) in the Çankırı-Çorum Basin, Central Turkey: Implications for Paleoclimate conditions, source–area weathering, provenance and tectonic setting. *Sedimentary Geology*, *341*, 289-303.

Moradi, M., Moussavi-Harami, R., Mahboubi, A., Khanehbad, M., & Ghabeishavi, A. (2017). Rock typing using geological and petrophysical data in the Asmari reservoir, Aghajari Oilfield, SW Iran. *Journal of Petroleum Science and Engineering*, *152*, 523-537.

Morton, A. C. (1985). Heavy minerals in provenance studies. In *Provenance of arenites* (pp. 249-277). Dordrecht: Springer Netherlands.

Morton, A. C., & Hallsworth, C. (1994). Identifying provenance-specific features of detrital heavy mineral assemblages in sandstones. *Sedimentary Geology*, *90*(3-4), 241-256.

Morton, A. C., Davies, J. R., & Waters, R. A. (1992). Heavy minerals as a guide to turbidite provenance in the Lower Palaeozoic Southern Welsh Basin: a pilot study. *Geological Magazine*, *129*(5), 573-580.

Najman, Y., Bickle, M., BouDagher-Fadel, M., Carter, A., Garzanti, E., Paul, M., ... & Vezzoli, G. (2008). The Paleogene record of Himalayan erosion: Bengal Basin, Bangladesh. *Earth and Planetary Science Letters, 273*(1-2), 1-14.

Nandy, D. R. (2001). *Geodynamics of Northeastern India and the Adjoining Regions*. (p. 209), ACB Publications, Kolkata, India.

Nandy, D. R. (2017). *Geodynamics of Northeastern India and the adjoining region*. Scientific book centre.

Nandy, D. R., & Sarkar, K. (1973). Geological mapping and mineral survey in parts of Aizawl District, Mizoram. *Geological Survey of India. Progress Report for FS 1971*, *72*.

Nandy, D. R., Dasgupta, S., Sarkar, K. & Ganguly, A. (1983). Tectonic evolution of Tripura Mizoram Fold Belt, Surma Basin, North East India. *Quaternary Journal of Geology Mineral and Metallurgical Society of India, 35*(4), 186-194.

Nesbitt, H. W., & Young, G. M. (1984). Prediction of some weathering trends of plutonic and volcanic rocks based on thermodynamic and kinetic considerations. *Geochimica et cosmochimica acta*, *48*(7), 1523-1534.

Nesbitt, H. W., & Young, G. M. (1996). Petrogenesis of sediments in the absence of chemical weathering: effects of abrasion and sorting on bulk composition and mineralogy. *Sedimentology*, *43*(2), 341-358.

Nesbitt, H., & Young, G. M. (1982). Early Proterozoic climates and plate motions inferred from major element chemistry of lutites. *nature*, *299*(5885), 715-717.

Parker, A. (1970). An index of weathering for silicate rocks. *Geological Magazine*, *107*(6), 501-504.

Passega, R. (1957). Texture as characteristic of clastic deposition. *AAPG Bulletin*, *41*(9), 1952-1984.

Passega, R. (1964). Grain size representation by CM patterns as a geologic tool. *Journal of Sedimentary Research*, *34*(4), 830-847.

Pettijohn, F. J. (1975). *Sedimentary rocks* (Vol. 3, p. 628). New York: Harper & Row.

Pettijohn, F. J., Potter, P. E., & Siever, R. (1972). Sand and Sandstone. Springer-Verlag, Berlin Heidelberg New York. *pp 618 Pitman WC*.

Pettijohn, F. J., Potter, P. E., & Siever, R. (2012). *Sand and sandstone*. Springer Science & Business Media.

Posamentier, H. W., & Allen, G. P. (2014). *Siliciclastic sequence stratigraphy: concepts and applications*. GeoScienceWorld.

Quasim, M. A., Khan, S., Srivastava, V. K., Ghaznavi, A. A., & Ahmad, A. H. M. (2021). Role of cementation and compaction in controlling the reservoir quality of the Middle to Late Jurassic Sandstones, Jara dome, Kachchh Basin, western India. *Geological Journal*, *56*(2), 976-994.

Rahman, M. J. J., & Suzuki, S. (2007). Geochemistry of sandstones from the Miocene Surma Group, Bengal Basin, Bangladesh: Implications for Provenance, tectonic setting and weathering. *Geochemical Journal*, *41*(6), 415-428.

Rajganapathi, V. C., Jitheshkumar, N., Sundararajan, M., Bhat, K. H., & Velusamy, S. (2013). Grain size analysis and characterization of sedimentary environment along Thiruchendur coast, Tamilnadu, India. *Arabian Journal of Geosciences*, *6*, 4717-4728.

Ramamoorthy, A., & Ramasamy, S. (2015). Petrography and provenance of surface barail sandstones, Kohima, Nagaland, India. *Int J Eng Econ*, *4*, 2278-2540.

Ramamoorthy, A., & Ramasamy, S. (2016). Petrography and Heavy Mineral Analysis of Barail Sandstones, Zubza Village, Kohima District, Nagaland India. *International Journal Geology and Earth Sciences*, *2*, 43-53.

Ramanathan, A. L., Rajkumar, K., Majumdar, J., Singh, G., Behera, P. N., Santra, S. C., & Chidambaram, S. (2009). Textural characteristics of the surface sediments of a tropical mangrove Sundarban ecosystem India.

Reading, B. G. (1978). Sedimentary environments and facies.

Rezaee, M. R., & Tingate, P. R. (1997). Origin of quartz cement in the Tirrawarra sandstone, southern Cooper basin, South Australia. *Journal of Sedimentary Research*, *67*(1), 168-177.

Roser, B. P., & Korsch, R. J. (1986). Determination of tectonic setting of sandstone-mudstone suites using SiO2 content and K2O/Na2O ratio. *The Journal of Geology*, *94*(5), 635-650.

Sahu, B. K. (1964). Depositional mechanisms from the size analysis of clastic sediments. *Journal of Sedimentary Research*, *34*(1), 73-83.

Samad, S. K., Mishra, D. K., Mathews, R. P., Ghosh, S., Mendhe, V. A., & Varma, A. K. (2020). Geochemical attributes for source rock and palaeoclimatic reconstruction of the Auranga Basin, India. *Journal of Petroleum Science and Engineering*, *185*, 106665.

Sarma, J. N., & Chutia, A. (2013). Petrography and heavy mineral analysis of Tipam Sandstones exposed on the Tipam Hill of Sita Kunda area, Upper Assam, India. South East Asian. *Journal of Sedimentary Basin Research*, *1*, 28-34.

Schoenborn, W. A., & Fedo, C. M. (2011). Provenance and paleoweathering reconstruction of the Neoproterozoic Johnnie Formation, southeastern California. *Chemical Geology*, *285*(1-4), 231-255.

Selley, R. C. (1998). *Elements of petroleum geology*. Gulf Professional Publishing.

Sengupta, P., Dasgupta, S., Bhui, U. K., Ehl, J., & Fukuoka, M. (1996). Magmatic evolution of mafic granulites from Anakapalle, Eastern Ghats, India: Implications for tectonic setting of a Precambrian high-grade terrain. *Journal of Southeast Asian Earth Sciences*, *14*(3-4), 185-198.

Sengupta, S. M. (2004). *Introduction to Sedimentology*. Oxford, New Delhi. 295p.

Sengupta, S. M., (1994). *Introduction to sedimentology,* Oxford and IBH Pub. Co

Sengupta, S., Acharyya, S. K., & De Smeth, J. B. (1996). Geochemical characteristics of the Abor volcanic rocks, NE Himalaya, India: nature and early Eocene magmatism. *Journal of the Geological Society*, *153*(5), 695-704.

Singh, B. P., Pawar, J. S., & Karlupia, S. K. (2004). Dense mineral data from the northwestern Himalayan foreland sedimentary rocks and recent river sediments: evaluation of the hinterland. *Journal of Asian Earth Sciences*, *23*(1), 25-35.

Sinha, R. N., & Sastri, V. V. (1973). Correlation of the Tertiary geosynclinal sediments of the Surma valley, Assam, and Tripura state (India). *Sedimentary Geology*, *10*(2), 107-134.

Sloss, L.L., Krumbein, W.C., & Dapples, E.C. (1949). Integrated Facies analysis. In: Sedimentary Facies in Geologic History (Longwell, C.R. (Eds.*), Geological Society of America Memoir 39,* 91-124.

Sonowal, R., Swimm, A., Sahoo, A., Luo, L., Matsunaga, Y., Wu, Z., ... & Kalman, D. (2017). Indoles from commensal bacteria extend healthspan. *Proceedings of the National Academy of Sciences*, *114*(36), E7506-E7515.

Srivastava, A. K., & Mankar, R. S. (2009). Grain size analysis and depositional pattern of upper Gondwana sediments (Early Cretaceous) of Salbardi area, districts Amravati, Maharashtra and Betul, Madhya Pradesh. *Journal of the Geological Society of India*, *73*, 393-406.

Srivastava, A. K., Ingle, P. S., Lunge, H. S., & Khare, N. (2012). Grain-size characteristics of deposits derived from different glacigenic environments of the Schirmacher Oasis, East Antarctica. *Geologos*, *18*(4), 251-266.

Sutherland, R. A., & Lee, C. T. (1994). Application of the log-hyperbolic distribution to Hawai'ian beach sands. *Journal of Coastal Research*, 251-262.

Suttner, L. J. (1974). Sedimentary petrographic provinces: An evaluation, in Ross, C. A, ed., Paleogeographic provinces and provinciality. *Society of Economic Paleontologists and Mineralogists. Special Publication 21,* 75-84.

Suttner, L. J., & Dutta, P. K. (1986). Alluvial sandstone composition and paleoclimate; I, Framework mineralogy. *Journal of Sedimentary Research*, *56*(3), 329-345.

Suttner, L. J., Basu, A., & Mack, G. H. (1981). Climate and the origin of quartz arenites. *Journal of Sedimentary Research*, *51*(4), 1235-1246.

Swift, D., Kofoed, J., Saulsbury, F., & Sears, P. (1972). Holocene evolution of the shelf surface, central and southern Atlantic shelf of North America. In D. Swift, D. Duane, & O. Pilkey (Eds.), *Shelf sediment transport: Process and pattern* (pp. 499-574). Hutchinson and Ross.

Tao, S., Xu, Y., Tang, D., Xu, H., Li, S., Chen, S., ... & Gou, M. (2017). Geochemistry of the Shitoumei oil shale in the Santanghu Basin, Northwest China: Implications for paleoclimate conditions, weathering, provenance and tectonic setting. *International Journal of Coal Geology*, *184*, 42-56.

Taylor, S. R., & McLennan, S. M. (1985). *The continental crust: Its composition and evolution*. Blackwell.

Teichert, C. (1958). Concepts of facies. *AAPG Bulletin*, *42*(11), 2718-2744.

Thomas, R. L., Kemp, A. L. W., & Lewis, C. F. M. (1972). Distribution, composition and characteristics of the surficial sediments of Lake Ontario. *Journal of Sedimentary Research, 42*(1), 66-84.

Tingate, P. R., & Rezaee, M. R. (1997). Origin of quartz cement in Tirrawarra Sandstone, Southern Cooper Basin, South Australia. *Journal of Sedimentary Research, 67,* 168-177.

Tiwari, R. P., & Kachhara, R. P. (2003). Molluscan biostratigraphy of the Tertiary sediments of the Mizoram, India. *Jour. Pal. Soc. India*, *48,* 59-82.

Tiwari, R. P., and Mehrotra, R. C. (2002). Plant impressions from the Barail Group of Champhai-Aizawl Road section, Mizoram, India. *Phytomorphology, 52*(1), 69-76.

Tiwari, R. P., Rajkonwar, C., & Patel, S. J. (2013). Funalichnus bhubani isp. nov. from Bhuban Formation, Surma Group (Lower-Middle Miocene) of Aizawl, Mizoram, India. *Plos One*, *8*(10), e77839.

Tiwari, R. P., Sangode, S. J., Patil, S. K., Sivaji, C., and Arora, B. R. (2006). Status of palaeomagnetic and magnetostratigraphic studies in Northeast India and the new initiatives. *DCSDST Newsletter*, *16*(2), 16-20.

Tiwari, R.P., Rajkonwar, C., Lalchawimawii, Lalnuntluanga, P., Malsawma, J., Ralte, V.Z., & Patel, S.J. (2011). Trace fossils from Bhuban Formation, Surma Group

(Lower to Middle Miocene) of Mizoram India and their paleoenvironmental significance. *Journal of Earth System Science*, *120*(6) 1124-1143.

Tortosa, A., Palomares, M., & Arribas, J. (1991). Quartz grain types in Holocene deposits from the Spanish Central System: some problems in provenance analysis. *Geological Society, London, Special Publications*, *57*(1), 47-54.

Touche, L. (1981). Note on the geology of Lushai Hills. *Rec. Geol. Surv. India*, *24*(2), 83-181.

Udden, J. A. (1914). Mechanical composition of clastic sediments. *Bulletin of the Geological Society of America*, *25*, 655–744.

Uddin, A., & Lundberg, N. (1998). Unroofing history of the Eastern Himalaya and the Indo–Burman ranges: Heavy mineral study of Cenozoic sediments from the Bengal Basin, Bangladesh. *Journal of Sedimentary Research*, *68*(3), 465-472.

Uddin, A., & Lundberg, N. (1999). A paleo-Brahmaputra? Subsurface lithofacies analysis of Miocene deltaic sediments in the Himalayan–Bengal system, Bangladesh. *Sedimentary Geology*, *123*(3-4), 239-254.

Uddin, A., Kumar, P., Sarma, J. N., & Akhter, S. H. (2007). Heavy mineral constraints on the provenance of Cenozoic sediments from the foreland basins of Assam and Bangladesh: erosional history of the eastern Himalayas and the Indo-Burman Ranges. *Developments in Sedimentology*, *58*, 823-847.

Van Wagoner, J. C., Posamentier, H. W., Mitchum, R. M., Vail, P. R., Sarg, J. F., Loutit, T. S., & Hardenbol, J. (1988). An overview of the fundamentals of sequence stratigraphy and key definitions. In C. K. Wilgus, B. S. Hastings, C. G. St. C. Kendall, H. W. Posamentier, C. A. Ross, & J. C. Van Wagoner (Eds.), *Sea-level changes—An integrated approach* (SEPM Special Publication No. 42, pp. 39–45).

Vincent, C. E., Stolk, A., & Porter, C. F. C. (1998). Sand suspension and transport on the Middelkerke Bank (southern North Sea) by storms and tidal currents. *Marine Geology*, *150*(1-4), 113-129.

Visher, G. S. (1969). Grain size distributions and depositional processes. *Journal of Sedimentary Research*, *39*(3).

Weljte, G. J. (1994). Provenance and dispersal of sand-sized sediments: recognition of dispersal pattern and sources of sand-sized sediments by means of inverse modelling techniques. *Geol. Ultraiectina, 121*, 208.

Wentworth, C. K. (1922). *The shapes of beach pebbles*. US Government Printing Office.

Worden, R.H. & Burley, S.D. (2003). Sandstone diagenesis: the evolution from sand to stone. In: Burley, S.D. &Worden, R.H. (eds) *Sandstone Diagenesis, Recent and Ancient*. International Association of Sedimentologists Reprint Series, Oxford, 3–44.

Wu, J., Li, H., Goodarzi, F., Min, X., Cao, W., Huang, L., Jiang, Y., Luo, Q., & Jiang, Y. (2022). Geochemistry and depositional environment of the Mesoproterozoic Xiamaling shales, northern North China. *Journal of Petroleum Science and Engineering, 215*, 110730.

Yuan, G., Cao, Y., Schulz, H. M., Hao, F., Gluyas, J., Liu, K., ... & Li, F. (2019). A review of feldspar alteration and its geological significance in sedimentary basins: From shallow aquifers to deep hydrocarbon reservoirs. *Earth-science reviews*, *191*, 114-140.

Zhang, Q. Q., Zhang, S. H., Zhao, Y., & Hu, G. H. (2021). Geochronology, geochemistry and petrogenesis of the Neoarchean magmatism in the Jiefangyingzi area, northern North China Craton: Implications for crustal growth and tectonic affinity. *Precambrian Research*, *357*, 106144.

Zhang, Q., Wu, X. S., Radwan, A. E., Wang, B. H., Wang, K., Tian, H. Y., & Yin, S. (2022). Diagenesis of continental tight sandstone and its control on reservoir quality: A case study of the Quan 3 member of the cretaceous Quantou Formation, Fuxin uplift, Songliao Basin. *Marine and Petroleum Geology*, *145*, 105883.

Zhang, Y. L., Bao, Z. D., Zhao, Y., Jiang, L., Zhou, Y. Q., & Gong, F. H. (2017). Origins of authigenic minerals and their impacts on reservoir quality of tight sandstones: Upper Triassic Chang-7 Member, Yanchang Formation, Ordos Basin, China. *Australian Journal of Earth Sciences*, *64*(4), 519-536.

Zhao, G., Kroener, A., Wilde, S. A., Sun, M. I. N., Li, S., Li, X., ... & He, Y. (2007). Lithotectonic elements and geological events in the Hengshan–Wutai–Fuping belt: A synthesis and implications for the evolution of the Trans-North China Orogen. *Geological Magazine*, *144*(5), 753-775.

Zhao, Q., Zhai, D., Wang, J., Liu, J., & Williams-Jones, A. E. (2021). The geochemistry and geochronology of Permian granitoids from central Inner Mongolia, NE China: Petrogenesis and tectonic implications. *Lithos*, *404*, 106489.

Zoramthara, C., Ralte, V. Z., & Lalramdina. (2015). Grain size analysis of Tipam sandstones near Buhchang village, Kolasib district, Mizoram. *Science Vision, 15,* 42-51.

ABSTRACT

Tectonically, Mizoram is a part of the Surma Basin, is associated with the eastward subduction of the Indian plate along the Arakan Yoma suture during the Miocene period, followed by the subsequent formation of the Indo-Burmese Orogenic belt (Nandy, 1982). The Cenozoic rocks of Mizoram are represented by the Surma Basin, often referred to as the Greater Bengal Basin's northern extension in the geological past. The Surma Basin has evolved similarly to the Bengal Basin which was initiated by the collision between the Indian plate and the Burmese plate (Nandy et al. 1983; Dasgupta, 1984; Bharali et al. 2017).

Geologically, the Mizoram part is encompassed within the Neogene Surma Basin, which is characterized by a Succession of elongated and folded hill ranges exhibiting an arcuate shape with westward convexity. Based on the lithological variations, the Tertiary sequence of the Mizoram Fold Belt (MFB) has been classified into the Barail Group (Late Oligocene), Surma Group (Upper Oligocene-Miocene), and Tipam Group (Late Miocene-Early Pliocene). It extends across an area of approximately 21,081 km2 and is located between the latitudes of 22º00'N and 24o30'N, along with longitudes 92°15′E and 93°25′E, respectively. The Miocene succession of Mizoram is one of the thickest sedimentary columns of the region and is a repeated succession of Paleogene to Neogene argillaceous and arenaceous rocks. According to the previous investigations, the entire basin is composed of sandstone, silty-sandstone, shale, mudstone, and their combination along with a few pockets of calcareous sandstone, fossiliferous siltstone and intraformational conglomerate (Tiwari and Kachhara, 2003).

The previous researchers La Touche (1891), Hayman (1937), and Franklin (1948) laid the foundation. Nevertheless, Ganju (1975), Nandy et al. (1983), Dasgupta (1984), and Tiwari et al. (2003, 2007, 2011) extensively worked on the Surma Basin, providing valuable information on the regional geological framework, tectonic settings, paleontology, magneto stratigraphy, etc.

This present research work has been selected for consolidating the discrepancies in the litho-unit division as suggested by the earlier researchers and a

deficiency in adequate geological information. Consequently, the present study involves a comprehensive outcrop mapping and preparation of a vertical litho-column for the Bhuban Formation in the selected sections. A comprehensive petrographic analysis, encompassing diagenesis of the Bhuban sandstones has been carried out. This study also includes an attempt at the granulometric analysis, heavy mineral analysis, and whole-rock geochemistry of sandstones in parts of the Aizawl district. Additionally, a Sequence stratigraphic model has been prepared for the Bhuban Formation of the study area. Furthermore, the study area is also an important aspect of its distinctive geodynamic setting, and the rocks are geologically suitable for hydrocarbon prospects.

The study area encompasses the Surma Group of the Miocene Bhuban Formation, which falls within the Upper Bhuban Formation and Middle Bhuban Formation of the Aizawl District of Mizoram ranging from lower to middle Miocene age. Geographically, the study area extends from latitude 23°38' to 23°46' N and longitude 92°43' to 92°49' E, with a maximum elevation of 1159 meters (MSL) covering toposheets no. 84-A/10, 84-A/14, 84-A/15 (Fig. 1.2). The examined Bhuban sandstones are characterized by fine to medium grains, buff in color, and exhibit massive bedding with limited outcrops (Fig1.3). Conversely, the shales are described as dark grey, firm, and compact. In the present research work, geological mapping is conducted in four road sections of the Aizawl district of Mizoram where rocks are mainly from the Upper and Middle Bhuban Formation of Surma Group. Thickness measurements of various sedimentary beds are recorded to prepare a litho-column for each section.

The thesis comprises nine chapters including references. Chapter 1 introduces the study area, including its location, coordinates, sample names, accessibility, physiography, climate, and geological significance. Field assessments along the proposed four sections in Aizawl District were conducted, focusing on sedimentary structures, lithology, and detailed mapping. Rock samples, field data (GPS location, dip, and strike), and images were collected for further analysis. Additionally, this chapter also includes the Geological setting and study area along with the Geological Significance.

Chapter 2 includes details of the methodology, materials, and techniques which are to accomplish the objectives of the present study. Grain analysis employed the sieving method with a Mechanical Sieve Shaker Machine, utilizing ASTM sieves with mesh sizes ranging from 35, 45, 60, 80, 120, 170, 230, 325 and collecting pan, along with ½ Phi (Ø) intervals for petrography, Modal analysis using the Point counting technique following the Gazzi-Dickinson method was conducted. Thin sections made from collected samples were analyzed using a LeicaDM4500 P polarizing microscope equipped with a Leica DFC420 camera and Leica Image Analysis software. Each thin section underwent a 500-step count. Heavy mineral separation utilized the Gravity settling method with Bromoform as a liquid medium, following the Funnel separation method of Krumbein and Pettijohn 1938. The ZTR Index by Hubert was used to express the maturity of the samples. For geochemical analysis, major, trace, and rare earth elements were examined in rock samples at CSIR-National Geophysical Research Institute, Hyderabad, India. Trace and rare earth elements were analyzed using HR-ICP-MS, while major elements were examined using XRF. Additionally, this chapter also includes a paragraph on previous research surveys of relevant to the study.

Chapter 3 comprises the sedimentological investigation, focusing primarily on the preparation of lithocolumns during field observations and the study of sequence stratigraphy. These lithocolumn columns were constructed based on meticulous measurements of various litho-units, measurements of bed thickness, observations of sedimentary structures, grain size, and fossil content exposed in the study region. Furthermore, from the sequence stratigraphic framework, four primary types of system tracts i.e. falling stage system tract (FSST), low stand system tract (LST), transgressive system tract (TST), and high stand system tract (HST) have been identified based on field observations and sedimentary structures. In this present study, an attempt has been made 3 to establish the sequence stratigraphic framework by analyzing the lithostratigraphic column from field observations and the presence of sedimentary structures. An attempt has also been made to conceptualize a depositional regime for Bhuban sediments (Surma Group) of the study area based on lithology, bed geometry, and sedimentary structures. The Study area dominantly a fluvio–tidal environment has been envisaged with also minor contribution to the Shallow marine Environment.

The chapter 4 covers mainly an analysis of Bhuban sandstone Petrography unveiled insights into the source area characteristics, provenance, climatic conditions and weathering history, as well as tectonic settings. Quartz emerged as the predominant detrital grain, comprising an average of 83.59% followed by feldspars (average 7.94%), and lithic fragments (average 8.47%), as well as matrix, cement, secondary and accessory minerals. Additionally, other accessory minerals such as micas and heavy mineral inclusions were also identified. Based on the petrographical textural relationships, it can be inferred that the sandstones are primarily sub-litharenite and arkosic wacke, possessing a fine-to-medium grain size and poor to moderate sorting. The grains are sub-rounded to sub-angular in shape. the examined area underwent a complex diagenetic process, which affected the Bhuban Sandstones in various ways, including compaction, cementation, replacement, recrystallization, dissolution, and mineral overgrowths. Studied sandstones are derived from a granitic source rock composition, with a significant detritus contribution from a medium- to high-rank metamorphic source. The analysis of tectono-provenance settings using petrographic ternary plots Q_mFL_t and Q_tFL revealed that the sediments were sourced from a recycled orogen, under humid climatic conditions, with minimal contributions from the craton interior.

Granulometric analysis of Bhuban Sandstone is included in Chapter 5 which mainly deals with the sandstone to understand the nature of the transporting medium, the energy flow of the sediments, and the depositional environments. Based mostly on univariate grain size parameters, bivariate plots, linear discriminant function, and log–log probability curves, and the C–M pattern it is inferred that Bhuban sediments are predominantly fine-grained, poorly sorted to moderately sorted, platykurtic to mesokurtic and mainly the coarse skewed, low to moderate energy condition and deposited in a shallow marine environment under the influence of fluvial action. The C–M pattern also signifies the transport mechanisms of the analyzed where sediments were mostly deposited by suspension with some rolling sediments, which resulted in finer to medium fractions under the influence of fluvial action in a shallow marine condition.

Heavy minerals analysis of Bhuban Sandstone covers chapter 6 where the heavy mineral assemblage of Bhuban sandstones included both non-opaque in the form of mainly zircon, rutile, tourmaline, apatite, staurolite, kyanite, garnet, epidote, augite and opaque minerals. The abundance of zircon and rutile in the form of euhedral suggests that these rocks originated from acidic igneous and crystalline metamorphic rocks as well as short to a moderate distance of sediment transportation. Additionally, ZTR index for Bhuban sediments displays a low value which indicates that the sediments are mineralogically immature.

Chapter 7 deals with the geochemical analysis of the Bhuban sandstones. The whole-rock geochemical analysis reveals a higher concentration of SiO2, followed by Al_2O_3, Fe_2O_3, MgO, K_2O, Na_2O, CaO, MnO, and P_2O_5. The SiO_2/Al_2O_3 ratio is high, averaging 5.065. This suggests that the ratio increases due to weathering, recycling processes, and sediment transport processes. As a result, the population of quartz grains increases, indicating the leaching of less resistant minerals over time. The analysis of the Bhuban sandstone's Rare Earth Elements (REE) concentration, when compared to a chondrite normalized patterns, reveals that the Light Rare Earth Elements (LREE: La-Gd) are enriched over Heavy Rare Earth Elements (HREE: Tb-Lu), with avg. LREE/HREE ratio of 9.803 ppm, with a Negative Eu anomaly of 0.62. Additionally, there are relatively lower concentrations of Sr due to the fractionation of Ca-rich plagioclase from the source rocks. These findings suggest that the sandstone likely originated from fractionated felsic source rocks, such as granitoids, as indicated by the REE ratio and chondrite normalized pattern. (Slack and Stevens, 1994).

By integrating various geochemical classification schemes, the Bhuban sandstones are primarily classified as litharenite, with arkose and wacke types, according to classification schemes proposed by Pettijohn *et al.* (1972) and Blatt *et al.* (1980). By assimilation, different provenance plots based on Geochemistry analysis indicate that the sediments were derived from the felsic rocks viz. granite, granodiorite, and their metamorphic equivalents of upper to middle grade viz. schist, gneisses, etc. The tectonic setting of Bhuban sandstones is primarily characterized by the active continental margin based on geochemical analysis with less weathered from the source rocks under semi-humid to humid climatic conditions.

In Chapter 8, the entire research is summarized and concluded. Based on field observations, laboratory studies, and interpretations, as well as various sedimentary structures it's likely that the Bhuban sandstones were deposited in a shallow marine environment to deltaic under the strong influence river. Grain size analysis and sedimentary structures observed in the field support this inference, along with the preservation of burrows. Regarding mineralogy, the analysis of heavy mineral assemblages, ZTR maturity index, and petrographic analysis suggests that the Bhuban sandstones both Upper and Middle Bhuban formation originated from immature sediments derived from mixed sources, including granite, granodiorite, and their metamorphic equivalents of upper to middle grade viz. schist, gneisses etc. Again, based on Geochemical and petrological investigations the Bhuban sandstones are believed to have been sourced from various provenances, including recycled sedimentary terrain, and felsic sources. It's hypothesized that the tectonic settings of the Bhuban sandstones originated from the Continental Island Arc, linked to the Active Continental Margin. These sediments are thought to have been transported from uplifted and eroded terrain in the Himalayan orogenic belts, the crystalline Proterozoic upliftment in northeast India, and the nearby Indo-Myanmar tectonic belt.